UCTEA Turkish Chamber of Civil Engineers

# Teknik Dergi

## *Technical Journal*

Volume 32 Issue 6 November 2021

## TEKNİK DERGİ PUBLICATION PRINCIPLES

Teknik Dergi is a scientific and technical journal indexed by the Science Citation Index Expanded. Annually six issues are published, three in Turkish in the months of January, May and September, three in English in March, July and November. Its main principles of publication are summarized below:

1. Articles reporting original scientific research and those reflecting interesting engineering applications are accepted for publication. To be classified as original, the work should either produce new scientific knowledge or add a genuinely new dimension to the existing knowledge or develop a totally new method or substantially improve an existing method.
2. Articles reporting preliminary results of scientific studies and those which do not qualify as full articles but provide useful information for the reader can be considered for publication as technical notes.
3. Discussions received from the readers of the published articles within three months from publication are reviewed by the Editorial Board and then published together with the closing remarks of the author.
4. Manuscripts submitted for publication are evaluated by two or three reviewers unknown to the authors. In the light of their reports, final decision to accept or decline is taken by the Editorial Board. General policy of the Board is to get the insufficient manuscripts improved in line with the reviewers' proposals. Articles that fail to reach the desired level are declined. Reasons behind decisions are not declared.
5. A signed statement is taken from the authors, declaring that the article has not been published as a "journal article or book chapter". In case the Editorial Board is in the opinion that the article has already been published elsewhere with minor changes or suspects plagiarism or a similar violation of ethics, then not only that article, but none of the articles of the same authors are published.
6. Papers reporting works presented as conference papers and developed further may be considered for publication. The conference it was presented to is given as a footnote in the first page.
7. Additionally, a document signed by all authors, transferring the copyright to UCTEA Chamber of Civil Engineers is submitted together with the manuscript.

UCTEA Turkish Chamber of Civil Engineers

# Teknik Dergi

## *Technical Journal*

Volume 32 Issue 6 November 2021

**UCTEA *(TMMOB)***
**Turkish Chamber of Civil Engineers *(İnşaat Mühendisleri Odası)***
Necatibey St. No: 57, Kızılay 06440 Ankara, Turkey
Tel: +90.312.294 30 00 - Faks: +90.312.294 30 88
E-mail: imo@imo.org.tr - www.imo.org.tr

**Publisher *(Sahibi)*:**
Taner YÜZGEÇ
On behalf of UCTEA Turkish Chamber of Civil Engineers

**Administrative Officer *(Yazı İşleri Müdürü)*:**
Özer AKKUŞ

Volume 32 - Issue 6 - November 2021 *(Cilt 32 - Sayı 6 - Kasım 2021)*
Published bi-monthly. Local periodical. *(İki ayda bir yayınlanır, yerel süreli yayın)*
Date of Print: 1 November 2021 *(Baskı Tarihi: 1 Kasım 2021)*
Number of copies: 1.000 *(1.000 adet basılmıştır)*


**ISSN: 1300-3453**

Teknik Dergi is indexed by
- Science Citation Index Expanded
- Scopus
- Journal Citation Reports / Science Edition
- Engineering Index
- Concrete Abstracts (American Concrete Institute)
- National Technical Information Service (US NTIS)
- CITIS
- Ulrich's International Periodical's Directory
- TR Index

Teknik Dergi is a peer reviewed open access periodical publishing papers of original research and interesting practice cases. It addresses both the research community and the practicing engineers.

Teknik Dergi ekidir.

---

**Printed by *(Baskı)*:**
Boyut Tanıtım Matbaa Basım Yayın San. Tic. Ltd. Şti.
İvedik Organize Sanayi 1354. Cad. Fora İşmerkezi No: 138/18 - Yenimahalle /Ankara
Tel: 0.312.385 72 12 - Faks: 0.312.385 72 13

UCTEA Turkish Chamber of Civil Engineers
# Teknik Dergi

## Reviewers:

This list is renewed each year and includes reviewers who served in the last two years of publication.

Süleyman ADANUR
Ali Mardani AGHABAGLOU
Ayda Şafak AĞAR ÖZBEK
Perviz AHMEDZADE
Ragıp AKBAŞ
Sami Oğuzhan AKBAŞ
Şeref Doğuşcan AKBAŞ
Rıfat AKBIYIKLI
Özge AKBOĞA KALE
Hüseyin AKBULUT
Burcu AKÇAY ALDANMAZ
Cihan Taylan AKDAĞ
Adem AKPINAR
Muhammet Vefa AKPINAR
Atakan AKSOY
Hafzullah AKSOY
Hakan AKSU
Tülay AKSU ÖZKUL
Büşra AKTÜRK
Güzin AKYILDIZ ALÇURA
Zuhal AKYÜREK
Uğurhan AKYÜZ
Sadık ALASHAN
Cenk ALHAN
Sinan ALTIN
Selim ALTUN
Adlen ALTUNBAŞ
Ahmet Can ALTUNIŞIK
Yalçın ALVER
Egemen ARAS
Ergin ARIOĞLU
Yalçın ARISOY
Musa Hakan ARSLAN
Deniz ARTAN İLTER
Şenay ATABAY
Ali Osman ATAHAN
Hakan Nuri ATAHAN
Abdullah AVEY
Ersin AYDIN
İsmail AYDIN
Mustafa Tamer AYVAZ
Ela BABALIK
Can Elmar BALAS
Selim BARADAN
Türkay BARAN
Bekir Oğuz BARTIN
Eyüp Ensar BAŞAKIN
Cemal BAŞARAN
Özgür BAŞKAN
İdris BEDİRHANOĞLU
Niyazi Özgür BEZGİN
Senem BİLİR MAHÇİÇEK
Ahmet BİRİNCİ
İlknur BOZBEY
Zafer BOZKUŞ
Atıl BULU
Burcu BURAK BAKIR
Halil İbrahim BURGAN
Yusuf CALAYIR
Erdem CANBAY
Zekai CELEP
Cihan CENGİZ
Halim CEYLAN
Hüseyin CEYLAN
Ömer CİVALEK
Özgür ÇAKIR
Melih ÇALAMAK
Gülben ÇALIŞ
Erkan ÇELEBİ
Kutay ÇELEBİOĞLU
Tevfik Kutay ÇELEBİOĞLU
Ahmet Ozan ÇELİK
Oğuz Cem ÇELİK
Osman Nuri ÇELİK
Semet ÇELİK
Hilmi Berk ÇELİKOĞLU
Mecit ÇETİN
Gökhan ÇEVİKBİLEN
Mesut ÇİMEN
Safiye Feyza ÇİNİCİOĞLU
Erdal ÇOKÇA
Şevket ÇOKGÖR
İsa ÇÖMEZ
Atilla DAMCI
Yakup DARAMA
Osama M.F. DAWOUD
Özgür DEĞERTEKİN
Abdullah DEMİR
Cem DEMİR
Uğur DEMİR
Ender DEMİREL
Mehmet Cüneyd DEMİREL
Fatih DİKBAŞ
Seyyit Ümit DİKMEN
İrem DİKMEN TOKER
Ali Ersin DİNÇER
Selim DÜNDAR
Nurhan ECEMİŞ ZEREN
Alper ELÇİ
Şebnem ELÇİ
Muhammet Emin EMİROĞLU
Hakan ERDEM
Sinan Turhan ERDOĞAN
Esin ERGEN PEHLEVAN
Ayşen ERGİN
Gökmen ERGÜN
Ebru ERİŞ
Bülent ERKMEN
Barış ERKUŞ
Esra Ece ESELLER BAYAT
Tuğba ESKİŞAR TEFÇİ
Burak FELEKOĞLU
Okan FISTIKOĞLU
Abdullah GEDİKLİ
Ergun GEDİZLİOĞLU
Mohammad Ali GHORBANİ
Ömer GİRAN
Konuralp GİRGİN
Zehra Canan GİRGİN
Ilgın GÖKAŞAR
Çağlar GÖKSU
Serdar GÖKTEPE
Fazlı Erol GÜLER
Hakan GÜLER
Ilgın GÜLER
Gürkan GÜNAY
Taylan GÜNAY
Abdurrahman GÜNER
Samet GÜNER
Ülker GÜNER BACANLI
Oğuz GÜNEŞ
Mehmet Şükrü GÜNEY
Tuba GÜRBÜZ
BÜYÜKKAYIKÇI
Melike GÜREL
İbrahim GÜRER
Aslı Pelin GÜRGÜN
Gürşans GÜVEN IŞIN
Iman HAJİRASOULİHA
Soner HALDENBİLEN
Murat HAMDERİ
Ufuk HANCILAR
Ingo A. HANSEN
Mustafa HATİPOĞLU
Nejan HUVAJ SARIHAN
Metin HÜSEM
Zeynep IŞIK
Hande IŞIK ÖZTÜRK
Sabriye Banu İKİZLER
Ragıp İNCE
Eren İNCİ
Pınar İNCİ KOÇAK
Sedat KABDAŞLI
Volkan KAHYA
Mehmet Rifat KAHYAOĞLU
Volkan KALPAKÇI
Alper KANYILMAZ
Murat KARACASU
Tanay KARADEMİR
Halil KARAHAN
Ali KARAİPEKLİ
Cenk KARAKURT
Mustafa KARAŞAHİN
Zülküf KAYA
Mustafa Kubilay KELEŞOĞLU
Mustafa Erol KESKİN
Havvanur KILIÇ
İsmail Emrah KILIÇ
Sami And KILIÇ
Fahriye KILINÇKALE
Ufuk KIRBAŞ
Veysel Şadan Özgür KIRCA
Güven KIYMAZ
Young Hoon KİM
Gökhan KİRKİL
Salih KOÇAK
Niyazi Uğur KOÇKAL
Önder KOÇYİĞİT
Mehmet Melih KOŞUCU
Baha Vural KÖK
Mete KÖKEN
Fuat KÖKSAL
Şerife Yurdagül KUMCU
Murat KURUOĞLU
Akif KUTLU
Semih KÜÇÜKARSLAN
Abdullah KÜRKÇÜ
Hilmi LUŞ
Kasım MERMERTAŞ
Mehmet Murat MONKUL
Hamid MORTEZAİE
Yetiş Şazi MURAT
Sepanta NAİMİ
Öcal NECMİOĞLU
Sinan Melih NİĞDELİ
Elif OĞUZ
Didem OKTAY
Derviş Volkan OKUR
Volkan OKUR
Mehmet Hakkı OMURTAG
Engin ORAKDÖĞEN
Şeref ORUÇ
Akın ÖNALP
Halil ÖNDER
Jülide ÖNER
Bihrat ÖNÖZ
Mustafa ÖZAKÇA
Bergüzar ÖZBAHÇECİ
Ceyhun ÖZÇELİK
Gökhan ÖZDEMİR
İlker ÖZDEMİR
Osman Nuri ÖZDEMİR
Halit ÖZEN
Murat ÖZEN
Pelin ÖZENER
Cem ÖZER
Hasan ÖZER
Serkan ÖZGEN
Eren Arman ÖZGÜVEN
Hakkı Oral ÖZHAN
Yener ÖZKAN
M. Hulusi ÖZKUL
Gülen ÖZKULA
Turan ÖZTURAN
Hasan Tahsin ÖZTÜRK
Mustafa ÖZUYSAL
Polat ÖZYİĞİT
Gülizar ÖZYURT
TARAKÇIOĞLU
Onur PEKCAN
Elişan Filiz PİROĞLU
Cengiz POLAT
Selim PUL
Selçuk SAATÇİ
Selman SAĞLAM
Mehmet SALTAN
İlyas SARIBAŞ
Afşin SARITAŞ
Altuğ SAYGILI
Serdar SELAMET
Senem SEYİS
Alper SEZER
Faiz Uddin Ahmed SHAİKH
Osman SİVRİKAYA
Behzad SOLTANBEİGİ
Celal SOYARSLAN
Serdar SOYÖZ
Tayfun Altuğ SÖYLEV
Aleksandar STEVANOVİC
Erol ŞADOĞLU
Güvenç ŞAHİN
Remzi ŞAHİN
Yuşa ŞAHİN
Mustafa ŞAHMARAN
Nermin ŞARLAK
Ömer Lütfi ŞEN
Burak ŞENGÖZ
Aynur ŞENSOY ŞORMAN
Okan ŞİRİN
Ali Arda ŞORMAN
Ali Ünal ŞORMAN
Özcan TAN
Gülüm TANIRCAN
Kürşat TANRIÖVEN
Serhan TANYEL
Yüksel TAŞDEMİR
Kerem TAŞTAN
Gökmen TAYFUR
İlker TEKİN
Beytullah TEMEL
Egemen TEOMETE
Serdal TERZİ
Berrak TEYMUR
H. Onur TEZCAN
Hüseyin Onur TEZCAN
Mesut TIĞDEMİR
Şahnaz TİĞREK
Salih TİLEYLİOĞLU
Vedat TOĞAN
Onur Behzat TOKDEMİR
Cengiz TOKLU
Nuray TOKYAY
Ali TOPAL
İlker Bekir TOPÇU
Cem TOPKAYA
Selçuk TOPRAK
Kamile TOSUN FELEKOĞLU
Gökçe TÖNÜK
Nursu TUNALIOĞLU
Kağan TUNCAY
Gürsoy TURAN
Ö. Tuğrul TURAN
Cüneyt TÜZÜN
Latif Onur UĞUR
Mehmet Fevzi UĞURYOL
Berna UNUTMAZ
Volkan Emre UZ
Nihal UZCAN ERATLI
İbrahim Mert UZUN
Deniz ÜLGEN
Mehmet ÜLKER
Cüneyt VATANSEVER
Syed Tanvir WASTI
Nazmiye YAHNİOĞLU
Cem YALÇIN
Mehmet Cem YALÇIN
Aslı YALÇIN DAYIOOĞLU
Ahmet Cevdet YALÇINER
İsmail Özgür YAMAN
Arcan YANIK
Mert Yücel YARDIMCI
Ufuk YAZGAN
Anıl YAZICI
Halit YAZICI
Kasım YENİGÜN
Seda YEŞİLMEN
İrem Zeynep YILDIRIM
Mehmet YILDIRIMOĞLU
Osman YILDIZ
Çetin YILMAZ
Fatih YILMAZ
Koray Kamil YILMAZ
Mehmet YILMAZ
Murat YILMAZ
Mustafa Tuğrul YILMAZ
Veysel YILMAZ
Yüksel YILMAZ
Fatih YONAR
Recep YURTAL
İsmail YÜCEL
Ömer YÜKSEK
Ercan YÜKSEL
Yeliz YÜKSELEN AKSOY
Ahmet Şahin ZAİMOĞLU
Abdullah Can ZÜLFİKAR

UCTEA Turkish Chamber of Civil Engineers

# Teknik Dergi

Volume: 32 Issue: 6 November 2021

## CONTENTS

*Teknik Dergi, 2021 11227-11256, Paper 632*

# Evaluation of Intersection Properties Using MARS Method for Improving Urban Traffic Performance: Case Study of Tekirdağ, Turkey

**Görkem GÜLHAN**[1]
**Mustafa ÖZUYSAL**[2]
**Hüseyin CEYLAN**[3]

## ABSTRACT

Increasing urban traffic performance is a technical problem that has been investigated by many researchers these days. Traffic performance can be increased in many ways, as part of the transportation planning process, on smaller scales, or with different methods and techniques. The determination of traffic intervention areas in urban transportation planning is an intervention type that determines the rate at which the traffic performance will increase. Although transportation planning is an integrated issue, the type of traffic modification and prior intervention on intersections are often determined with partitive paradigms and strategies. It is a significant opportunity for decision makers to be informed in advance of the effects of intersection characteristics on the overall traffic performance. However, it is not an attempted or tested concept to perform a general assessment of the impact of the intersection characteristics on the overall performance of the intersections. In this study, a four-stage integrated analysis including the multivariate adaptive regression splines (MARS) method is proposed for the overall traffic performance evaluation. The traffic characteristics of intersections are first indexed and categorized. The intersection performance results are then obtained using the VISSIM traffic simulation software. Subsequently, the relationship between them is determined with the MARS method, and the effects of the intersection characteristics on the traffic performance are investigated. Tekirdağ, a metropolitan city located in northwestern Turkey, is selected for the case study. According to the obtained simulation results, the suggestions related to the development of intersection performances are made and tested.

Note:
- This paper was received on April 8, 2019 and accepted for publication by the Editorial Board on May 23, 2020.
- Discussions on this paper will be accepted by January 31, 2022.
- https://dx.doi.org/10.18400/tekderg.551032

1 Pamukkale University, Dept. of Urban and Regional Planning, Denizli, Turkey - ggulhan@pau.edu.tr https://orcid.org/0000-0003-2715-0984

2 Dokuz Eylül University, Department of Civil Engineering, İzmir, Turkey - mustafa.ozuysal@deu.edu.tr https://orcid.org/0000-0002-3276-3075

3 Pamukkale University, Department of Civil Engineering, Denizli, Turkey - hceylan@pau.edu.tr https://orcid.org/0000-0002-8840-4936

**Keywords:** Traffic performance, VISSIM, intersection, Multivariate Adaptive Regression Splines.

## 1. INTRODUCTION

In the last decades, the spread of land use and motorized travel demand in urban areas have increased based on the growing urbanization. On the other hand, people are spending more time in traffic owing to the increasing travel distances and durations even on normal (steady state) traffic conditions. Considering the typical incidents (i.e., accidents, car breakdowns, lane blockages from construction activities, bad weather conditions), traffic flow is interrupted and unpredictable delays occur [1]. In this context, many researchers have handled delay and travel time minimization problems on the network and arterial levels. Most typical studies on the network level focus on the transportation network design problem, in which some traffic control strategies are introduced to calculate the intersection signal timings more accurately, or topologies of the network elements (i.e., parking places, road closure schemes, lane addition, lane allocation) are redesigned [2-8]. On the other hand, the performance analyses of urban arterials are primarily evaluated in terms of the average travel time, which is a function of signal timing parameters of adjacent intersections and traffic flow patterns under different levels of congestion [9-10]. Therefore, several studies focus on signal timing and offset optimization on urban arterials [11-15]. When viewed from this aspect, intersections appear to be the key point to provide shorter travel times and decrease the level of congestion on the roads. Because the intersections are the most critical components of the road transportation systems, they must be designed and operated based on the advanced methodologies to determine the most appropriate solution. Thus, the project level requirements can be satisfied by addressing the site constraints [16]. In the relevant literature, congestion management strategies have widely been investigated based on the geometric designs or operational improvements of signalized intersections (i.e., cycle time determination, green split calculations, phase planning).

Intersection geometry and physical element improvements may be interpreted as the most recognized intersection intervention types. The total delay time, queue length, capacity, and safety performance of an intersection is directly related to the geometric design itself. Otković and Dadić [17] compared the delays at a roundabout and a conventional signal-controlled intersection in Osijek city. They found that the delay times could be decreased significantly at roundabouts in comparison with the signalized intersections. Furthermore, a number of studies outlined that the roundabouts provided safer driving environments by decreasing all crashes from 21% to 61% [18-20]. While the increasing trend on replacing conventional signalized intersections with roundabouts has continued, designing unconventional intersections has also been emphasized by researchers [21-30]. As reported in the previous research, geometrically different designed intersections provide different levels of operational and safety performance. Apart from the geometric adjustments on isolated intersections via converting them into roundabouts or unconventional types, signal timing improvements has widely been studied in the past. Lan [31] proposed a new cycle time calculation approach based on nonlinear regression analysis to reveal the relationship between cycle time and traffic flow pattern based on the total lost time, critical flow ratio, and duration of analysis period. Results of the study showed that the generated optimal cycle length is only 5.7% deviated from the analytical solution. Talmor and Mahalel [32] proposed

a signal timing design method for an isolated intersection under severe congestion conditions. They showed that designing the signal timing parameters by considering the throughput function, instead of the saturation flow function, might increase the discharge capacity of a signalized intersection. Yu et al. [33] presented a multi-objective optimization problem including capacity, delay time, number of stops, and emissions with their related weights determined by the fuzzy compromise programming approach. In their study, the objective function value is minimized using genetic algorithm, and the results showed that the capacity of the intersection could be improved by reducing the vehicle delays and number of stops. As shown above, several studies concerning intersection performance improvements have focused on either the intersection geometry or signal timing calculations based on prior decisions. In other words, the planner has already decided to convert a signalized intersection into a roundabout or an unconventional intersection; subsequently, the research is built on this prior decision. Likewise, the planner may have decided to increase the performance of a signalized intersection by only changing the stage plan, cycle time, and green times. In either case, it is assumed that the planner can provide the right decision. However, considering a significant variety of factors affecting the performance of an intersection, developing an integrated approach would be useful for policy makers and planners because prejudiced decisions may lead to time loss or missing a better solution alternative. This approach may be developed using regression models by identifying the intersection performance as the dependent variable within different perspectives (i.e., average speed, travel time, delay time, and number of stops). Meanwhile, several factors affecting the intersection performance may be treated as the independent variables. Therefore, the most important determinants of the intersection performance would be identified and policy makers can be supported for the efficient use of resources.

This study employs a novel estimation technique, the multivariate adaptive regression spline (MARS) model that has been widely applied in many scientific fields. MARS is a method providing flexibility to consider nonlinear effects of explanatory variables using the partial adaptation of spline functions [34]. Additionally, MARS can provide threshold values of explanatory variables where the effects on dependent variables considerably change [35]. As the intersection performance depends on miscellaneous factors such as traffic characteristics (volume, composition, moving directions, etc.), control type (signalization, give way, etc.), geometry (lane number and width, dimensions, medians, etc.) and immediate surroundings (close intersections, bus stops, etc.), linear approaches cannot adequately predict the intersection performance. Additionally, parametric predictions including threshold values of independent variables that should not be exceeded in intersection design (maximum cycle time, maximum roundabout diameter, etc.) are essential to obtain the basic principles for practitioners. Thus, more accurate and substantive results may be obtained in performance prediction using the MARS approach. As mentioned before, studies on intersection performance improvements are based on the assumption that intersection control type and geometric structure are predetermined. However, improving a particular intersection depending on the parameters initially adopted may prevent the planner from making a much more efficient planning. By using the proposed approach in this study, it may be possible to simultaneously evaluate a great variety of data reflecting geometric characteristics, control type and traffic flow patterns in terms of the performance of a given intersection. Once the model results are justified on a valid sample size, intersection performance estimation can be obtained without using expensive and time-consuming micro simulation models. Therefore,

it is expected to bring a new perspective, which may be identified as a holistic point of view, to the investigation of intersection performance analysis.

In this context, a four-step integrated approach is developed to determine several independent variables' (i.e., intersection control type, intersection geometry type, number of legs, number of enter/exit lanes, signal timings, traffic flow characteristics, number and distance of bus stops around, intersection size) impact on eight intersection performance indicators by employing the MARS model. The values of the performance indicators are obtained using microsimulations by the VISSIM software. Based on the modelling results, the most efficient relationships between the intersection properties and performance indicators are determined, and explanatory information on how to achieve targeted improvements in the intersection performance is provided for policy makers and planners. At the final step of the proposed approach, a demonstration is provided to show that the MARS model predictions may effectively be used to examine and improve the performance of an existing intersection.

The remainder of the paper is organized as follows: The next section presents the method and study area. The analyses are provided in section 3 including the indexing of intersections, the MARS model results, and the selection and testing of intersection design parameters. Finally, section 4 presents the conclusions and some suggestions for future directions.

## 2. METHOD & STUDY AREA

### 2.1. Method

The aim of this study is to offer an effective traffic improvement planning by considering the intersection characteristics and performance on decision levels. Hence, a stepwise paradigm has been offered and each level has been defined, as shown in Fig. 1.

**Step 1;** starts with the description and indexing of intersection features. Intersections have many characteristics, and the determination of those characteristics to use them for generating intersection modification strategies is substantial. Those characteristics may be the leg green times according to their directions, saturated leg flows, traffic volumes and ratios according to their types and directions, saturation rate, square diameters, square lane numbers, average approach square existence, existence of roundabouts, average number of lane widths, existence of bus stop and their distances to the intersections, number of lanes, existence of intermediate refuge, turn pads, existence of intersections nearby, dimensions of intersection, number of legs, phase numbers, signal cycle times, and signaling status. These can be grouped into four primary parts: traffic-, geometric-, and control-related features and immediate surroundings. The derived intersection characteristics for the study are shown in Tables 1a and 1b. While the characteristics, especially the control-related ones are specific, most of the traffic-related and geometric parameters are generic except the roundabout diameter, saturation flow, etc. Traffic-related parameters are generally derived according to the volume moves for different directions (through passing, right turn, left turn) and their average percentages. Passenger car equivalent (PCE) volumes are obtained using the coefficients suggested in the Highway Capacity Manual (HCM) 2010 [36]. The geometric layout of intersections is also considered in detail with the lane width and number, existence of turning bays and medians, distances between stop lines, etc. Control-related characteristics are generally based on signalization such as average green time and their percentages for

each movement, number of phases, etc. The critical components in the immediate surrounding of each intersection are also described. In particular, the existence, number and distance of close intersections, and bus stops are indexed. As stated in HCM 2010, transit buses that stop for picking up or discharging passengers within 75 m of the stop line, block the traffic flow. Thus, the number and distance of upstream and downstream bus stops within 75 m of the stop line are indexed. Furthermore, the number of upstream and downstream intersections within 400 m of the stop line is considered during the modeling process by considering a 50 km/h progressive speed for urban areas, where the traffic volumes are spread over several streets [37]. The mentioned parameters may be correlated with the intersection performance results and thus the relation between performance and characteristics may be established. Hence, policy makers may use those results for decision making and scenario generation processes of transportation planning at low levels.

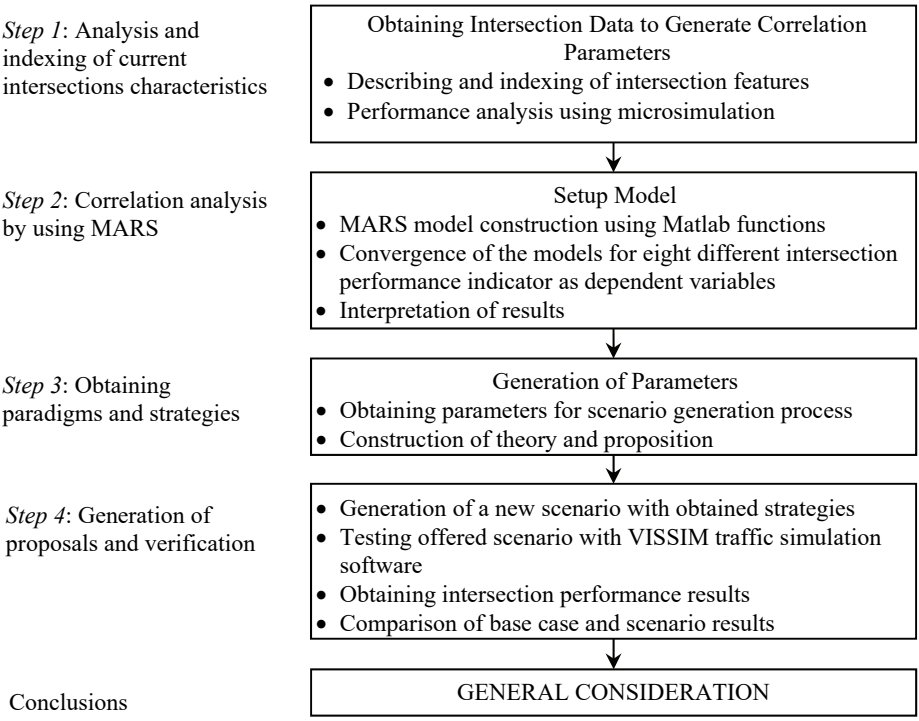


*Fig. 1 - Flowchart of the traffic improvement stepwise paradigm*

At the second stage of Step 1 in the stepwise paradigm, intersection performances are obtained using microsimulations. The VISSIM traffic simulation software is preferred for the study. It is utilized for visual analysis, and to measure the overall intersection performance. VISSIM was originally developed at the University of Karlsruhe, Germany. VISSIM may be used to analyze traffic and transit operations, traffic composition, bus stops, traffic signals,

and evaluating different alternatives under various scenarios. It is a time-step, micro and behavior-based simulation model, which is developed to model traffic operations and analyze traffic performance. The simulation necessitates the input parameters like the geometry of traffic lanes, vehicle composition, speed, traffic volumes and movements at each intersection leg, vehicle routes in the intersection and conflict areas. The measurement parameters are the average delay time per vehicle (s), average speed (km/h), average number of stops per vehicles, average stopped delay per vehicle (s), total delay time (h), number of stops, total stopped delay (h), and total travel time (h). The mentioned software is a microscopic multimodal traffic flow simulation software package developed by PTV Planung Transport Verkehr AG in Karlsruhe [38].

**Step 2;** consists of a correlation analysis using the MARS approach. MARS is a multivariate nonparametric and nonlinear regression method, introduced by Friedman [39, 40]. The model consists of spline basis functions, where the basis functions and the parameters associated with each one (product degree and knot locations) are automatically determined by the data. This procedure is motivated by the recursive partitioning approach to regression and shares its attractive properties. It has more power and flexibility to model relationships that are nearly additive or involve interactions. Additionally, the model can be represented in a form that separately identifies the additive contributions and those associated with different multivariable interactions [39].

Because of the promising prediction power and interpretation simplicity of the MARS method, it is preferred in novel models, specifically where the nonlinearity between predictors and response are under question. Unlike other prediction models, a prior assumption for the relationship between dependent and independent variables is not required. Additionally, MARS is not a black-box model as much as the other nonlinear prediction techniques, e.g., artificial neural networks, fuzzy-logic, etc. because it provides an interpretable equation that includes coefficients according to the intervals produced by the model structure [35].

In recent years, transportation investigations use the MARS method in many studies such as accident analysis [41-43] and air passenger demand forecasting [34]. Although the application of MARS is limited in traffic engineering, the capability and interpretability of this approach is clearly introduced especially in traffic flow prediction [44, 45]. In these studies, short-term traffic flow prediction on interstate freeway segments is performed by considering spatio-temporal effects in the MARS method, and its superior prediction accuracy is revealed by comparing with many other advanced modeling techniques such as the parametric model autoregressive integrated moving averaging (ARIMA) and the kernel method support vector regression. This encourages the use of MARS in intersection-related analyses where multiple varieties of short run affects are under question.

In the MARS method, the relation between dependent and independent variables is described in intervals by piecewise regression functions. The term “piecewise” means that MARS divides the space of predictors into multiple knots and subsequently fits a spline function between them [42]. The general MARS function can be expressed using the following equation (1):

*Table 1a - List of explanatory (1-55) variables examined in MARS models.*

| No | Variable Name | Short Name | Description |
|---|---|---|---|
| **1** | Intersection control type | Cont | 1: signalized, 0: unsignalized |
| **2** | Intersection geometry type | Geo | 1: roundabout, 0: others |
| **3** | Cycle time* | Cyc | If the intersection is signalized (sec) |
| **4** | Number of phases* | No.phases | If the intersection is signalized |
| **5** | Number of legs | No.legs | |
| **6** | Number of entering flows | No.enter | |
| **7** | Intersection dimension in East-West direction | Dim_EW | Distance between E-W bound stop lines (m) |
| **8** | Intersection dimension in North-South direction | Dim_NS | Distance between N-S bound stop lines (m) |
| **9** | Existance of close intersection | Ex_close | yes:1, no:0 (closer than 400 m) |
| **10** | Number of close intersections | No.close | If Ex_close is 1 |
| **11** | Number of left-turn moves with turning bay | No.LT_bay | |
| **12** | Number of left-turn moves without turning bay | No.LT_nobay | |
| **13** | Number of enters in which left-turns do not exist | No.noLT | |
| **14** | Number of right-turn moves with turning bay | No.RT_bay | |
| **15** | Number of right-turn moves without turning bay | No.RT_nobay | |
| **16** | Number of enters in which right-turns do not exist | No.noRT | |
| **17** | Number of legs with median (central refuge) | No.Med | |
| **18** | Number of legs without median (central refuge) | No.noMed | |
| **19** | Total number of enter lanes | No.EntLanes | |
| **20** | Total number of exit lanes | No.ExtLanes | |
| **21** | Average number of lanes per leg | Lane/Leg | |
| **22** | Difference between the numbers of enter and exit lanes | Ent-Ext_lanes | No of enter lanes minus no of exit lanes |
| **23** | Existance of close bus stops at enter flows | BusStop_Ent | 1:yes, 0: no (closer than 75 m) (HCM 2010) |
| **24** | Average distance of close bus stops at enter flows | Dist_BS_Ent | If BusStop is 1 |
| **25** | Number of close bus stops at left turns of exit flows | No.BS_Ext_LT | |
| **26** | Number of close bus stops at through passing exit flows | No.BS_Ext_Str | |
| **27** | Number of close bus stops at right turns of exit flows | No.BS_Ext_RT | |
| **28** | Average distance of close bus stops at left turns of exit flows | Dist_BS_Ext_LT | If No.BS_Ext_LT is at least 1 |
| **29** | Average distance of close bus stops at through passing exit flows | Dist_BS_Ext_Str | No.BS_Ext_Str is at least 1 |
| **30** | Average distance of close bus stops at right turns of exit flows | Dist_BS_Ext_RT | No.BS_Ext_RT is at least 1 |
| **31** | Average lane width | LaneWidth | (m) |
| **32** | Roundabout diameter | RA_dia | If the intersection is roundabout (m) |
| **33** | Cycling lane number | RA_no.lane | If the intersection is roundabout |
| **34** | Average width of approach median | RA_appr | If the intersection is roundabout (m) |
| **35** | Average green time for through passing flow* | GT_Thr | (sec) |
| **36** | Average green time for right turn flow* | GT_RT | (sec) |
| **37** | Average green time for left turn flow* | GT_LT | (sec) |
| **38** | Average green to cycle ratio for through passing flow* | G/C_Thr | |
| **39** | Average green to cycle ratio for right turn flow* | G/C_RT | |
| **40** | Average green to cycle ratio for left turn flow* | G/C_LT | |
| **41** | Average saturated flow of enter legs* | Sat.Flow | (veh./hour) |
| **42** | Entering passenger car volume | Vpc | (veh./hour) |
| **43** | Entering heavy vehicle volume | Vhv | (veh./hour) |
| **44** | Entering total volume | Vtot | (veh./hour) |
| **45** | Heavy vehicle ratio | HVR | |
| **46** | Entering passenger car volume per lane | VperLpc | |
| **47** | Entering heavy vehicle volume per lane | VperLhv | |
| **48** | Entering total volume per lane | VperLtot | |
| **49** | Average of leg based heavy vehicle ratio | HVRleg | |
| **50** | Average of leg based saturation ratios | SatRat | |
| **51** | Through passing passenger car volume | Vpc_Thr | (veh./hour) |
| **52** | Through passing heavy vehicle volume | Vhv_Thr | (veh./hour) |
| **53** | Through passing passenger car equivalent (PCE) volume | Vpce_Thr | (pce/hour) |
| **54** | Number of through passing flows | No.Thr | |
| **55** | Ratio of through passing flow number to enter flow number | no.Rat_Thr | |

** For signalized intersections*

*Table 1b - List of explanatory (56-75) and dependent (P1-P8) variables examined in MARS models.*

| No | Variable Name | Short Name | Description |
|---|---|---|---|
| **56** | Average ratio of through passing over entering flow | AvRat_Thr | |
| **57** | Leg based average ratio of through passing over entering flow | AvRat_Leg_Thr | |
| **58** | Right turn passenger car volume | Vpc_RT | (veh./hour) |
| **59** | Right turn heavy vehicle volume | Vhv_RT | (veh./hour) |
| **60** | Right turn PCE volume | Vpce_RT | (pce/hour) |
| **61** | Number of right turn flows | No.RT | |
| **62** | Ratio of right turn flow number to enter flow number | no.Rat_RT | |
| **63** | Average ratio of right turn over entering flow | AvRat_RT | |
| **64** | Leg based average ratio of right turn over entering flow | AvRat_Leg_RT | |
| **65** | Left turn passenger car volume | Vpc_LT | (veh./hour) |
| **66** | Left turn heavy vehicle volume | Vhv_LT | (veh./hour) |
| **67** | Left turn PCE volume | Vpce_LT | (pce/hour) |
| **68** | Number of left turn flows | No.LT | |
| **69** | Ratio of left turn flow number to enter flow number | no.Rat_LT | |
| **70** | Average ratio of left turn over entering flow | AvRat_LT | |
| **71** | Leg based average ratio of left turn over entering flow | AvRat_Leg_LT | |
| **72** | Entering PCE volume | Vpce | (pce/hour) |
| **73** | Average green time per entering vehicle for through passing flow* | GTr_Thr | (sec/(pce/hour)) |
| **74** | Average green time per entering vehicle for right turn flow* | GTr_RT | (sec/(pce/hour)) |
| **75** | Average green time per entering vehicle for left turn flow* | GTr_LT | (sec/(pce/hour)) |
| **P1** | Average delay time per vehicle | P1.DelpVeh | (sec) |
| **P2** | Average speed | P2.AvSpeed | (km/h) |
| **P3** | Total delay time | P3.TotDelay | (hour) |
| **P4** | Total distance traveled | P4.TotDist | (km) |
| **P5** | Number of stops | P5.No.Stops | |
| **P6** | Number of vehicles that have left the network | P6.No.VehLeft | |
| **P7** | Total travel time | P7.Tot_TrlTime | (hour) |
| **P8** | Average travel time per vehicle | P8.Ave_TrlTime | (hour/veh.) |

** For signalized intersections*

$$y = b_o + \sum_{m=1}^{M} b_m B_m(x) \tag{1}$$

where $y$ is the dependent variable; $x$ is the explanatory variable; $b_o$ and $b_m$ are the estimated coefficients to yield the best fit of data; $M$ is the number of basis functions included into the model. $B_m(x)$ is the $m^{th}$ basis function, which can be either a single function or the product of two or more functions for different explanatory variables [34, 46]. The piecewise-linear form of the basis function is shown below:

$$B_m(x) = \prod_{k=1}^{k_m} \left[ S_{km} \left( X_{v(k,m)} - t_{k,m} \right) \right] \tag{2}$$

In the equation, $km$ is the number of knots, $S_{km}$ can be either 1 or -1 to indicate the right/left regions of the associated step function, $v(k,m)$ is the label of the explanatory variable, and $t_{k,m}$ is the knot location [34]. A cubic version of this piecewise-linear form also exists for the basis functions, in which a power function is applied for each multiplication segment. However, the piecewise-linear form is preferred in this study to provide simple interpretability.

In the modeling process, two primary steps are applied. The first step is the "construction where basis functions are added to the model using a forward stepwise procedure." The predictors and their knot locations (thresholds) that contribute to the model are defined. In the second step, or the "pruning phase," the basis functions with the least contribution are eliminated using backward deletion. To avoid overfitting, a generalized cross-validation statistic is typically used, where a penalty for model complexity is accounted for [42]. The Generalized Cross-Validation (GCV) criterion is estimated using the following equation:

$$GCV(M) = \frac{1}{N} \frac{\sum_{i=1}^{N} (y_i - \hat{y})^2}{(1 - C\left(\tilde{M}\right)/N)^2} \tag{3}$$

where $N$ is the number of observations; $y_i$ is the response for observation $i$; $\hat{y}$ is the predicted response for observation $i$; $C(\tilde{M})$ is the complexity penalty factor.

**Step 3;** obtains the process for paradigms and strategies. It consists of the generation of design parameters. In this section, the relationship between intersection characteristics and intersection performance results is determined. To obtain the most effective intersection properties that should be considered as the top priority, explanatory variables are analyzed in terms of occurrence frequency and relative importance in the MARS predictions of intersection performance indicators.

Because of the mentioned relationship, the intersection characteristics to be evaluated during the scenario production phase and the intersection characteristics that are meaningful in the model are determined. Hence, the theory of the proposition to be developed has been determined. The most related variables in terms of performance indicators have been chosen to be utilized in the determination process.

**Step 4;** consists of the generation of design proposals and design verification. At this stage, the design parameters obtained are evaluated and the intervening intersections and method of intervention are determined. The strategies for the selected intersection are determined and a scenario is generated using the determined parameters. The intersection design is generated towards the scenario, and the mentioned intersection design is simulated with the equal traffic demand. Subsequently, the intersection performance indicators are obtained for the designed case, and the intersection design parameters are determined by comparing with the base case intersection performance indicators.

### 2.2. Study Area

Tekirdağ is a metropolitan seaport that attracts attention oflarge organized industrial zones. The city has significant tourism investments and several advantages due to its location. Tekirdağ is near Istanbul and it is one of the most notable cities in the Marmara region [47]. Tekirdağ has 11 counties, and the most important ones are Süleymanpaşa, Çorlu, and Çerkezköy in terms of economy andpopulation. Çorlu and Çerkezköy lead the industrial sector, while Süleymanpaşa leads the service sector.

The macroform of Süleymanpaşa is adjacent to the seaside. It has a linear urban development between the East–West axis. A belt highway in the north of the city is located as an artificial threshold. The population of the county is 176,848. Çorlu is the largest county of Tekirdağ, and it is 38 km away from the city center. It is one of Turkey's largest counties. Rapid urbanization, intense industrialization, and outside-in migration are the significant problems of the county. The population of the county is 273,362, and it is at the intersection point of large-scaled transportation corridors. Çerkezköy has an increasing population, and it has the highest population density. Many access opportunities to the city exist in terms of transportation modes. The county containing industrial zones has a population of 146,319. Malkara is another significant settlement and it has four intersections with traffic surveys. Locations of four counties are given in Fig. 2.

Traffic surveys and counts are conducted by drones and subsequently counted in the office environment. Counts are conducted for evening and morning peak hours. However, in the study only the morning peak hour count results are evaluated. Traffic counts were performed when the schools were open, and the actual traffic pattern was observed. Counts are conducted in categories such as cars, minibuses, trucks, and buses. The speed and behavior patterns are also observed. The traffic characteristics of the settlements in Tekirdağ are similar to each other. In fact, they are similar to the traffic characteristics of the other medium-sized cities of Turkey. Heavy vehicle traffic and urban public transport traffic constitute only a fraction of the overall traffic. Private car use is relatively high in the overall traffic. Traffic congestion is observed at peak hours in specific central regions. The transportation infrastructure shows that the city is located at the seashore, and some traffic axes are not accessible.

## 3. ANALYSIS

### 3.1. Indexing of intersection properties

Traffic surveys and simulations are conducted for 64 intersections. The simulations have been conducted using the VISSIM traffic software. In the calibration section, the vehicle speed and behavior pattern are iteratively updated until the number of vehicles passing through the intersection arms are equalized to the traffic counts. The obtained performance results are generated by a network performance analysis and supported by visual captures. Performance indicators are calculated for the base case. More than 75% of these intersections are located in four sites (Çerkezköy, Çorlu, Malkara, and Süleymanpaşa). Others are scattered in different districts and on intercity roads, including roundabouts, and intersections with signalized and unsignalized intersections. Fig. 3 shows the locations of the intersections in Çerkezköy, Çorlu, Malkara, and Süleymanpaşa.

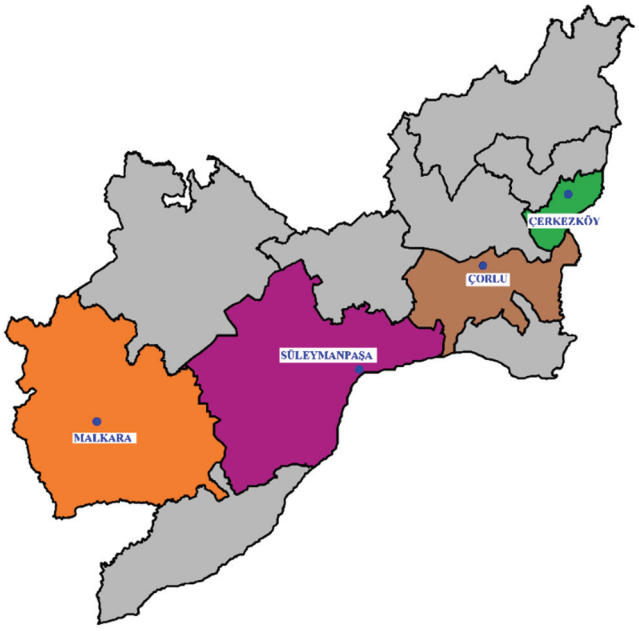


*Fig. 2 - Locations of Çerkezköy, Çorlu, Malkara, and Süleymanpaşa*


*Fig. 3 - Locations of intersections in Çerkezköy, Çorlu, Malkara, and Süleymanpaşa*

In this study, we performed a calibration process based on field volumes and number of vehicles that have left the network through 64 intersections. Comparison of field and

simulation volumes are given in Fig. 4. As can be seen in the figure, R-squared value is about 0.89 which represents smaller differences between the field data and the fitted values.

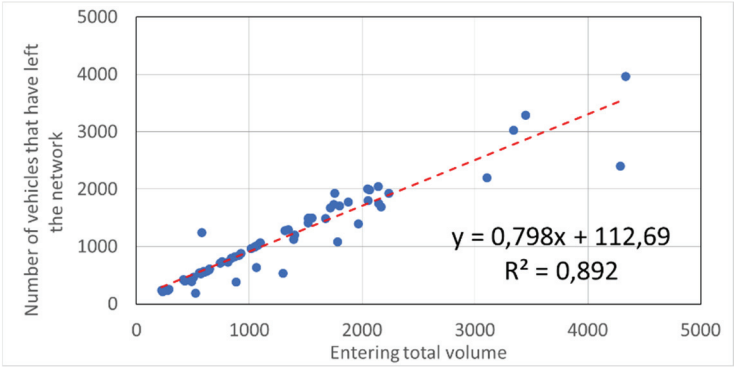


*Fig. 4 - Comparison of field and simulation volumes*

### 3.2. MARS model results

The derived intersection characteristics based on geometry, control, and traffic, are examined to estimate eight different intersection performance indicators using the MARS method. In MARS modeling, the functions developed by Jekabsons [48] based on Friedman's method [39, 40] in Matlab programming language are utilized with some modifications according to the scope of the study.

As the first step, data standardization process is added to generated codes. Before performing a MARS model, it is recommended to pre-scale the explanatory and dependent variables to the 0–1 interval [39]. Hence, the transformation equation used is shown below:

$$X_i^s = (X_i^o - X_{\min}^o)/(X_{\max}^o - X_{\min}^o) \quad (4)$$

where $X_i^s$ is the standardized value of the $i^{\text{th}}$ observation of the explanatory variable, $X_i^o$ is the observed value, and $X_{min}^o$ and $X_{max}^o$ are the minimum and maximum values of the related observations, respectively.

For the second step of the code modification, basic functions of Jekabsons [48] are combined to construct, converge and evaluate MARS models. The three main steps used in the modeling process are creating structure of model configuration parameters, building MARS model with dependent and independent variables, performing ANOVA decomposition and variable importance assessment. Also a conditional loop is constructed for repeating the process until obtaining a model with significant dependent variables by comparing relative importance values. The relative importance of a variable is defined as the square root of the GCV of the model with all basis functions involving that variable removed, minus the square root of the GCV score of the corresponding full model, scaled such that the relative importance of the most important variable has a value of 100 [35, 40].

In the initial modeling stage, the maximum number of basis functions is limited to 20 in the piecewise linear form, and all of the 75 explanatory variables (intersection characteristics) are included. After the first convergence of the MARS model, the explanatory variables with relative importance smaller than 5% are eliminated, and the model is converged again. This process is repeated until all of the remaining explanatory variables have a relative importance of over 5%.

For clarifying the estimation capability of the models, in addition to the MARS model specific indicators (GCV, $R^2_{GCV}$), the calculation of some well-accepted statistics that are based on the prediction residuals and widely used for comparing the performance in nonlinear predictions are attached to Jekabsons' functions [48]: root mean square error (RMSE), efficiency factor (EF), post regression statistics for observed and predicted values (slope (m), intercept (b), and coefficient of correlation (r)), and discrepancy ratio percentages (DRP) [49]. DR percentages are provided for both the 10% and 25% discrepancies (see Table 2). Besides, the predictive power of the models are examined by using training and testing stages. For this purpose, randomly selected 42 of 64 intersection data are implemented for training and the generated models are tested by using the remaining 22 intersection data.

As shown in Table 2, all the intersection performance indicators have been considerably predicted by the explanatory variables. All of the models exhibit $R^2_{GCV}$ values over 0.80, and efficiency factors over 0.85. Generally, the MARS model appears to be useful in the estimation of any intersection performance according to the all data-based trainings. The most distinctive differences between the prediction capabilities are obtained by comparing the post regression and discrepancy statistics. When the discrepancy is considered as 25% for all data models, the average speed is shown to be estimated properly for all of the observations. The number of vehicles that have left the network, average travel time per vehicle, total distance travelled, and total travel time also indicate high proper estimation percentages, while the others present considerable percentages for high predictions. When the post regression statistics are compared, the prominent performances can be found as the average speed, total delay time, number of stops, and total travel time, in which the coefficient of correlation (r) is approximately 0.98.

Although convergence performances are increased with randomly divided data, prediction performances with testing set are generally decreased (compared with all data) as expected. According to F-test probability values which should be smaller than 0.05 for a significant performance, average speed (P2), total delay time (P3), number of stops (P5) number of vehicles that have left the network (P6) and average travel time per vehicle (P8) models have high predictive power with testing data. These models still have coefficient of determination (R-squared) and efficiency factors over 0.65. Consequently, it can be said that MARS modeling approach shows prominent estimation capability for these five performance indicators.

According to $R^2_{GCV}$ statistics which is the main indicator of MARS modeling, the performance indicators average speed (P2), number of stops (P5) and total travel time (P7) are found to be the most predictable indicators. Since total travel time is strongly related with the number of vehicles using the intersections, it is preferred to focus on average travel time per vehicle (P8). Consequently, for the brevity of the study, three of the indicators were selected for the comprehensive analysis: average speed (P2), number of stops (P5), and average travel time per vehicle (P8).

*Table 2 - General prediction performances of MARS models for eight different intersection performance indicators*

| Intersection Performance Indicator | | No: | | P1 | P2 | P3 | P4 | P5 | P6 | P7 | P8 |
|---|---|---|---|---|---|---|---|---|---|---|---|
| | | Descpriction: | | Average delay time per vehicle | Average speed | Total delay time | Total distance traveled | Number of stops | Number of vehicles that have left the network | Total travel time | Average travel time per vehicle |
| | | Short name: | | DelpVeh | AvSpeed | TotDelay | TotDist | No.Stops | No.VehLeft | Tot_TrlTime | Ave_TrlTime |
| MARS model convergence | *all data (64 intersections)* | GCV | : | 0.01001 | 0.00819 | 0.00586 | 0.00819 | 0.00693 | 0.00346 | 0.00326 | 0.00780 |
| | | $R^2_{GCV}$ | : | 0.880 | 0.924 | 0.914 | 0.789 | 0.924 | 0.919 | 0.935 | 0.819 |
| | *training data (42 intersections)* | GCV | | 0.00349 | 0.00665 | 0.00556 | 0.00600 | 0.00491 | 0.00178 | 0.00176 | 0.00667 |
| | | $R^2_{GCV}$ | | 0.949 | 0.930 | 0.904 | 0.860 | 0.938 | 0.960 | 0.961 | 0.828 |
| | Number of basis functions | | : | 11 | 9 | 11 | 8 | 11 | 4 | 10 | 10 |
| General prediction performances | *all data (64 intersections)* | R | : | 0.972 | 0.979 | 0.980 | 0.934 | 0.982 | 0.966 | 0.983 | 0.953 |
| | | R-squared | : | 0.944 | 0.958 | 0.960 | 0.872 | 0.964 | 0.934 | 0.967 | 0.908 |
| | | F | : | 89.467 | 155.436 | 126.632 | 54.610 | 143.531 | 281.214 | 173.723 | 59.032 |
| | | Pf | : | 0 | 0 | 0 | 0 | 0 | 0 | 0 | 0 |
| | | RMSE | : | 0.067 | 0.066 | 0.051 | 0.069 | 0.056 | 0.052 | 0.040 | 0.062 |
| | | EF | : | 0.944 | 0.958 | 0.960 | 0.872 | 0.964 | 0.934 | 0.967 | 0.908 |
| | *testing data (22 intersections)* | R | : | 0.702 | 0.865 | 0.803 | 0.581 | 0.894 | 0.830 | 0.703 | 0.834 |
| | | R-squared | : | 0.493 | 0.747 | 0.645 | 0.337 | 0.800 | 0.688 | 0.494 | 0.695 |
| | | F | : | 1.582 | 9.467 | 5.807 | 3.053 | 6.498 | 5.525 | 1.074 | 13.673 |
| | | Pf | : | 0.22188 | 0.00024 | 0.00304 | 0.05507 | 0.00164 | 0.00338 | 0.45126 | 0.00007 |
| | | RMSE | : | 0.230 | 0.176 | 0.170 | 0.144 | 0.144 | 0.110 | 0.168 | 0.140 |
| | | EF | : | 0.493 | 0.747 | 0.645 | 0.337 | 0.800 | 0.688 | 0.494 | 0.695 |
| Post regression statistics | *all data (64 intersections)* | m | : | 0.944 | 0.958 | 0.960 | 0.872 | 0.964 | 0.934 | 0.967 | 0.908 |
| | | b | : | 0.013 | 0.024 | 0.007 | 0.025 | 0.008 | 0.017 | 0.006 | 0.027 |
| | | r | : | 0.972 | 0.979 | 0.980 | 0.934 | 0.982 | 0.966 | 0.983 | 0.953 |
| | *testing data (22 intersections)* | m | : | 0.579 | 0.780 | 1.046 | 1.099 | 0.995 | 1.277 | 1.212 | 0.515 |
| | | b | : | 0.038 | 0.176 | -0.004 | 0.014 | 0.007 | -0.042 | -0.003 | 0.105 |
| | | r | : | 0.754 | 0.885 | 0.870 | 0.814 | 0.912 | 0.943 | 0.881 | 0.930 |
| Discrepancy ratio percentages (10% discrepancy) | *all data (64 intersections)* | $DRP_{low}$ | : | 14.06 | 3.13 | 15.63 | 21.88 | 14.06 | 1.56 | 25.00 | 14.06 |
| | | $DRP_{proper}$ | : | 37.50 | 87.50 | 37.50 | 42.19 | 35.94 | 89.06 | 45.31 | 70.31 |
| | | $DRP_{high}$ | : | 48.44 | 9.38 | 46.88 | 35.94 | 50.00 | 9.38 | 29.69 | 15.63 |
| | *testing data (22 intersections)* | $DRP_{low}$ | : | 72.73 | 13.64 | 22.73 | 36.36 | 9.09 | 22.73 | 45.45 | 27.27 |
| | | $DRP_{proper}$ | : | 9.09 | 50.00 | 13.64 | 9.09 | 27.27 | 50.00 | 9.09 | 45.45 |
| | | $DRP_{high}$ | : | 18.18 | 36.36 | 63.64 | 54.55 | 63.64 | 27.27 | 45.45 | 27.27 |
| Discrepancy ratio percentages (25% discrepancy) | *all data (64 intersections)* | $DRP_{low}$ | : | 9.38 | 0.00 | 10.94 | 4.69 | 4.69 | 1.56 | 14.06 | 4.69 |
| | | $DRP_{proper}$ | : | 51.56 | 100.00 | 48.44 | 87.50 | 56.25 | 93.75 | 76.56 | 92.19 |
| | | $DRP_{high}$ | : | 39.06 | 0.00 | 40.63 | 7.81 | 39.06 | 4.69 | 9.38 | 3.13 |
| | *testing data (22 intersections)* | $DRP_{low}$ | : | 59.09 | 0.00 | 4.55 | 13.64 | 4.55 | 0.00 | 22.73 | 4.55 |
| | | $DRP_{proper}$ | : | 31.82 | 86.36 | 59.09 | 59.09 | 45.45 | 100.00 | 50.00 | 90.91 |
| | | $DRP_{high}$ | : | 9.09 | 13.64 | 36.36 | 27.27 | 50.00 | 0.00 | 27.27 | 4.55 |

### *3.2.1. Average Speed (P2)*

A high average speed at an intersection can indicate that queuing and delays are at the minimum, and traffic flows without any considerable interruptions. In the MARS models, the average speed provides a successive estimation of the intersection performance. The model converges with 0.00819 GCV value, and nine basis functions (including intercept). Equation 5 shows the final form of the MARS estimation function. The standardized forms of the basis functions are also shown in Table 3. As shown in the equation, the number of phases (No.phases), cycle time (Cyc), entering heavy vehicle volume (Vhv), and entering total volume per lane (VperLtot) are the effective variables in the prediction. According to Eq. 5, No.phases in the MARS prediction indicates that if the number of phases is under four, it increases the average speed by 1.32 km/h for every decreasing number. The critical threshold for Vhv is found to be 714.6 and this variable has two different basis functions. Each additional heavy vehicle over this threshold decreases its average speed by 0.579 km/h, and each vehicle decreasing under this rate also increases by 0.479 km/h. This means that the number of heavy vehicles influences significantly on the average speed. Cycle time values of under 88.956 s present an adverse effect with a -0.775 coefficient. The VperLtot variable has a more complicated effect on the average speed than the other explanatory variables, because of four different basis functions and several threshold values. It can be inferred that a VperLtot of over 151.715 negatively affects the average speed, while it can increase it for values under 138.275 veh/h/lane. A sensitivity analysis, which will be discussed in the next paragraphs, can be more expressive for this type of variables.

$$\begin{aligned} &\text{P2.AvSpeed} = 31.556 + 1.32*\max(0, 4 - \text{No.phases}) - 0.579*\max(0, \text{Vhv} - 714.6) \\ &+ 0.479*\max(0, 714.6 - \text{Vhv}) - 2.09*\max(0, 310.615 - \text{VperLtot}) \\ &- 0.775*\max(0, 88.956 - \text{Cyc}) + 2.23*\max(0, \text{VperLtot} - 238.675) \\ &- 2.98*\max(0, \text{VperLtot} - 151.715) + 1.99*\max(0, 138.275 - \text{VperLtot}) \end{aligned} \tag{5}$$

*Table 3 - Basis function coefficient statistics of MARS model for P2.AvSpeed*

| No | Basis function | Coefficient | Standard error | t statistics | P-value |
|---|---|---|---|---|---|
| BF0 | Intercept | 0.586 | 0.118 | 4.950 | 0 |
| BF1 | max(0, 0.8 - No.phases) | 1.324 | 0.152 | 8.710 | 0 |
| BF2 | max(0, Vhv - 0.636) | -0.579 | 0.204 | -2.833 | 0.0064 |
| BF3 | max(0, 0.636 - Vhv) | 0.479 | 0.092 | 5.190 | 0 |
| BF4 | max(0, 0.337 - VperLtot) | -2.094 | 0.480 | -4.367 | 0.0001 |
| BF5 | max(0, 0.706 - Cyc) | -0.775 | 0.164 | -4.733 | 0 |
| BF6 | max(0, VperLtot - 0.246) | 2.234 | 0.790 | 2.829 | 0.0065 |
| BF7 | max(0, VperLtot - 0.136) | -2.981 | 0.830 | -3.592 | 0.0007 |
| BF8 | max(0, 0.119 - VperLtot) | 1.993 | 0.627 | 3.178 | 0.0024 |

The relative importance of the variables in the model is shown in Table 4. The $R^2_{GCV}$ values in the table show the prediction capability of the MARS model for the case of excluding the considered variable. It is clear that the most important variable in the model is the number of phases. The entering heavy vehicle volume follows this variable. Because limiting the number of heavy vehicles using an intersection is only possible with transportation network management, the number of phases may be considered for maintaining average speed performance.

The relative importance of each basis function in the model can be investigated using Table 3. Considerably small and zero values of probabilities (P) of the t statistics show that every basis function is essential in the prediction of the average speed. When the absolute values of t statistics are compared, BF1 that included No.phases appears to be the most effective basis function. BF3, the intercept, and BF5 follow BF1.

*Table 4 - MARS model ANOVA for P2.AvSpeed model.*

| ANOVA function | Basis functions numbers | Variables | Standard deviation | GCV | $R^2_{GCV}$ | Relative importance |
|---|---|---|---|---|---|---|
| 1 | 5 | Cyc | 0.25596 | 0.01061 | 0.901 | 28.75 |
| 2 | 1 | No.phases | 0.47400 | 0.01793 | 0.833 | 100.00 |
| 3 | 2, 3 | Vhv | 0.11558 | 0.01344 | 0.875 | 58.60 |
| 4 | 4, 6, 7, 8 | VperLtot | 0.07731 | 0.01211 | 0.887 | 45.04 |

Fig. 5 demonstrates a graphical sensitivity analysis of the average speed model. For obtaining each line of the figure, the model is simulated 401 times with a range of each considered model parameter between -2 and 2 times of its mean value of observations with 0.01 increment. At every 401 simulations of the considered parameter, the other model parameters are fixed at their mean observation values. Consequently, the corresponding proportional change in model predictions with respect to the model in which all of the model parameters are taken as mean are obtained. The horizontal axis shows the proportional change in each model parameter around the average of observations and the vertical axis indicates the corresponding proportional change in the average speed model. The complicated effect of VperLtot is clearer from the figure. The changes in slopes of the VperLtot line indicates several thresholds in the model. In general, this variable exhibits the largest adverse effect on the average speed performance, when its steepest average slope is considered. While a low Vhv increases the average speed as much as VperLtot, this cannot be assumed for high Vhv. Although the number of phases is the most important variable in the model, the sensitivity graph demonstrates a lower impact than the ones of VperLtot and Vhv. Additionally, the effect of No.phases diminishes over (approximately) a 0.4 increase. The cycle time also decreases the average speed for low ratios (according to the mean of observations); however, it is ineffective for high ratios. It is noteworthy that the sensitivity lines are related to the magnitude and sign of the explanatory variable coefficients. The coefficients may or may not relate to the significance of the explanatory variable in explaining the variance of the dependent variable.

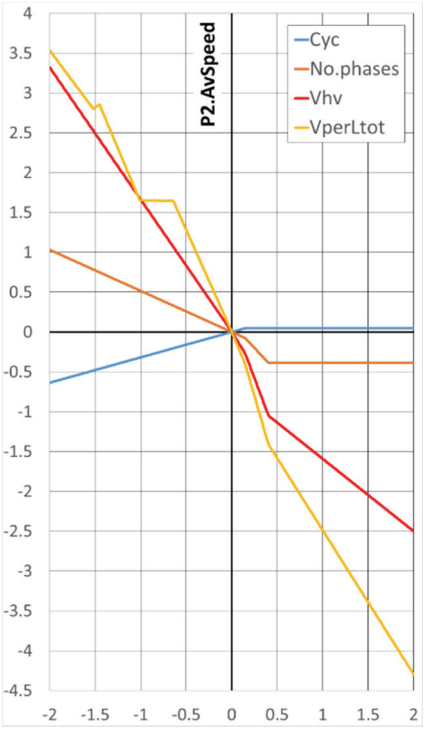


*Fig. 5 - Sensitivity analysis for MARS variables in P2.AvSpeed model.*

### *3.2.2. Number of Stops (P5)*

The number of stops can be used as a measure of interruptions in traffic flows. The less number of stops means more fluent flows at the intersections. The MARS model of number of stops converges with 0.00693 GCV and 11 basis functions. The final form of the basis functions and their standardized version are shown in Eq. 6 and Table 5, respectively. Seven different parameters are found to be significant in the prediction: average width of approach median of roundabout (RA_appr), entering heavy vehicle volume (Vhv), through passing passenger car equivalent volume (Vpce_Thr), leg-based average ratio of right turn over entering flow (AvRat_Leg_RT), left turning passenger car volume (Vpc_LT), entering passenger car equivalent volume (Vpce), and average green time per entering vehicle for right turn flow (GTr_RT). It can be inferred that the estimation of P5 is rather complicated and related with several parameters depending on vehicle movements, signalization and geometry. Vpce of over 1030 (approximately), and Vhv of over 296 appear to increase the number of stops as threshold values. Additionally, vehicle movements such as Vpc_LT of under 290, and Vpce_Thr of under 410 cause a decreasing effect on this performance. Further, 14% is found to be the threshold for the right turn ratio with two basis functions. Unlike other variables, the roundabout approach width has a linear effect with 0.242 coefficient, implying that this width raises the number of stops in all conditions. Additionally, the average green time per right turning vehicle of over 0.679 s increases the stops.

$$\begin{aligned} P5.No.Stops = {} & 516.817 + 0.71*\max(0, Vpce - 1029.735) + 0.217*\max(0, GTr\_RT - 0.679) - 0.98*\max(0, 290.241 - Vpc\_LT) + 0.242*\max(0, RA\_appr + 0) \\ & + 0.294*\max(0, Vhv - 295.5) + 0.21*\max(0, AvRat\_Leg\_RT - 0.139) \\ & + 0.637*\max(0, 0.139 - AvRat\_Leg\_RT) - 2.07*\max(0, 410.142 - Vpce\_Thr) \\ & + 1.93*\max(0, 1252.237 - Vpce) - 0.492*\max(0, 448.4 - Vhv) \end{aligned} \quad (6)$$

Table 5 shows that the basis functions including Vpce, Vpc_LT, and RA_appr variables are the most effective basis functions according to the t statistics. Table 6 that includes the relative importance of each variable also shows similar results in the variable-based form. Although Vpc_LT includes only one basis function, it is the second important variable in the MARS model, and this proves the critical significance of left turns in the intersection performance. Fig. 6 demonstrates the sensitivity of the model for each variable, while the others are maintained in their average values. Interestingly, Vpce and GTr_RT show similar sensitivities. This may arise from the site-specific observation correlations of these parameters. Contrary to the regression model, the MARS model does not require multicollinearity analysis and thus the elimination of this type of correlations is simply a modeller preference. Some fluctuations are observed on the sensitivity for the low values of the AvRat_Leg_RT, Vpce, and GTr_RT variables. The emergence of these nonlinear differences is an important advantage of the MARS modeling approach. Although RA_appr is found to be the third most important variable according to the ANOVA statistics, it gives the lowest sensitivity when it is compared with the other variables. This may arise from the limited number of roundabouts and the small range of approach width observations.

*Table 5 - Basis function coefficient statistics of MARS model for P5.No.Stops*

| No | Basis function | Coefficient | Standard error | t statistics | P-value |
|---|---|---|---|---|---|
| BF0 | Intercept | 0.101 | 0.033 | 3.046 | 0.0036 |
| BF1 | max(0, Vpce - 0.155) | 0.711 | 0.072 | 9.922 | 0 |
| BF2 | max(0, GTr_RT - 0.143) | 0.217 | 0.045 | 4.809 | 0 |
| BF3 | max(0, 0.271 - Vpc_LT) | -0.980 | 0.115 | -8.521 | 0 |
| BF4 | max(0, RA_appr + 0) | 0.242 | 0.034 | 7.156 | 0 |
| BF5 | max(0, Vhv - 0.255) | 0.294 | 0.086 | 3.418 | 0.0012 |
| BF6 | max(0, AvRat_Leg_RT - 0.227) | 0.210 | 0.052 | 4.011 | 0.0002 |
| BF7 | max(0, 0.227 - AvRat_Leg_RT) | 0.637 | 0.156 | 4.083 | 0.0002 |
| BF8 | max(0, 0.0963 - Vpce_Thr) | -2.072 | 0.502 | -4.131 | 0.0001 |
| BF9 | max(0, 0.201 - Vpce) | 1.926 | 0.309 | 6.241 | 0 |
| BF10 | max(0, 0.394 - Vhv) | -0.492 | 0.163 | -3.030 | 0.0038 |

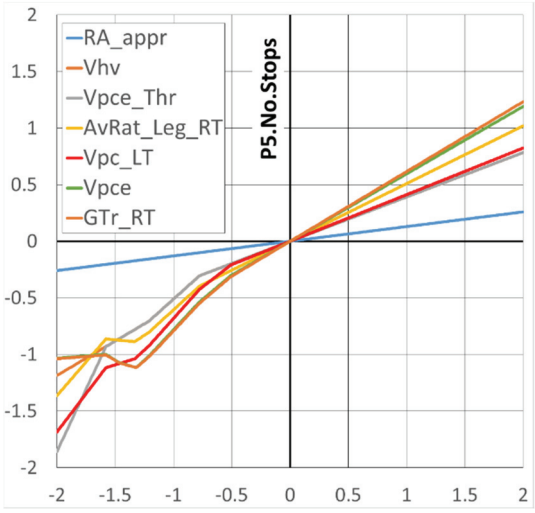


*Fig. 6 - Sensitivity analysis for MARS variables in P5.No.Stops model.*

*Table* 6. MARS model ANOVA for P5.No.Stops model.

| ANOVA function | Basis functions numbers | Variables | Standard deviation | GCV | $R^2_{GCV}$ | Relative Importance |
|---|---|---|---|---|---|---|
| 1 | 4 | RA_appr | 0.05983 | 0.01243 | 0.863 | 41.74 |
| 2 | 5, 10 | Vhv | 0.11046 | 0.01013 | 0.888 | 25.74 |
| 3 | 8 | Vpce_Thr | 0.04767 | 0.00836 | 0.908 | 12.11 |
| 4 | 6, 7 | AvRat_Leg_RT | 0.04250 | 0.00824 | 0.909 | 11.11 |
| 5 | 3 | Vpc_LT | 0.09449 | 0.01499 | 0.835 | 57.85 |
| 6 | 1, 9 | Vpce | 0.12968 | 0.02280 | 0.748 | 100.00 |
| 7 | 2 | GTr_RT | 0.04163 | 0.00908 | 0.900 | 17.83 |

### *3.2.3. Average Travel Time (P8)*

The average travel time per vehicle can be considered as a convenient performance tool that can be an indicator of many intersection characteristics such as dimensions, management, saturation, etc. Although the P8 MARS model is less successful than P7 according to Table 2, it is preferred for examination because of two aspects: the average travel time can reflect the critical intersection performances average speed and delay together, and it is an indicator independent from traffic counts. Additionally, this measure has prominent discrepancy ratio statistics with a high proper percentage and balanced values for low and high percentages. The model adequately converges with 0.0078 GCV and 10 basis functions. The efficient variables on the prediction of the average travel time are found as the average of the leg-based saturation ratios (SatRat), intersection dimensions in the North–South and East–West directions (Dim_NS and Dim_EW), average green-to-cycle ratio for right turn flow

(G/C_RT), left turn passenger car volume (Vpc_LT), difference between the numbers of enter and exit lanes (Ent-Ext_lanes), and through passing heavy vehicle volume (Vhv_Thr). The prediction equation (7) shows the critical thresholds and coefficients of these variables. The standardized forms and statistics of the basis function can also be found in Table 7. The saturation ratio for signalized intersections occurs in two different basis functions with the same threshold, 0.132. Meanwhile, a SatRat smaller than 0.132 decreases the travel time with a -0.17 coefficient, and also decreases it with a -0.33 coefficient for values over this threshold. This may arise from the signalized intersection observations with small saturations in general. The intersection dimensions are measured as the distance between stop lines for the NS and EW bounds. The related basis functions show that if the dimensions are higher than 50 m in the NS bound, it increases the average travel time with a 0.564 coefficient, while Dim_EW decreases it with a -0.26 for distances under 54 m (approximately). The green-to-cycle ratio of over 0.146 for the right turn flow decreases the average travel time with a -0.296 coefficient. The left turn passenger car volume of over 177 increases the travel time with a 1.71 coefficient, and it decreases if it is over 315 with a -1.72 coefficient. If the similar and opposite signs of the coefficients of these basis functions are considered, it can be said that the Vpc_LT effect diminishes for the counts over 315. The average left turn passenger car is 208 for the observed roundabouts; thus, this reduction is shown for some extreme observations.

$$\begin{aligned} P8.Ave\_TrlTime = {} & 0.041 - 0.33*\max(0, SatRat - 0.132) - 1.17*\max(0, 0.132 \\ & - SatRat) + 0.564*\max(0, Dim\_NS - 50.032) - 0.296*\max(0, G/C\_RT - 0.146) \\ & + 1.71*\max(0, Vpc\_LT - 176.715) - 0.78*\max(0, 0.002 - Ent\text{-} Ext\_lanes) \\ & + 0.494*\max(0, Vhv\_Thr - 375.25) - 0.26*\max(0, 53.974 - Dim\_EW) - 1.72*\max(0, \\ & Vpc\_LT - 314.874) \end{aligned} \quad (7)$$

*Table 7 - Basis function coefficient statistics of MARS model for P8.Ave_TrlTime.*

| No | Basis function | Coefficient | Standard error | t statistics | P-value |
|---|---|---|---|---|---|
| BF0 | Intercept | 0.416 | 0.026 | 15.790 | 0 |
| BF1 | max(0, SatRat - 0.171) | -0.331 | 0.092 | -3.579 | 0.0007 |
| BF2 | max(0, 0.171 - SatRat) | -1.169 | 0.167 | -6.989 | 0 |
| BF3 | max(0, Dim_NS - 0.296) | 0.564 | 0.098 | 5.734 | 0 |
| BF4 | max(0, G/C_RT - 0.143) | -0.296 | 0.068 | -4.376 | 0.0001 |
| BF5 | max(0, Vpc_LT - 0.165) | 1.713 | 0.230 | 7.450 | 0 |
| BF6 | max(0, 0.286 - Ent-Ext_lanes) | -0.780 | 0.194 | -4.013 | 0.0002 |
| BF7 | max(0, Vhv_Thr - 0.475) | 0.494 | 0.128 | 3.865 | 0.0003 |
| BF8 | max(0, 0.578 - Dim_EW) | -0.260 | 0.073 | -3.562 | 0.0008 |
| BF9 | max(0, Vpc_LT - 0.294) | -1.716 | 0.303 | -5.662 | 0 |

The entering lane number over exit lanes (positive Ent-Ext_lanes) may be observed in improper intersection designs. The related basis function show that it decreases the average travel time if it is negative, as expected. Through passing heavy vehicle volume (Vhv_Thr) is also found to be an increase factor (with a positive 0.494 coefficient) on the travel time for the observations of over 375.

According to the t statistics in Table 7, the most effective basis functions can be sorted as BF5 (Vpc_LT over knot with a positive coefficient), BF2 (SatRat under knot with a negative coefficient), and BF3 (Dim_NS over knot with a positive coefficient). According to the ANOVA analysis of the variables shown in Table 8, Vpc_LT is the most important variable for the average travel time prediction. The $R^2_{GCV}$ value decreases to 0.649 from 0.819 when this variable is excluded. SatRat and Dim_NS follow this variable. It can be inferred that, especially the left turning passenger car volume should be maintained under 176, saturation ratio under 0.132, and intersection dimensions under 50 m for an acceptable travel time performance. It is noteworthy that these threshold values may be case specific, and similar modeling processes should be performed for intersection observations from other countries or cities where the driver behavior may differ under various intersection geometry, traffic composition, and management conditions.

*Table 8 - MARS model ANOVA for P8.Ave_TrlTime model.*

| ANOVA function | Basis functions numbers | Variables | Standard deviation | GCV | $R^2_{GCV}$ | Relative importance |
|---|---|---|---|---|---|---|
| 1 | 8 | Dim_EW | 0.04426 | 0.00883 | 0.795 | 16.31 |
| 2 | 3 | Dim_NS | 0.05497 | 0.01150 | 0.733 | 54.65 |
| 3 | 6 | Ent-Ext_lanes | 0.03579 | 0.00928 | 0.785 | 23.16 |
| 4 | 4 | G/C_RT | 0.04132 | 0.00968 | 0.775 | 29.14 |
| 5 | 1, 2 | SatRat | 0.08107 | 0.01317 | 0.695 | 76.30 |
| 6 | 7 | Vhv_Thr | 0.04051 | 0.00913 | 0.788 | 20.84 |
| 7 | 5, 9 | Vpc_LT | 0.09253 | 0.01512 | 0.649 | 100.00 |

A graphical sensitivity analysis of the average travel time model is shown in Fig. 7. Except for the dimensions variables (Dim_NS and Dim_EW), the lower values of all other variables appear to have a higher decreasing effect on the travel time, when it is compared with their increasing effect for higher values (according to the average) because the sensitivity slopes are generally larger at the left side. Therefore, maintaining these variables under some acceptable averages is preferable.

### 3.3. Selection of Intersection Design Parameter(s)

In this section, the model results are interpreted and new design parameters are generated to modify the existing intersections. An intersection has been selected for modification and a design is generated.

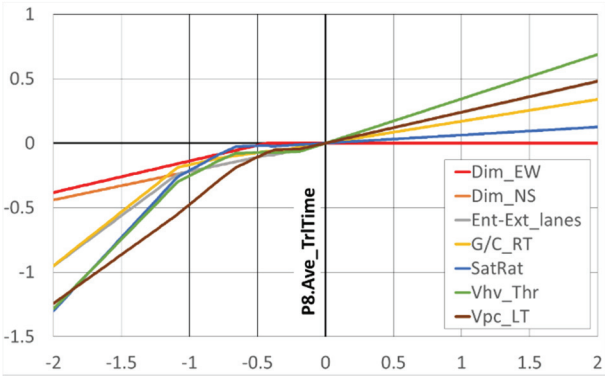


*Fig. 7 - Sensitivity analysis for MARS variables in P8.Ave_TrlTime model.*

*Table 9 - The selected intersection design parameters and performance indicators*

| | ***Intersection Performance*** | ***Intersection dimension in North-South direction (Dim_NS)*** | | | | | ***Left turn passenger car equivalent volume (Vpc_LT)*** | | | | |
|---|---|---|---|---|---|---|---|---|---|---|---|
| | | Relative Importance | No of BF | Coef. | t stat. | Basis Function(s) [BF] | Relative Importance | No of BF | Coef. | t stat. | Basis Function(s) [BF] |
| **P1** | Average delay time per vehicle | 88.26 | 1 | 0.715 | 6.748 | max(0, Dim_NS -50.032) | 21.62 | 1 | 0.368 | 3.739 | max(0, Vpc_LT -117.81) |
| **P2** | Average speed | - | - | - | - | - | - | - | - | - | - |
| **P3** | Total delay time | 43.64 | 1 | 0.397 | 5.073 | max(0, Dim_NS -50.032) | - | - | - | - | - |
| **P4** | Total distance traveled | - | - | - | - | - | - | - | - | - | - |
| **P5** | Number of stops | - | - | - | - | - | 57.85 | 1 | -0.98 | -8.521 | max(0,290.241 -Vpc_LT) |
| **P6** | Number of vehicles that have left the network | - | - | - | - | - | - | - | - | - | - |
| **P7** | Total travel time | 6.22 | 1 | 0.26 | 4.174 | max(0, Dim_NS -53.014) | 12 | 3 | -2.011<br>1.151<br>0.969 | -5.246<br>3.986<br>3.792 | max(0,299.88 -Vpc_LT)<br>max(0,134.946 -Vpc_LT)<br>max(0,404.838 -Vpc_LT) |
| **P8** | Average travel time per vehicle | 54.64 | 1 | 0.564 | 5.734 | max(0, Dim_NS -50.032) | 100 | 2 | 1.713<br>-1.716 | 7.445<br>-5.662 | max(0, Vpc_LT -176.715)<br>max(0, Vpc_LT -314.874) |

To obtain the intersection design parameters that should be considered as a first priority, 75 explanatory variables are analyzed in terms of occurrence frequency and relative importance in the MARS predictions of eight different intersection performances. The intersection dimensions (North–South direction) and left turn passenger car volume are found to be the most frequently included parameters in the performance prediction, with inclusion in four different prediction models for both. The model statistics regarding these variables are shown in Table 9. The average delay, and the total and average travel times are typical performance indicators for these intersection features. The "t" statistics of the intersection dimensions are over "4," and the threshold values in the basis function varies between 50–53 m. The dimensions over these threshold values adversely affect many performance indicators with positive coefficients. The influence of the left turning passenger car volume is rather complicated especially for the travel-time-based performances. It occurs with two or more basis functions with several thresholds in the prediction models. For example, according to

Table 9, while a Vpc_LT higher than 118 veh./h increases the average delay per vehicle with a 0.368 coefficient, it decreases the number of stops with a -0.98 coefficient for Vpc_LT values smaller than 290 veh./h. The MARS models reflect many nonlinearities regarding the traffic count dynamics. Meanwhile, improving the traffic volume-based variables is more difficult than improving the geometric variables. This requires the implementation of network management tools such as one-way applications and left-turn constraints. Therefore, the intersection dimensions are chosen as the basic design parameter. It is worth noting that the prominence of intersection dimensions is a case-specific result, and different intersection observations and driver behaviors from another city may cause alternative conclusions. The proposed stepwise paradigm should be followed for each site study to obtain sound results.

### 3.4. Testing of Intersection Design Parameter

To test the improvement, a traffic simulation for the chosen intersection has been performed for the base case and for the proposed solution. Subsequently, before and after analysis have been conducted to evaluate the improvement.

The chosen intersection to test is called “Narin Kavsağı”. It is a signalized roundabout with a diameter of 64 m. The vehicle volumes of the intersection legs are presented in Table 10. The intersection demand in the proposed solution is assigned the same as the base case. Five arms and four routes exist for each intersection arm; therefore, 20 routes are available. The traffic speed values are calibrated by surveys as follows: passenger car, 50 km/h; HGV, 30 km/h; bus, 30 km/h; minibus, 40 km/h.

*Table 10 - Vehicle input for the intersection (veh/hour)*

| Departure leg / Approach leg | A | | | | B | | | | C | | | | D | | | | E | | | |
|---|---|---|---|---|---|---|---|---|---|---|---|---|---|---|---|---|---|---|---|---|
| | Car | HGV | Bus | Minibus | Car | HGV | Bus | Minibus | Car | HGV | Bus | Minibus | Car | HGV | Bus | Minibus | Car | HGV | Bus | Minibus |
| A | 0 | 0 | 0 | 0 | 20 | 0 | 0 | 5 | 34 | 0 | 0 | 11 | 7 | 0 | 0 | 3 | 6 | 0 | 0 | 4 |
| B | 26 | 1 | 1 | 2 | 0 | 0 | 0 | 0 | 50 | 5 | 6 | 9 | 60 | 7 | 4 | 9 | 0 | 0 | 0 | 0 |
| C | 195 | 15 | 12 | 33 | 10 | 1 | 1 | 3 | 0 | 0 | 0 | 0 | 65 | 7 | 3 | 15 | 70 | 4 | 3 | 8 |
| D | 59 | 4 | 4 | 8 | 48 | 5 | 4 | 13 | 363 | 7 | 8 | 27 | 0 | 0 | 0 | 0 | 330 | 10 | 11 | 29 |
| E | 190 | 0 | 0 | 0 | 135 | 0 | 0 | 0 | 0 | 0 | 0 | 0 | 0 | 0 | 0 | 0 | 0 | 0 | 0 | 0 |

Intersection layout, signal groups and phase diagrams for base case and proposed solution are given in Fig. 8. The intersection has been simulated for the base case and subsequently redesigned in terms of dimensions. It has been transformed into an intersection that is narrower and not a roundabout, by following a new intersection design paradigm. The

redesigned intersection has also been simulated in the VISSIM traffic simulation software. The visual comparison of the mentioned simulations in the 3000$^{th}$ second is shown in Fig. 9.

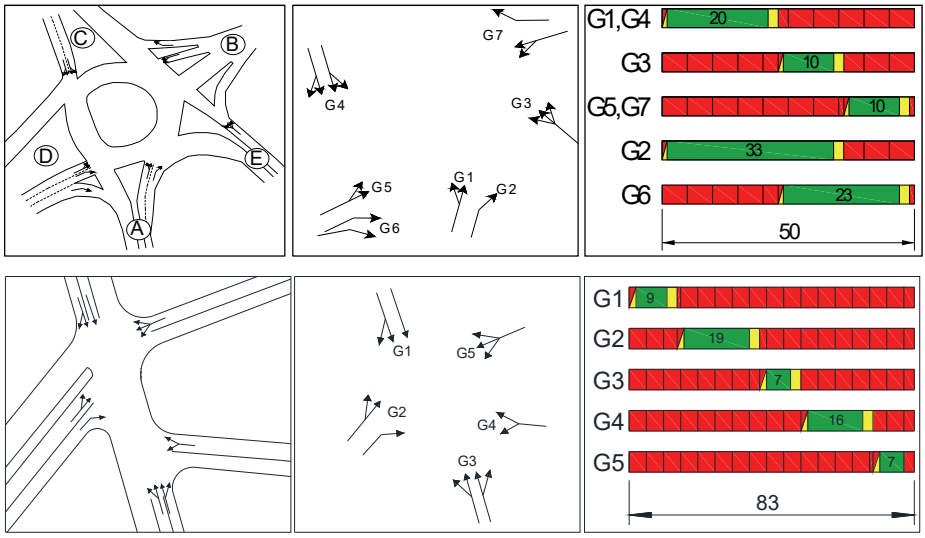


*Fig. 8 - Intersection layouts, signal groups and phase diagrams of "Narin" Intersection for base case (a) and for the proposed solution (b)*

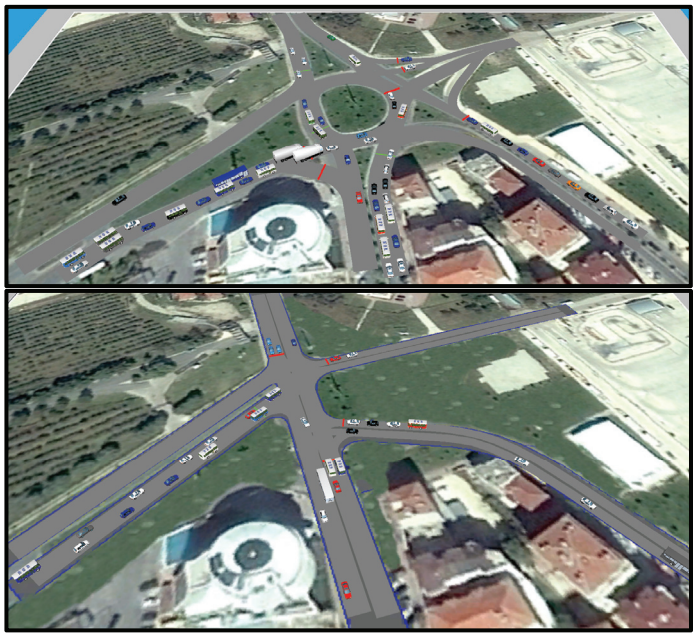


*Fig. 9 - The visual comparison of intersection for base case (a) and for the proposed solution (b) (3000$^{th}$ second of the simulation).*

As shown in Fig. 9, the dimensions of the intersection have been reduced, and the traffic jam has decreased. The performance indicators for the base case and proposed solution has been compared in Table 11. The performance indicators: average delay time per vehicle, average speed, total delay time, and total distance travelled are the primary correlated indicators with variables. Thus, the improvements on those indicators are validations of the test section. Table 11 shows noteworthy change percentages at performance indicators between 2% and 29%. The increase in the total distance travelled is likely due to the rising number of vehicles that have successfully left the network. Except for that, all the performance indicators were improved. The average speed and number of stops are the most improved performances, i.e., of over 25%. Consequently, using the proposed stepwise analysis, only one critical intervention can significantly improve the crucial intersection performances such as the average delay and speed.

*Table 11 - Comparison of intersection performance indicators for base case and proposed solution*

| | Performance indicators | Base case | Proposed solution | Change |
|---|---|---|---|---|
| P1 | Average delay time per vehicle (s) | 45.25 | 35.93 | -20.6% |
| P2 | Average speed (km/h) | 10.95 | 14.11 | 28.9% |
| P3 | Total delay time (h) | 21.67 | 19.35 | -10.7% |
| P4 | Total distance travelled (km) | 307.00 | 386.19 | 25.8% |
| P5 | Number of stops | 2572 | 1870 | -27.3% |
| P6 | Number of vehicles that have left the network | 1698 | 1912 | 12.6% |
| P7 | Total travel time (h) | 28.04 | 27.36 | -2.4% |
| P8 | Average travel time per vehicle (min.) | 0.99 | 0.86 | -13.3% |

## 4. CONCLUSIONS

In the study, a stepwise analysis briefly including intersection indexing and microsimulation, MARS-based performance prediction, selection of intersection design parameters, and testing were conducted. It was aimed to provide a holistic strategy for the description of fundamental components that decrease the intersection-based highway network performance. An average of 80 intersections in Tekirdağ were investigated with eight performance indicators. Using the MARS method, which is a promising modeling technique providing nonlinear and parametric estimations, many intersection parameters such as heavy vehicle volume, number of phase, cycle time, total entering vehicle per lane, saturation ratio, and intersection dimensions were found to be critical factors affecting the intersection performance with several threshold values. The variable of intersection dimensions of over 50 m was found to show the most significant effect on the average speed, average delay time per vehicle, total delay time, average delay time per vehicle, and number of stops indicators. According to the obtained result, a new intersection design was created, which was below the 50 m threshold. The intersection design was simulated and compared with the base case situation, and the improvement results were obtained. According to the results obtained, the

offered intersection type was more efficient in terms of all the performance indicators, i.e., up to 29%.

Many intersections, intersection characteristics, and performance indicators exist in the model. Therefore, it generated a backdrop for interpretations and subjective perspectives. It is helpful for planners to determine which design parameters to be prioritized, and which intersections should be prioritized. Many options are available for setting the mentioned priorities in the proposed model.

It is meaningful to evaluate the general characteristics of the intersections before intervening in the interchanges. The analytical nature of the assessment performed will provide a more accurate decision-making process. The mentioned model may be utilized in the urban transportation studies of local administrations. It may also be used at the lower stages of transportation planning.

There are several traffic related problems in big cities of both developing and developed countries. As known, most of these problems arise from low performance of the intersections. In such cases, specific intersection redesign proposals may provide improved results in terms of delays and congestion. The model developed in this study reveals the major intersection design parameters, which may be useful to evaluate by the planners and decision-makers in intersection redesign process. For the case area of this study, as it is stated in Table 9, planning process should start with improvements on intersection dimensions (in the north direction) and left turn volumes. The model may be utilized in new planning processes since the data generated by the model provides an essential information for decision makers.

Various policies should be developed before the interventions at crossroads in future work. These intervention policies can be determined by the proposed model or by the evaluation of many different data. Finally, since there are still many other significant variables affecting the intersection performance, the proposed model will be extended considering some other key determinants which can impact on the model.

**Acknowledgements**

The authors gratefully acknowledge the contribution of the PTV Traffic Mobility Logistics for the VISSIM traffic planning software. The authors are also grateful to the Metropolitan Municipality of Tekirdağ for providing the reference for the background of this paper.

## References

[1] Saka, A. A., Jeihani, M., James, P. A., Estimation of Traffic Recovery Time for Different Flow Regimes on Freeways. Morgan State University Department of Transportation and Urban Infrastructure Studies School of Engineering, Report No: MD-09-SP708B4L, 2008.

[2] Ceylan, H., Bell, M. G. H., Traffic signal timing optimisation based on genetic algorithm approach, including drivers' routing. Transportation Research Part B: Methodological, 38 (4), 329–342, 2004.

[3] Chiou, S. W., Joint optimization for area traffic control and network flow. Computers and Operations Research, 32 (11), 2821–2841, 2005.

[4] Cantarella, G. E., Vitetta, A., The multi-criteria road network design problem in an urban area. Transportation, 33 (6), 567–588, 2006.

[5] Chiou, S. W., A hybrid approach for optimal design of signalized road network. Applied Mathematical Modelling, 32 (2), 195–207, 2008.

[6] Ceylan, H., Ceylan, H., A Hybrid Harmony Search and TRANSYT hill climbing algorithm for signalized stochastic equilibrium transportation networks. Transportation Research Part C: Emerging Technologies, 25, 152–167, 2012.

[7] Szeto, W. Y., Jiang, Y., Wang, D. Z. W., Sumalee, A., A sustainable road network design problem with land use transportation interaction over time. Networks and Spatial Economics, 15 (3), 1–32, 2013.

[8] Di, Z., Yang, L., Qi, J., Gao, Z., Transportation network design for maximizing flow-based accessibility. Transportation Research Part B: Methodological, 110, 209–238, 2018.

[9] Sun, W., Wang, Y., Yu, G., Liu, H. X., Quasi-optimal feedback control for a system of oversaturated intersections. Transportation Research Part C: Emerging Technologies, 57, 224–240, 2015.

[10] Chen, P., Sun, J., Qi, H., Estimation of delay variability at signalized intersections for urban arterial performance evaluation. Journal of Intelligent Transportation Systems, 21 (2), 94–110, 2017.

[11] Liu, Y., Chang, G. L., An arterial signal optimization model for intersections experiencing queue spillback and lane blockage. Transportation Research Part C: Emerging Technologies, 19, 130–144, 2011.

[12] Lim, K., Kim, J. H., Shin, E., Kim, D. G., A signal control model integrating arterial intersections and freeway off-ramps. KSCE Journal of Civil Engineering, 15 (2), 385–394, 2011.

[13] Song, X., Tao, P., Chen, L., Wang, D., Offset optimization based on queue length constraint for saturated arterial intersections. Discrete Dynamics in Nature and Society, Volume 2012, 1–13, 2012.

[14] Chen, F., Wang, L., Jiang, B., Wen, C., An Arterial Traffic Signal Control System Based on a Novel Intersections Model and Improved Hill Climbing Algorithm. Cognitive Computation, 7 (4), 464–476, 2015.

[15] Xinwu, Y., Qiaohui, W., Huibin, X., Xiaoyan, X., A coordinated signal control method for arterial road of adjacent intersections based on the improved genetic algorithm. Optik, 127 (16), 6625–6640, 2016.

[16] Stamatiadis, N., Kirk, A., Improving Intersection Design Practices Final Report - Phase I. Kentucky Transportation Center Research, Report No: KTC-10-09/SPR 380-09-1F, 2010.

[17] Otković, I. I., Dadić, I., Comparison of delays at signal-controlled intersection and roundabout. Promet Traffic & Transportation, 21 (3), 157–165, 2009.

[18] Persaud, B., Retting, R., Garder, P., Lord, D., Safety effects of roundabout conversions in the United States: empirical Bayes observational before-and-after study. Transportation Research Record, 1751, 1–8, 2001.

[19] Rodegerdts, L., Bansen, J., Tiesler, C., Knudsen, J., Myers, E., Roundabouts: An Informational Guide. Report 672 - Second Edition, Transportation Research Board – National Cooperative Highway Research Program, Washington DC, USA, 2010.

[20] Gross, F., Lyon, C., Persaud, B., Srinivasan, R., Safety effectiveness of converting signalized intersections to roundabouts. Accident Analysis and Prevention, 50, 234–241, 2013.

[21] Kramer, R. P., New combinations of old techniques to rejuvenate jammed suburban arterials. In: Strategies to alleviate traffic congestion. Proceedings of ITE's 1987 national conference, Washington, DC, Institute of Transportation Engineers, 139–148, 1987.

[22] Hummer, J. E., Boone, J. L., The travel efficiency of unconventional arterial intersection designs. Transportation Research Record: Journal of the Transportation Research Board, 1500, 153–161, 1995.

[23] Hummer, J. E., Reid, J. D., Unconventional left-turn alternatives for urban and suburban arterials: an update. In: Transportation research circular E-C019: Urban Street Symposium Conference Proceedings, 28–30 June, Dallas, TX, 1999.

[24] Jagannathan, R., Bared, J., Design and operational performance of crossover displaced left-turn intersections. Transportation Research Record: Journal of the Transportation Research Board, 1881, 1–10, 2004.

[25] Shahi, J., Choupani, A., Modelling the operational effects of unconventional U-turns at a highway intersection. Transportmetrica, 5 (3), 173–191, 2009.

[26] El Esawey, M., Sayed, T., Unconventional USC intersection corridors: evaluation of potential implementation in Doha, Qatar. Journal of Advanced Transportation, 45 (1), 38–53, 2011.

[27] El Esawey, M., Sayed, T., Analysis of unconventional arterial intersection designs (UAIDs): state-of-the-art methodologies and future research directions. Transportmetrica A: Transport Science, 9 (10), 860–895, 2013.

[28] Autey, J., Sayed, T., El Esawey, M., Operational performance comparison of four unconventional intersection designs. Journal of Advanced Transportation, 47 (5), 536–552, 2012.

[29] Naghawi, H., Idewu, W., Analysing delay and queue length using microscopic simulation for the unconventional intersection design superstreet. Journal of the South African Institution of Civil Engineering, 56 (1), 100–107, 2014.

[30] Xiang, Y., Li, Z., Wang, W., Chen, J., Wang, H., Li, Y., Evaluating the operational features of an unconventional dual-bay U-turn design for intersections. Plos One, 11 (7), 1–18, 2016.

[31] Lan, C-J., New optimal cycle length formulation for pretimed signals at isolated intersections. Journal of Transportation Engineering, 130 (5), 637–647, 2004.

[32] Talmor, I., Mahalel, D., Signal design for an isolated intersection during congestion. Journal of the Operational Research Society, 58 (4), 454–466, 2007.

[33] Yu, D., Tian, X., Xing, X., Gao, S., Signal timing optimization based on fuzzy compromise programming for isolated signalized intersection. Mathematical Problems in Engineering, Volume 2016, 1–12, 2016.

[34] Chang, L., Analysis of bilateral air passenger flows: A non-parametric multivariate adaptive regression spline approach. Journal of Air Transport Management, 34, 123–130, 2014.

[35] Ozuysal, M., Caliskanelli, S. P., Reliability estimation of public bus routes: applicability of MARS approach. Canadian Journal of Civil Engineering, 45 (10), 852-865, 2018.

[36] Transportation Research Board (TRB), Highway Capacity Manual. National Research Council, Washington DC, 2010.

[37] Gluck, J., Levinson, H. S., Stover, V., Impacts of access management techniques. National Cooperative Highway Research Program Report 420, Washington DC, 1999.

[38] PTV AG, VISSIM 5.40-01-User Manual. PTV Planung Transport Verkehr AG, Karlsruhe, 2011.

[39] Friedman, J.H., Multivariate adaptive regression splines. The Annals of Statistics, 19 (1), 1–67, 1991.

[40] Friedman, J. H., Estimating functions of mixed ordinal and categorical variables using adaptive splines. California: Laboratory for Computational Statistics, Technical Report No. 108, Department of Statistics, Stanford University, USA, 1991.

[41] Abdel-Aty, M., Haleem, K., Analyzing angle crashes at unsignalized intersections using machine learning techniques. Accident Analysis and Prevention, 43 (1), 461–470, 2011.

[42] Haleem, K., Gan, A., Lu, J., Using multivariate adaptive regression crash splines (MARS) to develop modification factors for urban areas freeway interchange influence. Accident Analysis and Prevention, 55, 12–21, 2013.

[43] Chang, L., Chu, H., Lin, D., Lui, P., Analysis of freeway accident frequency using multivariate adaptive regression splines. Procedia Engineering, 45, 824–829, 2012.

[44] Xu, Y., Kong, Q. J., Liu, Y., A spatio-temporal multivariate adaptive regression splines approach for short-term freeway traffic volume prediction. Proceedings of the 16th International IEEE Annual Conference on Intelligent Transportation Systems (ITSC 2013), The Hague, The Netherlands, October 6-9, 217-222 (in the proceedings book), 2013.

[45] Xu, Y., Kong, Q. J., Klette, R., Liu, Y., Accurate and interpretable bayesian MARS for trafic flow prediction. IEEE Transactions on Intelligent Transportation Systems, 15 (6), 2457–2469, 2014.

[46] Salford Systems, SPM User Guide: Introducing MARS. https://www.salford-systems.com/support/spm-user-guide/help/mars, 2016.

[47] TMM, Preperation of Traffic Regulation, Road and Intersection Preliminary Projects. Tekirdağ Metropolitian Municipality, Final Report (in Turkish), Tekirdağ, 2015.

[48] Jekabsons, G., ARESLab: Adaptive regression splines - toolbox for Matlab/Octave. http://www.cs.rtu.lv/jekabsons, 2016.

[49] Ozuysal, M., Caliskanelli, S. P., Tanyel, S., Baran, T., Capacity prediction for traffic circles: applicability of ANN. Proceedings of the Institution of Civil Engineers: Transport, 162 (4), 195–206, 2009.

*Teknik Dergi, 2021 11257-11286, Paper 633*

# Investigation of Organizational and Regional Perceptions on the Changes in Construction Projects

**Osman İLTER**[1]
**Tahir ÇELİK**[2]

## ABSTRACT

One of the most common concern in construction projects is changes during execution. Changes can increase the cost and duration of the construction project hereby, can lead to conflict between the parties involved in construction projects. Causes of the changes may differ depending on the organizations and regions characteristics. The aim of this study is to investigate the impact of organizational and regional characteristics on key change factors. In this regard, top risky change factors were identified with respect to contractors, consultants, and owners located in North Cyprus, Turkey, and the U.S.A. The research findings showed that the most risky change factors differed in accordance with the characteristics of organizations and regions. It was concluded that "Errors/Inadequacies in Contract Drawing" was the riskiest factor according to contractors while "Low price due to high competition" was noted to be the riskiest change causes with respect to consultants and owners. If different countries were compared, "Inconsistency between different design disciplines" was identified as the top risky change factor according to the respondents in the U.S.A. located organizations, but "Low contract price" was designated as the top risky change factor according to the respondents in North Cyprus and Turkey. In addition, key measures were suggested to mitigate changes in accordance with organizational and regional characteristics.

**Keywords:** Changes in construction, cost-time over-run, claims, mitigation measures.

## 1. INTRODUCTION

Changes during the construction process are one of the most common problems in construction projects. Ming et al. [1], stated that changes are one of the most common distress in construction. Ibbs et al. [2], were defined "Any addition, deletion, or any other revision to project goals and scope of work are considered to change, whether they increase or decrease the project cost or schedule". Almost all construction projects are subject to various changes during the execution process. Changes made during execution trigger many problems in the construction project.

Note:
- This paper was received on July 24, 2019 and accepted for publication by the Editorial Board on April 23, 2020.
- Discussions on this paper will be accepted by January 31, 2022.
- https://doi.org/10.18400/tekderg.595995

1 Eastern Mediterranean University, Department of Civil Engineering, Cyprus - osman.ilter@cc.emu.edu.tr https://orcid.org/0000-0002-3270-3523

2 Cyprus International University, Department of Civil Engineering, Cyprus - tcelik@ciu.edu.tr https://orcid.org/0000-0002-2943-0640

Increasing project cost and time are called as the most important problems caused by the changes in construction projects. Aness et al [3], indicated that the average cost and time overrun due to change orders is between 11 and 15% of the original contract value and between 10 and 20% of the original project duration in large projects in Egypt. Problems created by changes are serious aside from the quality, budget and time are considered as the most important parameters of a project. Moselhi et al. [4], emphasized that changes are one of the major issues that cause poor project performance, such as degradation of productivity, delay [5], and cost overruns [6]. As a result, it is almost become impossible to complete construction projects within the targeted budget and time frame, so the projects are completed in failures. Such problems are often seen in Northern Cyprus and Turkey. Arditi et al. [7], stated that frequent change orders are the most important source of delay in public projects in Turkey. Kazaz et al. [8], emphasized that "design and material changes" is the main delay reason on construction projects carried out in Turkey. Most cases in courts related to the construction sector are related to disputes between the parties as a result of changes [9]. The owner, project manager, and contractor as main stakeholders exhibit different approaches with respect to the requirements and evaluation of changes. The contractor is usually in a struggle to claim additional payment and time as a consequence of any changing case in the project [10, 11] however, clients are often not volunteer to meet the contactors 'claims, and therefore the projects could not be terminated at the targeted budget and time, so the parties suffer various losses [11].

## 2. RESEARCH BACKGROUND

### 2.1. Change Causes and Effects

Many researchers have investigated and analysed the causes and effects of change factors in construction projects on the basis of different regions and project characteristics. For this reason, the causes and effects of changes have been examined extensively with a comprehensive literature survey. The most significant change causes according to the different regions and organizational characteristics were presented as high factor findings as follows.

Assaf and Hejji [12], were stated that change orders are the most common cause of delay in the Saudi Arabia construction sector according to consultant, contractor, and owners. Kazaz et al [8], were emphasized that design and material changes are becoming the most significant delay causes in the Turkish construction sector based on contractor's views. Kaming et al. [13], have demonstrated that design changes and material costs increased due to inflation is becoming the most significant factors that cause time and cost overruns in the Indonesia construction sector according to project manager's evaluation. Zaneldin [14] was designated that change orders are the most frequent claim causes in construction projects implemented in Dubai and Abu Dhabi. Ijaola and Iyagba [15], and Oladapo [16], were determined the type of causes, effects, and sources as well as benefits and remedial actions of change orders for construction projects in Nigeria and Oman. It was concluded that additional work and modification to design were the most common change order factors both in Nigeria and Oman and project cost and time overruns were as around 79 and 68 percent as a result of a change order in Nigeria. Hassanein and Nemr [17], were demonstrated that 54% of causes of claims in the Egyptian construction sector have been resulted due to change orders. Besides, change orders can be allowed in 57 % of the projects in Egypt due to poor documentation practices by the contractor's team were identified [17]. Enshassi et al. [18], were identified 64 causes of change order through literature review to demonstrate the most

common and important type of change orders with respect to different party's perceptions operating in the Gaza strip. "Lack of construction material and equipment" and "change in design" were emphasized to be the most significant change causes according to all parties in Gaza Strip. Stare [19], was clarified that 90% of project changes are the reason for project delay and cost overrun in construction projects carried out in Slovenia. Arain and Pheng [11], were specified that changes in plan or scope, unforeseen problems, and defective problems were the most frequent were most significant causes of change orders for institutional buildings in Singapore [20], and their effect on project cost was determined [20]. Wu et al. [21], were explored 90 metropolitan public work projects in Taiwan to identify causes and impact of change orders on project cost and duration under two main evaluation dimensions as technical and administrative. It was concluded that "changed orders owing to legislative or policy changes" were designated as the most significant causes of a change order in highway construction projects carried out in Taiwan.

Akinsola et al. [22], were identified the types and quantified factors influencing change order on the total cost of change and the average rate of change in construction projects. Lu and Issa [23], were demonstrated that the most frequent and most costly changes were often related to design changes and design errors. The time-cost relationship of the building projects in Turkey was investigated by taking into consideration the changes in exchange rate and the number of working days due to climatic effects [24]. Ahbab et al. [25] were concluded that design changes and poor project management and supervision are the main causes that severely affect time management in large transportation projects financed by the Asian Development Bank. Project variables have been investigated with hypothesis testing to predict whether the project is impacted [26] and loss of labor efficiency were quantified by linear regression equation as 40.05% due to change orders [27]. Wambeke et al.[28], were examined the causes of changes in construction projects in order to evaluate the effect on the starting time and duration of tasks as well as the number and type of people impacted as a result of changes. Moselhi et al. [4], were explored 117 projects implemented in the U.S.A. and Canada to examine productivity loss of labor due to change orders by developing the Neural Network Model. Lee et al. [29], were analyzed the amount and number of loss events due to change orders that occurred in apartment projects in South Korea by using the Loss Distribution Approach method. Diekman and Nelson, [30] were indicated that the most common causes of claims were resulted by change orders. Bröchner and Badenfelt [31], were investigated 16 contractual relationships in Sweden to identify change reasons and explored their frequencies according to contract type and contractual incentives respectively. Bakr [32] was identified as the most common cause of changes in the Jordan construction industry by exploring the historical data of change cases that occurred in construction projects. Ezgi et al. [33] were investigated the effect of tendering procedure and contract type on the contract price by analysing 19.546 tender procedures of construction work data between the years 2007 and 2017 in Turkey. The likelihood of disagreement due to changes was emphasized to be high in lump sum contracted compared to the unit price contracted construction projects in Turkey. In addition, authors were revealed that most of contract price of the works between 2007 and 2017 were below the threshold value.

At the end of the comprehensive literature review, it has been realized that the key change causes vary depending on the organizational, regional and project characteristics since organizations and regions have their own particular characteristics, construction law, cultures, economies, and construction technologies. Hence, this paper aims to examine the top risky change factors for a lump sum and design-bid-build contracted building construction projects according to the construction organizations located in North Cyprus-Turkey and the U.S.A. Furthermore, this

study aimed to suggest mitigation measures in accordance with organizational and regional characteristics.

### 2.2. Measures to Reduce Changes

In this study, suggestions were referred to reduce changes hereby, the measures suggested to mitigation changes were monitored in the literature and presented as follow.

Hassanein and Nemr [17], were clarified that formation of standard form of contract conditions along the same line of FIDIC contracts for international project can be effective solution to proper change order claims management in the Egyptian construction industry. Besides, awareness of good contract document of site team will be beneficial for contractor organizations to be able to manage change order claims. Aness et al. [3], were stated that "adding clause regulating change order procedures to have clear procedures for handling the change orders in construction contracts" and "negotiation of change order cases by knowledgeable person" were the most effective change management process to reduce the negative impact of change in Egypt construction industry. Improvement on contractual procedure, common understanding amongst professionals when interpreting customer's requirements and application of new technology in design phase as Building Information Modelling (BIM) were designated as the most effective potential methods to reduce frequency of change on educational building projects in Nigeria [34]. Ijaola and Iyagba [15], were noted that, assigned of specialized quantity surveyor and project manager and development of standard document from beginning to completion of projects were the most effective change order remedies in construction projects in Nigeria and Oman. Taylor et al. [35], were stated that "front end planning" could be beneficial to mitigate change orders due to owner-induced enhancement, contract item overrun and contract omissions in highway construction projects. Dumont et al. [36], were emphasized that design and construction cost are reduced by 20% and total design and construction schedule is reduced by as much as 39 % by front end planning (pre project planning) process in industrial based projects. Zaneldin [14], was referred that "reasonable time for design"," efficient quality control techniques", "clearly written contracts"," good contract awareness", "establishment of risk sharing philosophy" and "proper job records" were the most effective claim preventive factors for United Arab Emirates construction projects. Chan and Kumaraswamy [37], were indicated that "effective site management and data communication", "good site investigation" and "value management techniques to minimize client initiated changes" the most effective factors to minimize time overruns in Hong Kong construction projects.

At the end of the comprehensive literature review, it has been realized that, various mitigation measures have been suggested to be able to control changes and to reduce its negative effects on projects according to the regional and project characteristics. At this point, the changes need to be managed by different methods in accordance with the organization and regional characteristic. Applying the most appropriate mitigation measure according to the factor influencing the change is required in order to get the most benefits in this regard, this study aimed to suggest the key mitigation measures in accordance with the characteristics of organizations and regions.

## 3. RESEARCH METHOD

### 3.1. Determination the Change Factors in Construction Projects

In the first phase of the study, the causes of changes in construction projects were identified based on the validity of the literature. Factors that are commonly accepted as change causes in literature were listed. At the end of a comprehensive literature survey, it was targeted to include all kinds of change factors representing almost all kinds of events encountered in construction projects. Furthermore, the change causes have been categorized in order to provide a better orientation. In this regard, change factors were listed whether to represent events originated due to technical, administrative, construction process, persons and external issues. In this regard, change factors were listed whether to represent events originated due to technical, administrative, construction process, persons and external issues. Hereby, a total of 25 different factors that influence changes were identified through 33 different research sources (See in Table 1).

*Table 1 - Change Factors and References*

| | Change Factors | References |
|---|---|---|
| Planning and Design | Errors in Contract Drawings | Hsieh et al. [38], Memon et al. [39], Motawa, I.A.[40] , Lee et al. [29], Love et al. [41], Chen, [42], Sun and Meng [43], Enshassi [18] |
| | Inconsistencies between different Designs | Sun and Meng [43], Chan and Kumaraswamy [37],Hsieh et al. [38],Wu et al. [21], |
| | Errors and Inadequacy in Specification | Hsieh e al. [38], Sun and Meng [43],Wu et al. [21] ,Assaf and Hejji [12], Enshassi [18], Kazaz et al. [8], |
| | Conflict among contract documents | Hsieh e al. [38], Odeh and Battaineh, [44], Lo et al. [45], Zaneldin [14], Arain and Pheng [20], Motawa, I.A. [40], Enshassi [18] |
| | Use of Poor design software | Assaf and Hejji [12] |
| | Constructability Ignored | Motawa, I.A. [40],Rosenfeld,[46],Assaf and Hejji [12] |
| | Error in Cost Estimating and budgeting | Hsieh e al. [38], Sun and Meng [43], Zaneldin [14], Kazaz et al. [8], Sha'ar et al. [47], Mansfield et al. [48] |
| | Unrealistic imposed contract duration | Sun and Meng [43], Zaneldin [14],Memon et al. [39],Odeh and Battaineh [44], Doloi et al. [49], Sha'ar et al.[47] |

*Table 1 - Change Factors and References (continue)*

| | | |
|---|---|---|
| Construction-Site | Inadequate site investigation in pre-construction | Mohamad et al.[50],Wu et al.[21], Assaf and Hejji [12], Kazaz et al. [8] |
| | Uncertainties / problems of Subsurface | Hsieh e al.[38], Lee et al. [29],Mohamad et al. [50],Wu et al.[21], Assaf et al. [48], Odeh and Battaineh [44], Zaneldin, [14] |
| | Provision of additional shop drawings | Yap et al. [52],Cox et al.[53],Cox and Hamilton, [54], Odeh and Battaineh [44], Assaf and Hejji [12], Enhassi et al.[55] |
| | Errors in execution | Sun and Meng [43], Zaneldin [14] ,Kazaz et al. [8], Sha'ar et al. [47], Assaf and Hejji [12] |
| | Material / Equipment / Manpower shortage | Memon et al. [39],Yap et al.[52], O'Brien [10], Kazaz et al.[8], Arditi et al. [7], Arain and Pheng[20], Enshassi [18], Arain et al [56], |
| | Additions / Omissions of work | Mohamad et al.[50], Ijaola and Iyagba [15] |
| People | Lack of Experience of Project Participants | Motawa [40], Sun and Meng [46], Chan and Kumaraswamy [40], Assaf and Hejji [12], Enshassi [18],Kazaz et al. [8], O'Brien [10] |
| | Poor communication between Parties | Motawa, [40],Sun and Meng [43], Assaf and Hejji [12], Enshassi [18], Doloi et al.[49], Kazaz et al. [8] |
| | Owners Level of Construction Sophistication | Chan and Kumaraswamy [37] , Assaf and Al-Hejji[12], Enshassi [18], Ling et al.[57] |
| Administrative | Poor Contract Management | Hsieh et al.[38], Odeh and Battaineh [44], Doloi et al.[49], Sha'ar et al.[47], Faridi and El-Sayegh [58] |
| | Inappropriate choice of project delivery system | Assaf and Hejji [12], Doloi et al.[49],Ling et al. [57], Sha'ar et al. [47] |
| | Inappropriate choice of contract type | Assaf and Hejji,[12],Sha'ar et al.[47], Ling et al. [57] |
| | Low Contract Price (Competitive Bidding) | Arain and Pheng [20], Assaf and Hejji [12], Sha'ar et al.[47], Doloi [59], Holt et al.[60] |

*Table 1 - Change Factors and References (continue)*

| | | |
|---|---|---|
| External | Unforeseeable Natural Conditions | Motawa [40], Hsieh et al.[38], Wu et al [21], Kazaz et al. [8],Sha'ar et al.[47], Enshassi [18] |
| | Fluctuation in Tax / Interest Rate / Material and Labor Cost | Sun and Meng [43], Andersen et al. [61], Love et al.[62], Doloi et al [49], Zaneldin, [14], Enshassi [18] |
| | Change in government laws/ regulations | Motawa [40], Hsieh et al. [38] ,Andersen et al.[61], Assaf and Hejji [12], Doloi et al. [49], Yap et al.[52], Enshassi [18] |
| | Shortening / Compression in Project Schedule | Motawa [40], Sun and Meng [43], Chan and Kumaraswamy [37], Odeh and Battaineh [44], Enshassi [18] |

### 3.2. Categorization of Causes that result in Changes

In this study, it was deemed appropriate to evaluate change factors within certain categories in order to obtain more focused results. In this respect, the change factors were evaluated in 5 different categories. In accordance with factor types, 5 different change categories were formed based on the validity of 18 different research studies in literature as shown in table 2. Change factors are placed in the relevant category according to factor types based on the literature. (See in Table 1). Definitions of change categories were presented as follow:

#### *3.2.1. Planning and Design Related Causes:*

Hsieh et al.[38] and Motawa [40], were defined that causes of changes are basically related to errors, omissions, and defects in design and planning, such as inconsistency between drawings and site conditions, mistaken quantity estimates, planning mistakes, citation of inadequate specifications, etc. In general, the design and planning team is responsible for changes caused by factors in this category [38]. Love et al. [63], were stated that documentation errors and omissions have resulted as a consequence of the lack of communication between client and design team members in the design phase of construction projects. It was reported that almost 75% of problems or rework on the construction projects were connected to the design phase [63].

In this respect, eight factors were included in the planning and design category (See in Table 1) which regarding design documents, design coordination and quantity estimates.

#### *3.2.2. Construction and Site Related Causes:*

Motawa [40] and Lee et al.[29], were demonstrated that change causes are generally related to construction execution process due to adopting new construction techniques / methods, site

conditions, difficulties in labour, and difficulties in work execution and control methods. Location and underground conditions are becoming the main project-specific dynamics that affect the construction process [50, 62, 64]. Frimpong et al. [65], were stated that the execution of the project is affected by inherent site conditions. Yap et al [66], were denoted that the unavailability of material and equipment in the market in execution may cause changes in projects.

Six factors were placed in construction and site category which associated with construction methods, site inspections and site conditions, resource availability and shop drawings in the construction process (See in Table 1).

### *3.2.3. Human Factor Causes Changes:*

Motawa [40], was stated that knowledge and experience of the project team are the key components to undertake successful projects. The study denoted that, lack of effort of individuals and poor communication as a result of the cultural issues of organizations participating in the project may lead to changes. Hwang et al [67], were emphasized that "client-related rework" due to client and client's representatives are the main cause of rework in construction. "Replacement of materials by the client" and "change of plans or scope by the client" are reported as the highest frequent cause and contributed the most to client-related rework.

Three factors were placed in people category which, regarding the experience, effort, communication level and attitude of the parties involved in the construction project (See in Table 1).

### *3.2.4. Administrative and Contract Related Causes:*

Akinsola et al. [22], were referred that different contract strategies and organizational structures, and management style, are the dynamics of the construction organization. The study was clarified that organization and administrative factors may lead to changes in projects such as the administrative method of procurement, type of contract, method of tendering, type of tender document used, bidding environment and percentage of the adequacy of design document before tender [22]. Arain and Pheng [11] and O'Brien [10], were stated that in the case of the low contract price in competitive bids. the contractor's desired profitability can be a potential cause of changes in construction projects by strive to convince the project owner to allow certain changes, leading to additional financial benefits for him.

In this regard, four factors were included in the administrative and contract category (See in Table 1) which, related to the quality and type of the contract, tendering method and bidding competitiveness.

### *3.2.5. External Causes for Changes:*

Alaghbari et al. [68], were stated that economic conditions, law, and regulation are external factors that can lead to changes. Physical environmental conditions, economic policy, and socio-political conditions are considered as external factors of change causes [62]. Aiyetan et al [69], were referred that the external factors had the most effect on the project parameter as a consequence of

the change of governmental regulation. Hsieh et al. [38], were reported that works in project may change by the effect of government rules/regulation government agencies.

Four change factors were included in the external category which, associated with the uncertain economic conditions, weather conditions, rules/regulations and decisions of authority (See in Table 1). These factors are basically related to the effects arising outside of the project and are not composed of the project's technical and administrative facilities and not related to the performance of the project and performance of the parties.

Categories of change factors and references were presented in table 2 as follow:

*Table 2 - Categories of Changes and References.*

| Groups | References |
|---|---|
| Planning and Design | Motawa [40], Sun and Meng [43],Yap et al. [66], Love et al [63],Chan and Kumaraswamy [37], |
| Construction and Site | Motawa [40], Lee et al.[29], Doloi, et al.[49], Sun and Meng [43],Yap et al.[66], Love et al.[62], Mohamad et al.[50] ,Hsieh et al.[38], Lo et al.[45], Kazaz et al.[8] |
| Human Factors | Motawa [40], Lo et al.[45], Doloi, et al.[49], Yap et al.[66], Hwang et al.[67],Sun and Meng [43], Yap et al.[52], Kazaz et al.[8], Sha'ar et al. [47], Enshassi et al [18] |
| Administrative | Faridi and El-Sayegh [58], Akinsola et al.[22], Kazaz et al.[8] |
| External | Motawa [40],Sun and Meng [43], Yap et al.[66], Hsieh et al.[38],Yap et al.[52],Lo et al.[45], Sha'ar et al.[47], Faridi and El-Sayegh [58], Enshassi et al [18] |

### 3.3. Demographic Information of the Correspondents

In the following phase, change factors were examined based on a survey of professionals in the construction industry in North Cyprus, Turkey, and the U.S.A.

Civil engineers and architects were interviewed on behalf of their organizations in North Cyprus and Turkey and in the U.S.A. A participant was included in the survey for each organization in order to perform an organizational based assessment. Since they had participated on behalf of the organization, they were asked to evaluate the questionnaire based on the organization's experience. Survey document was sent as hardcopy to the organizations located in North Cyprus however; an electronic file of survey document has been sent to organizations located in Turkey and the U.S.A. by using an online survey tool. A total of 96 organizations have participated in the survey. The distribution of regions, organizations and participants' profiles were presented in Table 3.

*Table 3 - Distribution of the Regions, Organizations and Participant Profile*

| | | North Cyprus and Turkey | | | | U.S.A. | | | | **Total** |
|---|---|---|---|---|---|---|---|---|---|---|
| | | Experience (Years) | | | | Experience (Years) | | | | |
| | Position | 0-5 | 5-15 | >15 | Total | 0-5 | 5-10 | >15 | Total | |
| Contractor | Site Engineer | 4 | 7 | 10 | 21 | 2 | 0 | 0 | 2 | 23 |
| | Design Engineer (Head Office) | 0 | 4 | 5 | 9 | 0 | 4 | 2 | 6 | 15 |
| | Site Architect | 0 | 1 | 1 | 2 | 0 | 0 | 0 | 0 | 2 |
| | Design Architect (Head Office) | 0 | 0 | 3 | 3 | 0 | 1 | 1 | 2 | 5 |
| | Total | 4 | 12 | 19 | **35** | 2 | 5 | 3 | **10** | **45** |
| Consultant-Owner | Site Engineer | 1 | 1 | 6 | 8 | 0 | 0 | 2 | 2 | 10 |
| | Design Engineer (Head Office) | 2 | 5 | 12 | 19 | 0 | 0 | 9 | 9 | 28 |
| | Site Architect | 0 | 0 | 2 | 2 | 0 | 0 | 1 | 1 | 3 |
| | Design Architect (Head Office) | 0 | 6 | 2 | 8 | 0 | 2 | 0 | 2 | 10 |
| | Total | 3 | 12 | 22 | **37** | 0 | 2 | 12 | **14** | **51** |
| **Total** | | 7 | 24 | 41 | **72** | 2 | 7 | 15 | **24** | **96** |

In this study, two different organizational and regional characteristics are discussed based on the factors of change. The first organization type was considered to be contractor who represents the party in which undertakes the implementation of the construction projects and as a result, the party that aims to achieve financial success. The second type of organization is together the consultant and the owner where both of them have authority to produce technical and administrative decisions in project phases and to supervise the contractors as well as to decide on the financial return in which the contractor is entitled. In this way, the number of contractors and consultant owners participating in the survey has been fairly balanced.

On the other hand, the selected first region type is Northern Cyprus and Turkey together where both of them are similar characteristics and developing countries. The selected second region is the United States (U.S.A.), where has quite different characteristics and as representative of the developed countries. Northern Cyprus and Turkey were discussed together since they have similar however, the USA, which has different characteristics, is discussed as the second region type. Research findings were categorized and discussed in order to emphasize the impact of organizational and regional characteristics between organizations and region types. The data collection and the analysis methods were explained in the following section of the article.

### 3.4. Importance Index Scores for Different Factors

In the survey, change factors were assessed based on three parameters designated by the order as the frequency of occurrence, impact on cost and impact on time on the construction projects.

Participants have been asked to examine the change factors on the basis of lump-sum contracted and design bid build procured reinforced concrete building projects sized up to 5000 m2. Since this study was intended to make an organizational based assessment, the participants were asked to evaluate the change factors based on the experience of the organization rather than their personal experience.

Factors weighting method were chosen to obtain the opinions of participant's ideas through the survey. Five-point Likert scale were used in order to examine the change factors based on the frequency of occurrence, impact on cost and impact on time on the construction projects. The factor's level of significance was determined by calculating factors relative Importance Index scores (R.I.I.) based on the frequency of Occurrence (F.I.), impact on project cost (C.I.) and impact on project time (T.I.). Factors Relative Importance Index scores were calculated by using equation (1):

$$R.I.I.(\%) = \frac{\sum W_i \times X_i}{A \times N} \tag{1}$$

Where,

R.I.I. (%): Relative Importance Index for Frequency of Occurrence (F.I.); Relative Importance Index for impact on project cost (C.I.); Relative Importance Index for impact on project time (T.I.).

Wi: The weight assigned on Likert's scale given to each factor by the respondents and ranges from 0 to 4, where; 0: Never, 1: Rare, 2: Moderate, 3: Frequent, 4: Very Frequent for Frequency of Occurrence; 0: No Effect, 1: Weak, 2: Moderate, 3: Strong, 4: Very Strong for impact on project cost and time; 0: No Effect, 1: Weak, 2: Moderate, 3: Strong, 4: Very Strong for impact on project time;

$X_i$: Number of choice of the (i) th weight in the Likert's scale for the change factor.
A: is the highest weight (i.e. 4 in this case) and;
N: is the total number of respondents

### *3.4.1. Risk Significance Index of Change Factors*

The top risky change factors were identified depending on the outcome of the frequency, cost and time indexes. For this, the levels of risk of change factors were determined by calculating the Risk Significance index (R.S.I.) scores. The factor that has the highest risk significance index (R.S.I.) was expressed as the riskiest factor. Factors Risk Significance Index (R.S.I.) scores were calculated by using frequency index as multiplier effect and aggregating, cost and time impact indexes (See equation 2 and 3).

$$AV..S.I.(\%) = \frac{C.I + .T.I.}{2} \tag{2}$$

Where;

AV.S.I. = Average Severity Index; C.I. = Cost Impact Index; T.I. = Time Impact Index

$$R.S.I.(\%) = \frac{F.I. \times AV.S.I.}{100} \tag{3}$$

Where; R.S.I. = Risk Significance Index; F.I. = Frequency Index; AV.S.I. = Average Severity Index (equation 2)

### *3.4.2. Risk Significance Index of Change Categories*

The risk significance index for change categories (Av. R.S.I.) was calculated by calculating the average of the risk importance index (Av. R.S.I.) of factors within the category (See equation 4).

$$Av.R.S.I.(\%) = \frac{\sum_{I=1}^{n} R.S.I.}{n} \tag{4}$$

Where;

AV.R.S.I. = Risk Significance Index of change category; R.S.I. = Risk significance index of the (i) th factor in change category; n = Number of factors in the change category.

## 4. RESEARCH FINDINGS AND DISCUSSION

The research findings were presented and discussed according to the types of organizations and regions.

### 4.1. Top Risky Change Factors according to the Different Organizational Characteristics

Risk Significance Index (R.S.I.) of change factors according to organization types were presented in Table 4. According to the contractors, the top risky changes were comprised due to poor quality

of the contract drawings. This finding has indicated that the most frequent most severe changes according to contractors were originated due to errors and poor quality in project drawings. The project owners have major responsibility for drawing documents since the preparation of project drawings is carried out by consultants under the owner's responsibility in design-bid-build procured projects. In this context, contractors have made effort to state that there is a lack of responsibility for the project owners and consultants as project drawing documents are issued under the responsibility of the owners and consultants.

On the other hand, "Low contract price due to competition" was specified as the most risky change factor according to consultants and owners which means, most frequent and severe factor on cost and time overruns. Consultants and owners interpreted that top risky changes occurred due to the low bid price associated with the contractor selection method. There are more chance to cost/time overruns when the bidding environment is highly competitive [11].

It has been observed that the likelihood of a tendency of cost and time overruns increases when contractors have a strong desire to get awarded as a result of keeping their costs below other bidders.

Adding or omitting of work items related to circumstances of the construction execution process and poor scope definition were ranked the second-highest risky change factor according to both organization characteristics. Adding or omitting items may be requested by any party due to many reasons. In fact, this can be a consequence of the side effects of many factors. Both quality of the design, as well as the comprehensiveness of other project documents as well as the level of organization and communication, may generate the consequence of adding extra work items. The contractor's desired profitability can be a potential cause of changes in construction projects. Addition of work items could be used as a means of achieving extra income. In this respect, additional works could be interpreted as a common source for the contractors to be able to achieve desired profitability since contractors may in efforts to include additional works in order to achieve financial benefits [10]. This can be interpreted as the unethical behaviour of contractors to achieve the highest possible level of profit. Besides, poor scope definition is one of the major triggers that may cause additions of works during execution [39, 47]. The addition of extra works items could be reduced by detailed project designing and scope definition together with the preparation of comprehensive project documents.

These findings were also pointed out that, consultants and owners have higher concerns about changes since risk index average was higher in consultants-owners than contractor (See table 4). The consultants have a great responsibility in case of any disruption caused by the changes and the disagreement between the parties. This finding could be interpreted that, consultants are experiencing great challenging in resolving problems regarding changes so that the project can progress smoothly. On the other hand, project owners may incur additional costs due to the need for a financial source for the change.

According to these findings, potential measures were suggested in accordance with the organizational characteristics in the following section that aim to prevent top risky change factors were suggested in accordance with the organizational characteristics in the following section.

*Table 4 - Factors R.S.I. according to the organization types*

| | Causes of Change | Contractor | | Consultant - Owner | |
|---|---|---|---|---|---|
| | | R.S.I. | Rank | R.S.I. | Rank |
| Planning And Design | Errors/Inadequacies in Contract Drawings | 48.6 | 1 | 37.2 | 3 |
| | Inconsistencies between different Designs | 34.7 | 3 | 34.7 | 4 |
| | Errors and Inadequacy in Specification | 31.7 | 6 | 28.3 | 13 |
| | Conflict among contract documents | 30.8 | 8 | 33.4 | 6 |
| | Un-use of advanced design software | 24.2 | 16 | 18.7 | 21 |
| | Constructability Ignored | 28.3 | 10 | 31.2 | 10 |
| | Error in Cost Estimating and budgeting | 26.1 | 13 | 22.7 | 17 |
| | Unrealistic imposed contract duration | 20.4 | 20 | 32.3 | 8 |
| Construction-Site | Inadequate site investigation in pre-construction | 30.2 | 9 | 31.6 | 9 |
| | Uncertainties / problems of Subsurface | 22.7 | 17 | 25.8 | 14 |
| | Provision of additional shop drawings | 31.0 | 7 | 29.7 | 12 |
| | Errors in execution | 16.4 | 24 | 25.2 | 15 |
| | Material / Equipment / Manpower shortage | 18.1 | 23 | 18.2 | 22 |
| | Additions / Omissions of work items | 41.7 | 2 | 38.5 | 2 |
| People | Lack of Experience of Project Participants | 32.3 | 5 | 33.5 | 5 |
| | Poor communication between Parties | 28.0 | 12 | 33.3 | 7 |
| | Owners Level of Construction Sophistication | 24.2 | 15 | 22.5 | 18 |
| Administrative | Poor Contract Management | 28.3 | 11 | 30.9 | 11 |
| | Inappropriate choice of project delivery system | 22.2 | 18 | 22.7 | 19 |
| | Inappropriate choice of contract type | 24.3 | 14 | 23.6 | 16 |
| | Low Contract Price (Competitive Bidding) | 34.3 | 4 | 43.6 | 1 |
| External | Unforeseeable Natural Conditions | 21.6 | 19 | 17.3 | 24 |
| | Fluctuation in Tax / Interest Rate / Material and Labor Cost | 19.1 | 22 | 17.5 | 23 |
| | Change in government laws/ regulations | 10.7 | 25 | 10.2 | 25 |
| | Shortening / Compression in Project Schedule | 20.3 | 21 | 22.3 | 20 |
| Average R.S.I. (%) | | | 26.80 | | 27.40 |

### *4.1.1. Contractors' view on Change Causes*

Contractors stressed that the top risky changes are due to weaknesses and flaws in the project drawings. Contractors were in a struggle to express that they have no obligations and responsibilities regarding project designing since contractors are not involved in the design phase in design-bid-build procured projects [11, 56]. In this context, contractors conclude that other major organizations such as owners and consultants are in charge of design-related issues. At this point, contractors are in an effort to state that they have right to claim additional payment and time as a result of changes which, originated from design issues since they express themselves as a victim in this case.

Globally standardized contract forms (i.e.: FIDIC) are used in construction projects [70]. However, there is no standard form and content for the drawings in the global sense. At this point, the contract drawings should be prepared based on specific standards in terms of structure, requirement, scope, and format that can be validated globally. With this structure and philosophy, the suffering and weakness caused by the drawings could be minimized [15, 70]. Hereby, the drawing standard certification would be requested from the design firms. On the other hand, it would be beneficial to involve the contractors in the design process to take initiative for the design process in order to ensure the legalization of responsibilities all parties with respect to design documents. At this point, Design-Build procurement models could be effective to overcome this issue [12, 47]. The integration of similar obligations in the Design-Build procurement method into the contracts could be effective to minimize design-related issues. In addition, high quality, broad participatory and comprehensive design process could also contribute to reducing the change necessity in the project.

In addition, factors' risk significance index score was quite to be higher in contractors' assessment compared to consultants-owners. These findings were interpreted that defects in the drawing may constitute a high risk for contractors than consultants and owners.

### *4.1.2. Consultants and Owners View on Change Causes*

The top risky changes were originated due to the contractor's low bid price according to the consultants and owners. This finding was indicated that the low bidding price could have serious intense that precipitating change cases in construction projects.

Today, competitive and economic conditions are becoming more challenging. Generally, contractors may tend to offer a low bid price due to high competition to get awarded and to continue their activities [71].

Changes could be a major opportunity for contractors to be able to claim extra payments in order to reduce the distress of low bid prices [11]. The money and time claimed by the contractor for changes may be higher since competitive environment no longer present in the execution process. For this reason, contractors would tend to request changes in the purpose of increasing their earnings during the execution process [10,11]. Mohamad et al [50], emphasized that contractors may lead to design changes by offering to use available materials and alternative construction methods in the purpose of saving money and time. In this way, financial losses are tried to being reduced. Tan et al. [72] stated that contractors would tend to offer a lower bid price than those other competitors in a sacrifice of the profit margin and hence, financial damage may compensate by change orders during the execution process in order to claim extra financial resources from the

owner [73]. It is believed and experienced that "low contract price due to competition" is highly risky for contractors as well, due to the reality that every change order of the contractor may not be awarded by owners. This issue could be able to defuse with the determination of base price offer as the tender threshold value in the purpose of not accepting any bid below of base price [12, 44]. The base price to be determined should also provide financial conditions to contractors to enable the project to be completed smoothly. In addition, it would be beneficial to evaluate bids by giving less weight to quantitative and more weight to qualitative criteria by applying qualitative based evaluation rather than quantitative-based for the contract awarding process.

At this point, bidding is becoming an important process to prevent forthcoming problems. For this reason, high-quality consultancy services are needed to be able to carry out the tender process in the most accurate way and to award the most accurate contractor for execution. This finding could interpret that, construction projects are subject to low quality of consultancy services. It will be beneficial for project owners to carry out their projects by experienced consultancy firms.

### 4.2. Top Risky Change Categories on the basis of Organizational Characteristics

Risk Significance index (R.S.I.) of change categories were presented in Table 5. The highest risk significance index was resulted in "Planning and Design" according to the contractors. In general, the activities in the "Planning and Design" phases are more concerned to the owner's obligations. Besides, this category has been resulted as one of the most risky category (second highest) by consultants and project owners. In this context, the greatest importance in project organizations should be given to the planning and design process. On the other hand, Consultant-Owner was emphasized that most risky change causes were originated due to administrative based issues which are more associated with the contract management and tendering process. The bottom line is that poor planning; design and administrative structure which are all regarding with pre-construction process can trigger changes significantly and therefore have a major impact on the cost and time of the project. These findings have pointed out that, obligations of organizations in the design and tendering processes have constitutes the greatest risks on construction projects. In addition, the risk index levels in both organization characteristics were fairly close in all categories except "external".

*Table 5 - Risk Significance Index of Change Categories according to the organization types*

| | Contractor | | Consultant-owner | |
|---|---|---|---|---|
| **Change Category** | Av. R.S.I. | Rank | Av. R.S.I. | Rank |
| Planning and Design | 30.6 | 1 | 29.81 | 2 |
| Construction and Site | 26.7 | 4 | 28.17 | 4 |
| People | 28.2 | 2 | 29.77 | 3 |
| Administrative | 27.3 | 3 | 30.20 | 1 |
| External | 17.9 | 5 | 16.83 | 5 |
| Average | 26.10 | | 26.95 | |

### 4.3. Top Risky Change Factors according to the Different Countries and Regions

The top risky change factors were examined according to the opinions of organizations located in different regions. In this context, the following results were categorized and discussed according to the regions of organizations.

#### *4.3.1. North Cyprus and Turkey*

R.S.I. of change causes according to the organizations in North Cyprus-Turkey was presented in table 6. "Low contract price due to competition" which associated with bidding evaluation and tendering process was identified as the most risky change factor according to the respondents in North Cyprus and Turkey. Generally, contractors in these regions are awarded based on prices. For this reason, quantification (price) based evaluation is mostly preferred rather than qualification, and therefore owners tend to award the lowest bidder contractors. In this context, contractors are in an effort to offer the lowest bid price in order to get awarded [71]. Construction projects face many difficulties due to the low bid price contracts, such as slow progress and quality degradations [9], hereby contractors may claim changes to compensate for financial loss due to low bid price [10,11]. Changes can be a potential opportunity for the contractor's desired profitability. Additional works due to changes could be a common source for the contractors to increase earnings [10]. Thereby, contractors' financial difficulties due to lower bid may be covered by additional payments due to changes.

*Table 6 - Factors Risk Significance Index (R.S.I.) according to the Region Types*

| | | North Cyprus and Turkey | | | | | |
|---|---|---|---|---|---|---|---|
| | Causes of Change | Contractor | | Consultant - Owner | | Total | |
| | | R.S.I. | Rank | R.S.I. | Rank | R.S.I. | Rank |
| Planning And Design | Errors in Contract Drawings | 49.9 | 1 | 37.8 | 3 | 43.1 | 2 |
| | Inconsistencies between different Designs | 36.3 | 5 | 29.2 | 11 | 32.2 | 6 |
| | Errors and Inadequacy in Specification | 32.2 | 7 | 29.2 | 12 | 30.5 | 10 |
| | Conflict among contract documents | 32.2 | 6 | 36.8 | 4 | 34.6 | 5 |
| | Un-use of advanced design software | 18.3 | 21 | 13.8 | 23 | 15.9 | 23 |
| | Constructability Ignored | 25.6 | 13 | 33.9 | 6 | 29.8 | 11 |
| | Error in Cost Estimating and budgeting | 26.1 | 12 | 22.2 | 19 | 23.9 | 17 |
| | Unrealistic imposed contract duration | 21.3 | 18 | 33.2 | 8 | 27.3 | 13 |

*Table 6 - Factors Risk Significance Index (R.S.I.) according to the Region Types (continue)*

| | | North Cyprus and Turkey | | | | | |
|---|---|---|---|---|---|---|---|
| | **Causes of Change** | **Contractor** | | **Consultant - Owner** | | **Total** | |
| | | **R.S.I.** | **Rank** | **R.S.I.** | **Rank** | **R.S.I.** | **Rank** |
| Construction-Site | Inadequate site investigation in pre-construction | 31.6 | 10 | 32 | 10 | 31.8 | 9 |
| | Uncertainties / problems of Subsurface | 23.8 | 14 | 28.3 | 13 | 26.5 | 14 |
| | Provision of additional shop drawings | 32.1 | 8 | 25.6 | 16 | 28.5 | 12 |
| | Errors in execution | 14.2 | 24 | 22.4 | 18 | 18.7 | 19 |
| | Material / Equipment / Manpower shortage | 16.2 | 23 | 17.3 | 21 | 16.8 | 22 |
| | Additions / Omissions of work | 39.1 | 3 | 33.6 | 7 | 35.9 | 4 |
| People | Lack of Experience of Project Participants | 38.3 | 2 | 39.1 | 2 | 40.7 | 3 |
| | Poor communication between Parties | 28.4 | 11 | 35.8 | 5 | 32.2 | 8 |
| | Owners Level of Construction Sophistication | 21.3 | 19 | 24.2 | 17 | 22.9 | 18 |
| Administrative | Poor Contract Management | 31.9 | 9 | 32.5 | 9 | 32.2 | 7 |
| | Inappropriate choice of project delivery system | 22.2 | 16 | 27.1 | 14 | 24.8 | 16 |
| | Inappropriate choice of contract type | 21.9 | 15 | 24.9 | 15 | 25.1 | 15 |
| | Low Contract Price (Competitive Bidding) | 36.9 | 4 | 48.9 | 1 | 44 | 1 |
| External | Unforeseeable Natural Conditions | 22.1 | 17 | 16.2 | 22 | 18.6 | 20 |
| | Changes in Tax /Interest Rate / Material and Labor Cost | 19 | 20 | 13.4 | 24 | 15.9 | 24 |
| | Change in government laws/ regulations | 10.7 | 25 | 11.2 | 25 | 11 | 25 |
| | Shortening / Compression in Project Schedule | 17.4 | 22 | 18.3 | 20 | 17.9 | 21 |
| Average R.S.I. (%) | | 26.76 | | 27.48 | | 27.2 | |

Low prices can be more attractive to project owners in the short term. However, project owners may experience difficulties due to the tendency of contractors to increase incomes with additional works in the long term. At this point, potential forthcoming problems can be mitigated by choosing the most accurate contractor through a qualitative based evaluation method. In this regard, it is necessary to make legal arrangements to force on using a qualification based method in the tender process.

### *4.3.2. Change Factors in the U.S.A.*

R.S.I. of change causes according to the respondents in the U.S.A. was presented in table 7. According to the participants in the USA, the riskiest changes are caused by "discrepancies between different designs". In this context, this has been stated that the conflict between project designs is the most common cause of changes in construction projects in the USA. These kinds of problems are encountered more particularly in large-scale projects. Today, the scale and the scope of the projects are in a growing trend. Multi-functional buildings are being built with an increasing global competitive environment trend. The compatibility and integrity between different designs are being more difficult due to the increase in project complexity. Nowadays the quality and function of the contract drawings gradually become more important with the growing trend of complex designs. In this regard, the consistency of different designs becomes one of the most significant factors influencing changes due to the implementation of large-scale, multifunctional and complex projects in the global construction industry today.

At this point, it is required to enhance and develop compatibility and integrity in a project to overcome conflicts between different designs. Different designs need to be combined in one holistic design to ensure integrity. In addition, it is necessary to create an environment in which different design units can work together. For this purpose, a holistic project design unit needs to be established in the design phase of the construction project. In this regard, different design units will better be managed through holistic project design unit. It is possible to reduce such problems

*Table 7 - Factors R.S.I. according to the organization Types*

| | | U.S.A. | | | | | |
|---|---|---|---|---|---|---|---|
| | **Causes of Change** | **Contractor** | | **Consultant-Owner** | | **Total** | |
| | | **R.S.I.** | **Rank** | **R.S.I.** | **Rank** | **R.S.I.** | **Rank** |
| Planning And Design | Errors in Contract Drawings | 43.3 | 1 | 30.2 | 7 | 35.2 | 3 |
| | Inconsistencies between different Designs | 36 | 3 | 48.5 | 1 | 43.5 | 1 |
| | Errors and Inadequacy in Specification | 30.9 | 5 | 23.6 | 16 | 26.7 | 11 |
| | Conflict among contract documents | 27.9 | 9 | 27.6 | 9 | 26.9 | 10 |
| | Un-use of advanced design software | 24.6 | 13 | 21.7 | 18 | 22.9 | 17 |

*Table 7 - Factors R.S.I. according to the organization Types (continue)*

| | | U.S.A. | | | | | |
|---|---|---|---|---|---|---|---|
| | **Causes of Change** | **Contractor** | | **Consultant-Owner** | | **Total** | |
| | | **R.S.I.** | **Rank** | **R.S.I.** | **Rank** | **R.S.I.** | **Rank** |
| Planning and Design | Constructability Ignored | 27.1 | 11 | 30.2 | 6 | 28.9 | 7 |
| | Error in Cost Estimating and budgeting | 24 | 14 | 24.2 | 15 | 24.5 | 15 |
| | Unrealistic imposed contract duration | 18.8 | 21 | 26.7 | 10 | 23.6 | 16 |
| Construction-Site | Inadequate site investigation in pre-construction | 28.8 | 8 | 31.4 | 5 | 30.3 | 6 |
| | Problems of Subsurface | 21.6 | 17 | 20.1 | 20 | 20.7 | 19 |
| | Provision of additional shop drawings | 29.8 | 6 | 34.2 | 3 | 32.5 | 5 |
| | Errors in execution | 16.8 | 23 | 26.1 | 12 | 22.6 | 18 |
| | Shortage in Materials/ Equipment / Manpower | 16.7 | 24 | 16.8 | 22 | 17.1 | 23 |
| | Additions / Omissions of work | 40 | 2 | 44.1 | 2 | 42.4 | 2 |
| People | Lack of Experience of Project Participants | 26.8 | 7 | 23.2 | 17 | 25.5 | 13 |
| | Poor communication between Parties | 25.8 | 12 | 26.6 | 11 | 28 | 8 |
| | Owners Level of Construction Sophistication | 22.9 | 16 | 18.6 | 21 | 20.3 | 20 |
| Administrative | Poor Contract Management | 27.8 | 10 | 25.4 | 13 | 26.4 | 12 |
| | Inappropriate choice of project delivery system | 19.6 | 19 | 13.7 | 24 | 16.1 | 24 |
| | Inappropriate choice of contract type | 20.2 | 18 | 14.1 | 23 | 18.2 | 22 |
| | Low Contract Price | 31.2 | 4 | 32 | 4 | 33.4 | 4 |
| External | Unforeseeable Natural Conditions | 19.4 | 20 | 20.9 | 19 | 20.3 | 21 |
| | Changes in Tax / Interest Rate / Material and Labor Cost | 23.1 | 15 | 24.6 | 14 | 27.2 | 9 |
| | Change in government laws/ regulations | 9.9 | 25 | 10 | 25 | 10.1 | 25 |
| | Shortening / Compression in Project Schedule | 18.7 | 22 | 29.7 | 8 | 25.3 | 14 |
| Average R.S.I. (%) | | | 25.27 | | 25.77 | | 25.9 |

with BIM technology [34]. Today, the use of BIM in the United States is widely applied to ensure the compatibility between different project disciplines for construction projects. [74]. Different designs can be integrated easily and effectively by BIM tools. In addition, BIM tool ensures to integrate managerial information to the project design, so BIM is a powerful and effective method to enhance integrity in different design disciplines to overcome such problems in the construction industry. In this regard, it is necessary to make legal arrangements to enforce the use of the BIM tool in construction projects.

#### *4.3.3. Contractor's Perception according to the Different Regions*

Changes due to the weakness in drawings lead to the greatest risk according to the contractors in North Cyprus-Turkey and the U.S.A. In addition, these factors are constituted greater risk in Northern Cyprus and Turkey since the risk index score is much higher than in the U.S.A.

On the other hand, lack of experience of organizations and people involved in construction projects lead to one of the most risky changes in construction projects according to the contactors located in North Cyprus and Turkey, however, this factor has been stated to constitute a lower risk according to the contractors located in the U.S.A. Besides, changes that originated due to additions/omissions of work items were constituted almost the same risk level for contractors located both in North Cyprus-Turkey and the U.S.A.

#### *4.3.4. Consultant's and Owner's Perception according to the Different Regions*

The low bid price was leaded to the most risky changes according to the consultants and owners in North Cyprus-Turkey while it was emphasized to be much less risky according to the consultants and owner's in the U.S.A.

On the other hand, changes originated due to the inconsistencies between different designs that have constitutes the greatest risk in the U.S.A., while this was emphasized as to be much less risky for consultants and owners located in North Cyprus and Turkey.

### 4.4. Top Risky Change Categories on the basis of Regional Characteristics

R.S.I. of change categories according to the organizations in North Cyprus-Turkey and the U.S.A. were presented in tables 8 and 9 respectively.

#### *4.4.1. Discussion*

Most risky changes were caused due to the "Human" related factors according to the respondents in North Cyprus and Turkey whereas; this category has been stated to constitute a relatively low risk in the U.S.A because of the low R.S.I. On the other hand, changes composed due to the "Planning and Design" issues have been observed to create the same risk level in both regions since the risk index level is the same (See in table 8 and 9).

These findings show that the problem due to profile and performance of people involved in the project and project administrative status were indicated as source of very high risks in North

Cyprus and Turkey, while problems due to the design and construction execution phase has been observed as source of the greatest risky in the U.S.A. In this context, the main defects in North Cyprus and Turkey were mostly related to human and administrative defects, whereas it was observed that the main flaw in the US is mostly technical based.

*Table 8 - R.S.I. of Change Categories according to North Cyprus-Turkey*

| | **North Cyprus and Turkey** | | | | | |
|---|---|---|---|---|---|---|
| | **Contractor** | | **Consultant-Owner** | | **Overall** | |
| **Factor Group** | **Av. R.S.I.** | **Rank** | **Av. R.S.I.** | **Rank** | **Av. R.S.I.** | **Rank** |
| Planning and Design | 30.24 | 1 | 29.51 | 2 | 29.66 | 3 |
| Construction and Site | 26.17 | 4 | 26.53 | 4 | 26.37 | 4 |
| People | 29.33 | 2 | 33.03 | 3 | 31.33 | 1 |
| Administrative | 28.23 | 3 | 33.35 | 1 | 31.23 | 2 |
| External | 17.30 | 5 | 14.78 | 5 | 15.85 | 5 |
| Average | 26.25 | | 27.44 | | 26.89 | |

*Table 9 - R.S.I. of Categories according to the U.S.A*

| | **U.S.A.** | | | | | |
|---|---|---|---|---|---|---|
| | **Contractor** | | **Consultant-Owner** | | **Total** | |
| **Factor Group** | **Av. R.S.I.** | **Rank** | **Av. R.S.I.** | **Rank** | **Av. R.S.I.** | **Rank** |
| Planning and Design | 29.08 | 1 | 29.09 | 1 | 29.03 | 1 |
| Construction and Site | 25.62 | 2 | 28.78 | 2 | 27.60 | 2 |
| People | 25.17 | 3 | 22.80 | 3 | 24.27 | 3 |
| Administrative | 24.70 | 4 | 21.30 | 4 | 23.20 | 4 |
| External | 17.78 | 5 | 21.30 | 5 | 20.73 | 5 |
| Average | 24.47 | | 24.65 | | 24.96 | |

### *4.4.2. Discussion based on Contractors in Different Regions*

Most risky changes were composed due to issues in planning and design activities according to the contractors located in both regions. Contractors were also emphasized that changes originated due to the influence of the people involved in the project were constituted greater risk in North Cyprus-Turkey than the U.S.A.

On the other hand, contractors in the U.S.A. have been observed to be less concerned with respect to change risks since risk index score is rather low compared to contractors in North Cyprus and Turkey in all categories.

### *4.4.3. Discussion based on Consultant-Owner in Different Regions*

Changes due to the administrative defects were composed more risk in construction projects according to the consultants and owners located in North Cyprus and Turkey; however, this was stated to be as much less risk for consultants and owners in the USA since risk index score was fairly low in the U.S.A.

On the other hand, changes due to planning and design flaws were constituted the same risk level for consultants and owners located in North Cyprus-Turkey and the U.S.A. In addition, changes due to administrative defects are constituted of greater risk according to contractors compared to the consultants and owners located in the U.S.A.

It is known that such changes causing both cost and time overruns and this leads to serious disagreements and disputes among parties involved in construction projects. In this regard, organizations may show a stance towards their interests while stating the reason for changes. Organizations might be in an effort to be insistent that counter organizations be responsible for changes. Results obtained in the study confirm this idea. According to results, it was observed that contactors, consultants and project owners have basically headed to point out to those change factors where they subject to less responsibility.

In general, most risky changes were emphasized to be composed due to design based issues according to the contractors however; most risky changes were resulted due to the low contact price according to the consultants and owners. In general, consultants and owners have major responsibility with respect to documents of drawing while; the bid price is more relevant to the responsibilities of the contractor's organizations.

On the other hand, it has been observed that the characteristics of the regions have a significant effect when interpreting the most risky change factors. The findings showed that the top risky change factor was identified as coherent in accordance with the regional characteristics. In North Cyprus and Turkey, "Low contract price" were designated as to be riskiest change factor, whereas "Inconsistency between different design" were identified in the U.S.A. In general, organizations located in North Cyprus and Turkey are preferred to carry out the project by achieving the lowest cost rather than high quality. This is because; more importance is given to cost not a quality while selecting contractors in North Cyprus and Turkey. This finding could be interpreted that short-term success is more attractive than long-term for organizations in North Cyprus and Turkey. On the other hand, the biggest difficulties encountered in the U.S.A. are related to inconsistency between different design disciplines. Today, the most common technical challenge in construction

projects is to be an incompatibility between project disciplines due to the need for large-scale, multi-functional and complex projects in the global construction sector.

All sectors in North Cyprus are suffered from weaknesses in institutionalization and comprehensiveness. This is due to the lack of global integrity of sectors in North Cyprus as a result of the implementation of global isolation by the international community. The isolation of North Cyprus from a global trend could be attributed to this fact. Lack of integrated to global standards leads to differences in tender laws in Northern Cyprus. The way of projects are carried out is different in Northern Cyprus; this is because the administrative and technical obligations of the projects differ according to global standards. This creates differences in perception and qualities in North Cyprus organizations compared to international organizations. In this regard, great importance should be given to the concept of institutionalization and this structure needs to be developed and implemented throughout the whole project phases.

## 5. CONCLUSION

A lot of changes are experienced in construction projects carried out in North Cyprus and Turkey. The reason for so many changes in construction projects is often the lack of quality consultancy services. The quantity-based selection method is often applied in North Cyprus and Turkey and thus, poor quality of consultancy services are provided due to the fact that the technical consultants are selected based on bid price (Quantity based) rather than quality based. This fact is very effective in this regard since the quality of the project outcomes (from design to execution) is subject to the efforts of consultancy services. Nowadays, the U.S.A. as a developed country is in trend in choosing consultants by applying a quality-based selection method. In this regard, project owners in North Cyprus and Turkey should assign the consultants by applying quality based evaluation rather than quantity. Project performances are affected dramatically as a consequence of project changes and claims and thus, any organization involved in the project may be condemned to pay the cost of changes. As general terms, the findings were pointed out that, the better preparation of project documents and comprehensive organization in terms of both technical and managerial aspects prior to construction execution may significantly help to reduce change necessity and will definitely more accomplished project will be terminated. The findings in this paper has only been proved according to the ideas of the construction organizations in North Cyprus, Turkey and the U.S.A. for lump sum contracted design bid build procured building projects because of the chosen region and project characteristics. Therefore, researchers are encouraged to examine the risk level of change causes and to examine the effectiveness of change mitigation measures with respect to different regional and project characteristics.

### Symbols

AV. S.I. : Average of Cost and Time Overrun Index

R.S.I. : Risk Significance Index

AV. R.S.I. : Average Risk Significance Index

C.I. : Cost Overrun Index

F.I. : Frequency Index

I.I. : Importance Index

T.I. : Time Overrun Index

Wi : The weight assigned on Likert's scale given to each factor

Xi : Number of choice of the ith weight in the Likert's scale for the change factor

**Acknowledgments**

Authors of this study would like to thank Organizations for their participation to survey and contributions.

## References

[1] Ming, S., Sexton, M., Aouad, G., Fleming, A., Senaratne, S., Anumba, C., Industrial Report: Managing Changes in Construction Projects Retrieved, Bristol UWE: School of the Built and Natural Environment, Bristol UWE, 2004.

[2] Ibbs, W., Wong, C., Kwak, H., Project Change Management Systems, Journal of Management in Engineering, 17, (3), 159–165, 2001.

[3] Anees, M.M., Mohamed, H.E., Abdul Razek, M.E., Evaluation of change management efficiency of construction contractors, Housing and Building National Research Center, 9,(1), 77-85,2013

[4] Moselhi, O., Assem, I., El-Rayes, K., Change Orders Impact on Labor Productivity, Journal of Construction Engineering and Management, 131, (3), 354–359,2005.

[5] Alnuami, A.S., Taha, R.A., Al Mohsin, M., Al-Harthi, A.S., Causes, Effecrs, Benefits, and Remedies of Change Orders on Public Construction Projects in Oman, Journal of Construction Engineering and Management, 136, (5), 615–622, 2010.

[6] Serag, E., Oloufa, A., Malone, L., Radwan, E., Model for Quantifying the Impact of Change Orders on Project Cost for U.S. Roadwork Construction, Journal of Construction Engineering and Management, 136, (9), 1015–1027, 2010.

[7] Arditi, D. Akan, T.A., Gurdamak, S., Reasons for Delay in Public Projects in Turkey, Cosntruction Management and Economics, 3, (2), 171-181, 1985

[8] Kazaz, A., Ulubeyli, S., Tuncbilekli, N.A., Causes of Delay in Construction Projects in Turkey, Journal of Civil Engineering and Management, 18, (3), 426–435,2012.

[9] İlter, O., Çelik, T., The Effect of Project Variables on Cost and Time of Construction Projects, 5th international Project and Construction Management Conference (IPCMC2018), North Cyprus, 2018

[10] O'Brien, J.J., 1998, Construction Change Orders, New York, McGraw Hill

[11] Arain, F.M., Pheng, L.S., How Design Consultants Perceive Potential Causes of Variation Orders for Institutional Buildings in Singapore, Architectural Engineering and Design Management, 1, (3), 181-196, 2005a.

[12] Assaf, S.A., Al-Hejji, S., Causes of Delay in Large Construction Projects, International Journal of Project Management, 24, (4), 349–357, 2006.

[13] Kaming, P.F., Olomolaiye, P.O., Holt, G.D., Harris, F.C., Factors Influencing Construction Time and Cost Overruns on High-Rise Projects in Indonesia, Construction Management and Economics, 15, (1), 83–94, 1997.

[14] Zaneldin, E.K., Construction Claims in United Arab Emirates: Types, Causes and Frequency, International Journal of Project Management, 24, (5), 453–459, 2006.

[15] Ijaola, I.A., Iyagba, R.O., A comparative Study of Causes of Change Orders in Public Construction Projects in Nigeria and Oman, Journal of Emerging Trends in Economics and Management Sciences, 3, (5), 495–501, 2012.

[16] Oladapo, A.A., A Quantitative Assessment of the Cost and Time Impact of Variation Orders on Construction Projects, Journal of Engineering Design and Technology, 5, (1), 35–48, 2007.

[17] Hassanein, A.A.G., Nemr, W.E., Claims Management in the Egyptian Industrial Construction Sector: A Contractor's Perspective, Engineering, Construction and Architectural Management, 15, (5), 456–469, 2007.

[18] Enshassi, A., Arain, F., Al-Raee, S., Causes of variation orders in construction projects in the Gaza Strip, Journal of Civil Engineering and Management, 16, (4), 540–551, 2010.

[19] Stare, A., Reducing Negative Impact of Project Changes with risk and change management, Zagreb International Review of Economics & Business, 14, (2), 71- 85, 2011

[20] Arain, F.M., Pheng, L.S., The Potential Effects of Variation Orders on Institutional Buildings Projects", Facilities, 23, (11), 496–510, 2005b.

[21] Wu, C., Hsieh, T., Cheng, W., Statistical Analysis of Causes for Design Change in Highway Construction on Taiwan, International Journal of Project Management, 23, (7), 554–563, 2005.

[22] Akinsola, A.O., Potts, K.F., Ndekugri, I., Harris, F.C., Identification and Evaluation of Factors Influencing Variations on Building Project Cost, International Journal of Project Management, 15, (4), 263–267, 1997.

[23] Lu, H., Issa,R.R.A., Extended production integration for construction: a loosely coupled project model for building construction. ASCE, Journal of Computing in Civil Engineering, 19, (1), 58-68, 2005

[24] Sönmez, M.., Dikmen, S.Ü., Akbıyıklı, R., Time - Cost Relationships for Superstructure Projects in Turkey, Teknik Dergi, 31, (2), 03-01, 2020

[25] Ahbab, C.., Daneshvar, S., Çelik, T., Cost and Time Management Efficiency Assessment for Large Road Projects Using Data Envelopment Analysis, Teknik Dergi, 30, (2), 8937 – 8959, 2019

[26] Hanna, A.S., Camlic, R., Peterson, P.A., Nordheim, E.V., Quantitative Definition of Project Impacted by Change Orders, Journal of Construction Engineering and Management, 128, (1), 57-64, 2002.

[27] Hanna, A.W., Gunduz, M., Impact of Change Orders on Small Labor-Intensive Projects, Journal of Construction Engineering and Management, 130, (5), 726-733, 2004.

[28] Wambeke, B.W., Hsiang, S., Liu, M., Causes of Variation in Construction Project Task Starting Times and Duration, Journal of Construction Engineering and Management, 137, (9), 663–677, 2011.

[29] Lee, S., Tae, S., Jee, N., Shin, S., LDA-Based Model for Measuring Impact of Change Orders in Apartment Projects and Its Application for Pre Risk Assessment and Post Evaluation, Journal of Construction Engineering and Management, 141, (7), 0401501, 2015.

[30] Diekman, J., Nelson, M., Construction Claims: Frequency and Severity, Journal of Construction Engineering and Management, 111, (1), 74–81,1985

[31] Bröchner, J., Badenfelt, U., Changes and Change Management in Construction and IT Projects, Automation in Construction, 20, (7), 767–775, 2011

[32] Bakr, G.A., Studying the Status of Variations in Construction Contract in Jordan, Computing in Civil and Building Engineering, 187–194, 2014.

[33] Kocaman, E.., Kuru, M., Çalış, G., Investigating the Effect of Tendering Procedure and Contract Type on the Construction Contract Price, Teknik Dergi, 31, (1), 9789 – 9812, 2020

[34] Oyewobi, L.O., Jimon, R., Olanrewaju, B., Shittu, A.A., Analysis of causes and impact of variation order on educational building projects, Journal of Facilities Management, 14, (2), 139-164, 2016

[35] Taylor, T.R.B., Uddin, M., Goodrum, P.M., McCoy, A., Shan Y., Change Orders and Lessons Learned: Knowledge from Statistical Analyses of Engineering Change Orders on Kentucky Highway Projects, Journal of Construction Engineering and Management, 138, (12), 1360–1369, 2012

[36] Dumont, P., Gibson, G.E., Fish, J., Scope Management using project definition rating index, Journal of Management in Engineering, 13, (5), 54-60,1997

[37] Chan, D.W.M. and Kumaraswamy, M.M., a comparative study of causes of time overruns in Hong Kong construction projects, International Journal of Project Management, 15, (1), 55-63,1997

[38] Hsieh, T., Lu, S., Wu, C.,Statistical Analysis of Causes for change orders in Metropolitan Public Works, International Journal of Project Management, 22, (8),679-686,2004

[39] Memon, A.H., Rahman, I.A., Hasan, M.F.A.,Significant causes and effects of variation orders in construction projects, Research Journal of Applied Sciences,7, (21),4494-4502, 2014

[40] Motawa, I.A.,A systematic approach to modelling change processes in construction projects, The Australian Journal of Construction Economics and Building, 5,(1), 2005

[41] Love, P.E.,Edwards, D.J., Zahir,I.,Forensic project management: An exploratory examination of the causal behavior of design-induced rework, IEEE Transportation Engineering Management, 55,(2), 234-247,2008

[42] Chen,J.L.,KNN-based knowledge sharing model for severe change order disputes in construction. Automation in Construction, 17,(6),773-779,2008

[43] Sun, M., Meng, X.,Taxonomy for change causes and effects in construction projects, International journal of Project Management, 27, (6),560-572,2009

[44] Odeh, A.M., Battaineh, H.T.,Causes of construction delay: traditional contracts, International Journal of Project Management, 20, (1), 67-73,2002

[45] Lo, T.Y., Fung, I.W.H., Tung, K.C.F, Construction Delays in Hong Kong Civil Engineering Projects, Journal of Construction Engineering and Management, 132, (6), 636-649,2006

[46] Rosenfeld,Y., Root-Cause Analysis of Construction-Cost Overruns, Journal of Construction Engineering and Management,140, (1), 4013039,2013

[47] Sha'ar, K.Z., Assaf, S.A., Bambang, T., Babsail, M. and Fattah, A.M.A.El., Design-construction interface problems in large building construction projects, International Journal of Construction Management, 17,(3), 238-250, 2017

[48] Mansfield, N., Ugwu, O., Doran, T., Causes of delay and cost overruns in Nigerian construction projects. International Journal of Project Management 12, (4), 254–260,1994

[49] Doloi, H., Sawhney, A., Iyer, K.C., Rentala, S.,Analysing factors affecting delays in Indian Contruction Projects, International Journal of project management,30, (4), 479-489,2012

[50] M. Mohamad, M. Nekooie, and A. Al-Harthy, "Design changes in residential reinforced concrete buildings: The causes, sources, impacts and preventive measures," J. Constr. Dev. Ctries,17, (2), 23–44, 2012

[51] Assaf, S.A., Al-Khalil, M. and Al-Hazmi, M., Causes of delay in large building construction projects. ASCE Journal of Management in Engineering, 11(2), 45–50,1995

[52] Yap, J.B.Y., Abdul-Rahman, H., Wang, H.,Collaborative model: Managing design changes with reusable project experiences through project learning and effective communication, International Journal of Project Management, 35, (7), 1253-1271, 2017

[53] Cox, I. D., Morris, J., Rogerson, J. H., and Jared, G. E., A quantitative study of post contract award design changes in construction, Construction Management and Economics., 17,(4), 427-439,1999

[54] Cox, S. and Hamilton, A.,Architect's Job Book, 6th edn, Royal Institute of British Architects, London, RIBA Publications,1995

[55] Enshassi A., Lisk R., Sawalhi I. and Radwan I.,Contributors to construction delays in Palestine, The Journal of American institute of constructors, 27, (2), 45-53, 2003

[56] Arain, F.M., Assaf, S., Low, S.P.,Causes of Discrepancies between Design and Construction. Architectural Science Review 47, (3), 237–249, 2004

[57] Ling, F.Y.Y., Chan, S.L., Chong, E., Ee, L.P., Predicting Performance of design-Build and Design-Bid-Build Projects, Journal of Construction Engineering and Management, 30, (1), 75-83,

[58] Faridi, A.S. and El-Sayeng,S.M.,Significant factors causing delay in the UAE construction industry, Construction Management and Economics, 24,(11),1167-1176,2006

[59] Doloi, H.,Analysis of pre-qualification criteria in contractor selection and their impacts on project success, Construction Management and Economics, 27, (12),1245-1263,2009

[60] Holt, G.D., Olomolaiye, P.O., Harris, F.C.,A review of contractor selection practice in the U.K. construction industry. Building and Environment 30, (4),553–561,1995

[61] Andersen, B., Olsson, N.O.E., Onsøyen, L.E., Spjelkavik, I.,Post project changes,: occurrence, causes, and countermeasures, International Journal of Project Business, 4, (2), 308-328,2011

[62] Love, P.E., Holt, G.D., Shen, L.Y., Li, H., Irani, Z.,Using systems dynamics to better understand change and rework in construction project management systems. International Journal of Project Management 20 (6), 425–436,2002

[63] P. E. D. Love, Z. Frani, and D. J. Edwards, "A rework reduction model for construction projects," IEEE Trans. Eng. Manag., 51, (4), 426–440, 2004

[64] Sambasivan, M. and Soon, Y.W., Causes and effects of delays in Malaysian construction industry. International Journal of Project Management, 25, (5),517–26, 2007

[65] Frimpong, Y., Oluwoye, J. and Crawford, L., Causes of delay and cost overruns in construction of groundwater projects in a developing countries: Ghana as a case study. International Journal of Project Management, 21, (5), 321–6, 2003

[66] Yap, J.B.Y., Abdul-Rahman, H., Wang, C., A Conceptual Framework for Managing Design Changes in Building Construction, MATEC Web of Conferences 66, 00021, 2016

[67] Hwang, B.-G., Zhao, X., Do, T.H. Van,Influence of Trade-Level Coordination Problems on Project Productivity,Project Management Journal,45, (5), 5-14,2014

[68] Alaghbari, M.W, Razali A. Khadir, Salim Azizah, Ernawati., The significant factors causing delay of building construction projects in Malaysia. Journal of Engineering, Construction and Architectural Management,14, (2), 192-206, 2007

[69] A. Aiyetan, J. Smallwood, and W. Shakantu, "A systems thinking approach to eliminate delays on building construction projects in South Africa," Acta Structilia,18,(2),19–39, 2011

[70] İlter, O., Çelik, T., Evaluation of Change Causes in Execution Process of Construction Projects, Project and Construction Management Conference, (PYYK 2016), Eskişehir, Turkey, 2016

[71] Drew, D., Skitmore, M., The effect of contract type and size on competitiveness in bidding, Construction Management and Economics, 15, (5), 469-489,1997

[72] Tan, Y., Shen, L., Khaled, A., Song S., An Examination of the Factors Affecting Contractor's Competition Strategy: a Hong Kong Study, International Journal of Project Organization Management, 1,(1), 4-23, 2008.

[73] Crowley, L.G., Hancher, D.E., Risk assessment of competitive procurement, Journal of Construction Management, 121, (2), 230-237, 1995

[74] Bryde, D., Broquetas, M.,Volm, J.M., Daneshvar, S., Çelik, T., The Project Benefits of Building Information Modelling (BIM), International Journal of Project Management, 31, (7), 971– 980, 2013

*Teknik Dergi, 2021 11287-11314, Paper 634*

# Buckling Analysis of Symmetrically Laminated Rectangular Thin Plates under Biaxial Compression

**Erkin ALTUNSARAY**[1]
**İsmail BAYER**[2]

## ABSTRACT

In this parametric study, the buckling analysis of symmetrically laminated rectangular thin plates subjected to biaxial compression is presented. The simply supported boundary condition is considered at the edges of the symmetrically laminated quasi-isotropic, cross-ply and angle-ply plates. The Rayleigh-Ritz Method is used to specify the critical buckling load of the plates based on the Classical Laminated Plate Theory (CLPT). A convergence study is achieved by increasing the number of parameters of assumed shape function. Validation of isotropic case is verified. The effects of the lamination types, plate aspect ratios (a/b, b/a) and thickness on the critical buckling load of the laminated plates under bi-axial compression were then investigated. The results were compared with Finite Element Method (FEM) solutions performed by ANSYS software package and fairly good agreement is obtained. Non-dimensional results were tabulated and presented for practical use for designers.

**Keywords**: Bi-axial buckling, symmetrically laminated thin plate, Rayleigh-Ritz Method, Finite Element Method, parametric study.

## 1. INTRODUCTION

Laminated composite thin plates have been extensively used in a diverse field of application in engineering structures such as civil, wind, aerospace, automotive and ship hull and superstructures etc., due to their excellent high strength-to-weight ratio and modulus-to-weight ratio. Being a structural element, buckling is a significant problem for these plates. Buckling of composite plates, which is often encountered in such structures, commonly occurs at a low applied stress levels and generates large deformations. Therefore, buckling

Note:
- This paper was received onAugust 19, 2019 and accepted for publication by the Editorial Board on April 17, 2020.
- Discussions on this paper will be accepted by January 31, 2022.

• https://doi.org/10.18400/tekderg.606620

1 Dokuz Eylul University, Institute of Marine Sciences and Technology, Izmir, Turkey - erkin.altunsaray@deu.edu.tr - https://orcid.org/0000-0003-3099-6059

2 Yildiz Technical University, Department of Naval Architecture and Marine Engineering, Istanbul, Turkey bayer@yildiz.edu.tr - https://orcid.org/0000-0002-8589-671X

of composite plates is a critical problem and focusing on the buckling phenomenon is of importance.

Early studies about uniaxial and biaxial buckling analysis of laminated rectangular composite plates were carried out by several researchers [1-19] before this century. Many researchers have investigated mechanical buckling of composite rectangular plates for the last two decades. Veres and Kollar [20] carried out buckling of orthotropic plates subject to biaxial load based on the Ritz method. Biaxial buckling behavior of anisotropic rectangular plates under simply supported, clamped and mixed boundary conditions was investigated analytically, experimentally and numerically by Romeo and Ferrero [21] and results demonstrated good correlation. Narita and Turvey [22] studied the optimum lay-ups and maximum buckling loads of symmetrically laminated rectangular plates by new layer-wise optimization (LO) iterative procedure. Ni et al. [23] presented buckling behavior for rectangular laminated composite plates subjected to biaxial loading by higher-order shear deformation theory and the pb-2 Ritz method for arbitrary boundary conditions. Shukla et al. [24] performed critical buckling analysis of cross-ply and angle-ply plates under uniaxial and biaxial loading based on the first-order shear deformation theory and von-Karman-type nonlinearity for different boundary conditions. Buckling of cross-ply square plates under uniaxial and biaxial loading on the basis of a unified five-degree-of-freedom shear deformable plate theory was presented by Timarci and Aydogdu [25].

Bert and Malik [26] analyzed buckling of cross-ply plates subject to uniaxial and biaxial compression using classical laminated plate theory, third order shear deformable theory and differential quadrature method for simply supported boundary condition. Qiao and Shan [27] studied buckling analysis of rotationally restrained plates subjected to biaxial load using the Ritz method. Aktaş [28] studied buckling of carbon/epoxy laminated composite plates under biaxial loading using The Veres-Kollar approach [20] and Finite Element Method software ANSYS. Good agreement was obtained between analytical and numerical results. Latalski [29] dealt with the ply thicknesses on optimal design of multi-layered laminated plates under uniaxial and biaxial compression. Sayyad and Ghugal [30] developed a trigonometric shear and normal deformation theory for buckling of isotropic, transversely isotropic, orthotropic composite rectangular plates subject to in-plane compressive forces. Bourada et al. [31] analyzed buckling of isotropic and orthotropic plates subject to uniaxial and biaxial compression by proposing a new four variable refined plate theory. Becheri et al. [32] presented exact analytical solution of buckling analysis of symmetrically cross-ply laminated plates subject to biaxial in-plane loads. Rajanna et al. [33] examined the effect of tension and compression buckling of cross-ply and angle-ply plates with circular and square cutouts subject to biaxial in-plane varying edge loads by Finite Element Method. Belkacem et al. [34] studied buckling behavior of hybrid (carbon/glass) laminated cross-ply plates under different boundary conditions, taking account the shear effect. Topal et al. [35] focused on the maximization of the critical buckling load of angle-ply plates resting on elastic foundation subjected to compressive loads using teaching learning based optimization method (TLBO) based on the governing equations of the first order shear deformation theory. Bourada et al. [36] have investigated buckling behavior of rectangular isotropic plates under uniaxial and biaxial compression by analyzing by the first order shear deformation theory. Fellah et al. [37] have presented a novel refined shear deformation theory for the buckling analysis of thick isotropic plates. Altekin [38, 39] has investigated bending, free vibration and buckling of super-elliptical plates.

In view of the literature, the majority of the articles are concerned with critical buckling loads of mainly orthotropic rectangular plates (such as cross-ply laminates) with different theories and methods. Recently, Altunsaray and Bayer [40] investigated buckling analysis of symmetrically laminated quasi-isotropic thin rectangular plates subject to uniaxial compressive loading by Galerkin Method and Finite Difference Method based on Classical Laminated Plate Theory. The authors also used Finite Element Method software package ANSYS to compare the results. The importance of using the symmetrically laminated quasi-isotropic plates which are constructed with -45°, +45°, 0° and 90° orientations used in engineering applications was indicated in the study of Altunsaray and Bayer [40]. An advantage of the symmetric laminate is that the bending-extension coupling matrix ($B_{ij}$) is zero. Thus, symmetrically laminated plates are preferred in production because such plates remain flat after curing due to thermal strains encountered during the curing process. To the best knowledge of the authors, no comparative parametric study has been done on the biaxial buckling analysis of symmetrically laminated quasi-isotropic, cross-ply and angle-ply thin plates by using Rayleigh-Ritz method and FEM in the literature. The motivation of this paper is to study the buckling analysis of symmetrically laminated quasi-isotropic, cross-ply and angle-ply thin rectangular plates under biaxial compressive load and to estimate the influence of lamination types, aspect ratio and plate thickness on these types of plates. The plates are analyzed as they are subjected to simply supported boundary condition at the edge. Rayleigh Ritz method is used for the solution of integral equations based on the Classical Laminated Plate Theory. Finite Element Method software package ANSYS is used to compare the results.

## 2. ANALYSIS

### 2.1. Geometry of plates, material properties and lamination types

Positive rotation of principle material with local and global axes is given by Figure 1.

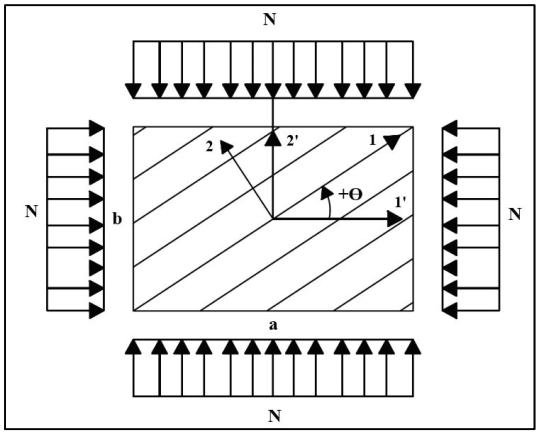


*Figure 1 - Positive Rotation of Principal Material Axes from 1'-2' Axes (1-2 local axes, 1'-2' global axes)*

Material properties of the carbon/epoxy composite, selected aspect ratios, lamination types and bending stiffness matrix are given in Tables 1, 2, 3 and 4, respectively. All laminated plates are symmetric, Quasi-isotropic plates have four different sequences (−45°, 0°, 45° and 90°), Cross-ply laminated plates consist of two different sequences (0° and 90°) and Angle-ply laminates have two different sequences (-45° and 45°). Thickness of each lamina (t) is equal to 0.2 mm thus the total thickness of a laminated plate is equal to 3.2 mm.

*Table 1 - Material properties of carbon/epoxy (T300-934) [41]*

| | |
|---|---|
| Longitudinal Young Modulus ($E_{11}$) | $148x10^9$ ($N/m^2$) |
| Transversal Young Modulus ($E_{22}$) | $9.65x10^9$ ($N/m^2$) |
| Longitudinal Shear Modulus ($G_{12}$) | $4.55x10^9$ ($N/m^2$) |
| Longitudinal Poisson ratio ($\nu_{12}$) | 0.3 |
| Lamina thickness (t) | $0.185x10^{-3}$ – $0.213x10^{-3}$ (m) |

*Table 2 - Aspect ratios*

| | | | | | | |
|---|---|---|---|---|---|---|
| **a/b** | 1 | 1.2 | 1.4 | 1.6 | 1.8 | 2 |
| **b/a** | 1 | 1.2 | 1.4 | 1.6 | 1.8 | 2 |

*Table 3 - Symmetrically laminated composite plate types*

| | | | |
|---|---|---|---|
| **LT1** | $[-45_2/0_2/45_2/90_2]_s$ | **LT15** | $[45_2/0_2/-45_2/90_2]_s$ |
| **LT2** | $[-45_2/0_2/90_2/45_2]_s$ | **LT16** | $[45_2/0_2/90_2/-45_2]_s$ |
| **LT3** | $[-45_2/45_2/0_2/90_2]_s$ | **LT17** | $[45_2/9_{02}/-45_2/0_2]_s$ |
| **LT4** | $[-45_2/45_2/90_2/0_2]_s$ | **LT18** | $[45_2/90_2/0_2/-45_2]_s$ |
| **LT5** | $[-45_2/90_2/0_2/45_2]_s$ | **LT19** | $[90_2/-45_2/0_2/45_2]_s$ |
| **LT6** | $[-45_2/90_2/45_2/0_2]_s$ | **LT20** | $[90_2/-45_2/45_2/0_2]_s$ |
| **LT7** | $[0_2/-45_2/45_2/90_2]_s$ | **LT21** | $[90_2/0_2/-45_2/45_2]_s$ |
| **LT8** | $[0_2/-45_2/90_2/45_2]_s$ | **LT22** | $[90_2/0_2/45_2/-45_2]_s$ |
| **LT9** | $[0_2/45_2/-45_2/90_2]_s$ | **LT23** | $[90_2/45_2/-45_2/0_2]_s$ |
| **LT10** | $[0_2/45_2/90_2/-45_2]_s$ | **LT24** | $[90_2/45_2/0_2/-45_2]_s$ |
| **LT11** | $[0_2/90_2/-45_2/45_2]_s$ | **LT25** | $[0_2/90_2/0_2/90_2]_s$ |
| **LT12** | $[0_2/90_2/45_2/-45_2]_s$ | **LT26** | $[90_2/0_2/90_2/0_2]_s$ |
| **LT13** | $[45_2/-45_2/0_2/90_2]_s$ | **LT27** | $[-45_2/45_2/-45_2/45_2]_s$ |
| **LT14** | $[45_2/-45_2/90_2/0_2]_s$ | **LT28** | $[45_2/-45_2/45_2/-45_2]_s$ |

When the laminate is symmetrical with respect to the mid-plane, it is referred to be a symmetrical laminate. Notation of the layup in LT1 $[-45_2/0_2/45_2/90_2]_s$ plate is given by Figure 2.

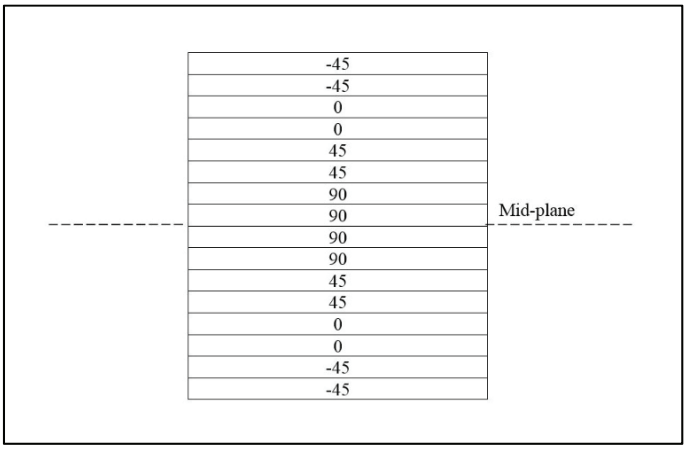


*Figure 2 - Notation of the layup in LT1* $[-45_2/0_2/45_2/90_2]_s$ *plate*

*Table 4 - Bending stiffness matrix of isotropic and symmetrically laminated plate types*

| **Plate Types** | **Bending Stiffness Matrix** | **Explanations** |
|---|---|---|
| Isotropic (single isotropic layer) | $\begin{bmatrix} D & \nu D & 0 \\ \nu D & D & 0 \\ 0 & 0 & \frac{(1-\nu)}{2}D \end{bmatrix}$ | $( D_{11} = D_{22} = D )$ |
| Symmetrical Orthotropic (Cross-Ply)<br>Example: LT25= $[0_2/90_2/0_2/90_2]_s$ ,<br>LT26= $[90_2/0_2/90_2/0_2]_s$ | $\begin{bmatrix} D_{11} & D_{12} & 0 \\ D_{12} & D_{22} & 0 \\ 0 & 0 & D_{66} \end{bmatrix}$ | $( D_{16} = D_{26} = 0 )$ |
| Symmetrical Angle-ply<br>Example: LT27= $[-45_2/45_2/-45_2/45_2]_s$ ,<br>LT28=$[45_2/-45_2/45_2/-45_2]_s$ | $\begin{bmatrix} D_{11} & D_{12} & D_{16} \\ D_{12} & D_{22} & D_{26} \\ D_{16} & D_{26} & D_{66} \end{bmatrix}$ | $( D_{11} = D_{22} , D_{16} = D_{26})$ |
| Symmetrical Quasi-isotropic<br>Example: LT1=$[-45_2/0_2/45_2/90_2]_s$ | $\begin{bmatrix} D_{11} & D_{12} & D_{16} \\ D_{12} & D_{22} & D_{26} \\ D_{16} & D_{26} & D_{66} \end{bmatrix}$ | $( D_{16} = D_{26} )$ |

Bending stiffness matrix of isotropic and symmetrically laminated plate types are given in Table 4. It can be seen from the Table 4, bend-twist coupling terms are equal zero ($D_{16}$=$D_{26}$=0) for Isotropic and Cross-Ply plates, while these terms are different from zero for Angle-ply and Quasi-isotropic plates. Bending stiffness matrix elements ($D_{11} = D_{22}$) of Angle-ply plates are similar to isotropic plates. Explanations are given in Section 3.1 in detail.

### 2.2. Approximate solution methods in stability analysis of plates

Exact analytical solutions for certain geometries and boundary conditions are possible with methods such as Navier or Levy. Approximate solution methods such as Galerkin Method, which is one of the weighted residual methods, Rayleigh-Ritz Method which is one of the variational methods and Finite Element Method is one of the powerful numerical solution techniques can be used for different situations.

The mathematical model in the differential equation form can be solved by the Galerkin method, while the model in the form of integral equation can be solved by the Rayleigh-Ritz method. When the same trial function is used, the results obtained by Rayleigh-Ritz and Galerkin Method are identical.

The Rayleigh-Ritz method is based on the principle of minimum potential energy. An approximate trial function that satisfies the geometric boundary conditions of the system is selected and placed in the total potential energy equation. Then, the total potential energy is minimized with respect to the unknown coefficients of the approximate trial function, which gives a linear homogenous equation system. The determinant of the coefficient matrix should be equal to zero for a non-trivial solution, which leads to a characteristic equation involving a polynomial. Finally, the lowest critical buckling load may be found by the smallest root of this equation.

Galerkin method is another form of the Ritz Method. For the Galerkin method, the governing differential equation for the problem is needed. First, an approximate deflection function including unknown coefficients and shape functions is chosen. When the selected approximate deflection function is placed into the governing differential equation, there will be a remaining part different from zero which is called 'residual'. The Galerkin method minimizes the sum of the product of this residual by the shape functions over the entire region of the problem. The rest of the problem will be similar to R-R method mentioned above [42].

In the Finite Element Method, the system is divided into a finite number of elements (meshing). Each of the elements that make up the system is called a finite element and the corner points where they join are called nodal points. The deformation of the finite element surface is expressed depending on the displacement parameters (displacement components, displacement vectors such as displacement components, rotations and torsional curves). Thousands of nodes are often needed to achieve a reasonably accurate solution, so using a computer is inevitable. In general, the accuracy of the solution increases as the number of elements (and nodes) increases at the expense of calculation time [43,44].

In this parametric study, the Rayleigh-Ritz Method, an energy method which is one of the approximate solution methods, and ANSYS [45] software based on Finite Element Method developed since 1969 were used.

### *2.2.1. Isotropic Plate Case and Applying of the Rayleigh-Ritz Method*

According to energy approach the strain energy of isotropic plate is given below [46]

$$U = \frac{1}{2}\int_0^a \int_0^b \left[ D\left( \left( \frac{\partial^2 w}{\partial x^2} + \frac{\partial^2 w}{\partial y^2} \right)^2 - 2\,(1-\upsilon)\left( \left( \frac{\partial^2 w}{\partial x^2} \right)\left( \frac{\partial^2 w}{\partial y^2} \right) \left( \frac{\partial^2 w}{\partial x \partial y} \right)^2 \right) \right) \right] dx\, dy \tag{1}$$

Potential energy of the plate due to $N_x$ and $N_y$

$$V = -\frac{1}{2}\int_0^a \int_0^b \left[ N_x \left( \frac{\partial w}{\partial x} \right)^2 + N_y \left( \frac{\partial w}{\partial y} \right)^2 \right] dx\, dy \tag{2}$$

$$N_x = \gamma\, N_y \tag{3}$$

where $\gamma = 0$ for uniaxial loading and $\gamma = 1$ for bi-axial compressive loading ($N_x = N_y$). For this study $\gamma = 1$ is assumed and hence:

$$V = -\frac{1}{2}\int_0^a \int_0^b N \left( \left( \frac{\partial w}{\partial x} \right)^2 + \left( \frac{\partial w}{\partial y} \right)^2 \right) dx\, dy \tag{4}$$

The potential energy functional is given below

$$F=U+V \tag{5}$$

Substituting Eq. 1 and Eq. 4 into Eq. 5, the total potential energy is

$$F = \frac{1}{2}\int_0^a \int_0^b \left[ D\left( \left( \frac{\partial^2 w}{\partial x^2} + \frac{\partial^2 w}{\partial y^2} \right)^2 - 2\,(1-\upsilon)\left( \left( \frac{\partial^2 w}{\partial x^2} \right)\left( \frac{\partial^2 w}{\partial y^2} \right) \left( \frac{\partial^2 w}{\partial x \partial y} \right)^2 \right) \right) \right] dx\, dy$$

$$-\frac{1}{2}\int_0^a \int_0^b N \left( \left( \frac{\partial w}{\partial x} \right)^2 + \left( \frac{\partial w}{\partial y} \right)^2 \right) dx\, dy \tag{6}$$

Boundary conditions at edges of the plate;

(i) Simply supported; as the edges are free to rotate, the moment $M_x$ or $M_y$ must be zero,

$$w = M_x = \frac{\partial^2 w}{\partial x^2} = 0 \quad \text{at x = 0 and x = a} \tag{7}$$

$$w = M_y = \frac{\partial^2 w}{\partial y^2} = 0 \quad \text{at y = 0 and y = b} \tag{8}$$

(ii) Clamped edges; as the edges cannot rotate, the first derivative of w with respect to x and y must be zero,

$$w = \frac{\partial w}{\partial x} = 0 \quad \text{at x = 0 and x = a} \tag{9}$$

$$w = \frac{\partial w}{\partial y} = 0 \text{ at y = 0 and y = b} \tag{10}$$

Deflection function which satisfies the boundary conditions is given below;

$$\phi_{mn} = Xm.Yn = \sin\left(\frac{m\pi x}{a}\right)\sin\left(\frac{n\pi y}{b}\right) \quad \text{(for all edges simply supported)} \tag{11}$$

$$\phi_{mn} = Xm.Yn = x^{2m}(a-x)^{2m}y^{2n}(b-y)^{2n} \quad \text{(for all edges clamped)} \tag{12}$$

$$w(x,y) = \sum_{m=1}^{M}\sum_{n=1}^{N} C_{mn}\,\phi_{mn} \tag{13}$$

In order to find the lowest set of critical buckling loads, Equation (6) is minimized with respect to the coefficients $C_{mn}$

$$\frac{\partial F}{\partial C_{mn}} = 0 \tag{14}$$

Then, the following equation is obtained:

$$[K - \lambda_b M_b]\{C_{mn}\} = 0 \tag{15}$$

where $\lambda_b$ is the buckling load parameter including material properties, characteristic dimensions and in-plane uniform load of the plate. **K** is the stiffness matrix related with the strain energy and $M_b$ is the mass matrix related to potential energy. This is a generalized eigenvalue problem. For a non-trivial solution, the determinant of the coefficient matrix should be equal to zero:

$$|K - \lambda_b M_b| = 0 \tag{16}$$

Solution of equation (16) leads to a characteristic equation involving a polynomial, whose degree depends on the number of the terms of the deflection function, in $\lambda_b$, from which the lowest critical buckling loads ($N_{cr}$) may be found.

### *2.2.2. Symmetrically Laminated Composite Plate Cases and Applying of the Rayleigh-Ritz Method*

In this study buckling of symmetrically laminated Cross-Ply, Angle-Ply and Quasi-Isotropic thin plates were investigated based on the Classical Laminated Plate Theory (CLPT).

The strain energy (U) of the symmetrically laminated plate is given by the following [47]:

$$U = \frac{1}{2}\int_0^a \int_0^b \begin{bmatrix} D_{11}\left(\frac{\partial^2 w}{\partial x^2}\right)^2 + 2D_{12}\left(\frac{\partial^2 w}{\partial x^2}\right)\left(\frac{\partial^2 w}{\partial y^2}\right) + D_{22}\left(\frac{\partial^2 w}{\partial y^2}\right)^2 \\ +4D_{16}\left(\frac{\partial^2 w}{\partial x^2}\right)\left(\frac{\partial^2 w}{\partial x \partial y}\right) + 4D_{26}\left(\frac{\partial^2 w}{\partial y^2}\right)\left(\frac{\partial^2 w}{\partial x \partial y}\right) + 4D_{66}\left(\frac{\partial^2 w}{\partial x \partial y}\right)^2 \end{bmatrix} dx\,dy \tag{17}$$

Where $D_{11}$, $D_{12}$, $D_{22}$, $D_{16}$, $D_{26}$ and $D_{66}$ indicate the elements of bending stiffness matrix $D_{ij}$ which are found by the following [47]:

$$D_{ij} = \frac{1}{3}\sum_{k=1}^{n} \overline{Q}_{ij}^{k} (z_{k+1}^3 - z_k^3) \tag{18}$$

Where, $\overline{Q_{ij}}$ , n, $z_k$ and $z_{k-1}$ indicate the transformed reduced stiffness matrix, total number of plies and distance from the reference plane respectively [47]. The components of transformed reduced stiffness matrix, $\overline{Q_{ij}}$ , calculated for each lamina is:

$$\begin{aligned}
\overline{Q}_{11} &= Q_{11}c^4 + 2(Q_{12} + 2Q_{66})s^2c^2 + Q_{22}s^4 \\
\overline{Q}_{12} &= (Q_{11} + Q_{22} - 4Q_{66})s^2c^2 + Q_{12}(s^4 + c^4) \\
\overline{Q}_{22} &= Q_{11}s^4 + 2(Q_{12} + 2Q_{66})s^2c^2 + Q_{22}c^4 \\
\overline{Q}_{16} &= (Q_{11} - Q_{12} - 2Q_{66})sc^3 + (Q_{12} - Q_{22} + 2Q_{66})s^3c \\
\overline{Q}_{26} &= (Q_{11} - Q_{12} - 2Q_{66})s^3c + (Q_{12} - Q_{22} + 2Q_{66})sc^3 \\
\overline{Q}_{66} &= (Q_{11} + Q_{22} - 2Q_{12} - 2Q_{66})s^2c^2 + Q_{66}(s^4 + c^4)
\end{aligned} \tag{19}$$

Where c=cos(θ) and s=sin(θ) respectively. The reduced stiffness matrix elements, $Q_{ij}$, are given below:

$$\begin{aligned}
Q_{11} &= \frac{E_{11}}{1-\nu_{12}\nu_{21}}, \\
Q_{12} &= \frac{\nu_{12}E_{11}}{1-\nu_{12}\nu_{21}}, \\
Q_{22} &= \frac{E_{22}}{1-\nu_{12}\nu_{21}}, \\
Q_{66} &= G_{12}
\end{aligned} \tag{20}$$

For symmetrically laminated composite plate cases, only the simply supported boundary condition at the all four edges of plates is considered. Then the lowest critical buckling loads ($N_{cr}$) can be found as applying the same procedure as the isotropic case in Section 2.2.1.

### *2.2.3. Finite Element Method (FEM) software package ANSYS*

In this study, in order to compare the results obtained by Rayleigh-Ritz Method, Finite Element Method software ANSYS was used and the numerical results were given in Table 11, 12 and 13. It can be seen that the results of the two methods are correlated. Then, the non-dimensional results calculated by Rayleigh-Ritz Method and are presented in Table 14 and 15 to give practical data for designers.

A four nodal point shell element (SHELL 181) with six degrees of freedom at each node (see Figure 3) was used in finite element software package ANSYS [45]. SHELL181 element,

which is capable of modeling up to 250 plies, was selected for layered applications. The accuracy in modeling composite shells is governed by the first-order shear-deformation theory [45].

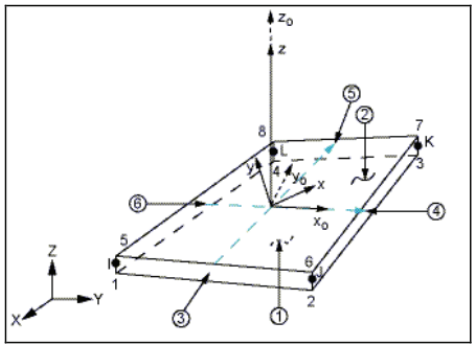


*Figure 3 - Four nodal point rectangular shell element SHELL181 (ANSYS, 2019)*

For meshing geometry, the rectangular element size was taken as 0.01 m. x 0.01 m. (Small edge of plate / Length of SHELL181 finite element=20). There are 400 elements in square plates (a/b=b/a=1) and 800 elements in rectangular plates (a/b=b/a=2). Convergence study with the number of finite elements is given in Table 5. The ratio of "Small edge of plate / Length of SHELL181 finite element" was taken to be 20 in order to obtain good convergence and high accuracy with low computational time.

*Table 5 - Convergence study with increasing number of finite elements for* LT1 $[-45_2/0_2/45_2/90_2]_s$ *plate*

| | **Critical buckling load Ncr (N/m)** | | | | | | |
|---|---|---|---|---|---|---|---|
| | **Small edge of plate / Length of SHELL181 finite element** | | | | | | |
| | **2** | **4** | **8** | **10** | **20** | **40** | **50** |
| **a/b** | Ncr (N/m) | Ncr (N/m) | Ncr (N/m) | Ncr (N/m) | **Ncr (N/m)** | Ncr (N/m) | Ncr (N/m) |
| **1** | 150604 | 93301 | 84726 | 83781 | **82537** | 82224 | 82186 |
| **2** | 58495 | 42770 | 40016 | 39706 | **39297** | 39194 | 39181 |

## 3. RESULTS

### 3.1. Isotropic plate case

A convergence study was done for the all edges simply supported case of isotropic plates. The results obtained by R-R method were compared with the results given in [48]. It can be seen from Table 6 that a convergence is observed after the 2nd terms (Table 5).

The critical buckling load equation obtained for the bi-axial buckling condition is given below [48]:

$$N_{cr} = \frac{\pi^2 D}{b^2}\left[1 + \left(\frac{b}{a}\right)^2\right] \tag{21}$$

The critical buckling load for isotropic plates may be found by equation (22). It can be noticed that when the aspect ratios a/b = b/a, the results will be equal . However, the situation is different in symmetrically laminated composite plates, which can be seen from the critical buckling load equation presented in Table 10.

$$N_{cr} = \frac{b^4 D_{11}\pi^2 + 2a^2 b^2 D_{12}\pi^2 + a^4 D_{22}\pi^2 + 4a^2 b^2 D_{66}\pi^2}{a^2 b^2 (a^2 + b^2)} \tag{22}$$

In this equation, while the coefficient of $a^4$ is $D_{22}$, and that of $b^4$ is $D_{11}$. Elements of bending stiffness matrix $D_{11}$ and $D_{22}$ are not equal for Cross-Ply laminated plates (LT25 and LT26) and Quasi-isotropic laminated plates (LT1-LT24) except Angle-Ply laminated plates (LT27 and LT28) in Table 8. Hence, if only a=b, the $N_{cr}$ (Equation.22) gives the same result, and the results for the different edge ratios of a and b are different for symmetrically laminated composite plate cases (Cross-Ply and Quasi-isotropic plates).

A comparison for the clamped case was not achieved for isotropic plates, because no results were found for this particular case in the literature, so no results were obtained by ANSYS software either. However, a convergence is observed in this present study for the all edges clamped case, which can be observed after the 3rd term (Table 7).

For the deflection function, a trigonometric trial function for the simply supported condition was selected, while an algebraic polynomial trial function given in Section 2.2.1 was selected for the clamped support condition.

$$\phi_{mn} = Xm.Yn = \sin\left(\frac{m\pi x}{a}\right)\sin\left(\frac{n\pi y}{b}\right) \tag{11}$$

$$\phi_{mn} = Xm.Yn = x^{2m}(a-x)^{2m}y^{2n}(b-y)^{2n} \tag{12}$$

*Table 6 - Convergence study of isotropic plates with all edges are simply supported*

| **Critical buckling load Ncr** | | | | | |
|---|---|---|---|---|---|
| **a/b** | **Ventsel and Krauthammer,2001 [48]** | **Present (Rayleigh-Ritz)** | | | |
| | | **1 term** | **2 terms** | **3 terms** | **4 terms** |
| **1** | 19,7392 D | 20,8000 D | 19,7392 D | 19,7392 D | 19,7392 D |
| **1,2** | 16,7235 D | 17,9308 D | 16,7235 D | 16,7235 D | 16,7235 D |
| **1,4** | 14,9051 D | 16,5957 D | 14,9051 D | 14,9051 D | 14,9051 D |
| **1,6** | 13,7249 D | 15,9579 D | 13,7249 D | 13,7249 D | 13,7249 D |
| **1,8** | 12,9158 D | 15,6553 D | 12,9158 D | 12,9158 D | 12,9158 D |
| **2** | 12,3370 D | 15,5200 D | 12,3370 D | 12,3370 D | 12,3370 D |

For the simply supported case of isotropic plates, even though the m and n values increase, the results remain the same after 2nd term. It is thought that it may be as a result of the trigonometric shape function which is widely used in the literature. The same situation is observed in the convergence analysis results given in Table 9 for symmetrically laminated composite plates.

*Table 7 - Convergence study of isotropic plates with all edges are clamped*

| **Critical buckling load Ncr** | | | | |
|---|---|---|---|---|
| | **Present (Rayleigh-Ritz)** | | | |
| **a/b** | **1 term** | **2 terms** | **3 terms** | **4 terms** |
| **1** | 54,0000 D | 53,2226 D | 52,5145 D | 52,5145 D |
| **1,2** | 46,5765 D | 46,0815 D | 45,2341 D | 45,2341 D |
| **1,4** | 43,1583 D | 42,7891 D | 41,7908 D | 41,7908 D |
| **1,6** | 41,5523 D | 41,2406 D | 40,0979 D | 40,0979 D |
| **1,8** | 40,8120 D | 40,5229 D | 39,2512 D | 39,2512 D |
| **2** | 40,5000 D | 40,2112 D | 38,8304 D | 38,8304 D |

### 3.2. Symmetrically laminated composite plates cases

#### *3.2.1. Elements of bending stiffness matrix of lamination types*

Elements of bending stiffness matrix of 28 different lamination types calculated by CLPT given are in Table 8.

*Table 8 – Elements of bending stiffness matrix of 28 different lamination types*

| | **$D_{11}$** (N.m) | **$D_{12}$** (N.m) | **$D_{16}$** (N.m) | **$D_{22}$** (N.m) | **$D_{26}$** (N.m) | **$D_{66}$** (N.m) |
|---|---|---|---|---|---|---|
| **LT1** | 206,80 | 71,10 | -44,53 | 99,92 | -44,53 | 75,58 |
| **LT2** | 197,60 | 62,49 | -53,44 | 126,35 | -53,44 | 66,96 |
| **LT3** | 153,95 | 88,33 | -26,72 | 118,33 | -26,72 | 92,80 |
| **LT4** | 118,33 | 88,33 | -26,72 | 153,95 | -26,72 | 92,80 |
| **LT5** | 126,35 | 62,49 | -53,44 | 197,60 | -53,44 | 66,96 |
| **LT6** | 99,92 | 71,10 | -44,53 | 206,80 | -44,53 | 75,58 |
| **LT7** | 286,08 | 45,27 | -17,81 | 72,32 | -17,81 | 49,74 |
| **LT8** | 276,88 | 36,66 | -26,72 | 98,74 | -26,72 | 41,13 |
| **LT9** | 286,08 | 45,27 | 17,81 | 72,32 | 17,81 | 49,74 |

*Table 8 – Elements of bending stiffness matrix of 28 different lamination types (continue)*

| | $D_{11}$ (N.m) | $D_{12}$ (N.m) | $D_{16}$ (N.m) | $D_{22}$ (N.m) | $D_{26}$ (N.m) | $D_{66}$ (N.m) |
|---|---|---|---|---|---|---|
| **LT10** | 276,88 | 36,66 | 26,72 | 98,74 | 26,72 | 41,13 |
| **LT11** | 258,47 | 19,43 | -8,91 | 151,59 | -8,91 | 23,91 |
| **LT12** | 258,47 | 19,43 | 8,91 | 151,59 | 8,91 | 23,91 |
| **LT13** | 153,95 | 88,33 | 26,72 | 118,33 | 26,72 | 92,80 |
| **LT14** | 118,33 | 88,33 | 26,72 | 153,95 | 26,72 | 92,80 |
| **LT15** | 206,80 | 71,10 | 44,53 | 99,92 | 44,53 | 75,58 |
| **LT16** | 197,60 | 62,49 | 53,44 | 126,35 | 53,44 | 66,96 |
| **LT17** | 99,92 | 71,10 | 44,53 | 206,80 | 44,53 | 75,58 |
| **LT18** | 126,35 | 62,49 | 53,44 | 197,60 | 53,44 | 66,96 |
| **LT19** | 98,74 | 36,66 | -26,72 | 276,88 | -26,72 | 41,13 |
| **LT20** | 72,32 | 45,27 | -17,81 | 286,08 | -17,81 | 49,74 |
| **LT21** | 151,59 | 19,43 | -8,91 | 258,47 | -8,91 | 23,91 |
| **LT22** | 151,59 | 19,43 | 8,91 | 258,47 | 8,91 | 23,91 |
| **LT23** | 72,32 | 45,27 | 17,81 | 286,08 | 17,81 | 49,74 |
| **LT24** | 98,74 | 36,66 | 26,72 | 276,88 | 26,72 | 41,13 |
| **LT25** | 287.7687 | 7.9519 | 0 | 145.2620 | 0 | 12.4245 |
| **LT26** | 145.2620 | 7.9519 | 0 | 287.7687 | 0 | 12.4245 |
| **LT27** | 124.6582 | 99.8091 | -35.6267 | 124.6582 | -35.6267 | 104.2817 |
| **LT28** | 124.6582 | 99.8091 | 35.6267 | 124.6582 | 35.6267 | 104.2817 |

### *3.2.2. Convergence study for composite plates*

For the study of the convergence of results, critical buckling load of LT1 ($[-45_2/0_2/45_2/90_2]_s$) a plate with simply supported boundary condition is investigated. The shape functions with increasing terms were employed in order to reach convergence and the results are given in Table 9. It can be noticed from Table 9 that the convergence achieved is sufficient, if a shape function with 4 terms is selected. Four-term solutions are of more economical computational time than those of six or nine terms. Additionally, another important reason for why calculation with 4 terms is preferred, as shown in Table 10, is that bending-twisting coupling terms $D_{16}$ and $D_{26}$ are not included in the calculation with 3 terms, while they are included in 4-term calculation. Thus, this shape function with four terms will be used for all calculations in the rest of the study. The effect of bending-twisting coupling terms $D_{16}$ and $D_{26}$ for critical

buckling loads of plates demonstrated in Table 11. From the results it seems that bending-twisting coupling-terms decrease the critical buckling load.

*Table 9 - Convergence study of LT1 plate for aspect ratio=a/b=1 (* Xm=sin(m.Pi.x/a), Yn=sin(n.Pi.y/b) *)*

| **Critical buckling load Ncr (N/m)** | | | |
|---|---|---|---|
| **m/ n** | **1** | **2** | **3** |
| **1** | **1 term** | **2 terms** | **3 terms** |
| | X1.Y1 | X1.Y1+X1.Y2 | X1.Y1+X1.Y2+X1.Y3 |
| | 92680,5 | 92680,5 | 92680,5 |
| **2** | **2 terms** | **4 terms** | **6 terms** |
| | X1.Y1+X2.Y1 | X1.Y1+X2.Y1+X2.Y1+X2.Y2 | X1.Y1+X1.Y2+X1.Y3+X2.Y1+X 2.Y2 +X2.Y3 |
| | 92680,5 | 87154,6 | 86848,6 |
| **3** | **3 terms** | **6 terms** | **9 terms** |
| | X1.Y1+X2.Y1 +X3.Y1 | X1.Y1+X1.Y2+ X2.Y1+X2.Y2 +X3.Y1 +X3.Y2 | X1.Y1+X2.Y1+X3.Y1+X2.Y1+X 2.Y2 +X3.Y3+X3.Y1+X3.Y2+X3.Y3 |
| | 92680,5 | 87003,5 | 86286.9 |

*Table 10 - Comparison of three and four terms solution of critical buckling load of LT1 Plate*

| **Terms** | **Computations of critical buckling load Ncr (N/m) by Mathematica** | **a/b=1** |
|---|---|---|
| **3** | $\left\{\left\{N \to \frac{b^4 D11 \pi^2 + 2 a^2 b^2 D12 \pi^2 + a^4 D22 \pi^2 + 4 a^2 b^2 D66 \pi^2}{a^2 b^2 \left(a^2 + b^2\right)}\right\}\right\}$ | 92680.5 |
| **4** | $\left\{\left\{N \to \frac{1}{2\left(81 a^8 b^4 + 162 a^6 b^6 + 81 a^4 b^8\right)} \left(405 a^4 b^6 D11 \pi^2 + 405 a^2 b^8 D11 \pi^2 + 810 a^6 b^4 D12 \pi^2 + 810 a^4 b^6 D12 \pi^2 + 405 a^8 b^2 D22 \pi^2 + 405 a^6 b^4 D22 \pi^2 + 1620 a^6 b^4 D66 \pi^2 + 1620 a^4 b^6 D66 \pi^2 - \sqrt{\left(-405 a^4 b^6 D11 \pi^2 - 405 a^2 b^8 D11 \pi^2 - 810 a^6 b^4 D12 \pi^2 - 810 a^4 b^6 D12 \pi^2 - 405 a^8 b^2 D22 \pi^2 - 405 a^6 b^4 D22 \pi^2 - 1620 a^6 b^4 D66 \pi^2 - 1620 a^4 b^6 D66 \pi^2\right)^2 - 4\left(81 a^8 b^4 + 162 a^6 b^6 + 81 a^4 b^8\right)\left(-102\,400 a^2 b^6 D16^2 - 204\,800 a^4 b^4 D16 D26 - 102\,400 a^6 b^2 D26^2 + 324 b^8 D11^2 \pi^4 + 1296 a^2 b^6 D11 D12 \pi^4 + 1296 a^4 b^4 D12^2 \pi^4 + 648 a^4 b^4 D11 D22 \pi^4 + 1296 a^6 b^2 D12 D22 \pi^4 + 324 a^8 D22^2 \pi^4 + 2592 a^2 b^6 D11 D66 \pi^4 + 5184 a^4 b^4 D12 D66 \pi^4 + 2592 a^6 b^2 D22 D66 \pi^4 + 5184 a^4 b^4 D66^2 \pi^4\right)\right)\right)\right\}\right\}$, | 87154.6 |

*Table 11 - Effect of bending-twisting coupling terms ($D_{16}$, $D_{26}$) for critical buckling load Ncr*

| 4 terms solution (a/b=1) | | | | Critical buckling load Ncr (N/m) | |
|---|---|---|---|---|---|
| | | | | with $D_{16}$ and $D_{26}$ terms | neglecting $D_{16}$ and $D_{26}$ terms ($D_{16}$= $D_{26}$=0) |
| | | LT25 | LT26 | 61516 | 61516 |
| LT11 | LT12 | LT21 | LT22 | 66872 | 67183 |
| LT8 | LT10 | LT19 | LT24 | 73224 | 75682 |
| LT7 | LT9 | LT20 | LT23 | 78891 | 79932 |
| LT2 | LT5 | LT16 | LT18 | 80182 | 88431 |
| LT1 | LT6 | LT15 | LT17 | 87155 | 92681 |
| LT3 | LT4 | LT13 | LT14 | 99333 | 101180 |
| | | LT27 | LT28 | 103747 | 106846 |

### *3.2.3. Effect of thickness*

Critical buckling loads of symmetrically laminated rectangular plates for three different thicknesses (3.2, 4.8 and 6.4 mm) and six aspect ratios (a/b and b/a) were investigated and the results are presented in Table 12. It can be seen from the results that the critical buckling loads increase with the increase of the plate thickness. It can be noticed from Table 12 that the critical buckling loads decrease with the increase of the aspect ratio. From the tabulated results, differences between the results of Rayleigh-Ritz and FEM (ANSYS) grow with the increases of the thickness. In this study, because thin plates (t=3.2 mm) are studied, Classical Laminated Plate Theory (CLPT) is suitable. For thicker plates, shear deformable plate theories should be considered.

*Table 12 - Critical buckling load $N_{cr}$ (N/m) of different thinner or thicker plates*

| a/b | Critical buckling load (N/m) | | | | | |
|---|---|---|---|---|---|---|
| | $[-45_2/0_2/45_2/90_2]s$ | | $[-45_3/0_3/45_3/90_3]s$ | | $[-45_4/0_4/45_4/90_4]s$ | |
| | t=3.2 mm | | t=4.8 mm | | t=6.4 mm | |
| | Rayleigh-Ritz | FEM(ANSYS) | Rayleigh-Ritz | FEM(ANSYS) | Rayleigh-Ritz | FEM(ANSYS) |
| 1,0 | 87155 | 82537 | 291181 | 275262 | 698266 | 641889 |
| 1,2 | 69227 | 65368 | 229920 | 218516 | 552296 | 511192 |
| 1,4 | 57983 | 54732 | 191931 | 183233 | 461300 | 429522 |
| 1,6 | 50452 | 47695 | 166710 | 159836 | 400630 | 375192 |
| 1,8 | 45166 | 42812 | 149117 | 143575 | 358169 | 337350 |
| 2,0 | 41321 | 39297 | 136371 | 131855 | 327330 | 310035 |

*Table 12 - Critical buckling load $N_{cr}$ (N/m) of different thinner or thicker plates (continued)*

| b/a | Critical buckling load (N/m) | | | | | |
|---|---|---|---|---|---|---|
| | $[-45_2/0_2/45_2/90_2]s$ | | $[-45_3/0_3/45_3/90_3]s$ | | $[-45_4/0_4/45_4/90_4]s$ | |
| | t=3.2 mm | | t=4.8 mm | | t=6.4 mm | |
| | Rayleigh-Ritz | FEM(ANSYS) | Rayleigh-Ritz | FEM(ANSYS) | Rayleigh-Ritz | FEM(ANSYS) |
| 1,0 | 87155 | 82537 | 291181 | 275262 | 698266 | 641889 |
| 1,2 | 77739 | 74110 | 261746 | 247476 | 626008 | 578097 |
| 1,4 | 71597 | 68696 | 242862 | 229585 | 579251 | 536898 |
| 1,6 | 67340 | 64981 | 229941 | 217290 | 547043 | 508527 |
| 1,8 | 64265 | 62314 | 220689 | 208453 | 523866 | 488101 |
| 2,0 | 61971 | 60332 | 213835 | 201882 | 506630 | 472898 |

### *3.2.4. Effect of lamination types and aspect ratios*

Symmetrically laminated composite rectangular thin plates (Quasi-isotropic plates, Cross-Ply plates and Angle-Ply plates) consisting of 28 different types shown in Table 3 are used for the calculations of critical buckling loads $N_{cr}$ (N/m) of plates under simply supported boundary condition and the results are tabulated in Tables 13-14.

It is seen from the results that critical buckling loads depend on lamination types. Critical buckling loads increase with the decrease of the aspect ratios (a/b or b/a).

It is seen from the Table 13 (short edge is on the y axis: a/b) Angle-ply plates LT27 ( $[-45_2/45_2/-45_2/45_2]_s$ ) and LT28 ( $[45_2/-45_2/45_2/-45_2]_s$ ) have the highest value for the lowest critical buckling loads (103747 N/m) for aspect ratio a/b=1. For aspect ratio a/b =2, both of the Quasi-isotropic plates LT20 ($[90_2/-45_2/45_2/0_2]_s$) and LT23 ($[90_2/45_2/-45_2/0_2]_s$) have the highest value for the lowest critical buckling loads (71357 N/m).

It can be noticed from Table 14 (short edge is on the x axis: b/a), Angle-ply plates LT27 ( $[-45_2/45_2/-45_2/45_2]_s$ ) and LT28 ( $[45_2/-45_2/45_2/-45_2]_s$ ) have the highest value for the lowest critical buckling loads (103747 N/m) for aspect ratio b/a=1. For aspect ratio b/a =2, LT7 ($[0_2/-45_2/45_2/90_2]_s$) and LT9 ($[0_2/45_2/-45_2/90_2]_s$) have the highest value for the lowest critical buckling loads (71357 N/m).

*Table 13 - Critical buckling load (N/m), short edge is on the y axis*

| a/b | Method | Plate Types | | | | | | | | | |
|---|---|---|---|---|---|---|---|---|---|---|---|
| | | LT1 | L15 | LT2 | L16 | LT3 | LT13 | LT4 | LT14 | LT5 | LT18 |
| | | $N_{cr}$ (N/m) | | $N_{cr}$ (N/m) | | $N_{cr}$ (N/m) | | $N_{cr}$ (N/m) | | $N_{cr}$ (N/m) | |
| 1 | Rayleigh-Ritz | 87155 | | 80182 | | 99333 | | 99333 | | 80182 | |
| | FEM (ANSYS) | 82537 | | 73442 | | 97414 | | 97414 | | 73442 | |
| 1.2 | Rayleigh-Ritz | 69227 | | 64974 | | 81887 | | 84621 | | 70807 | |
| | FEM (ANSYS) | 65368 | | 59334 | | 80392 | | 83119 | | 65484 | |

*Table 13 - Critical buckling load (N/m), short edge is on the y axis (continued)*

| a/b | Method | Plate Types | | | | | | | | | |
|---|---|---|---|---|---|---|---|---|---|---|---|
| | | **LT1** | **L15** | **LT2** | **L16** | **LT3** | **LT13** | **LT4** | **LT14** | **LT5** | **LT18** |
| | | **$N_{cr}$ (N/m)** | | **$N_{cr}$ (N/m)** | | **$N_{cr}$ (N/m)** | | **$N_{cr}$ (N/m)** | | **$N_{cr}$ (N/m)** | |
| **1.4** | Rayleigh-Ritz | 57983 | | 55779 | | 70215 | | 74596 | | 65088 | |
| | FEM (ANSYS) | 54732 | | 51060 | | 69017 | | 73390 | | 60832 | |
| **1.6** | Rayleigh-Ritz | 50452 | | 49816 | | 61978 | | 67424 | | 61335 | |
| | FEM (ANSYS) | 47695 | | 45855 | | 60998 | | 66436 | | 57880 | |
| **1.8** | Rayleigh-Ritz | 45166 | | 45745 | | 55944 | | 62118 | | 58738 | |
| | FEM (ANSYS) | 42812 | | 42401 | | 55131 | | 61295 | | 55889 | |
| **2** | Rayleigh-Ritz | 41321 | | 42852 | | 51398 | | 58090 | | 56866 | |
| | FEM (ANSYS) | 39297 | | 40007 | | 50714 | | 57394 | | 54482 | |
| **a/b** | **Method** | Plate Types | | | | | | | | | |
| | | **LT6** | **LT17** | **LT7** | **LT9** | **LT8** | **LT10** | **LT11** | **LT12** | **LT19** | **LT24** |
| | | **$N_{cr}$ (N/m)** | | **$N_{cr}$ (N/m)** | | **$N_{cr}$ (N/m)** | | **$N_{cr}$ (N/m)** | | **$N_{cr}$ (N/m)** | |
| **1** | Rayleigh-Ritz | 87155 | | 78891 | | 73224 | | 66872 | | 73224 | |
| | FEM (ANSYS) | 82537 | | 77900 | | 71478 | | 66591 | | 71478 | |
| **1.2** | Rayleigh-Ritz | 77739 | | 58932 | | 55645 | | 53557 | | 69487 | |
| | FEM (ANSYS) | 74110 | | 58164 | | 54215 | | 53356 | | 68102 | |
| **1.4** | Rayleigh-Ritz | 71597 | | 47234 | | 45751 | | 46745 | | 67886 | |
| | FEM (ANSYS) | 68696 | | 46615 | | 44561 | | 46595 | | 66764 | |
| **1.6** | Rayleigh-Ritz | 67340 | | 39844 | | 39755 | | 43028 | | 67214 | |
| | FEM (ANSYS) | 64981 | | 39335 | | 38754 | | 42912 | | 66287 | |
| **1.8** | Rayleigh-Ritz | 64265 | | 34902 | | 35901 | | 40895 | | 66966 | |
| | FEM (ANSYS) | 62314 | | 34476 | | 35053 | | 40802 | | 66185 | |
| **2** | Rayleigh-Ritz | 61971 | | 31444 | | 33304 | | 39618 | | 66915 | |
| | FEM (ANSYS) | 60332 | | 31085 | | 32578 | | 39542 | | 66246 | |
| **a/b** | **Method** | Plate Types | | | | | | | | | |
| | | **LT20** | **LT23** | **LT21** | **LT22** | **LT25** | | **LT26** | | **LT27** | **LT28** |
| | | **$N_{cr}$ (N/m)** | | **$N_{cr}$ (N/m)** | | **$N_{cr}$ (N/m)** | | **$N_{cr}$ (N/m)** | | **$N_{cr}$ (N/m)** | |
| **1** | Rayleigh-Ritz | 78891 | | 66872 | | 61516 | | 61516 | | 103747 | |
| | FEM (ANSYS) | 77900 | | 66591 | | 61399 | | 61399 | | 100801 | |
| **1.2** | Rayleigh-Ritz | 75251 | | 61650 | | 58739 | | 47995 | | 86698 | |
| | FEM (ANSYS) | 74457 | | 61424 | | 58629 | | 47937 | | 84345 | |
| **1.4** | Rayleigh-Ritz | 73373 | | 59710 | | 58663 | | 41440 | | 74887 | |
| | FEM (ANSYS) | 72722 | | 59522 | | 58557 | | 41412 | | 72975 | |
| **1.6** | Rayleigh-Ritz | 72335 | | 59150 | | 59539 | | 38112 | | 66343 | |
| | FEM (ANSYS) | 71788 | | 58987 | | 59434 | | 38100 | | 64766 | |
| **1.8** | Rayleigh-Ritz | 71728 | | 59175 | | 60684 | | 36375 | | 59974 | |
| | FEM (ANSYS) | 71259 | | 59031 | | 60578 | | 36373 | | 58656 | |
| **2** | Rayleigh-Ritz | 71357 | | 59440 | | 61833 | | 35461 | | 55115 | |
| | FEM (ANSYS) | 70946 | | 59309 | | 61723 | | 35466 | | 54001 | |

*Table 14 - Critical buckling load (N/m), short edge is on the x axis*

| b/a | Method | Plate Types | | | | | | | | | |
|---|---|---|---|---|---|---|---|---|---|---|---|
| | | **LT1** | **L15** | **LT2** | **L16** | **LT3** | **LT13** | **LT4** | **LT14** | **LT5** | **LT18** |
| | | **$N_{cr}$ (N/m)** | | **$N_{cr}$ (N/m)** | | **$N_{cr}$ (N/m)** | | **$N_{cr}$ (N/m)** | | **$N_{cr}$ (N/m)** | |
| **1** | Rayleigh-Ritz | 87155 | | 80182 | | 99333 | | 99333 | | 80182 | |
| | FEM (ANSYS) | 82537 | | 73442 | | 97414 | | 97414 | | 73442 | |
| **1.2** | Rayleigh-Ritz | 77739 | | 70807 | | 84621 | | 81887 | | 64974 | |
| | FEM (ANSYS) | 74110 | | 65484 | | 83119 | | 80392 | | 59334 | |
| **1.4** | Rayleigh-Ritz | 71597 | | 65088 | | 74596 | | 70215 | | 55779 | |
| | FEM (ANSYS) | 68696 | | 60832 | | 73390 | | 69017 | | 51060 | |
| **1.6** | Rayleigh-Ritz | 67340 | | 61335 | | 67424 | | 61978 | | 49816 | |
| | FEM (ANSYS) | 64981 | | 57880 | | 66436 | | 60998 | | 45855 | |
| **1.8** | Rayleigh-Ritz | 64265 | | 58738 | | 62118 | | 55944 | | 45745 | |
| | FEM (ANSYS) | 62314 | | 55889 | | 61295 | | 55131 | | 42401 | |
| **2** | Rayleigh-Ritz | 61971 | | 56866 | | 58090 | | 51398 | | 42852 | |
| | FEM (ANSYS) | 60332 | | 54482 | | 57394 | | 50714 | | 40007 | |

| b/a | Method | Plate Types | | | | | | | | | |
|---|---|---|---|---|---|---|---|---|---|---|---|
| | | **LT6** | **LT17** | **LT7** | **LT9** | **LT8** | **LT10** | **LT11** | **LT12** | **LT19** | **LT24** |
| | | **$N_{cr}$ (N/m)** | | **$N_{cr}$ (N/m)** | | **$N_{cr}$ (N/m)** | | **$N_{cr}$ (N/m)** | | **$N_{cr}$ (N/m)** | |
| **1** | Rayleigh-Ritz | 87155 | | 78891 | | 73224 | | 66872 | | 73224 | |
| | FEM (ANSYS) | 82537 | | 77900 | | 71478 | | 66591 | | 71478 | |
| **1.2** | Rayleigh-Ritz | 69227 | | 75251 | | 69487 | | 61650 | | 55645 | |
| | FEM (ANSYS) | 65368 | | 74457 | | 68102 | | 61424 | | 54215 | |
| **1.4** | Rayleigh-Ritz | 57983 | | 73373 | | 67886 | | 59710 | | 45751 | |
| | FEM (ANSYS) | 54732 | | 72722 | | 66764 | | 59522 | | 44561 | |
| **1.6** | Rayleigh-Ritz | 50452 | | 72335 | | 67214 | | 59150 | | 39755 | |
| | FEM (ANSYS) | 47695 | | 71788 | | 66287 | | 58987 | | 38754 | |
| **1.8** | Rayleigh-Ritz | 45166 | | 71728 | | 66966 | | 59175 | | 35901 | |
| | FEM (ANSYS) | 42812 | | 71259 | | 66185 | | 59031 | | 35053 | |
| **2** | Rayleigh-Ritz | 41321 | | 71357 | | 66915 | | 59440 | | 33304 | |
| | FEM (ANSYS) | 39297 | | 70946 | | 66246 | | 59309 | | 32578 | |

| b/a | Method | Plate Types | | | | | | | | | |
|---|---|---|---|---|---|---|---|---|---|---|---|
| | | **LT20** | **LT23** | **LT21** | **LT22** | **LT25** | | **LT26** | | **LT27** | **LT28** |
| | | **$N_{cr}$ (N/m)** | | **$N_{cr}$ (N/m)** | | **$N_{cr}$ (N/m)** | | **$N_{cr}$ (N/m)** | | **$N_{cr}$ (N/m)** | |
| **1** | Rayleigh-Ritz | 78891 | | 66872 | | 61516 | | 61516 | | 103747 | |
| | FEM (ANSYS) | 77900 | | 66591 | | 61399 | | 61399 | | 100801 | |
| **1.2** | Rayleigh-Ritz | 58932 | | 53557 | | 47995 | | 58739 | | 86698 | |
| | FEM (ANSYS) | 58164 | | 53356 | | 47937 | | 58629 | | 84345 | |

*Table 14 - Critical buckling load (N/m), short edge is on the x axis (continue)*

| b/a | Method | Plate Types | | | | | | | |
|---|---|---|---|---|---|---|---|---|---|
| | | LT20 | LT23 | LT21 | LT22 | LT25 | LT26 | LT27 | LT28 |
| | | $N_{cr}$ (N/m) | | $N_{cr}$ (N/m) | | $N_{cr}$ (N/m) | $N_{cr}$ (N/m) | $N_{cr}$ (N/m) | |
| 1.4 | Rayleigh-Ritz | 47234 | | 46745 | | 41440 | 58663 | 74887 | |
| | FEM (ANSYS) | 46615 | | 46595 | | 41412 | 58557 | 72975 | |
| 1.6 | Rayleigh-Ritz | 39844 | | 43028 | | 38112 | 59539 | 66343 | |
| | FEM (ANSYS) | 39335 | | 42912 | | 38100 | 59434 | 64766 | |
| 1.8 | Rayleigh-Ritz | 34902 | | 40895 | | 36375 | 60684 | 59974 | |
| | FEM (ANSYS) | 34476 | | 40802 | | 36373 | 60578 | 58656 | |
| 2 | Rayleigh-Ritz | 31444 | | 39618 | | 35461 | 61833 | 55115 | |
| | FEM (ANSYS) | 31085 | | 39542 | | 35466 | 61723 | 54001 | |

### *3.2.5. Non-dimensional results*

Non-dimensional critical buckling loads of symmetrically laminated composite plates are tabulated for practical data for designer and given in Table 15 and 16.

*Table 15 - Non-dimensional critical buckling load, short edge is on the x axis,*

$$N'_{cr} = N_{cr}\frac{b^2}{t^3 E_{22}}$$

| Plate Type | Aspect ratio a/b | | | | | |
|---|---|---|---|---|---|---|
| | 1 | 1,2 | 1,4 | 1,6 | 1,8 | 2 |
| LT1 | 45158 | 35869 | 30043 | 26141 | 23402 | 21410 |
| LT15 | | | | | | |
| LT2 | 41545 | 33665 | 28901 | 25811 | 23702 | 22203 |
| LT16 | | | | | | |
| LT3 | 51468 | 42428 | 36381 | 32113 | 28987 | 26631 |
| LT13 | | | | | | |
| LT4 | 51468 | 43845 | 38651 | 34935 | 32185 | 30098 |
| LT14 | | | | | | |
| LT5 | 41545 | 36688 | 33724 | 31780 | 30434 | 29464 |
| LT18 | | | | | | |
| LT6 | 45158 | 40279 | 37097 | 34891 | 33298 | 32109 |
| LT17 | | | | | | |
| LT7 | 40876 | 30535 | 24474 | 20645 | 18084 | 16292 |
| LT9 | | | | | | |

*Table 15 - Non-dimensional critical buckling load, short edge is on the x axis, $N'_{cr} = N_{cr}\frac{b^2}{t^3 E_{22}}$ (continued)*

| Plate Type | Aspect ratio a/b | | | | | |
|---|---|---|---|---|---|---|
| | **1** | **1,2** | **1,4** | **1,6** | **1,8** | **2** |
| **LT8** | 37940 | 28832 | 23705 | 20598 | 18602 | 17256 |
| **LT10** | | | | | | |
| **LT11** | 34649 | 27750 | 24220 | 22294 | 21189 | 20527 |
| **LT12** | | | | | | |
| **LT19** | 37940 | 36004 | 35174 | 34826 | 34697 | 34671 |
| **LT24** | | | | | | |
| **LT20** | 40876 | 38990 | 38017 | 37479 | 37165 | 36973 |
| **LT23** | | | | | | |
| **LT21** | 34649 | 31943 | 30938 | 30648 | 30661 | 30798 |
| **LT22** | | | | | | |
| **LT25** | 31874 | 30435 | 30395 | 30849 | 31443 | 32038 |
| **LT26** | 31874 | 24868 | 21472 | 19747 | 18847 | 18374 |
| **LT27** | 53755 | 44921 | 38802 | 34375 | 31075 | 28557 |
| **LT28** | | | | | | |

*Table 16 - Non-dimensional critical buckling load, short edge is on the y axis, $N'_{cr} = N_{cr}\frac{a^2}{t^3 E_{22}}$*

| Plate Type | Aspect ratio b/a | | | | | |
|---|---|---|---|---|---|---|
| | **1** | **1,2** | **1,4** | **1,6** | **1,8** | **2** |
| **LT1** | 45158 | 40279 | 37097 | 34891 | 33298 | 32109 |
| **LT15** | | | | | | |
| **LT2** | 41545 | 36688 | 33724 | 31780 | 30434 | 29464 |
| **LT16** | | | | | | |
| **LT3** | 51468 | 43845 | 38651 | 34935 | 32185 | 30098 |
| **LT13** | | | | | | |
| **LT4** | 51468 | 42428 | 36381 | 32113 | 28987 | 26631 |
| **LT14** | | | | | | |
| **LT5** | 41545 | 33665 | 28901 | 25811 | 23702 | 22203 |
| **LT18** | | | | | | |

*Table 16 - Non-dimensional critical buckling load, short edge is on the y axis, $N'_{cr} = N_{cr}\frac{a^2}{t^3 E_{22}}$ (continued)*

| Plate Type | Aspect ratio b/a | | | | | |
|---|---|---|---|---|---|---|
| | **1** | **1,2** | **1,4** | **1,6** | **1,8** | **2** |
| **LT6** | | | | | | |
| **LT17** | 45158 | 35869 | 30043 | 26141 | 23402 | 21410 |
| **LT7** | | | | | | |
| **LT9** | 40876 | 38990 | 38017 | 37479 | 37165 | 36973 |
| **LT8** | | | | | | |
| **LT10** | 37940 | 36004 | 35174 | 34826 | 34697 | 34671 |
| **LT11** | | | | | | |
| **LT12** | 34649 | 31943 | 30938 | 30648 | 30661 | 30798 |
| **LT19** | | | | | | |
| **LT24** | 37940 | 28832 | 23705 | 20598 | 18602 | 17256 |
| **LT20** | | | | | | |
| **LT23** | 40876 | 30535 | 24474 | 20645 | 18084 | 16292 |
| **LT21** | | | | | | |
| **LT22** | 34649 | 27750 | 24220 | 22294 | 21189 | 20527 |
| **LT25** | 31874 | 24868 | 21472 | 19747 | 18847 | 18374 |
| **LT26** | 31874 | 30435 | 30395 | 30849 | 31443 | 32038 |
| **LT27** | | | | | | |
| **LT28** | 53755 | 44921 | 38802 | 34375 | 31075 | 28557 |

## 4. CONCLUSIONS

Biaxial buckling analysis of symmetrically laminated quasi-isotropic, cross-ply and angle-ply rectangular thin plates has been examined in this study. Plates were considered as simply supported at the edges. Effects of thickness, aspect ratios and lamination types on critical buckling loads have been investigated parametrically by Rayleigh Ritz Method based on the Classical Lamination Plate Theory (CLPT). The Finite Element Method software package ANSYS has been used for verification calculations in order to compare the results. Good correlation was obtained.

For the calculation of Rayleigh Ritz Method integral equations were initially solved by using Mathematica [49] then the code prepared by using the MATLAB [50] programming language for different conditions. Results obtained using Rayleigh Ritz Method were obtained much faster than those of FEM calculations with ANSYS software package.

The critical buckling load of isotropic plates increases with decreasing of the aspect ratio (a/b or b/a). This situation was observed for the symmetrically composite laminates (Cross-Ply, Angle-Ply and Quasi-isotropic plates) similarly.

The present paper also indicates that the thick plates have a larger buckling strength compared to thin plates. However, shear deformable theories should be considered for thick plates.

Symmetrically laminated cross-ply plates are orthotropic and their bending-twisting coupling terms $D_{16}$ and $D_{26}$ are zero, but these terms are taken into account for quasi-isotropic and angle-ply laminates. Jones [51] mentioned that for laminated plates with bending-twisting coupling decrease buckling loads. The same situation was observed that considering Angle-ply and Quasi-isotropic plates for four-terms solutions in this study. When the bending-twisting coupling terms ($D_{16}$, $D_{26}$) are not taken into account, the critical buckling load is higher.

Results show that bending stiffness matrix elements $D_{11}$ and $D_{22}$ are equal for symmetrically laminated Angle-Ply plates (LT27= $[-45_2/45_2/-45_2/45_2]_s$ and LT28=$[45_2/-45_2/45_2/-45_2]_s$) similar to isotropic plates. Thus, the critical buckling load for equal aspect ratios (a/b = b/a) gives the same result for angle-ply plates and isotropic plates. One of the most important results of this study is that, in terms of largest value for the lowest critical buckling loads ($N_{cr}$), the angle-ply plates are more advantageous than Cross-ply and Quasi-isotropic plates for lowest aspect ratio is (a/b=1, 1.2 and 1.4). Symmetrically laminated Quasi-isotropic plates have the highest value for the fundamental critical buckling loads for highest aspect ratios (a/b=1.6, 1.8 and 2). It is demonstrated that the bending stiffness matrix elements play an important role in the bi-axial buckling of symmetrically laminated plates.

It was aimed to determine the most appropriate stiffest plate types (having highest value for the lowest critical buckling loads) and this aim was accomplished for all conditions (results given in Section 3).

Therefore, it can be concluded that the most suitable plate types may be quickly determined at the design stage of composite engineering structures, with the use of tabulated non-dimensional results obtained by the Rayleigh Ritz method. In addition, the tabulated results should be valuable to engineers as well as researchers working in this field.

Some mode shapes of Quasi-isotropic, Cross-ply and Angle-ply laminates have been obtained and given in Appendix (Figure A1 and Figure A2).

In future studies, stress and strain distributions along the thickness of laminated plates and failure theories can be examined, supported by experimental studies and advantageous lamination types can be investigated by optimization techniques.

**Acknowledgements**

The authors thank Prof. Dr. İzzet Deniz ÜNSALAN (Dokuz Eylul University) for his valuable help.

## References

[1] Lekhnitskii, S. G., Anisotropic plates, second ed, translated from the Russian by S. W. Tsai and T. Cheron, Gordon and Breach, New York.,1968.

[2] Ambartsumyan, S. A.,Theory of anisotropic plates, Technomic Publishing, Stamford CT., 1970.

[3] Ashton, J. E. and Whitney, J. M., Theory of laminated plates, Technomic [43 Publishing, Stamford CT. 1970.

[4] Szilard R., Theory and analysis of plates: classical and numerical methods. Englewood Cliffs, New Jersey: Prentice-Hall, 1974.

[5] Jones, R. M., Mechanics of composite materials, Scripta, Washington DC, 1975.

[6] Chia, C.Y, Nonlinear analysis of plates, McGraw-Hill, New York, 1980.

[7] Leissa, A. W., A review of laminated composite plate buckling, Appl Mech Rev vol 40, no 5, May, 575-591, 1987.

[8] Tung, T. K. and Surdenas, J., Buckling of Rectangular Orthotropic Plates Under Biaxial Loading, Journal of Composite Materials, Vol. 21-February, 124-128, 1987.

[9] Nagendra, S., Haftka, R.T. and Gurdal, Z., Stacking sequence optimization of simply supported laminates with stability and strain constraints, AIAA-92-2310-CP-2526-2535, 1992.

[10] Zhang, J.W., Buckling and Postbuckling of Unsymmetrically Laminated Angle-ply Plates in Uniaxial and Biaxial Compression, Thin- Walled Structures 15, 271-290, 1993.

[11] Kim Y.S. and Hoa S.V., Bi-axial buckling behavior of composite rectangular plates, Composite Structures 31, 247-252, 1995.

[12] Nair, S., Singh, G.L. and G. Rao, V., Stability of Laminated Composite Plates Subjected To Various Types of In-Plane Loadings, Int. J. Mech. Sci., Vol. 38. No. 2, pp. 191-202, 1996.

[13] Sundaresan,P., Singh, G. and Rao,G.V., Buckling and post-buckling analysis of moderately thick laminated rectangular plates, Computers & Structures Vol. 61, No. I, pp.79-86, 1996.

[14] Walker,M., Adali, S. and Verijenko,V., Optimization of symmetric laminates for maximum buckling load including the effects of bending-twisting coupling, Computers&Structures, Vol.58, No.2, pp.313-319, 1996a.

[15] Walker, M., Adali, S. and Verijenko, V. E., Optimal design of symmetric angle-ply laminates subject to nonuniform buckling loads and in-plane restraints, Thin-Walled Structures Vol.26, No. I, pp. 45 60, 1996b.

[16] Adali,S., Richter,A. and Verijenko, K.E., Optimization of shear-deformable laminated plates under buckling and strength criteria, Composite Structures Vol. 39, No.3-4, pp. 167-178, 1997.

[17] Durban, D. and Zuckerman, Z., Elastoplastic buckling of rectangular plates in biaxial compression/tension, International Journal of Mechanical Sciences 41, 751—765, 1999.

[18] Sarma, M.A., Singh, G. and Rao,G.V., Stability behaviour of angle ply plates subjected to various types of inplane loadings, Indian Journal of Engineering& Materials Sciences, Vol.6, August, pp.173-181, 1999.

[19] Tuttle, M., Singhatanadgid, P. and Hinds, G., Buckling of Composite Panels Subjected to Biaxial Loading, Experimental Mechanics, VoI. 39, No. 3, September, pp.191-201, 1999.

[20] Kollar, L.P. and Veres, I.A., Buckling of Rectangular Orthotropic Plates Subjected to Biaxial Normal Forces, Journal of Composite Materials, Vol. 35, No. 07, 625-635, 2001.

[21] Romeo, G. and Ferrero, G., Analytical/Experimental Behavior of Anisotropic Rectangular Panels Under Linearly Varying Combined Loads, AIAA Journal, Vol. 39, No. 5, May, 932-941, 2001.

[22] Narita, Y. and Turvey, G. J., Proceedings of the Institution of Mechanical Engineers, Part C: Journal of Mechanical Engineering Science, Maximizing the buckling loads of symmetrically laminated composite rectangular plates using a layerwise optimization approach, 218: 681-691, 2004.

[23] Ni,Q., Xie, J. and Iwamoto, M., Buckling analysis of laminated composite plates with arbitrary edge supports, Composite Structures, 69, 209–217, 2005.

[24] Shukla, K. K., Nath, Y., Kreuzer, E. and Kumar, K.V.S., Buckling of Laminated Composite Rectangular Plates, J. Aerosp. Eng.18, 215-223, 2005.

[25] Timarci, T. and Aydogdu, M., Buckling of symmetric cross-ply square plates with various boundary conditions, Composite Structures 68, 381–389, 2005.

[26] Bert, C.W. and Malik,M., On the buckling characteristics of symmetrically laminated cross-ply plates, Mechanics of Composite Materials and Structures, 4:1, 39-67, 2007.

[27] Qiao, P. and Shan,L., Explicit local buckling analysis of rotationally restrained composite plates under biaxial loading, International Journal of Structural Stability and Dynamics, Vol. 7, No. 3, 487–517, 2007

[28] Aktaş,M., Buckling Behaviour Of Carbon/Epoxy Laminated Composite Plates Under Biaxial Loading, Advanced Composites Letters, Vol. 18, Iss. 3, 85-93, 2009.

[29] Latalski, J., Ply Thickness Tolerances In Stacking Sequence Optimization Of Multilayered Laminate Plates, Journal Of Theoretical And Applied Mechanics, 51, 4, pp. 1039-1052, Warsaw, 2013.

[30] Sayyad, A.S. and Ghugal,Y.M., On the Buckling of Isotropic, Transversely Isotropic and Laminated Composite Rectangular Plates, International Journal of Structural Stability and Dynamics, Vol. 14, No. 6, 1450020, 2014.

[31] Bourada,F., Amara, K. and Tounsi, A., Buckling analysis of isotropic and orthotropic plates using a novel four variable refined plate theory, Steel and Composite Structures, Vol. 21, No. 6, 1287-1306, 2016.

[32] Becheri,T. Amara,K., Bouazza, M. and Benseddiq,N., Buckling of symmetrically laminated plates using nth-order shear deformation theory with curvature effects, Steel and Composite Structures, Vol. 21, No. 6, 1347-1368, 2016.

[33] Rajanna, T. , Banerjee,S., Desai, Y.M. and Prabhakara, D.L., Vibration and buckling analyses of laminated panels with and without cutouts under compressive and tensile edge loads, Steel and Composite Structures, Vol. 21, No. 1, 37-55, 2016.

[34] Belkacem, A., Tahar,H.D., Abderrezak,R., Amine,B.M., Mohamed,Z. and Boussad,A., Mechanical buckling analysis of hybrid laminated composite plates under different boundary conditions, Structural Engineering and Mechanics, Vol. 66, No. 6, 761-769, 2018.

[35] Topal,U., Vo-Duy,T., Dede,T. and Nazarimofrad,E., Buckling load optimization of laminated plates resting on Pasternak foundation using TLBO, Structural Engineering and Mechanics, Vol. 67, No. 6, 617-628, 2018.

[36] Bourada, M., Bouadi,A., Bousahla,A.A., Senouci,A., Bourada,F., Tounsi,A. and Mahmoud, S.R., Buckling behavior of rectangular plates under uniaxial and biaxial compression, Structural Engineering and Mechanics, Vol. 70, No. 1, 113-123, 2019.

[37] Fellah, M., Draiche,K., Houari,M.S.A., Tounsi,A., Saeed,T., Alhodaly, M.Sh. and Benguediab,M., A novel refined shear deformation theory for the buckling analysis of thick isotropic plates, Structural Engineering and Mechanics, Vol. 69, No. 3, 335-345, 2019.

[38] Altekin, M., Bending of super-elliptical Mindlin plates by finite element method, Teknik Dergi, 29, No:4, 8469-8496, 2018.

[39] Altekin, M., Free linear vibration and buckling of super-elliptical plates resting on symmetrically distributed point-supports on the diagonals, Thin-Walled Structures, Vol.46, 10, 1066-1086, 2008.

[40] Altunsaray, E. and Bayer,İ., Buckling of symmetrically laminated quasi-isotropic thin rectangular plates, Steel and Composite Structures, Vol. 17, No. 3, 305-320, 2014.

[41] Tsai, S.W., Composites design, (4th Edition), Think Composites, 1988.

[42] Köksal, E. and Köksal, T.Çubuk Plak Kabuk Stabilitesi, Yıldız Teknik Üniversitesi Yayını, Yayın No:309, Yıldız Teknik Üniversitesi Matbaası, İstanbul ,1996 (In Turkish).

[43] Köksal, T., Sonlu Elemanlar Metodu, Yıldız Teknik Üniversitesi Yayını, Yayın No:304, Yıldız Teknik Üniversitesi Matbaası İstanbul ,1996 (In Turkish)

[44] Fish, J. and Belytschko, T., A first cours in Finite Elements, John Wiley&Sons,Ltd, 2007.

[45] ANSYS 2019.1, Academic version, Dokuz Eylul University, 2019.

[46] Iyengar,N.G.R., Structural stability of columns and plates, John Wiley&Sons,Ltd, 1988

[47] Reddy, J.N., Mechanics of laminated composite plates and shells: Theory and Analysis (2nd Ed.), Boca Raton, FL: CRC Press, 2004.

[48] Ventsel,E and Krauthammer,T., Thin plates and shells, theory, analysis, and applications, Marcel Dekker Inc., 2001

[49] Wolfram Mathematica 11.3.0, Dokuz Eylul University, 2019.

[50] Matlab R2018a, Dokuz Eylul University, 2019.

[51] Jones, R.M., Mechanics of composite materials, 2nd ed., Taylor&Francis, 1999.

## APPENDIX

In this section, critical buckling loads of some plate types for the first three mode shapes are given. It can be seen that the critical buckling load values of some different plate types for some edge ratios are equal. However, it has been observed that this situation may change as the edge ratio changes.

First three modes shapes and buckling loads of some quasi-isotropic, cross-ply and angle-ply laminates are presented in Figure A1 and Figure A2. It can be seen from Figure A1 (a/b=1) the critical buckling loads of LT8 and LT19 are equal but their modes shapes are different. LT27 (Angle-Ply plate) has the highest critical buckling loads for mode-1 and mode-2, while LT25 (Cross-Ply plate) has the highest critical buckling load for mode-3. It may be seen from Figure A2 for a different aspect ratio (a/b=2) the critical buckling loads of LT8 and LT19 are different this time. LT27 (Angle-Ply plate) has the highest critical buckling loads for mode-1, mode-2 and mode-3.

| | | |
|---|---|---|
| 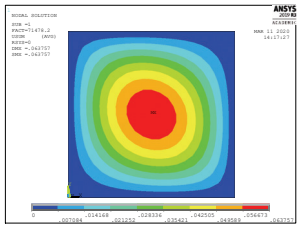 | 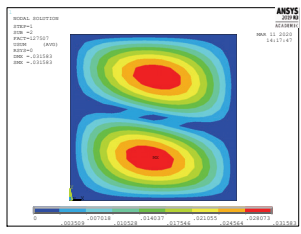 | 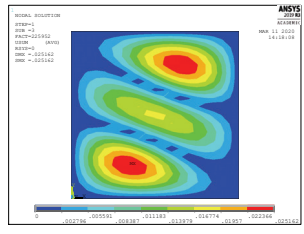 |
| LT8 $[0_2/-45_2/90_2/45_2]_s$ mode1= 71478 N/m | LT8 $[0_2/-45_2/90_2/45_2]_s$ mode2= 127507 N/m | LT8 $[0_2/-45_2/90_2/45_2]_s$ mode3= 225952 N/m |
| 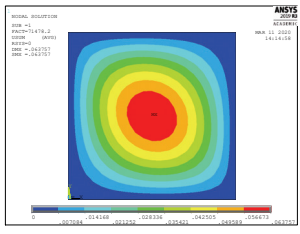 | 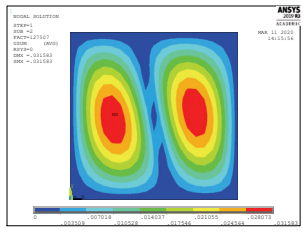 | 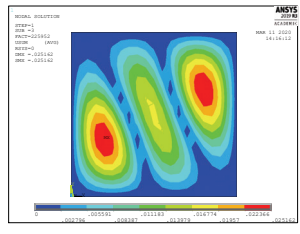 |
| LT19 $[90_2/-45_2/0_2/45_2]_s$ mode1= 71478 N/m | LT19 $[90_2/-45_2/0_2/45_2]_s$ mode2= 127507 N/m | LT19 $[90_2/-45_2/0_2/45_2]_s$ mode3= 225952 N/m |
| 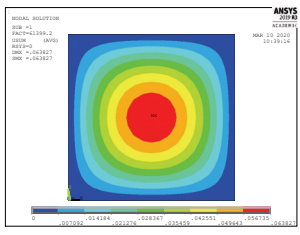 | 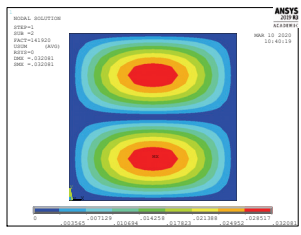 | 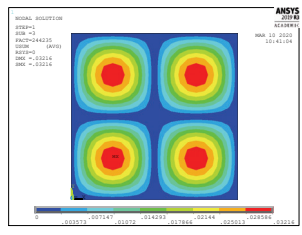 |
| LT25 $[0_2/90_2/0_2/90_2]_s$ mode1=61399 N/m | LT25 $[0_2/90_2/0_2/90_2]_s$ mode2=141920 N/m | LT25 $[0_2/90_2/0_2/90_2]_s$ mode3=244235 N/m |

| | | |
|---|---|---|
| 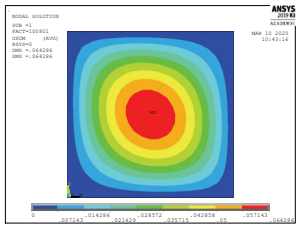 | 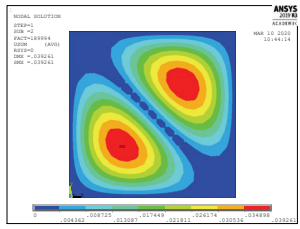 | 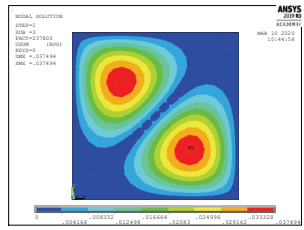 |
| LT27 $[-45_2/45_2/-45_2/45_2]_s$<br>mode1=100801 N/m | LT27 $[-45_2/45_2/-45_2/45_2]_s$<br>mode2=189994 N/m | LT27 $[-45_2/45_2/-45_2/45_2]_s$<br>mode3=237800 N/m |

*Figure A1 - Some mode shapes of laminated plates (quasi-isotropic, cross-ply, angle-ply) (a/b=1)*

| | | |
|---|---|---|
| 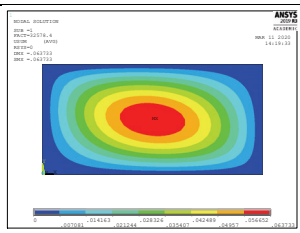 | 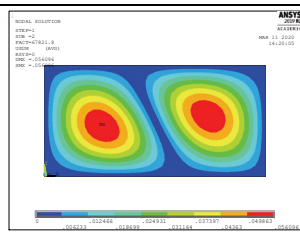 | 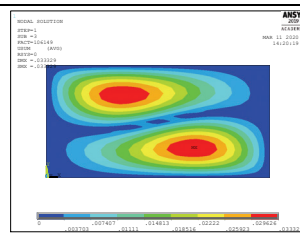 |
| LT8 $[0_2/-45_2/90_2/45_2]_s$<br>mode1= 32578 N/m | LT8 $[0_2/-45_2/90_2/45_2]_s$<br>mode2= 67821 N/m | LT8 $[0_2/-45_2/90_2/45_2]_s$<br>mode3= 106149 N/m |
| 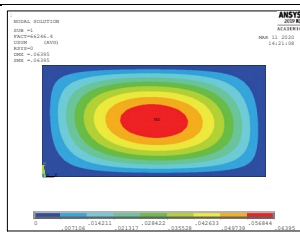 | 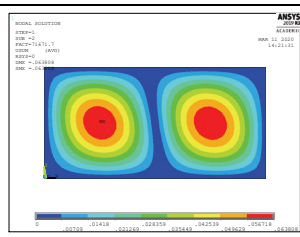 | 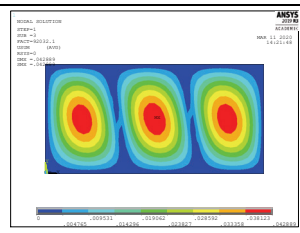 |
| LT19 $[90_2/-45_2/0_2/45_2]_s$<br>mode1= 66246 N/m | LT19 $[90_2/-45_2/0_2/45_2]_s$<br>mode2= 71671 N/m | LT19 $[90_2/-45_2/0_2/45_2]_s$<br>mode3= 92032 N/m |
| 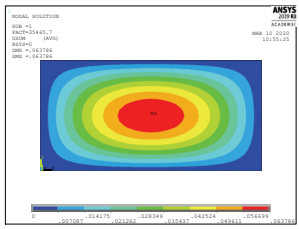 | 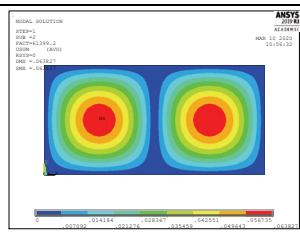 | 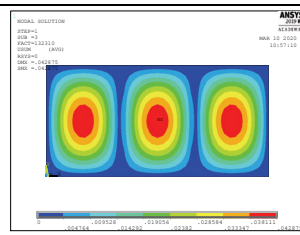 |
| LT25 $[0_2/90_2/0_2/90_2]_s$<br>mode1=35465 N/m | LT25 $[0_2/90_2/0_2/90_2]_s$<br>mode2=61399 N/m | LT25 $[0_2/90_2/0_2/90_2]_s$<br>mode3=132310 N/m |

| | | |
|---|---|---|
| 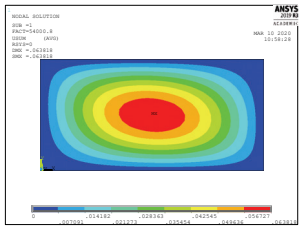 | 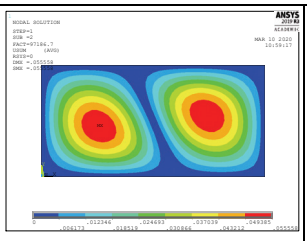 | 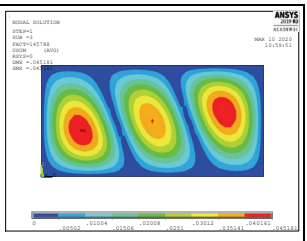 |
| LT27 $[-45_2/45_2/-45_2/45_2]_s$ mode1=54000 N/m | LT27 $[-45_2/45_2/-45_2/45_2]_s$ mode2=97186 N/m | LT27 $[-45_2/45_2/-45_2/45_2]_s$ mode3=145788 N/m |

*Figure A2 - Some mode shapes of laminated plates (quasi-isotropic, cross-ply, angle-ply) (a/b=2)*

*Teknik Dergi, 2021 11315-11336, Paper 635*

# Optimizing Non-linear Granular Layer Coefficients of a Flexible Pavement for Mechanistic-Empirical Method

**Murat BOSTANCIOĞLU**[1]

## ABSTRACT

In recent years, mechanistic-empirical (M-E) design methods are preferred in the design of flexible pavements instead of empirical methods using equations based on the road performance tests. However, the calibration of transfer equations that convert mechanical responses to pavement life and the definition of layer materials used in M-E methods have great importance for M-E methods.

In this study, mechanical analyses of a cross-section designed with the AASHTO-93 method were performed, and service life values were calculated with different empirical transfer equations. The obtained M-E design results were compared with the results calculated with the AASHTO-93 method, and transfer equations compatible with the AASHTO-93 method were determined. Among the transfer equations examined, it was found that the rutting equation of the Asphalt Institute gave the most consistent results with the AASHTO-93 method. In the mechanical analysis of the selected cross-section, granular base and sub-base layers were defined as non-linear elastic reflecting the actual in-situ conditions. K-Θ model was preferred for non-linear elastic layer definition, and $K_1$ and $K_2$ parameters of this model were optimized.

**Keywords:** Mechanistic-empirical design, AASHTO-93 method, non-linear layer coefficients, pavement life, rutting, fatigue.

## 1. INTRODUCTION

Flexible pavements consist of granular base and sub-base layers and a bituminous surface layer built on the subgrade to ensure the comfort and safety of vehicles and to resist the stresses caused by traffic loads and environmental conditions. The main purpose of pavement design is to determine the appropriate thickness of the layers subject to traffic loads and environmental effects. The methods used in flexible pavement design can be examined in five different categories as empirical methods, limiting shear failure method, limiting deflection method, regression method, and mechanistic-empirical (M-E) method [1-4].

Note:
- This paper was received on October 23, 2019 and accepted for publication by the Editorial Board on May 23, 2020.
- Discussions on this paper will be accepted by January 31, 2022.
- https://dx.doi.org/10.18400/tekderg.637166

1 Sivas Cumhuriyet University, Department of Civil Engineering, Sivas, Turkey - bostancioglu@cumhuriyet.edu.tr - https://orcid.org/0000-0001-6820-2213

AASHTO-93 method, which uses regression equations related to road performance tests, is preferred by Turkey General Directorate of Highways for the design of flexible pavements [1,5,6]. The AASHTO pavement design guide was first published in 1961 and was revised in 1972, 1981, 1986 and 1993 with the theoretical support added to the knowledge obtained from the road test. The equations used in the AASHTO method were obtained from the Ottowa Illinois road tests and used certain climatic conditions, specific layer materials, and a certain subgrade. The average annual rainfall in the region where the test track is 864 mm and the frost depth is 711 mm. The subgrade has inadequate drainage and the California bearing ratio (CBR) ranges from 2% to 4% [1-3]. In the AASHTO method, the number of load repetitions is a very important point to take into consideration and loads of all types of vehicles in traffic are converted to the equivalent axle load of 8.2 tonnes ($T_{8.2}$) [5]. The present serviceability index (PSI) is located in the design equation based on pavement roughness and distress conditions (fatigue, cracking and patching) [1,4,5]. The low traffic volumes, dated vehicle characteristics, short test times and limited material and climatic properties used in AASHTO road tests have led to questioning the usability of the method. Similar to the AASHTO method, these limitations observed in all empirical methods increased interest in M-E methods [2,4].

Unlike empirical procedures, the M-E design method is more adaptable to changing loading, material, construction, and environmental conditions. In the M-E method, the design is performed with different transfer equations for all types of distress modes (rutting, fatigue cracking, etc.) [2,7,8].

The mechanical part of the M-E design methods is based on basic material mechanics, and stress, strain and displacement values (outputs) are calculated at any depth of the cross-section depending on traffic loads, environmental loads and layer characteristics (inputs) on the road [1,9]. In the empirical part, these mechanical responses are converted to service life by transfer equations (pavement life estimation models) [8].

Burmister's layered theory [1,10] is one of the most practical methods for mechanical analysis of flexible pavements. In this theory, the layers are defined as linear elastic with the modulus of elasticity (E) and Poisson's ratio ($\upsilon$). The Burmister theory can also be used in mechanical analysis of multilayered systems containing viscoelastic and nonlinear layers with some modifications [1].

Material characterization is a crucial step for mechanical analysis. The mechanical responses of the pavement can be estimated by the theory of elasticity where stresses from external loads are relatively low. However, in real conditions, heterogeneous pavement layers can behave more differently than ideal. Where the bituminous surface layer is thick, the elastic theory applies, whereas in relatively thin surface layers the mechanical response is significantly affected by the nonlinear behavior of the granular layers and the subgrade [11].

The modulus of elasticity calculated based on the recoverable strain of material under repetitive loads is defined as the resilience module ($M_R$) of the material and is the ratio of deviator stress to recoverable strain in the three-axial test [1]. $M_R$ is the most important mechanical parameter used to characterize the subgrade, sub-base and base layers under repeated loads as the materials used in the layers exhibit permanent deformation under repeated loads [12,13].

In the literature, many studies are showing the variation of flexible pavement performances depending on the $M_R$ values of unbound layers and their characterization;

Shahji (2006) [14] and Masad and Little (2004) [15] stated in their studies that the total rutting on the pavement decreased as $M_R$ increased. Cerni et al. (2012) [16] and Masad and Little (2004) [15] revealed that load-related cracks occur easily due to the decreasing $M_R$ value. In their study, which presented the relationship between $M_R$ and thermal cracks, Şahin et al. (2013) [17] reported that thermal cracks accelerated due to $M_R$ decrease. Masad and Little (2004) [15] reported that the International Roughness Index (IRI) value decreased due to the increase in the base layer $M_R$.

Numerous models have been proposed in the literature for modeling granular layers and estimating $M_R$ values of unbound granular layers which are highly effective on flexible pavement performance as mentioned above. $M_R$ prediction models are categorized in the literature as follows [13, 18-23];

(1) Empirical regression models

(2) Nonlinear stress-dependent models

(3) Moisture-sensitive models

(4) Moisture-sensitive and stress-dependent models

(5) Stress-dependent and cross-anisotropic models

(6) Moisture-sensitive, stress-dependent, and cross-anisotropic model

(7) Regression models for stress-dependent model coefficients

(8) Regression models for moisture-sensitive and stress-dependent model coefficients

In the studies conducted in the literature, the importance of defining stress-dependency and anisotropic material in the determination of $M_R$ values of unbound layers was emphasized. In the study that investigated the effect of the definition of unbound layers on mechanical analysis, Masad et al. (2005) [24] showed that permanent deformation values increase significantly when non-linear and anisotropic properties are used. Adu-Osei et al. (2001) [25] reported that fatigue cracking life is reduced if cross-anisotropy is used in the base layer. Masad and Little (2004) [15] reported that total rutting and cracking, which led the IRI change, were affected by cross-anisotropy. Tutumluer (1995) [26] denoted that the $M_R$ and Poisson's ratio values of unbound layers are direction-dependent. Hence, cross-anisotropic elastic modeling is a better method to estimate the behavior of these layers than the isotropic elastic model.

In the studies carried out to determine the $M_R$ values of the unbound layers depending on the moisture content [27-31], it was stated that the moisture content is the main parameter especially in the prediction of the subgrade's $M_R$ value, and the high degree of moisture content change decreases the $M_R$. In the study investigating the effect of moisture content in the base layer on tensile strains under the surface layer, Luo et al. (2017) [23] found that tensile strains increased due to the increase in the moisture content of the base layer.

For the K-Θ, Uzan-Witczak and Lade-Nelson models are among the most well-known models for non-linear granular layer characterization. Among these models, the Uzan-

Witczak model provides the lowest surface displacement and horizontal strain under the surface layer at the same loading conditions, while the Lade-Nelson model gives the highest values. K-Θ model calculated the responses between the results of these two methods [32].

The K-Θ model (Equation 1), proposed by Seed et al. [19] where $M_R$ is a function of the sum of the principal stresses, is frequently used in $M_R$ estimation and is used in the definition of the non-linear elastic granular layer in the current study [33,34].

$$M_R = K_1 \theta^{K_2} \quad (1)$$

In Equation 1, Θ is the sum of the principal stresses in the dynamic three-axial test, and $K_1$ and $K_2$ are the regression constants obtained from the experimental data of the material. Because the model is simple and useful, there are many studies in which model parameters are determined for different soil types [35-40].

There are many studies for the use of the M-E method in pavement design, but it is not widely used because of limitations on the calibration of empirical transfer functions [2]. In this study, the empirical transfer equations used in the M-E design method were found to be compatible with the AASHTO-93 for a selected pavement cross-section. Thus, the mechanical responses and pavement life of a cross-section designed with the AASHTO-93 can be determined by the M-E method under different loading, material, and environmental conditions and compared with the AASHTO-93. The present study is original in comparing the transfer equations of the M-E method with an empirical one. Furthermore, the study aims to optimize the nonlinear granular layer coefficients ($K_1$ and $K_2$) used in the M-E method, which is highly effective on the mechanical responses and proposed in a wide range in the literature.

As a result of optimizing the layer coefficients, the material types and moisture contents of the unbound layers used in the M-E method will be more specifically defined. Thus, the error rate for defining materials will be minimized in the calculation of cross-section responses.

## 2. MATERIAL AND METHODS

A conventional flexible pavement cross-section (Figure 1) was selected in the study, and layer thicknesses were determined following the studies in the literature [31,33,41-44]. The mechanical and physical properties of the layers are defined by the Highway Flexible Pavement Design Guide [5] and the maximum number of standard axle loads that the cross-section could be passed, over its economic life was determined by the AASHTO-93 method (Equation 2) [1,5].

$$\log(T_{8.2}) = Z_R x S_0 + 9.36x \log(SN+1) - 0.20 + \frac{\log(\frac{\Delta PSI}{4.2-1.5})}{0.40+\frac{1094}{(SN+1)^{5.19}}} + 2.32x \log(M_R) - 8.07 \quad (2)$$

Where,

$Z_R$: The standard normal deviation of reliability (R) is recommended as -1.645 for highways, -1.037 for state roads, and -0.524 for provincial roads.

$S_0$: The combined total standard deviation of traffic and performance estimation is suggested between 0.40-0.50 and is used as 0.45.

ΔPSI: The decrease in serviceability index ($P_0$-$P_t$). $P_0$ is the initial serviceability index between 4.2-4.5 when the road is first opened to traffic. In this study, this value was used as 4.2. $P_t$ is the terminal serviceability index and 2.5 for highways and state roads, 2.0 for provincial roads.

$M_R$: Resilient modulus (psi)

SN: Structural number (inches), is calculated by Equation 3 based on the thicknesses (Di, Dj) of the layers, the layer coefficients (ai, aj) and the drainage coefficients (mj) of the granular layers.

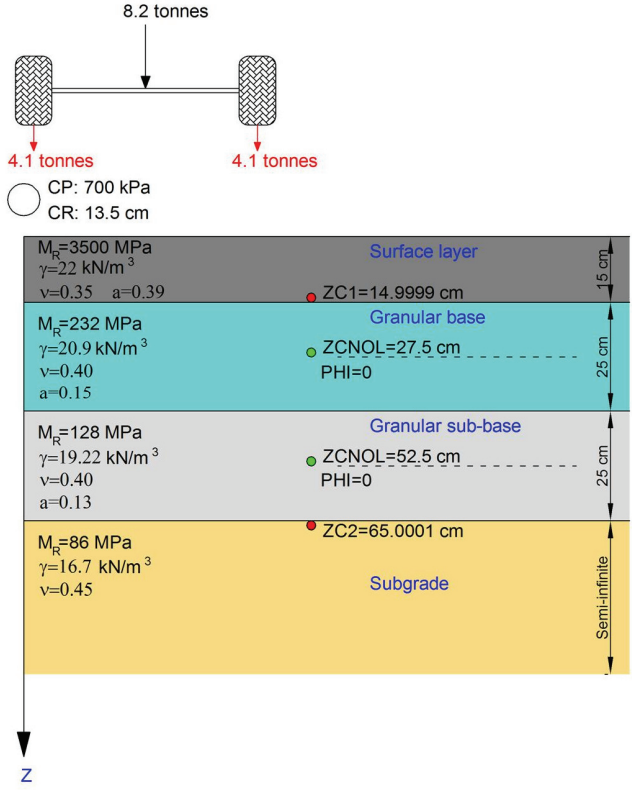


*Figure 1 - Model geometry*

$$SN = \sum_{i=1}^{k} a_i D_i + \sum_{j=1}^{n} a_j D_j m_j \quad (3)$$

Where,

k denotes the number of hot mix asphalt (HMA) layers and n denotes the number of granular layers. Granular layer drainage coefficients were taken as 1.0. The layer coefficients to be

used in the AASHTO-93 method were obtained with the help of Figure 2, Equations 4 and 5 respectively for surface, base and sub-base layers depending on the layer resilient modulus values and are given in Figure 1 [1].


*Figure 2 - Layer coefficients due to HMA resilient modulus [1]*

$$a_{base} = 0.249x \log\left(M_{R\,base}\right) - 0.977 \quad (4)$$

$$a_{sub-base} = 0.227x \log\left(M_{R_{sub-base}}\right) - 0.839 \quad (5)$$

In Equations 4 and 5, the $M_{R\ base}$ and $M_{R\ sub\text{-}base}$ indicate the resilient modulus (psi) of the base and sub-base layers.

In the M-E design method, the mechanical responses (displacement, stress, and strain) should be converted to a parameter that reflects the pavement performance (rutting, fatigue, cracking, etc.). The most commonly used mechanical parameters for this purpose are the horizontal strain ($\varepsilon_r$) under the surface layer (ZC1 in Figure 1) and the vertical strain ($\varepsilon_v$) on the subgrade (ZC2 in Figure 1). If horizontal strains are excessive, cracks occur on the surface, and this is called fatigue criterion. If vertical strains are excessive, deformations occur on the pavement, and this is called the rutting criterion [8,45,46]. In the literature, there are various models for fatigue and rutting criteria, and the general forms of these models are given in Equations 6 and 7, and the coefficients (f1-f5) used in the equations are given in Table 1 [8,47].

$$N_f = f1\varepsilon_r^{-f2} M_{R_{surface}}^{-f3} \quad (6)$$

$$N_r = f4(\varepsilon_v)^{-f5} \quad (7)$$

Where $N_f$ is the number of load repetitions required for fatigue, $N_r$ is the number of load repetitions required for rutting distress, $M_{R\ surface}$ is the resilient modulus (psi) of the surface layer.

*Table 1 - Distress model coefficients for different agencies [8,47]*

| | Asphalt Institute | Shell Research | US Army Corps of Engineers | Belgian Road Research Center | Transport and Road Research Laboratory | Federeal Highway Administration | ILLINOIS Department of Transportation | Austin Research Engineers |
|---|---|---|---|---|---|---|---|---|
| f1 | 0.0795 | 0.0685 | 497.156 | 4.92E-14 | 1.66E-10 | 0.1001 | 5.00E-06 | 4.88E-01 |
| f2 | 3.291 | 5.671 | 5 | 4.76 | 4.32 | 3.565 | 3 | 3.0312 |
| f3 | 0.854 | 2.363 | 2.66 | 0 | 0 | 1.474 | 0 | 0.6529 |
| f4 | 1.37E-09 | 6.15E-07 | 1.81E-15 | 3.05E-09 | 1.13E-06 | --- | --- | --- |
| f5 | 4.477 | 4 | 6.527 | 4.35 | 3.75 | --- | --- | --- |

To determine which of the empirical transfer equations used in the M-E design method yielding consistent results with the AASHTO-93 method, mechanical analysis of the cross-section was performed, and the strain values were obtained under the surface layer and on the subgrade. The obtained values were converted to pavement life and compared with the $T_{8.2}$ values of the AASHTO-93 method, and the transfer equations compatible with the AASHTO-93 method were obtained. KENLAYER software was used for mechanical analysis, which can be used successfully in the determination of displacement, stress and strain values of multilayered systems defined as linear elastic, non-linear elastic and viscoelastic under single, dual, dual tandem and dual tridem loading [1,7,48,49].

The layer thicknesses of the section are defined on the z-axis, and layer parameters ($M_R$ and $\upsilon$) and unit weights of the layers are given in Figure 1. The wheel load is defined as 4.1 tonnes on the single wheel following the AASHTO-93 method. The contact pressure (CP) of the wheel was selected as 700 kPa [50], and the circular wheel contact radius (CR) that would provide this internal pressure was determined as 13.5 cm. During the mechanical analysis, the contact surfaces between the layers were selected as bonded.

*Table 2 - Non-linear layer coefficients*

| Layer | $K_0$ | $K_1$ (kPa) | $K_2$ | PHI | ZCNOL(cm) |
|---|---|---|---|---|---|
| Base | 0.67 | Variable | Variable | 0 | 27.5 |
| Sub-base | 0.67 | Variable | Variable | 0 | 52.5 |

In addition to the linear elastic model, to perform non-linear analysis and to optimize non-linear layer coefficients, the base and sub-base layers are defined as non-linear using the

coefficients given in Table 2 [51]. To optimize the non-linear layer coefficients in accordance with the AASHTO-93 method, the $K_1$ and $K_2$ coefficients of the base and sub-base layers were determined as variables and analyses were made for 60 different $K_1$-$K_2$ combinations for the base layer and 360 combinations for the sub-base layer.

In Table 2, $K_0$ is the soil pressure at rest and is proposed as 0.8 or calculated by Equation 8 according to the Poisson's ratio of the layer [1].

$$K_0 = \upsilon/(1-\upsilon) \tag{8}$$

$K_1$ is a non-linear coefficient which varies with the moisture content of the granular layers, and $K_2$ is a non-linear exponent, the proposed $K_1$ and $K_2$ values for granular base layers are given in Tables 3 and 4, and the recommended $K_1$ and $K_2$ values for granular sub-base layers are given in Table 5. PHI is the internal friction angle of granular layers. The ZCNOL value is the depth of calculation of the modulus of elasticity for non-linear layers and is recommended to be taken as the mid-depth of the layer [1].

*Table 3 - Recommended $K_1$ and $K_2$ values for base layers*

| Reference | Material | $K_1$ (kPa) | $K_2$ |
|---|---|---|---|
| Hicks (1970) | Partially crushed gravel, crushed rock | 11032-34474 | 0.57-0.73 |
| Hicks and Finn (1970) | Untreated base at San Diego test road | 14479-37232 | 0.61 |
| Allen (1973) | Gravel, crushed stone | 12411-55159 | 0.32-0.70 |
| Kalcheff ve Hicks (1973) | Crushed stone | 27580-62053 | 0.46-0.64 |
| Boyce et al. (1976) | Well-graded crushed limestone | 55159 | 0.67 |
| Monismith and Witczak (1982) | In service base and sub-base materials | 19995-53435 | 0.46-0.65 |

*Table 4 - $K_1$ and $K_2$ values based on moisture content for base layers [1]*

| Mositure content | $K_1$ (kPa) | $K_2$ |
|---|---|---|
| Dry | 41369-68948 | 0.5-0.7 |
| Damp | 27580-41369 | 0.5-0.7 |
| Wet | 13790-27580 | 0.5-0.7 |

*Table 5 - $K_1$ and $K_2$ values based on moisture content for sub-base layers [1]*

| Moisture content | $K_1$ (kPa) | $K_2$ |
|---|---|---|
| Dry | 41369-55159 | 0.4-0.6 |
| Damp | 27580-41369 | 0.4-0.6 |
| Wet | 10343-27580 | 0.4-0.6 |

## 3. RESULTS AND DISCUSSION

### 3.1. Obtaining the Empirical Transfer Model Compatible with AASHTO-93 and Determining the Target Strain

$T_{8.2}$ values for different road types and reliability levels were calculated by the AASHTO-93 method and given in Table 6 depending on the subgrade resilient modulus, layer thickness, layer coefficients, and drainage coefficients given in Figure 1.

*Table 6 - AASHTO-93 design results*

| Road type | R (%) | ZR | Pt | $T_{8.2}(x10^6)$ |
|---|---|---|---|---|
| Highway | 95 | -1.645 | 2.5 | 23.35 |
| State road | 85 | -1.037 | 2.5 | 43.75 |
| Provincial road | 70 | -0.524 | 2.0 | 124.5 |

As a result of the mechanical analysis of the section by defining the layers linear elastic, the horizontal strain value under the surface layer was obtained as $2.124x10^{-4}$, and the vertical strain value on the subgrade was $2.345x10^{-4}$. Based on these responses, the pavement life values calculated by empirical transfer equations are shown in Table 7.

*Table 7 - M-E design results*

| | Asphalt Institute | Shell Research | US Army Corps of Engineers | Belgian Road Research Center | Transport and Road Research Laboratory | Federeal Highway Administration | ILLINOIS Department of Transportation | Austin Research Engineers |
|---|---|---|---|---|---|---|---|---|
| Nf | 1303655 | 1521195.97 | 765525.96 | 14952.36 | 1221238.80 | 4832.25 | 521802.87 | 12472426.51 |
| Nr | 24322215 | 203377885 | 890750781.7 | 18800892 | 46242655.65 | --- | --- | --- |

Table 7 shows that different transfer equations give quite different pavement life values. In particular, fatigue-related values are very low compared to pavement life due to rutting. When eight values related to fatigue and six values related to rutting are examined, it has been determined that the Nr equations of Asphalt Institute (AI) for highways and Transport and Road Research Laboratory for state roads are 96% and 94.6% compatible with the AASHTO-93 method respectively. For provincial roads with a low level of reliability, a highly compatible model could not be determined.

When the Highway Flexible Pavement Design Guide [5] is examined, the sum of the recommended bituminous layer thicknesses for all R and $T_{8.2}$ values is 19 cm and above (except only R = 70% and $T_{8.2}$=3-10x$10^6$).

In the current study, the bituminous surface layer thickness was chosen as 15 cm. Therefore, the main failure type for the section was determined as rutting since the surface layer was not thick enough according to the AASHTO-93 method, and therefore the load transmitted to the subgrade increased.

However, the most important point to be noted here is that when the cross-section type and thickness change, the prior failure can be changed, and the fatigue models of the M-E method can also be compatible with AASHTO-93.

Consequently, the rutting equation of AI was chosen as the transfer equation for the optimization of non-linear layer coefficients. In this equation, $\varepsilon_v$ value provides the $T_{8.2}$ of the AASHTO-93 method is obtained as the target strain ($2.366 \times 10^{-4}$) (Equation 7). In the following sections of the study, it is aimed to obtain non-linear layer coefficients which provide this target strain.

### 3.2. Obtaining Non-Linear Layer Coefficients for Base and Sub-base Layers

The $K_1$ and $K_2$ values used in the nonlinear elastic definition of the base and sub-base layers significantly affect the mechanical response values, and these values vary in a wide range according to the type, crush condition, moisture content and granulometry of the aggregate as shown in Table 3-5.

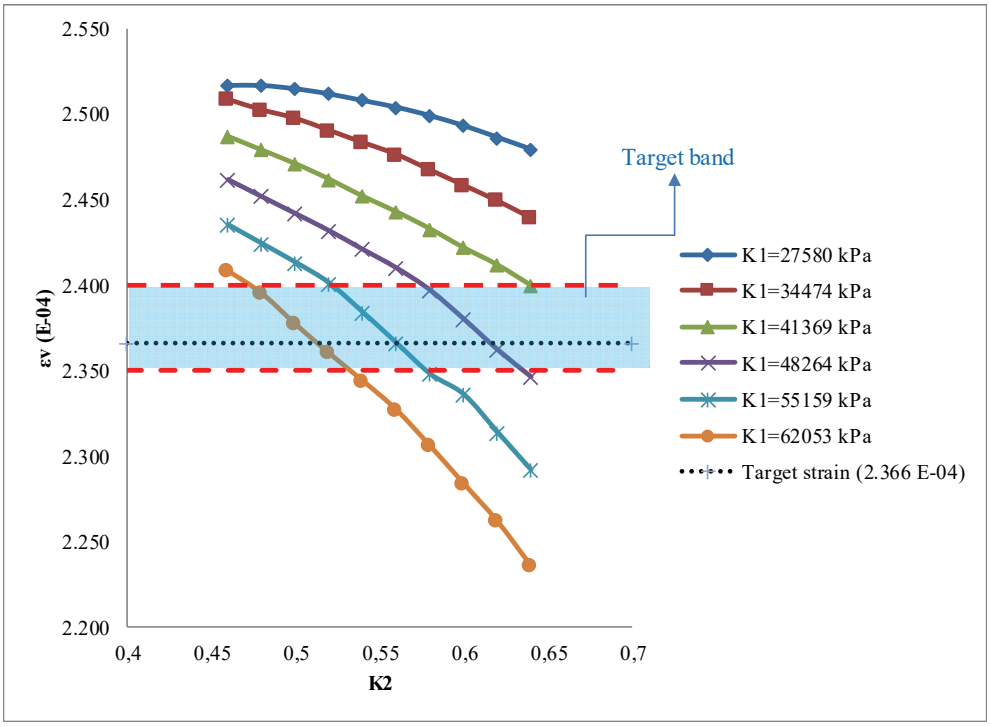


*Figure 3 - Analysis results for base layer optimization*

If the $K_1$ and $K_2$ values can be optimized for base and sub-base layers, a cross-section designed according to AASHTO-93 can be re-analyzed with various loading, material, contact, and environmental conditions and pavement responses and the pavement life values can be determined with M-E design for any distress mode. To determine the non-linear layer coefficients of these two layers, firstly the base layer was defined as non-linear elastic, and the other layers as linear elastic, and $K_1$ and $K_2$ values providing the target strain were obtained. The wet moisture content condition is neglected, and $K_1$ is determined between 27580 and 62053 kPa, $K_2$ is selected between 0.46 and 0.64 compatible to the literature, so 60 different combinations of $K_1$ and $K_2$ were performed mechanically and the results are shown in Figure 3.

In the graph given in Figure 3, $K_2$ increases for any fixed $K_1$ value, and $K_1$ increases for any fixed $K_2$ value with decreasing $\varepsilon_v$ values. That is the deformation resistance of the cross-section increases. The values of $K_1$ and $K_2$ of the base layer are not selected only from combinations that provide target strain, instead, combinations from the $2.4x10^{-4}$-$2.35x10^{-4}$ band (Figure 3) were selected, and the effects of non-linear definition of the sub-base in the next step were also considered. The target strain line intersects with the curves $K_1$ = 48264, 55159, and 62053 kPa. No matter how far the lower bound line of target band is positioned from the target strain, an intersection with a new $K_1$ value cannot be achieved. For this reason, the lower limit of the target band was kept at 2.35 E-04. The upper limit of the target band was determined at 2.4 E-04 to intersect with the curve of 41369 kPa, which is the lower limit value of $K_1$ for dry aggregate. Thus, the number of values to be worked on for optimization has been increased.

According to Figure 3, the combinations of $K_1$ and $K_2$ in the targeted strain band are shown in Table 8.

*Table 8 - $K_1$ and $K_2$ values that provide the target strain for the base layer*

| $K_1$ (kPa) | 62053 | 62053 | 55159 | 55159 | 55159 | 48264 | 48264 | 48264 | 41369 |
|---|---|---|---|---|---|---|---|---|---|
| $K_2$ | 0.48 | 0.52 | 0.52 | 0.54 | 0.56 | 0.58 | 0.60 | 0.62 | 0.64 |
| $\varepsilon_v$ ($x10^{-4}$) | 2.395 | 2.36 | 2.4 | 2.384 | 2.366 | 2.397 | 2.380 | 2.362 | 2.4 |

With the aim of obtaining the non-linear layer coefficients of the sub-base layer, mechanical analyses with various sub-base parameters were performed for each base combination shown in Table 8, and $K_1$ and $K_2$ values were obtained for the target strain. 360 analyses were performed by selecting $K_1$ values between 27580 and 55159 kPa and $K_2$ values between 0.4 and 0.6, and the results are given in Figures 4-12.

When the figures giving the results of the sub-base mechanical analysis are viewed, the $\varepsilon_v$ values decrease while increasing $K_2$ at relatively high $K_1$ values (48264-55159 kPa), and the $\varepsilon_v$ values increase as $K_2$ increases in combinations where $K_1$ has relatively lower values (27580-34474kPa). According to these results, $K_2$ value shows a reversible behavior in a weak sub-base layer under a high-strength base layer.

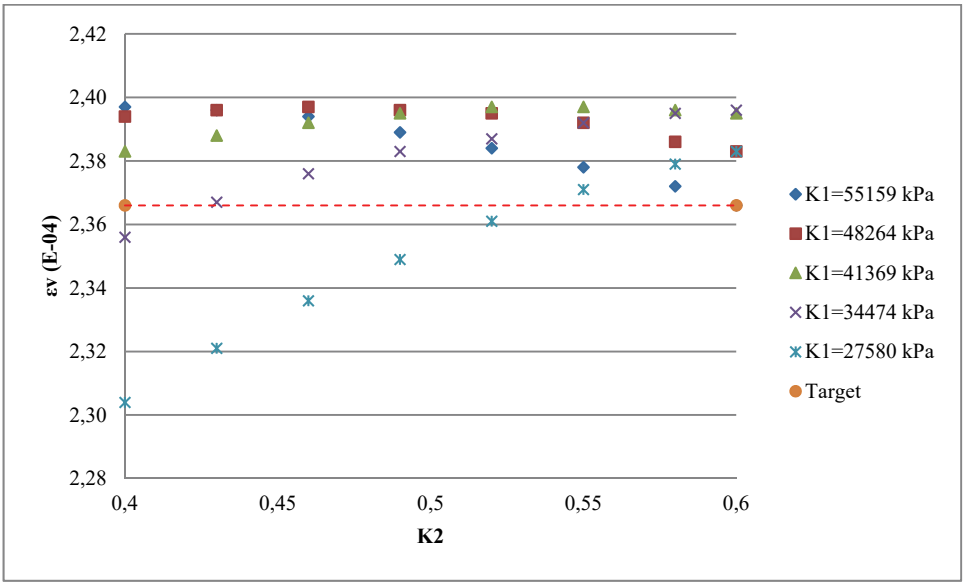


*Figure 4 - Analysis results for sub-base layer (Base layer $K_1$=62053 kPa, $K_2$=0.48)*

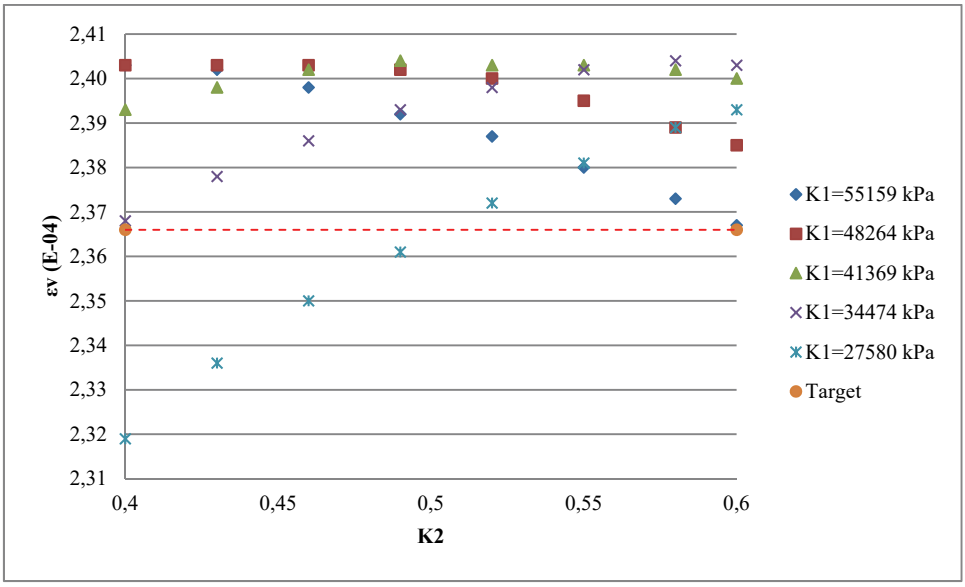


*Figure 5 - Analysis results for sub-base layer (Base layer $K_1$=62053 kPa, $K_2$=0.52)*

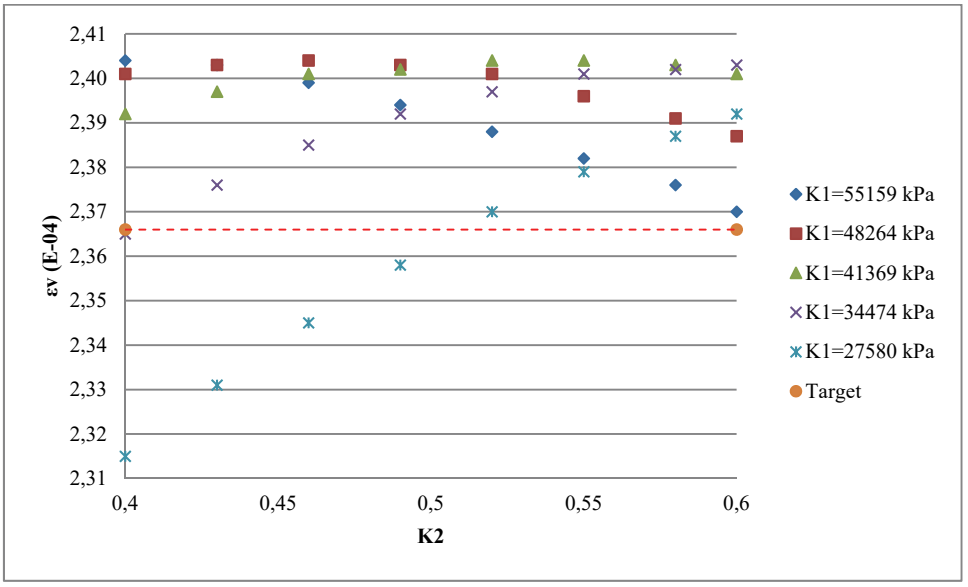


*Figure 6 - Analysis results for sub-base layer (Base layer $K_1$=55159 kPa, $K_2$=0.52)*

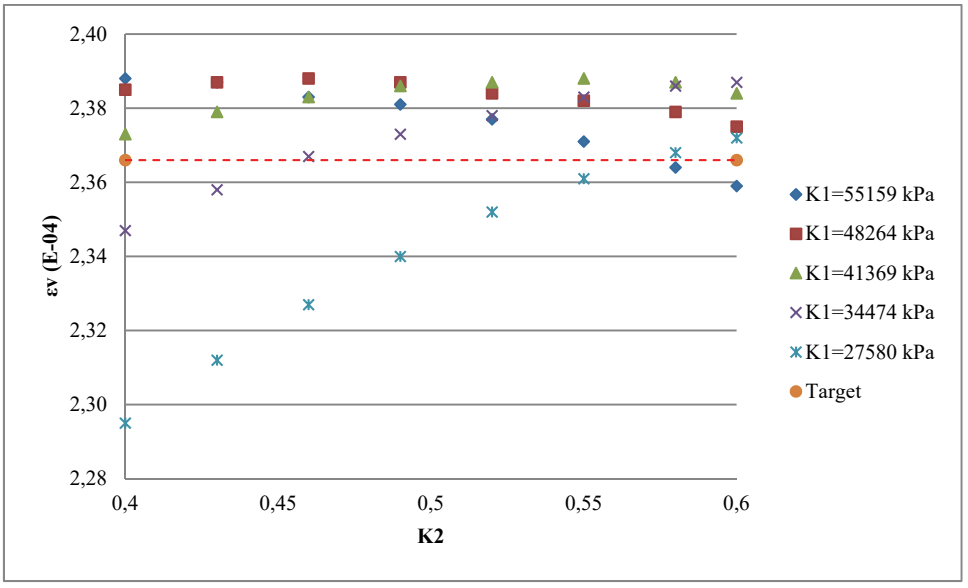


*Figure 7 - Analysis results for sub-base layer (Base layer $K_1$=55159 kPa, $K_2$=0.54)*

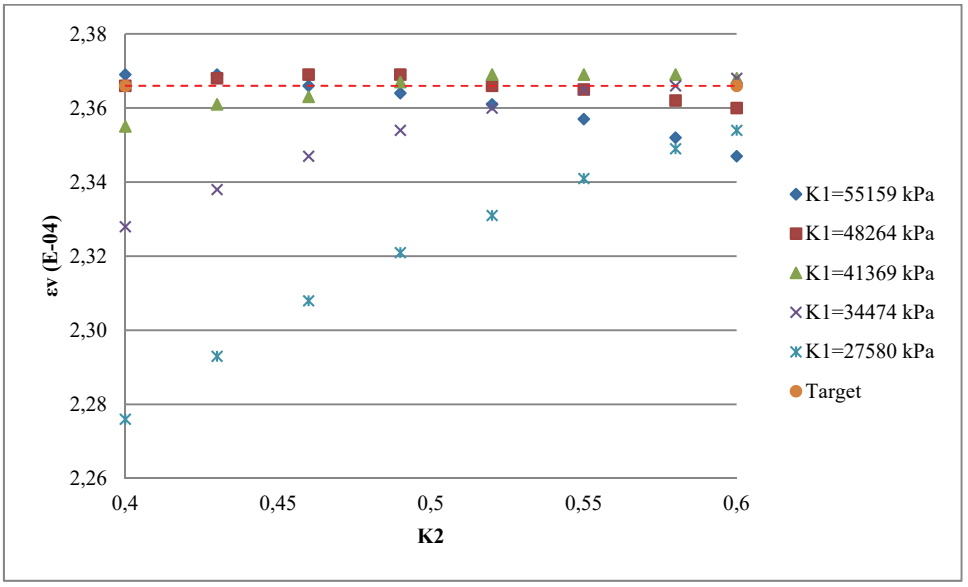


*Figure 8 - Analysis results for sub-base layer (Base layer $K_1$=55159 kPa, $K_2$=0.56)*

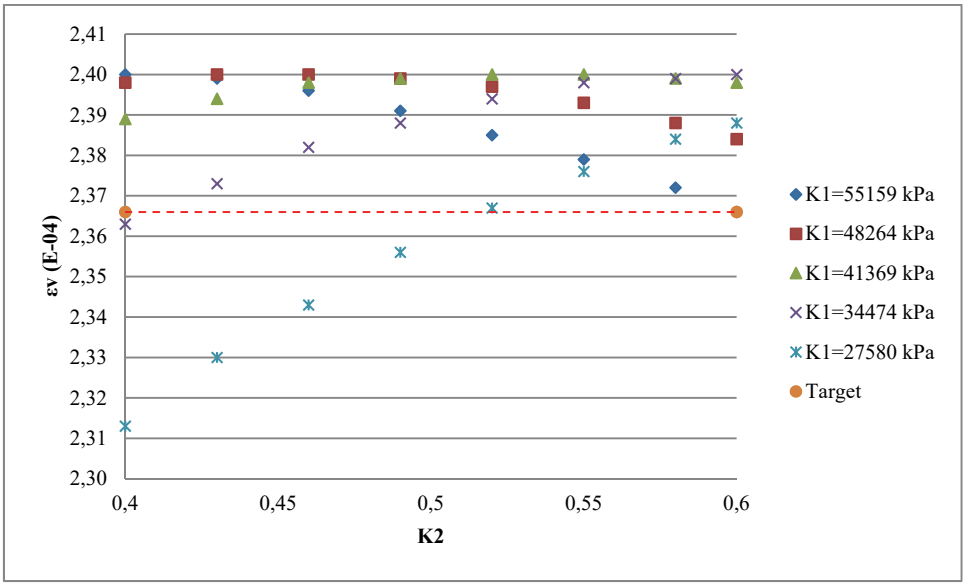


*Figure 9 - Analysis results for sub-base layer (Base layer $K_1$=48264 kPa, $K_2$=0.58)*

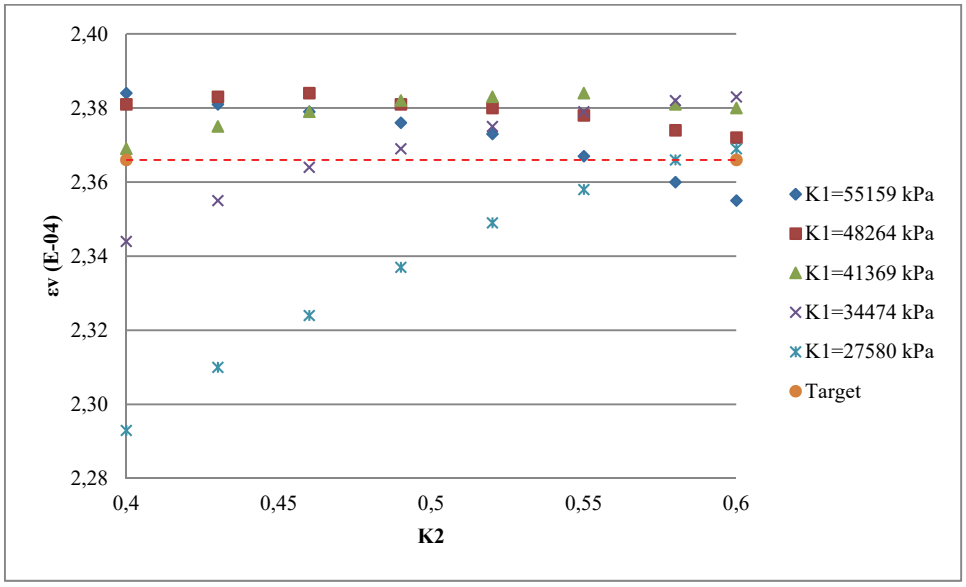


*Figure 10 - Analysis results for sub-base layer (Base layer $K_1$=48264 kPa, $K_2$=0.60)*

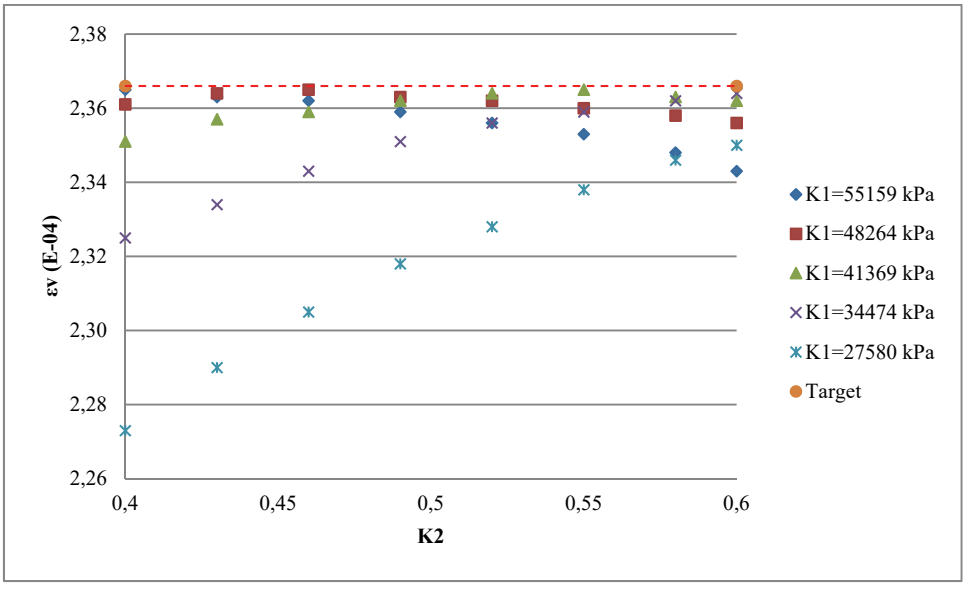


*Figure 11 - Analysis results for sub-base layer (Base layer $K_1$=48264 kPa, $K_2$=0.62)*

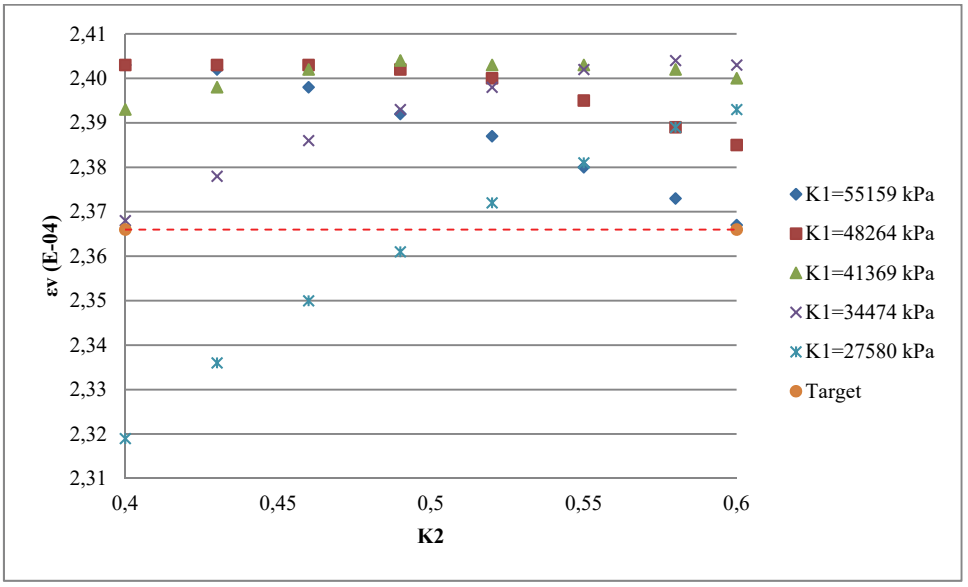


*Figure 12 - Analysis results for sub-base layer (Base layer $K_1$=41369 kPa, $K_2$=0.64)*

In Figures 4-12, the target strain values are shown with dashed lines, and the sub-base $K_1$ and $K_2$ combinations that intersect with these lines are determined. Accordingly, the combinations obtained as a result of defining both base and sub-base layers as non-linear elastic are shown in Table 9.

*Table 9 - Optimum base and sub-base coefficient combinations*

| | Base layer | | Sub-base layer | | |
|---|---|---|---|---|---|
| Combination number | $K_1$ (kPa) | $K_2$ | $K_1$ (kPa) | $K_2$ | $\varepsilon_v$ (x10$^{-4}$) |
| 1 | 55159 | 0.56 | 55159 | 0.46 | 2.366 |
| 2 | 55159 | 0.56 | 48264 | 0.40 | 2.366 |
| 3 | 55159 | 0.56 | 48264 | 0.52 | 2.366 |
| 4 | 55159 | 0.56 | 34474 | 0.58 | 2.366 |
| 5 | 62053 | 0.48 | 55159 | 0.60 | 2.366 |
| 6 | 48264 | 0.58 | 55159 | 0.60 | 2.366 |
| 7 | 48264 | 0.60 | 27580 | 0.58 | 2.366 |

When Table 9 is examined, it is seen that the optimum $K_1$ values obtained for the base layer are higher than the other tested values and provide high deformation resistance. In the 1, 2, 3 and 4 numbered combinations, the $K_1$ and $K_2$ values of the base layer remained the same, while the $K_1$ and $K_2$ values of the sub-base layer varied. In particular, when the combinations 2 and 3 were examined, the $K_1$ values of the sub-base layer under the same base were fixed

as 48264 kPa while the $K_2$ value increased from 0.40 to 0.52, and this change did not affect the strain values. Accordingly, the importance of the $K_2$ value of sub-base in pavements consisting of a rigid base and a rigid sub-base can be relatively smaller. Also, when all the base and sub-base combinations in Table 9 are evaluated together, it can be stated that the $K_1$ and $K_2$ values used for the M-E design to give similar results with the AASHTO-93 method reflect the dry, crushed and well-graded granular material properties.

According to the Turkish Highway Technical Specifications [52], gravel, crushed gravel, terrace gravel, crushed stone, and crushed slag as a base material, sand, gravel, terrace gravel, decomposed rock, slag, and crushed stone can be used as a sub-base material. When the values obtained in Table 9 are evaluated according to the material properties used in base and sub-base layers, the optimum values obtained for the base layer generally reflect dry and well-graded crushed stone aggregate properties (Table 3). Accordingly, the designer may find that the AASHTO-93 and M-E design methods will yield consistent results for a base layer to be constructed with well-graded and dry crushed stone aggregate. However, when the material type and moisture content used in the base layer change, the M-E design method must be included in the design as well as the AASHTO-93 method. For different $K_1$ and $K_2$ values selected from Tables 3 and 4 following the material type and moisture content to be used in construction, the results to be obtained will be different from the results of AASHTO-93.

When the optimum values obtained for the sub-base layer are compared with the $K_1$ and $K_2$ values depending on the moisture content given in Table 5, it can be seen that the dry sub-base material is generally compatible with the AASHTO-93 method. However, when using damp sub-base material (combination number 4 and 7), a compatible base layer must be defined.

## 4. CONCLUSIONS

According to the results obtained from the study, in which the AASHTO-93 method is compared with different empirical transfer models in the M-E design method in terms of pavement life, and the non-linear elastic layer parameters used in mechanical analysis are optimized, the following inferences can be made.

- Axle loads and configurations, tire pressures and patterns, mechanical properties of pavement layers, and climate and environmental conditions are constantly changing. For this reason, in the design of flexible pavements, the M-E design method must be taken into consideration together with empirical methods developed according to certain experimental parameters.
- The empirical pavement life estimation models used in the M-E design proposed by different organizations give quite different results from each other and the AASHTO-93 method. While the mean value obtained from the $N_f$ estimation models is calculated as $2.228 \times 10^6$, its standard deviation is $3.908 \times 10^6$, and the coefficient of variation is 175%, for rutting models the mean is $236.7 \times 10^6$, the standard deviation is $333.99 \times 10^6$, and the coefficient of variation is 141%. This high statistical values, especially in the coefficients of variation, show that calibration of the pavement life estimation model in M-E design methods is critical.

- In the flexible pavement design, the main type of deterioration the road will be exposed to should be prioritizedbecause different distress models of the same agency, show highly different design results. When Nr/Nf values are calculated for AI, Shell, US Army Corps of Engineers, Belgian Road Research Center, and Transport and Road Research Laboratory models, the results are obtained as 18.66, 133.7, 1163.6, 1257.4 and 37.9, respectively. When these results are taken into consideration, it is of great importance to estimate the prior distress type of pavement. Considering that the AASHTO-93 method, which is compared with the M-E methods in the present study, yields more consistent results with the transfer equations related to the rutting, the reliability of the AASHTO design decreases significantly for a cross-section subject to fatigue under heavy traffic.
- The cross-section analyzed in this study gave more consistent results with the rutting models in terms of layer thickness (especially 15 cm surface layer). However, if the cross-section type changes and thicker surface layers are used in the surface layer, the prior distress type may return to fatigue. In this case, while the unbound layer coefficients are optimized, tensile strain under the surface layer should be used as the target strain.
- In this study, the optimum layer coefficients obtained for the base and sub-base layers show that the materials used in the layers are constructed with well-graded and dry aggregates. In this case, the AASHTO-93 and M-E methods are compatible with each other. However, as the materials used in the base and sub-base layers and moisture contents change, M-E methods must be included in the design solution that takes into account the non-linear behavior of the materials.
- In the empirical pavement design methods related to the road tests, the change of the parameters used in the test affects the design results. It is a remarkable subject of study that the empirical method results are associated with an M-E method since it is not possible to examine a large number of parameters that affect the design of pavement. Thus, M-E design parameters (layer material characterization, contact type, etc.) can be optimized according to the empirical method outputs, and various analyses can be made with M-E design with different loading and environmental conditions.

**Funding**

This work is supported by the Scientific Research Project Fund of Sivas Cumhuriyet University under the project number M-753.

**References**

[1] Huang, Y. H., Pavement analysis and design. 2nd ed. Upper Saddle River, NJ: Pearson Prentice Hall, 1993.

[2] Mashayekhi, M., Amini, A.A., Behbahani, H., Nobakht, S., Comparison of mechanistic-empirical and empirical flexible pavement design procedures of AASHTO: A Case Study, 5th International Conference Bituminous Mixtures and Pavements, Thessaloniki, 2011.

[3] Alhasan, A., Ali, A., Offenbacker, D., Smadi, O., Lewis-Beck, C., Incorporating spatial variability of pavement foundation layers stiffness in reliability-based mechanistic-empirical pavement performance prediction, Transportation Geotechnics, 17, 1-13, 2018.

[4] Carvalho, R. L., Schwartz, C. W., Comparisons of flexible pavement designs: AASHTO empirical versus NCHRP project 1–37A mechanistic–empirical, Transportation Research Record, 1947(1), 167-174, 2006.

[5] Sağlık, A., Güngör, A.G., Highways flexible pavement design guide, Ankara, 2008.

[6] Çelik, O. N., Eyada, S. O., Assessment of flexible pavement fatigue life of Turkish typical sections using mechanistic empirical pavement design approach for coastal region, Ain Shams Engineering Journal, 10(1), 33-43, 2019.

[7] Muniandy, R., Aburkaba, E., Thamer, N., Comparison of flexible pavement performance using Kenlayer and Chev PC software program, Australian Journal of Basic and Applied Sciences, 7(9), 112-119, 2013.

[8] Behiry, A. E. A. E. M., Fatigue and rutting lives in flexible pavement, Ain Shams Engineering Journal, 3(4), 367-374, 2012.

[9] Mousa, M. R., Abo-Hashema, M.A., Gadallah, A.A., Mousa, R.M., Evaluation of pavement performance prediction models under different traffic and climatic conditions, The Proceedings of International Conference on Asphalt Pavement Engineering and Infrastructure, London, 2015.

[10] Singh, A. K., Sahoo, J. P., Analysis and design of two layered flexible pavement systems: A new mechanistic approach, Computers and Geotechnics, 117, 103238, 2020.

[11] Abd Alla, E. M., The rational use of finite element method in the analysis of flexible pavements, Journal of Engineering Sciences, Assiut University, 34(4), 1185-1211, 2006.

[12] Titi, H. H., Matar, M. G., Estimating resilient modulus of base aggregates for mechanistic-empirical pavement design and performance evaluation, Transportation Geotechnics, 17, 141-153, 2018.

[13] Ng, K., Henrichs, Z.R., Ksaibati, K., Wulff, S.S., Resilient modulus of subgrade materials for mechanistic-empirical pavement design guide, Road Materials and Pavement Design, 19(7), 1523-1545, 2018.

[14] Shahji, S. Sensitivity analysis of AASHTO'S 2002 flexible and rigid pavement design methods, Thesis (MSc), University of Central Florida, 2006.

[15] Masad, S.A., Little, D.N., Sensitivity analysis of flexible pavement response and AASHTO 2002 design guide to properties of unbound layers. Research report ICAR 504-1, International Center for Aggregates Research, 2004.

[16] Cerni, G., Cardone, F., Virgili, A., Camilli, S., Characterisation of permanent deformation behaviour of unbound granular materials under repeated triaxial loading, Construction and Building Materials, 28(1), 79-87, 2012.

[17] Sahin, H., Gu, F., Tong, Y., Luo, R., Lytton, R. L., Unsaturated soil mechanics in the design and performance of pavements, Advances in Unsaturated Soils, 105-118, 2013.

[18] Ahirwar, S. K., Mandal, J. N., Finite element analysis of flexible pavement with geogrids, Procedia Engineering, 189, 411-416, 2017.

[19] Seed, H. B., Mitry, F.G., Monismith, C.L., Chan, C.K., Prediction of flexible pavement deflections from laboratory repeated-load tests, Report No: 35, NCHRP, 1967.

[20] May, R. W., Witczak, M. W., Effective granular modulus to model pavement responses, Transportation Research Record, 810, 1-9, 1981.

[21] Uzan, J., Characterization of granular material, Transportation Research Record, 1022(1), 52-59, 1985.

[22] Ni, B., Hopkins, T.C., Sun, L., Beckham, T.L., Modeling the resilient modulus of soils, Proceedings of the 6th International Conference on the Bearing Capacity of Roads and Airfields, Lisbon, 2002.

[23] Luo, X., Gu, F., Zhang, Y., Lytton, R. L., Zollinger, D., Mechanistic-empirical models for better consideration of subgrade and unbound layers influence on pavement performance, Transportation Geotechnics, 13, 52-68, 2017.

[24] Masad, S., Little, D., Masad, E., Analysis of flexible pavement response and performance using isotropic and anisotropic material properties, Journal of Transportation Engineering, 132(4), 342-349, 2006.

[25] Adu-Osei, A., Little, D. N., Lytton, R. L., Cross-anisotropic characterization of unbound granular materials, Transportation Research Record, 1757(1), 82-91, 2001.

[26] Tutumluer, E., Thompson, M. R., Anisotropic modeling of granular bases in flexible pavements, Transportation Research Record, 1577(1), 18-26, 1997.

[27] Yang, S. R., Huang, W. H., Tai, Y. T. Variation of resilient modulus with soil suction for compacted subgrade soils, Transportation Research Record, 1913(1), 99-106, 2005.

[28] Butalia, T.S., Huang, J., Kim, D.G., Croft, F., Effect of moisture content and pore water pressure buildup on resilient modulus of cohesive soils in Ohio, ASTM Special Technical Publication, 1437, 70–84, 2003.

[29] Wolfe, W., Butalia, T., Continued monitoring of SHRP pavement instrumentation including soil suction and relationship with resilient modulus, Report No: FHWA/OH-2004/007, Department of Transportation, Federal Highway Administration, 2004.

[30] Gupta, S., Ranaivoson, A., Edil, T., Benson, C., Sawangsuriya, A., Pavement design using unsaturated soil technology, Report No: MN/RC-2007-11, University of Minnesota, 2007.

[31] Cary, C. E., Zapata, C. E., Resilient modulus for unsaturated unbound materials. Road Materials and Pavement Design, 12(3), 615-638, 2011.

[32] Ghadimi, B., Nikraz, H., A comparison of implementation of linear and nonlinear constitutive models in numerical analysis of layered flexible pavement, Road Materials and Pavement Design, 18(3), 550-572, 2017.

[33] Ghanizadeh, A. R., Ziaie, A., NonPAS: a program for nonlinear analysis of flexible pavements, International Journal of Integrated Engineering, 7(1), 2015.

[34] Karagöz, C., Analysis of Flexible pavements incorporating nonlinear resilient behavior of unbound granular layers, Thesis (PhD), Middle East Technical University, 2004.

[35] Hicks, R. G., Factors influencing the resilient properties of granular materials, Thesis (PhD), University of California, Berkeley, 1970.

[36] Hicks, R. G., Finn, F. N., Analysis of results from the dynamic measurements program on the San Diego test road, Proceedings, Association of Asphalt Paving Technologists, 39, 153-185, 1970.

[37] Allen, J. J., The effects of non-constant lateral pressure on the resilient response of granular materials, Thesis (PhD), University of Illinois at Urbana-Champaign, 1973.

[38] Kalcheff, I. V., Hicks, R. G., A test procedure for determining the resilient properties of granular materials, Journal of Testing and Evaluation, 1(6), 472-479, 1973.

[39] Boyce, J. R., Brown, S. F., Pell, P. S., The resilient behaviour of a granular material under repeated loading, Australian Road Research Board Conference Proceedings, 8, 1-12, 1976.

[40] Monismith, C. L., Witczak, M. W., Moderator's report, paper in session I, Pavement Design, Proceedings Fifth International Conference on the Structural Design of Asphalt Pavements, Netherlands, 2, 2-58, 1982.

[41] Pan, E., Chen, E., Alkasawneh, W., An exploratory study on functionally graded materials with applications to multilayered pavement design, Report No: FHWA/OH-2007/12, Department of Civil Engineering the University of Akron, 2007.

[42] Hafeez, I., Shan, A., Ali, A., Ahmed, I., Flexible pavement design evaluation using mechanistic-empirical approaches. Technical Journal, University of Engineering and Technology, 22, 27-33, 2017.

[43] Beskou, N. D., Tsinopoulos, S. V., Theodorakopoulos, D. D., Dynamic elastic analysis of 3-D flexible pavements under moving vehicles: A unified FEM treatment, Soil Dynamics and Earthquake Engineering, 82, 63-72, 2016.

[44] Al-Azzawi, A. A., Finite Element Analysis of Flexible Pavements Strengthed with Geogrid, ARPN Journal of Engineering and Applied Sciences, 7(10), 1295-1299, 2012.

[45] Ekwulo, E. O., Eme, D. B., Fatigue and rutting strain analysis of flexible pavements designed using CBR methods, African Journal of Environmental Science and Technology, 3(12), 2009.

[46] Perraton, D., Di Benedetto, H., Carter, A., Proteau, M., Link between different bottom-up fatigue's law coefficients of mechanical-empirical pavement design software, Construction and Building Materials, 216, 552-563, 2019.

[47] Priest, A., Calibration of fatigue transfer functions for mechanistic-empirical flexible pavement design, Thesis (PhD), Auburn University, 2005.

[48] Ziari, H., Khabiri, M. M., Interface condition influence on prediction of flexible pavement life, Journal of Civil Engineering and Management, 13(1), 71-76, 2007.

[49] Chegenizadeh, A., Keramatikerman, M., Nikraz, H., Flexible pavement modelling using Kenlayer, The Electronic Journal of Geotechnical Engineering, 21, 2467-2479, 2016.

[50] Hadi, M. N., Bodhinayake, B. C., Non-linear finite element analysis of flexible pavements, Advances in Engineering Software, 34(11-12), 657-662, 2003.

[51] Samad, E., Sensitivity analysis in flexible pavement performance using mechanistic empirical method (Case study: Cirebon–Losari road segment, West Java), Journal of the Civil Engineering Forum, 20(1), 1163-1174, 2011.

[52] Turkey General Directorate of Highways, Highways technical specification, Ankara, Turkey, 2013.

*Teknik Dergi, 2021 11337-11359, Paper 636*

# Evaluation of Load-Transfer Efficiency of Steel Mesh Reinforced Contraction Joints in Concrete Pavement: Accelerated Pavement Test and FE Analysis

**Muhammet ÇELİK[1]**
**Mehmet Tevfik SEFEROĞLU[2]**
**Muhammet Vefa AKPINAR[3]**
**Mohammad Manzoor NASERY[4]**
**Ayşegül Güneş SEFEROĞLU[5]**

## ABSTRACT

Transverse contraction joints are by far the most common type of joint in jointed plain concrete pavements. Early loading of contraction joints can create a weakened vertical plane and later grow as a full-depth crack. In this study, load transfer efficiency (LTE) of steel mesh reinforced transverse contraction joints were studied at accelerated pavement tests (APT). 3D finite element (FE) model of jointed plain concrete pavement (JPCP) was developed to study deflections and crack propagation in just under the joint of the concrete pavement. The APT tests were focused on the LTE values before and after the crack initiation under the contraction joint region. Experiments were performed on three slabs in which two of these slabs were prepared without reinforcement and one of them was reinforced with steel mesh. Data generated by APT was used for verification of crack propagation modeling in the finite element analysis. Steel mesh reinforced slab gave the lowest vertical deflections (51μm) and highest LTE (91.56%). The LTE value in the reinforced slab after 25,000 passes was 13.63% higher than the average of unreinforced slabs. The findings suggest that the load transfer efficiency was found to be a complex parameter and should be interpreted together with average displacement values when contraction joints are evaluated at early traffic loadings.

Note:
- This paper was received on November 5, 2019 and accepted for publication by the Editorial Board on April 17, 2020.
- Discussions on this paper will be accepted by January 31, 2022.
- https://doi.org/10.18400/tekderg.643027

1 Yalova University, Department of Civil Engineering, Yalova, Turkey
m.celik53@gmail.com - https://orcid.org/0000-0002-3998-8146

2 Gumushane University, Department of Civil Engineering, Gümüşhane, Turkey
mtseferoglu@gmail.com - https://orcid.org/0000-0003-4677-3335

3 Karadeniz Technical University, Department of Civil Engineering, Trabzon, Turkey
mvakpinar70@yahoo.com - https://orcid.org/0000-0001-7912-8274

4 Karadeniz Technical University, Department of Civil Engineering, Trabzon, Turkey
manzoor.nasery@gmail.com - https://orcid.org/0000-0003-3787-1355

5 Gumushane University, Department of Civil Engineering, Gümüşhane, Turkey
gnskaya61@gmail.com - https://orcid.org/0000-0002-1008-6456

**Keywords:** Accelerated pavement test, finite element analysis, concrete pavement, transverse contraction joint, steel mesh reinforcement.

## 1. INTRODUCTION

Concrete pavements are exposed to different stresses due to traffic loads and environmental conditions. These stresses cause uncontrolled cracks in concrete slabs over time. Contraction joints are made to ensure that these cracks occur in the weakened section [1]. Sawed concrete pavement joints are widely used in paving and industrial construction for efficient and cost-effective crack control [2, 3]. Saw cut joints minimize random cracking due to temperature changes and drying shrinkage. The weakened sections created by the joint cause the cracks to form at these locations. Cracking occurs beneath the sawed region as soon as the tensile stress overcomes the tensile strength of the concrete.

Contraction joints are one of the easiest and most economical methods to ensure the load transfer between the slabs [2, 3]. Contraction joints are usually cut 1/6-1/3 of the slab depth using wet or dry conventional contraction methods [4, 5]. Micro cracks just below the contraction joints start developing as soon as the road is open to traffic. However, these cracks also help to carry the vertical loads due to the internal friction between the aggregates at the joints [6-8].

Load transfer in concrete pavements is the capacity of a joint to transfer a portion of the wheel load from one side of the joint to the next. The load transfer is accomplished by steel reinforcement, aggregate interlock across adjacent edges of concrete slabs and friction between the concrete and stabilized base [6, 7]. For unreinforced jointed plain concrete pavement (JPCP), aggregate interlock underneath the saw cut portion of the joint provides the majority of the load transfer [5]. After the crack formation, the load transfer diminishes marginally [8, 9]. Over time these aggregate interlock faces can wear and load transfer can drop down, especially when there is no reinforcement. The field observation of the splits under a contraction joint is demonstrated in Fig. 1.

*Figure 1 - Crack observation under the contraction joint in-service pavement (Trabzon/Turkey).*

The repetitive traffic loading induced vertical deflections to cause the pavement to deteriorate early [10-12]. Vertical deflections vary according to many factors such as; concrete slab sizes, the thickness, load type, load repetition, base/sub-base conditions, joint type, joint depth, the presence of reinforcement, the vertical and horizontal slope of pavement,... etc. [13]. 'Load transfer efficiency', 'load transfer' and 'joint transfer efficiency' are terms that have been used by researchers to define the load transfer mechanism between the concrete slabs [14-15]. Deflection based LTE can be defined as a surface deflection measured on an unloaded slab relative to that on a loaded slab. Higher LTE at a joint indicates that traffic loading can result in lower vertical deflection [16].

The need for faster and more practical assessment methods that closely simulate service conditions has required the consideration of accelerated pavement testing (APT) facilities. APT develops road technology and provides an understanding of the performance of pavement systems while producing early, reliable and useful results [17, 18]. The APT system can be defined as a system that simulates the actual loading conditions that will affect the pavement in the field by simulating it in a controlled manner. The performance of the pavement in APT facilities can be achieved in a much shorter period than in the field. The 5-20 years of traffic loads can be carried out in 3-12 months with APT. Moreover, environmental conditions (temperature, humidity...) can be simulated and the response of the pavement in different ambient conditions can be obtained [19-23].

In this study load-transfer efficiency of steel mesh reinforced contraction joints in concrete pavement using the accelerated pavement test and FE analysis is evaluated. FE model of JPCP was developed using ABAQUS software to study deflections and crack propagation under the concrete pavement. The analysis focused on the LTE values before and after the crack initiation under the contraction joint. Finally, the cost-benefit analysis of using steel mesh reinforcement has been made.

## 2. EXPERIMENTAL PROGRAM

### 2.1. APT Facility

The scope of the APT facility was utilized to investigate 4 m × 2 m × 180 mm (thick) JPCP slabs as shown in Fig. 2 and Fig. 3. The test sections were constructed on top of a 300 mm thick base layer of natural gravel with a CBR of 80%. Average surface vertical deflections for each APT section were measured by LVDTs (linear variable differential transformers).

Each test section was applied for 1,000 passes/day with 0.80 MPa double wheels LVDTs were placed on both sides of the joint and the data were collected. During the testing program, the air temperature inside the APT facility varied between 21-25°C and the concrete surface temperature varied between 20-21°C and the bottom of the slab varied between 19-20°C. The difference between the top and bottom of the concrete was around 3°C which can be ignored when thermal effects are considered. The average relative humidity varied from 50 to 60%. Freeze-thaw effects were not considered in APT tests unless the tests were specifically designed to include these effects.

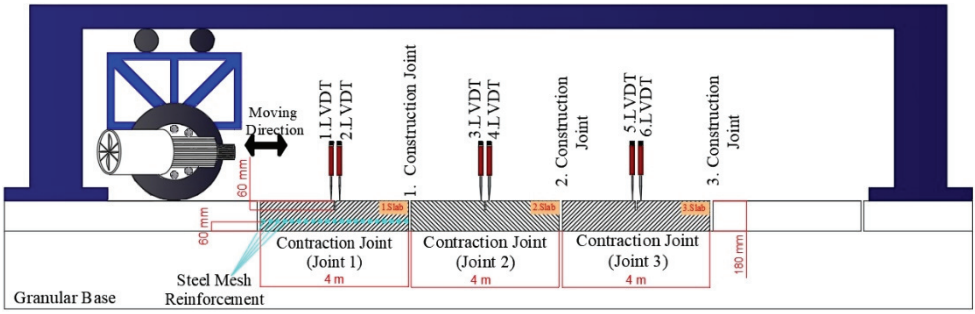


*Figure 2 - Side view of the test section*

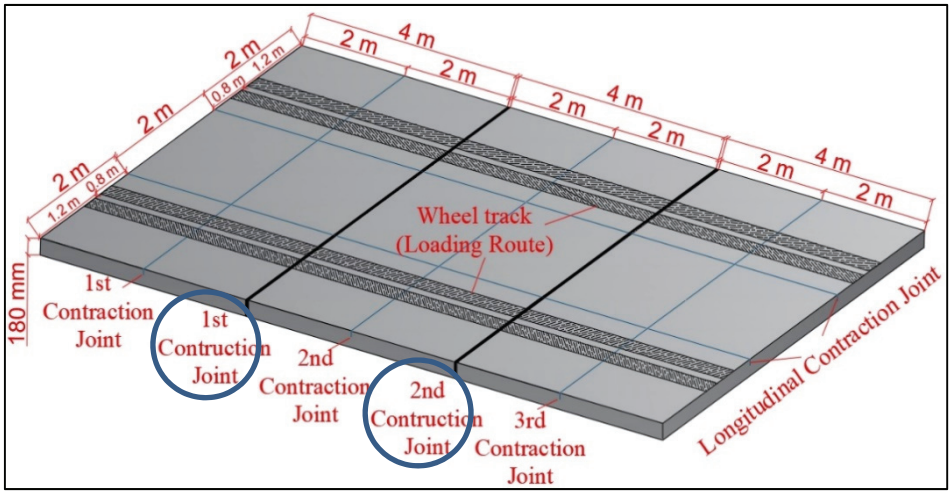


*Figure 3 - Construction and contraction joints*

## 2.2. Materials

### *2.2.1. Concrete Pavement, Base and Subbase Layer*

The existing 180 mm thick concrete pavement was made of CEM I 42.5 Portland cement having a characteristic compressive strength of 25 MPa. C25 standardized mix concrete is widely versatile and used in numerous commercial and domestic concrete pavement projects. The early core samples collected on the county roads showed that the concretes had typical C25 characteristics. The concrete density was 2,400 kg/m$^3$, tensile strength was 1.9-2 MPa. The testing program started three months after the concrete was paved in order to eliminate the strength parameter.

The most commonly specified steel mesh for paving works is A142 (6 mm wires), A193 (7 mm wires) and A252 (8 mm wires). A142 mesh is frequently utilized in 100 mm thick driveways and parking lots, although A252 is generally used in 150-200 mm thick slabs. As

shown in Fig. 4, the first slab was made of A252 steel mesh reinforced type, while the other two slabs were unreinforced. The section where steel mesh reinforcement spacing was 150 mm × 150 mm. The concrete slab was paved over a 300 mm thick granular base layer.

*Figure 4 - Mesh reinforcement was positioned 60 mm above the base layer*

*Table 1. Material Characteristics*

| Layer | Thickness (mm) | Dry unit weight ($kg/m^3$) | Elastic/ Modulus (MPa) | CBR (%) | Moisture Content (%) | Relative Compaction (%) |
|---|---|---|---|---|---|---|
| Concrete | 180 | 2,400 | 32,000 | - | - | - |
| Base | 300 | 2,100 | 300 | 80 | 5 | 98 |
| Subbase | 1,000 | 1,900 | 100 | 60 | 6 | 95 |


*Figure 5 - The base layer beneath the concrete pavement*

Figure 5 shows the compacted base and subbase layers and Table 1 shows the material characteristics. The base layer moisture content was maintained constant at 5% and no hydro-pumping effect was observed during the test. In terms of moisture content, the aggregate base moisture content of 5% was relatively low.

### *2.2.2. Contraction Joints*

Contraction joints were applied on the centerline of the concrete slabs (4 m × 2 m) as shown in Fig. 3. The slabs were apart from each other with construction joint (full depth joint), meaning that their deflections were not influenced by the adjacent ones. Full depth construction joints and contraction joints had 20 mm and 5 mm openings, respectively. The contraction joints were obtained by cutting down to 1/3 (60 mm) of the concrete slab depth (180 mm) as shown in Fig. 6. Consistent joint dimensions (same width and depth of each cut) were obtained. Typically, for jointed unreinforced concrete pavements, the joint spacing is about 30 times the thickness with the maximum spacing of 4.5 m. Generally, 3.7-4.6 m joint spacing is recommended as appropriate for concrete pavements with 180 mm thickness [24].


*Figure 6 - Saw-cut contraction joint and joint openings*

### 2.3. Test set-up

Vertical deflections under loading in contraction joints were monitored by LVDTs. To eliminate undesired excessive vibration deflections caused by moving wheels, the deflection sensors were mounted to the wall near the slab. The LVDT is capable of measuring up to 150 mm one hundred million translations from -20°C to +80°C. Figure 7 shows the locations of the LVDTs placed along the slab edges.

A uniform contact pressure of 0.8 MPa was maintained below each wheel passing. Pressure cells were placed on the slabs for calibration of the two wheels before and during the tests (Fig. 8). A total of 25,000 passes were made on the pavement lane and a total of 1,000 loads per a day were applied. The speed of the dual wheels was adjusted to 3 km/h in order to represent the heavy vehicle effect. In this study similar to literature the speed was adjusted

to 3 km/h in order to obtain an early crack at the joints. Similar loads and speeds were used by early studies [25-30].

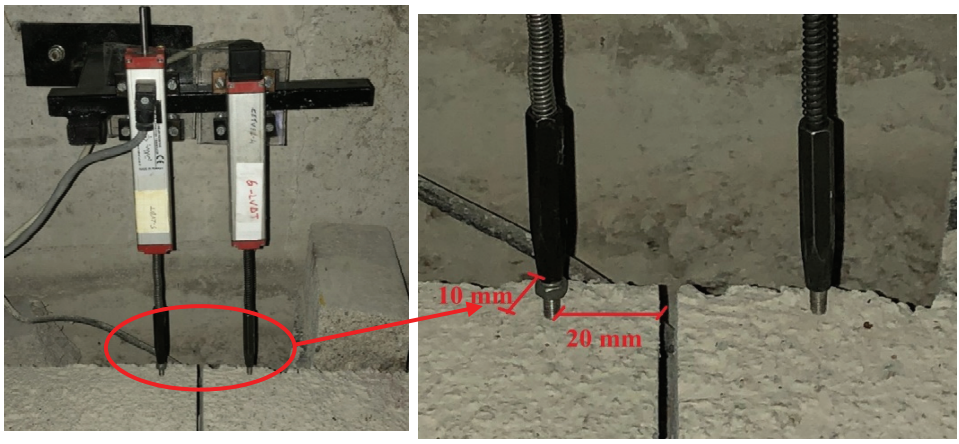


*Figure 7 - The LVDTs at both sides of the joint were mounted on the wall*


*Figure 8 - The pressure cell*

### 2.4. FE Modeling

A nonlinear 3D FE model was developed using ABAQUS version 6.12 to determine numerically the behavior of the contraction joints and induced cracks in the concrete slabs. As seen in Fig. 9, four different models (before and after the crack initiation) were examined in the finite element analysis.

To reduce the analysis time, only the space between the three joints was modeled. In the modeling process, the eight-node brick element with reduced integration (C3D8R) element

type was used in concrete slabs, base layer, and subbase layers. While for the reinforcement mesh a 2-node linear 3-D truss element (T3D2) was used (Fig. 10).

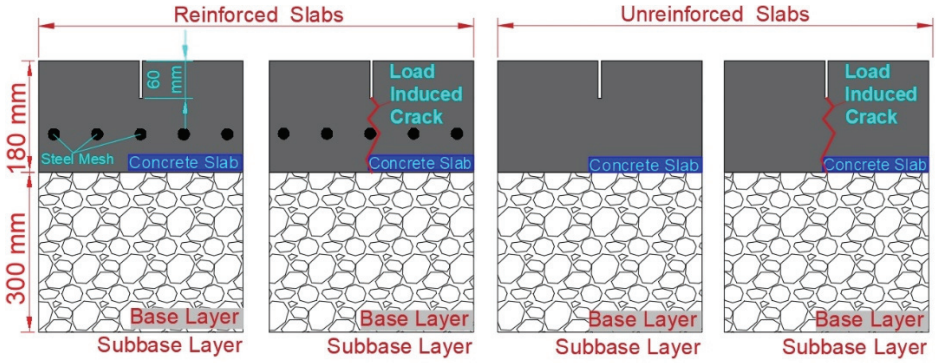


*Figure 9 - Reinforced and unreinforced FEM models before and after the crack initiation*

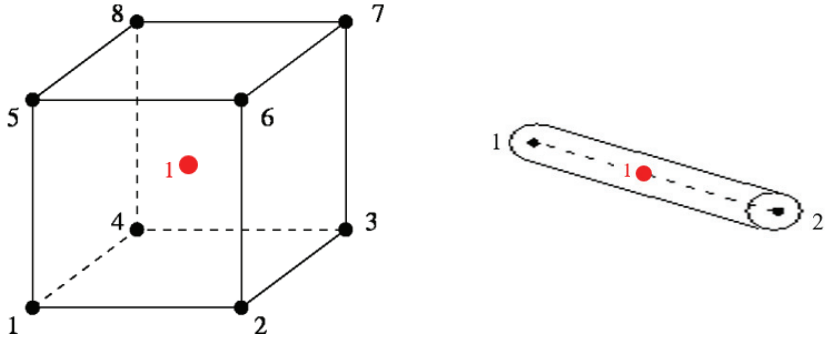


*(a)* *(b)*

*Figure 10 - (a) Eight-node brick element with reduced integration (C3D8R)*
*(b) 2-node linear 3-D truss element [31]*

To simulate the tire pressure during the nonlinear finite element analysis, two blocks were modeled with a similar dimension of the tire footprint 300 mm × 250 mm which was used in the experimental study. Frictional tangential behavior properties were used in the surface to surface contact elements representing the contact between the layers. To idealize the subgrade in FE models, built-in boundary condition were assigned to the bottom of the subbase layer. In this condition, all degrees of freedoms have been limited. The defined boundary condition, exerted tire pressure and three dimensional FE model with saw joint are presented in Fig.11.

One of the main aims of the study was the investigation of cracks in concrete slabs especially near the joints. To simulate the crack progression and stiffness degradation of the material, concrete damaged plasticity (CDP) material models were used. In ABAQUS, the stress-strain

curve must be defined to CDP model for both compression and tensile under uniaxial. During the study concrete slabs were paved with C25 class concrete, which means that the compressive strength of the concrete was 25 MPa. The idealized stress-strain curves of concrete in the experimental study were defined in the CDP model. Stiffness degradation parameters for both compression and tension were also defined by the mechanical properties of the CDP model. In addition, the material properties which were used in the CDP model are summarized in Table 2 [32]. For the simulation of the soil and compacted gravel layers, the most common material model is Drucker Prager Hardening model [33]. Therefore, in the base and subbase layers the Drucker Prager Hardening material model was used. The elasticity model was taken as 300 MPa for the base layer and 100 MPa for subbase layer. For both materials, the Poisson ratio was defined as 0.3 [34].

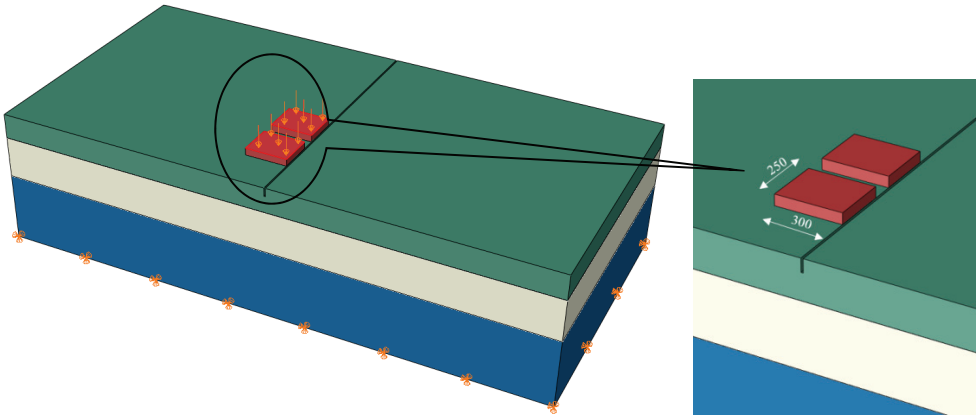


*Figure 11 - FE model with saw joint, tire pressure and boundary conditions*

*Table 2 - Material properties and parameters of C25 concrete [32]*

| | | | | | |
|---|---|---|---|---|---|
| Initial modulus of elasticity | $E_o$ (MPa) | 32,000 | Ratio of initial equi-biaxial compressive yield stress to initial uniaxial compressive yield stress | Fbo/Fco | 1.16 |
| Poisson ratio | ν | 0.2 | Max. damage parameter of tensile | dt | 0.99 |
| Density | ρ (kg/m³) | 2,400 | The ratio of the second stress invariant on the tensile meridian to that on the compressive meridian | Kc | 0.667 |
| Compressive Strength | Fck (MPa) | 25 | Eccentricity | *e* | 0.01 |
| Peak strain of compressive | ε | 0.002 | Dilation angle | Ψ | 36 |
| Ultimate strain | εu | 0.0034 | Tensile strength | Fctk (MPa) | 1.9 |

After a set of studies, the mesh element size of the concrete, base, and space was determined as 20 mm. However, the contraction distance was 5 mm, to optimize the analysis duration and obtain the best crack distribution, the area near to the joints were meshed as 5 mm. 3D finite element model with intensive mesh near the joint area is shown in Fig. 12.

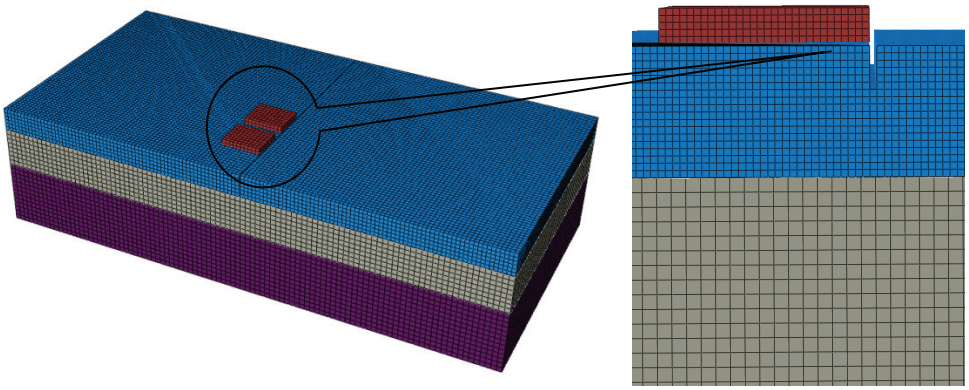

*Figure 12 - FE modeling of the saw cut contraction joint with intensive mesh near the joint area*

## 3. RESULTS AND DISCUSSION

### 3.1. APT Results

#### *3.1.1. Deflection Results*

In this study, LTE values were calculated using Eq. 1 [35] which is the most commonly used LTE AASHTO formula.

$$(\%)LTE = \frac{\delta_U}{\delta_L} \times 100 \quad (1)$$

Where, $\delta_L$ and $\delta_U$ are deflection values obtained from the joint on the loaded (approach) and unloaded (leave) slab, respectively.

Figure 13 shows the measured deflections at the initial and the final loadings (25,000), respectively. LVDT sensors numbered as 1, 3 and 5 measured deflections near the tire load. At the same time LVDTs 2, 4 and 6 measured the deflections on the opposite side of the joints, as shown in Fig. 13. As seen in Fig. 13, joint-1 is located on the center of the steel mesh reinforced slab; joint-2 and joint-3 is located on the slab with no steel reinforcement. Joint-2 and joint-3 refer to two contraction joints at adjacent slabs with the same characteristics (same dimensions and strength) with no mesh steel reinforcement.

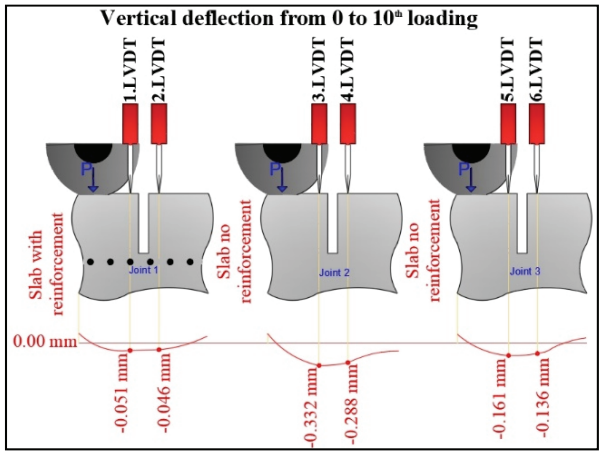


*(a)*

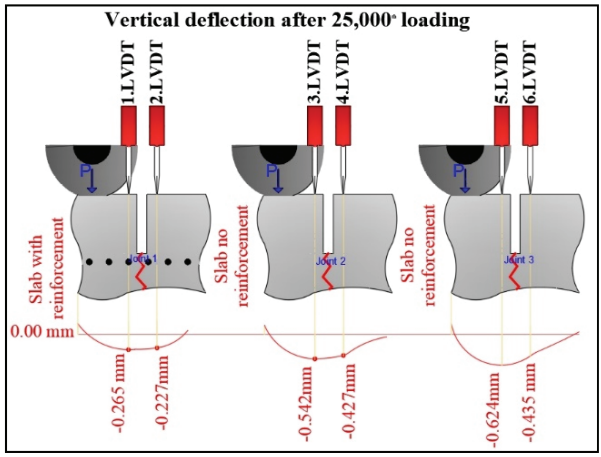


*(b)*

*Figure 13 - Vertical deflections (a) at first loading and (b) after 25,000 loadings*

Figure 14 shows the measured vertical deflections at the beginning of the slab and at the contraction joints. The positive values in Fig. 14 indicate that the displacement at the far end of the slab (A and C) whereas the negative ones indicate the deflection at the joint (B). B measuring negative and positive deflections at the same time indicates that the slab was behaving as a cantilever beam. This was expected due to the material used in the base layer as it was well compacted with a high CBR value of 80%. This also indicated that the bearing factor on the measurements could be neglected.

A summary of collected deflection data on the APT test sections is presented in Table 3 and Table 4 and shown in Fig. 15. The data show significant variability among the test sections.

Considering the vertical deflections, reinforced slab gave the lowest vertical deflections for loaded (51μm) and unloaded (46.7 μm) cases ($\delta_{ave}$ 48.85 μm).

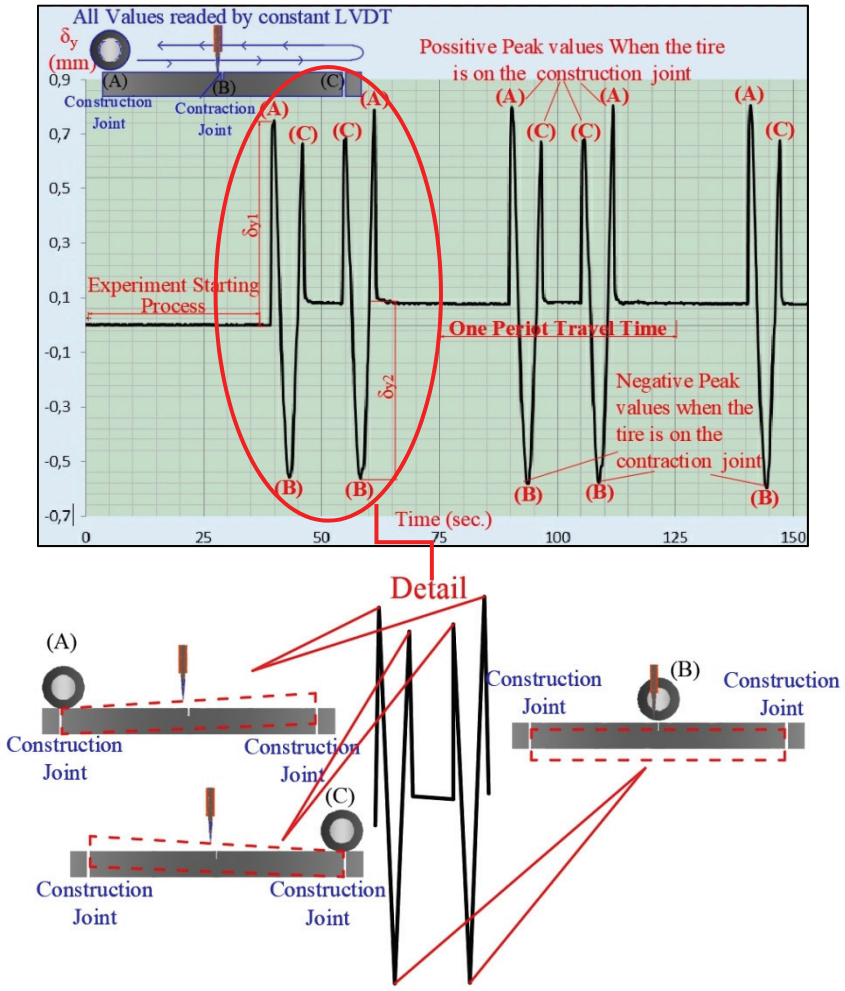


*Figure 14 - Measured vertical deflections versus time*

Figure 15 shows the graphics of each slab vertical deflection during 550 sec. (10 passes) measurement for reinforced slab and two unreinforced slabs (joint$_2$ and joint$_3$). The vertical deflection values did not change (0.02 mm) for reinforced slab under initial loadings (10 passes), but after 25,000 loads they increased up to 0.4 mm.

Average vertical deflection ($\delta_{ave}$) refers to the mean of deflections on the slab edges on both sides of the joint [35]. The $\delta_{ave}$ and LTE values obtained from the slabs in the first loading and the final (25,000 th) loading are given in Table 3 and Table 4, respectively.

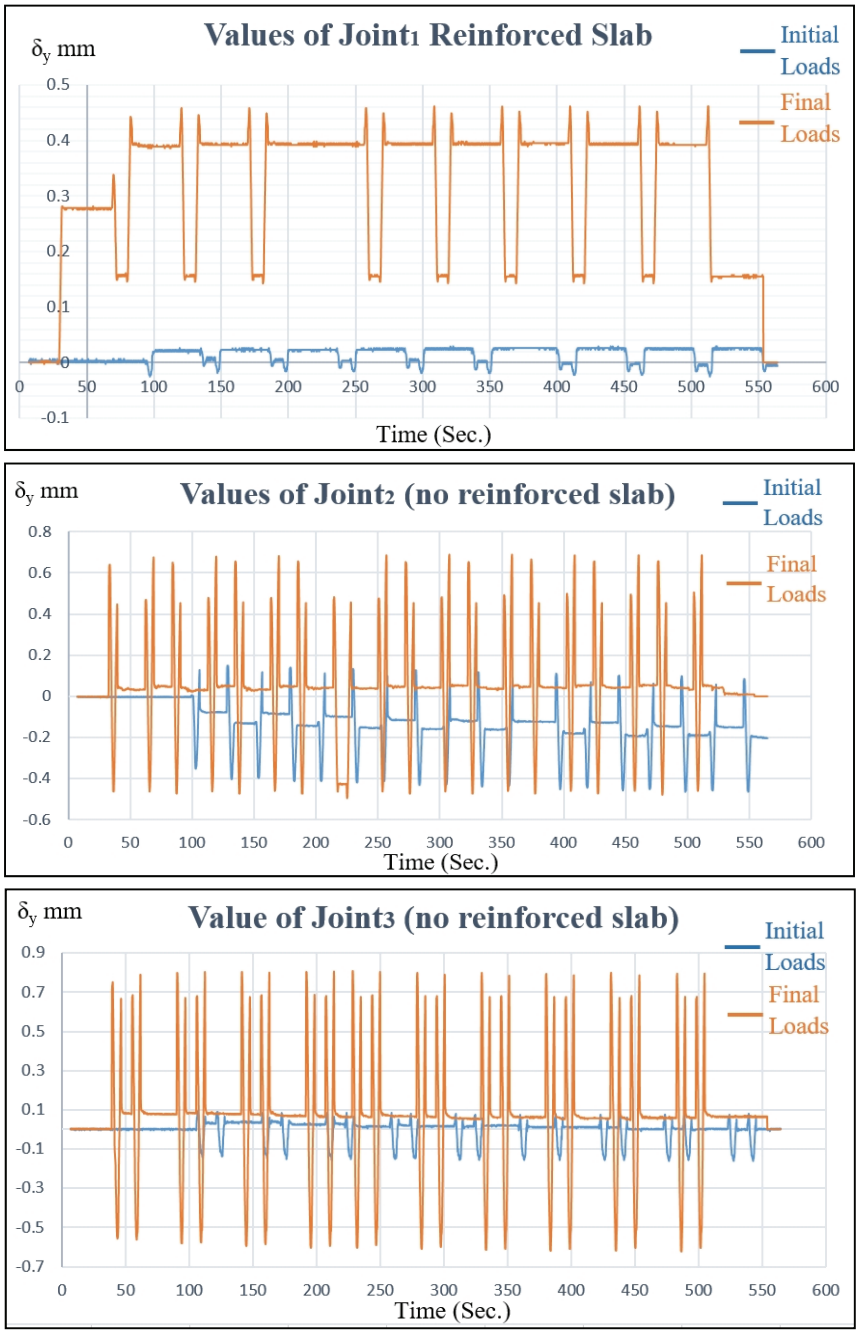


*Figure 15 - Curves of vertical deflection in each slab for (a) reinforced slab, (b) and (c) unreinforced slabs*

*Table 3 - δave and LTE values in the initial loadings (0-10 loading)*

| Joint Type | Vertical deflections (δ), μm | | LTE, % $(\delta_U/\delta_L)\times100$ | | $\delta_{ave}$, μm $(\delta_L+\delta_U)/2$ | |
|---|---|---|---|---|---|---|
| | Loaded side of the joint, $\delta_L$ | Unloaded side of the joint, $\delta_U$ | | | | |
| Steel reinforced joint$_1$ | 51 | 46.7 | 91.56 | | 48.85 | |
| No reinforcement joint$_2$ | 332 | 288 | 86.74 | Ave. 85.75 | 310 | Ave. 229.25 |
| No reinforcement joint$_3$ | 161 | 136 | 84.77 | | 148.5 | |

*Table 4 - $\delta_{ave}$ and LTE values after 25,000 loadings*

| Joint Type | Vertical deflections (μm) | | LTE (%) $(\delta_U/\delta_L)\times100$ | | $\delta_{ave}$ (μm) $(\delta_L+\delta_U)/2$ | |
|---|---|---|---|---|---|---|
| | Loaded side of the joint, $\delta_L$ | Unloaded side of the joint, $\delta_U$ | | | | |
| Steel reinforced joint$_1$ | 265 | 227.8 | 85.96 | | 246.4 | |
| No reinforcement joint$_2$ | 542 | 427 | 78.78 | Ave. 74.24 | 484.5 | Ave. 507 |
| No reinforcement joint$_3$ | 624 | 435 | 69.71 | | 529.5 | |

Significant differences were found between average vertical displacements, while the difference between LTE values was insignificant. There was a 6% difference between reinforced and unreinforced slabs in LTE values at initial loadings; however, the difference between the average displacement values was between 370%. The differences reduce to 3.7 times after 25,000 passes. The use of steel mesh in concrete pavements reduced, but did not prevent the increase of vertical displacement movement at the completion of 25,000 passes.

When comparing contraction joint performance, the average displacement values measured on both sides of the joint can be a good indicator. This finding suggests that the average displacement values should be taken into consideration besides LTE when contraction joints are evaluated at early traffic loadings.

The highest LTE value (91.56%) was measured in steel mesh reinforced concrete slab. Slab with reinforcement mesh gave the lowest LTE decrease rate of 6% after 25,000 passes. In contrast to mesh reinforced concrete slab, LTE rates decreased from 86.74% to 78.78% and 84.77% to 69.71% for second and third joints, respectively. The LTE difference between reinforced and unreinforced slabs was 6% before 25,000 passes and 13.6% when passes terminated.

Initial and final loading results showed major vertical deflection differences between the joints 2 and 3 even though both joints had the same thickness and the same material. A good explanation would be that the crack propagation at the joints was different and the interlock at the joints performed differently. But the visual inspection on the edges showed similar crack propagation. It is possible that the crack propagations were different elsewhere.

The cracks on the concrete slab edges were observed every 1,000 loadings as shown in Fig. 16. Table 5 shows the observed initial cracks versus the wheel loading. It is clear that steel mesh reinforcement delayed the early cracks (at least 50%) compared to the unreinforced slabs.

*Figure 16 - Dual wheel induced cracks under the unreinforced contraction joint*

*Table 5 - First observed cracks under varying dual tire loads*

| Joint type | Number of loading |
|---|---|
| $Joint_1$ (steel mesh reinforced) | 10,000-11,000 |
| $Joint_2$ (unreinforced) | 4,000-5,000 |
| $Joint_3$ (unreinforced) | 3,000-4,000 |

### 3.2. FE Analysis Results

The predicted finite element results were almost similar to the real-time test results from APT. As seen in Fig. 17 irregular formation of cracks similar to the actual experiments was observed.

It was not possible to measure the deflections between and under the tires at the center of the PCC slab during the APT test. The vertical displacement and LTE values calculated by the finite element method are shown in Fig. 18 and are given in Table 6. Fig. 18 shows the vertical deflection distribution through the unreinforced slab. Vertical displacement of joint-1 in the reinforced slab was approximately 10 times less than the $joint_2$. With the use of mesh reinforcement, LTE value was approximately at least 14% higher compared to the slabs without reinforcement.

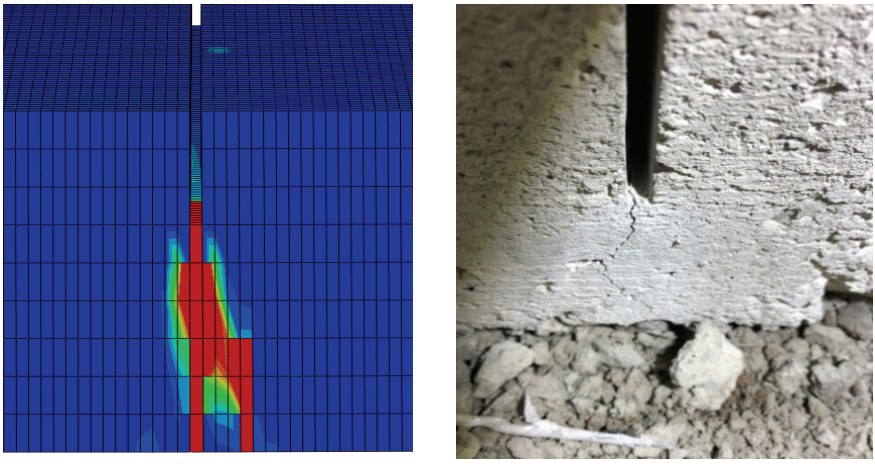

*(a) FEM* *(b) APT Observation*

*Figure 17 - Crack formations on the side views*

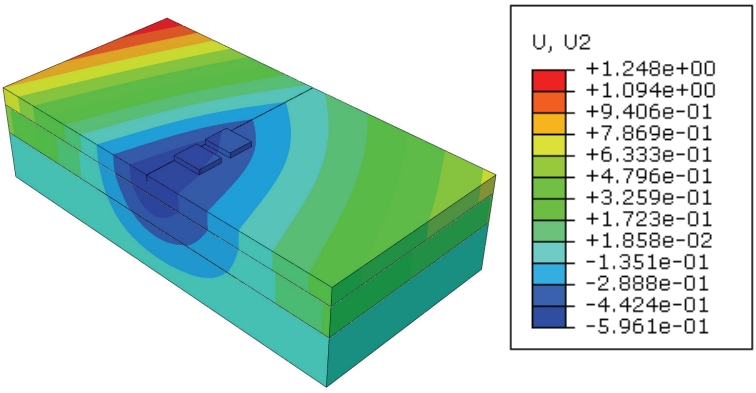


*Figure 18. Vertical deformation at joint$_2$*

*Table 6 - FE analysis results at the joints*

| Joint type | Vertical deflections (μm) | | LTE (%) | $\delta_{ave}$ (μm) |
|---|---|---|---|---|
| | Loaded slab, $\delta_L$ | Unloaded slab, $\delta_U$ | $(\delta_U/\delta_L)\times100$ | $(\delta_L+\delta_U)/2$ |
| Reinforced joint (no crack) | 63 | 55 | 87.30 | 59 |
| Reinforced joint (crack) | 179 | 153 | 85.47 | 166 |
| Unreinforced joint (no crack) | 596 | 432 | 72.48 | 514 |
| Unreinforced joint (crack) | 753 | 481 | 63.87 | 617 |

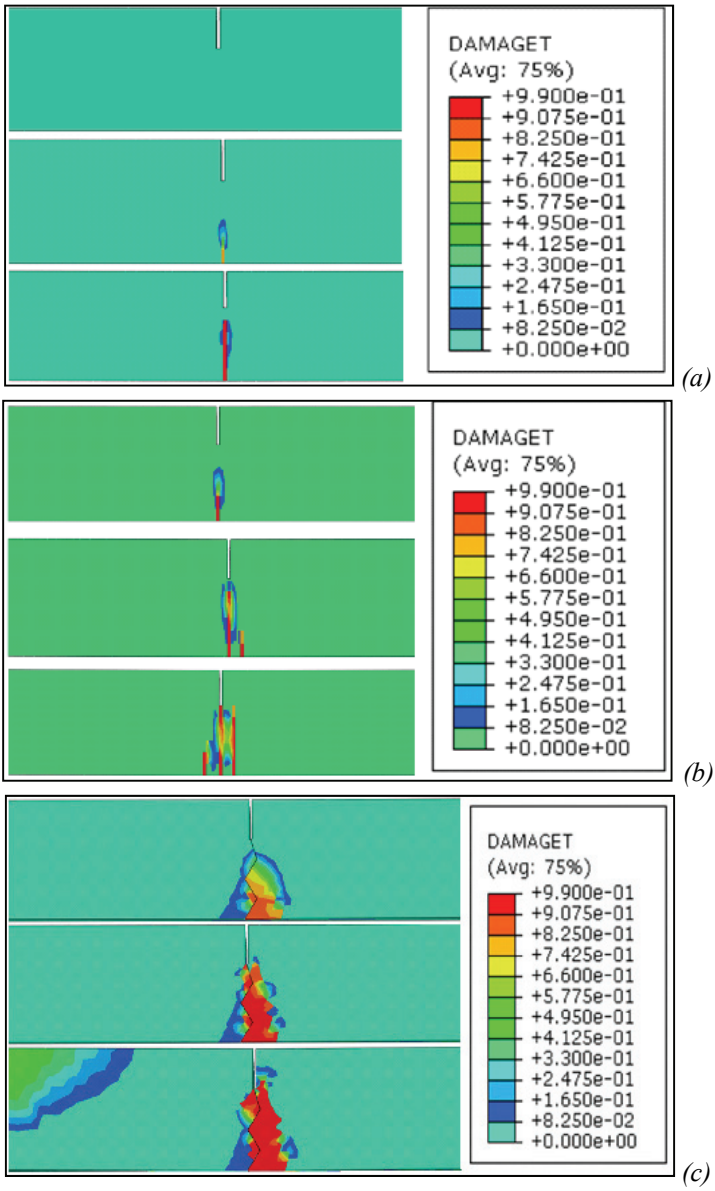


*Figure 19 - Cross section view of crack propagation (a) mesh reinforced slab, (b) unreinforced slab, (c) unreinforced slab with early crack*

The LTE difference between reinforced and unreinforced slabs was 16.9% before induced cracks occur, and 25.27% when cracks formed. The finite element analysis showed that contraction joint cracks tend to generate larger crack growth under the concrete slabs (Fig. 19 and Fig. 20). The cracks propagated from the bottom and merged to give continuity to the

joint. The cracked zone indicated that the propagation of cracks resulted in ultimate failure in aggregate and cementitious materials. The finite element results showed how joint cracks can become unstable and propagate further, and develop through the full depth of the slab. The results of FE analysis and the data obtained in the APT facility were similar. The difference between the results was due to small changes in the crack model.

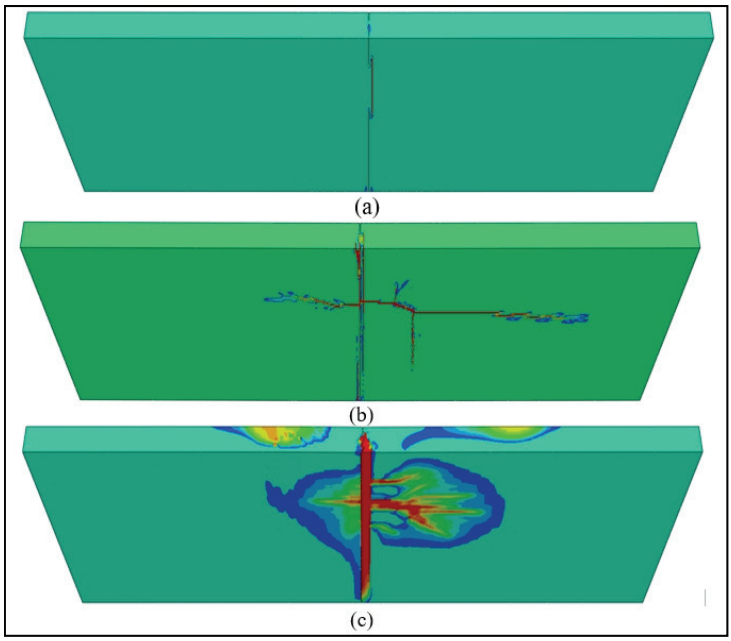


*Figure 20 - Maximum crack formation under (a) mesh reinforced slab, (b) unreinforced slab, and (c) unreinforced slab with early crack.*

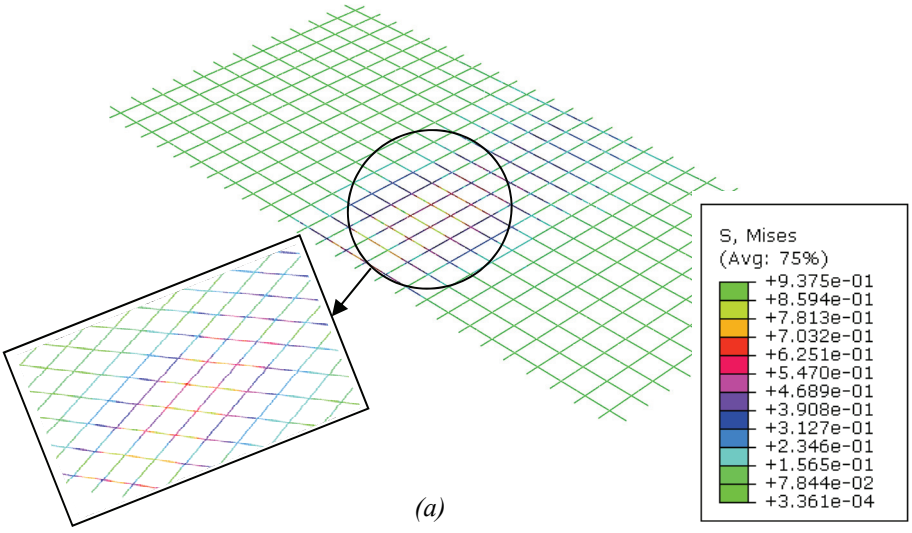


*(a)*

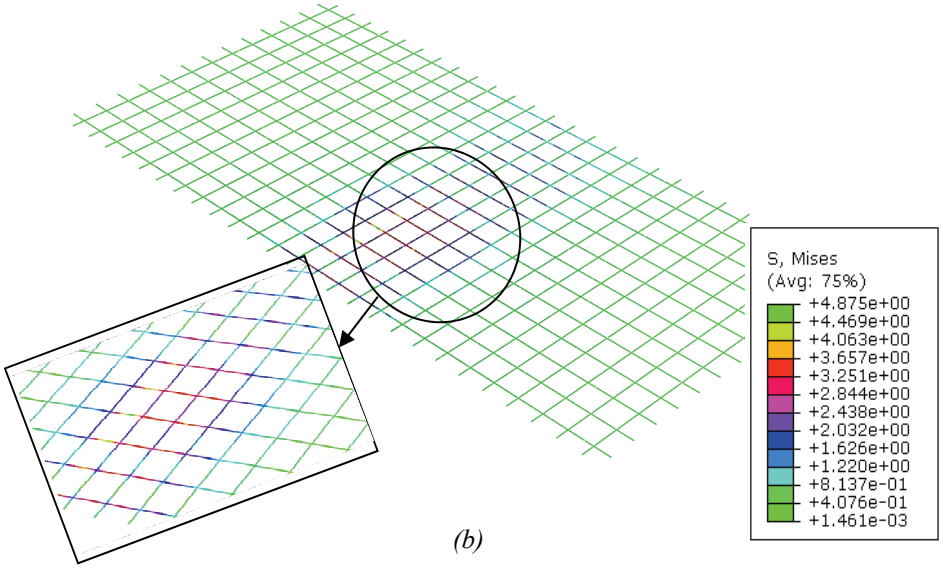


*(b)*

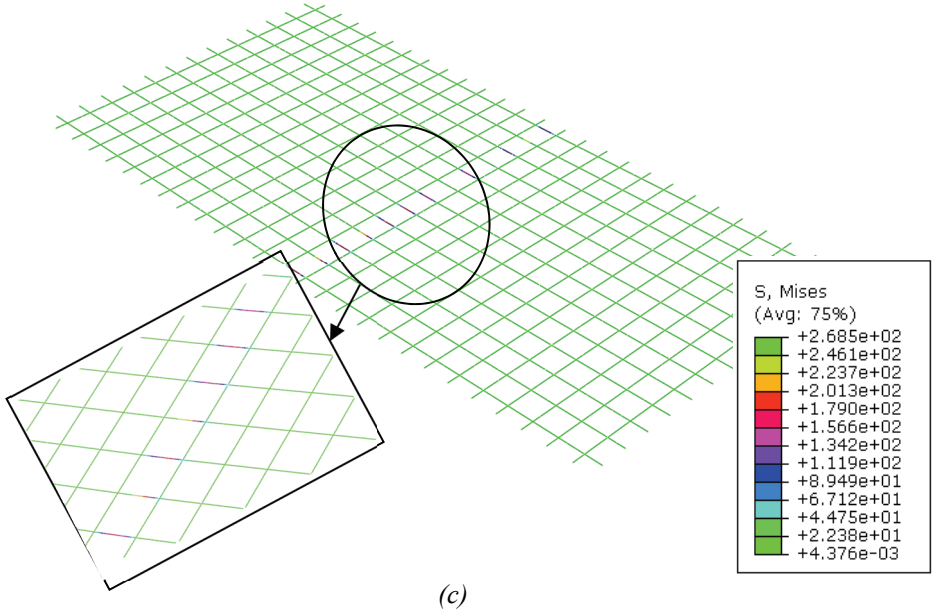


*(c)*

*Figure 21 - Von-Mises stress distribution through the 8 mm steel mesh (a) at the early stage of the loading, (b) the distribution in the middle of the loading and (c) at the end of the loading protocol*

Von-Mises stress distributions through the 8 mm steel mesh are shown in Fig. 21. When the stress distributions were examined, the maximum stress value in joint-1 (steel mesh reinforced) joint-2 and joint-3 was calculated as 13 MPa, 23 MPa and 36 MPa, respectively.

### 3.3. Cost Comparison

Two different cross-sections were prepared for cost comparison and shown in Table 7 and 8. The calculations were made according to reinforced or unreinforced concrete slabs. The cost analysis, item numbers used in Turkish institutions such as General Directorate of Highways (KGM) and The Ministry of Environment and Urbanization (ÇŞB) were used. The road platform width was accepted as 7 m and the length as 1 km for cost calculation. The distance of the aggregate crushing plant and the road was determined as 15 km. The base and subbase costs accepted as same in all comparisons.

*Table 7 - Cost of 1- km mesh reinforced concrete pavement (2018 bid unit prices)*

| Ins. | Item Number | Item Description | Unit | Unit Cost ($) | Amount | Cost ($) |
|---|---|---|---|---|---|---|
| MSB | MSB 322 | Concrete Pavement Construction | m³ | 35.79 | 1,260 | 45093.54 |
| KGM | KGM/6000 | Base/Subbase Construction (paving irrigation compression) | m³ | 5.51 | 1,400 | 7711.48 |
| ÇŞB | Y.23.010 | A252 (8 mm wires) mesh (casualty added) | Ton | 592.88 | 10.36 | 6142.22 |
| ÇŞB | NYF/03 | Transfer from Aggregate Crushing Plant to the Plant (15 km) | m³ | 0.49 | 1,540 | 752.33 |
| ÇŞB | NYF/07 | Transfer Steel Mesh to the Road | Ton | 8.47 | 10.36 | 87.74 |
| (Without any taxes) | | | **TOTAL:** | | | **59,787.30 $** |

*Table 8 - Cost of 1- km unreinforced concrete pavement (2018 bid unit prices)*

| Ins. | Item Number | Item Description | Unit | Unit Cost ($) | Amount | Cost ($) |
|---|---|---|---|---|---|---|
| MSB | MSB 322 | Concrete Pavement Construction | m³ | 35.79 | 1,260 | 45093.54 |
| KGM | KGM/6000 | Base/Subbase Construction (paving irrigation compression) | m³ | 5.51 | 1,400 | 7711.48 |
| ÇŞB | NYF/03 | Transfer from Aggregate Crushing Plant to the Plant (15 km) | m³ | 0.49 | 1,540 | 0.75 |
| (Without any taxes) | | | **TOTAL:** | | | **52,805.77 $** |

## 4. CONCLUSIONS

The information deduced from APT, together with FEM study, has provided useful understanding into the structural performance of reinforced and unreinforced jointed concrete pavements. The following specific conclusions are made from this study:

- LTE values of the steel mesh reinforced slab were approximately at least 14% higher compared to unreinforced slabs after 25,000 passes.

- Considering the vertical deflections, the reinforced slab gave the lowest vertical deflections for loaded (51μm) and unloaded (46.7 μm) cases. The values were almost 3-6 times lower than the unreinforced slabs.
- The average displacement values of both sides of the joint should be taken into consideration besides load transfer efficiency when contraction joints are evaluated at early traffic loadings.
- FE studies showed that while the stresses in the reinforcement were spread over a wide reinforcement area before the joint induced crack was formed, it was observed that after the cracking, the stress accumulations concentrated in a row of reinforcement under the joint.
- Evaluation of the LTE and vertical displacement values suggested that the use of mesh reinforcement is more favorable as it decreases both LTE and vertical displacements. Moreover, it was found that the application of the mesh reinforcement is a cost-beneficial approach, since it has been observed that 1 km of road costs increased by only 6,981.53 $ (13.2%).

**Acknowledgments**

This study was supported by the Scientific and Technical Research Council of Turkey (TUBITAK) (1001-Scientific and Technological Research Projects Funding Program Grant No: 217M481).

## References

[1] ACI (American Concrete Institute), Joints in Concrete Construction, ACI 224.3R-95, 2001.

[2] Springenschmid, R., Reimer, B., Fleischer, W., Construction of concrete pavements in West Germany. Transportation Research Record Journal of the Transportation Research Board, 1182, 12-17, 1988.

[3] Bautista, F. E., Basheer, I., Jointed plain concrete pavement (JPCP) preservation and rehabilitation design guide, California Department of Transportation (CDOT) Division of Design, 2008.

[4] Suprenant, A. B., Saw cutting joints in concrete, 1995. Available from: https://www.concreteconstruction.net/how-to/construction/sawcutting-joints-in-concrete_o [Accessed 1 January 1995].

[5] ACI (American Concrete Institute), Guide for design and construction of new jointed plain concrete pavements (JPCPs), Report No. ACI 325.12R-02, 2002.

[6] Colley, B. E., Humphrey, H. M., Aggregate interlock at joints in concrete pavements. Bulletin HRB National Research Council, 189, 1-18, 1967.

[7] Bishoff, D., Toepel, A., Dowel bar retrofit-STH 13 Construction and one-year performance report, Report No. WI-07-02, Wisconsin Department of Transportation, 2002.

[8] Hanekom, A. C., Horak, E., Visser, A.T., Comparison of South African and American aggregate interlock efficiency at concrete pavement joints. In: Proceedings of the 16th ASCE Engineering Mechanics Conference, University of Washington, Seattle, 2003.

[9] CDOT (California Department of Transportation), Guide for Design and Construction of New Jointed Plain Concrete Pavements (JPCPs), 2008.

[10] Darter, M., Barenberg, E., Yrjanson, W., Joint repair methods for Portland cement concrete pavements, National Cooperative Highway Research Program (NCHRP) Report No. 281, 1985.

[11] FHWA (Federal Highway Administration), Pavement subsurface drainage, Technical Guide Paper 90-01, 1990.

[12] Bennert, T. A., A rational approach to the prediction of reflective cracking in bituminous overlays for concrete pavements, Thesis (PhD), The State University of New Jersey, 2009.

[13] Khazanovich, L., Rita, L., Tompkins, D., Guidelines for the Rehabilitation of concrete pavements using asphalt overlays, Report No: FHWA TPF-5 (149), University of Minnesota, 2012.

[14] Shoukry, S. N., William, W. G., Riad, M.Y., Evaluation of load transfer efficiency measurement, Mid-Atlantic Universities Transportation Center, Report No: WVU-2002-04, 2005.

[15] Sadeghi, V., Hesami S., Investigation of load transfer efficiency in jointed plain concrete pavements (JPCP) using FEM. International Journal of Pavement Research and Technology, 11 (3), 253-264, 2018.

[16] Ioannides, A. M., Korovesis, G., Aggregate interlock: a pure-shear load transfer mechanism. Transportation Research Record, 1286, 14-24, 1990.

[17] Metcalf, J. B., Application of full-scale accelerated pavement testing, NCHRP Synthesis of Highway Practice 235, TRB National Research Council, 1996.

[18] McCullough, B. F., Dossey, T., Cho, Y. H., Case study of overlay performance on rigid pavement in Bowie Country. Transportation Research Record Journal of the Transportation Research Board, 1525 (1), 107-114, 1996.

[19] Metcalf, J. B., Rasoulian, M., Romanochi, S., Yongqi, L., Construction and comparison of Louisiana's conventional and alternative base courses under accelerated loading, Lousiana Transportation Research Center (LTRC) Report No. 93-1ALF, 1998.

[20] Romanoschi, S. A., Metcalf, J. B., Li, Y., Rasoulian, M., Assessment of pavement life at the first full-scale accelerated pavement test in Louisiana, In: 1998 TRB Annual Meeting, Transportation Research Board, Washington, D.C., 1998.

[21] Li, Y., Metcalf, J. B., Romanoschi, S. A., Rasoulian, M., Soil-Cement Base Pavements under Accelerated Loading, In: 1999 TRB Annual Meeting, Transportation Research Board, Washington, D.C., 1999.

[22] Saeed, A., Hall, J. W., Accelerated pavement testing: Data guidelines. Washington D.C.: National Cooperative Highway Research Program, NCHRP Report No. 512, 2003.

[23] Perez, S. A., Balay, J. M., Tamagny, P., Petit, Ch., Accelerated pavement testing and modelling of reflective cracking in pavements. Engineering Failure Analysis. 14 (8), 1526-1537, 2007.

[24] ACPA (American Concrete Pavement Association), Design of concrete pavement for city streets. IS184P1992, 2016.

[25] Changshun, H., Dongwei, C., Structural Study of Asphalt Concrete Overlays on the Existing Portland Cement Concrete Pavement. Journal of the Eastern Asia Society for Transportation Studies, 3 (3), 1999.

[26] Wu, R., Harvey, T., Signore, M. J., Cracking and rutting performance of composite pavements under testing with heavy vehicle simulator. Transportation Research Record Journal of the Transportation Research Board, 2304 (1), 177-184, 2012.

[27] Yin, H., Full-scale test of thermally induced reflective cracking in airport pavements. Road Materials and Pavement Design, 16 (1), 119-132, 2015.

[28] Plessis, L. D., Strauss, P. J., Perrie, B. D., Rossmann D., Accelerated pavement testing of load transfer through aggregate interlock and the influence of crack width and aggregate type - A case study, International Workshop on Best Practices for Concrete Pavements, South Africa, 2007.

[29] Joshi, S., Harle, S. M., Linear variable differential transducer (LVDT) & its application in Civil Engineering. International Journal of Transportation Engineering and Technology, 3 (4), 62-66, 2017.

[30] Huang, Y., Evaluating pavement response and performance with different simulative tests. Thesis (PhD).Virginia Polytechnic Institute and State University, 2017.

[31] ABAQUS/CAE v6.12 Programme, Dassault Systemes Simulia Corp. Providence, RI, USA, 2017.

[32] Hüsem, M., Coşğun, S. I., Behavior of reinforced concrete plates under impact loading: different support conditions and sizes. Computers and Concrete, 18(3), 389-404, 2016.

[33] Alejano, L. R., Bobet, A., Drucker–Prager criterion. In The ISRM Suggested Methods for Rock Characterization, Testing and Monitoring: 2007-2014, 247-252, Springer, Cham, 2012.

[34] Wayessa, G. S., Quezon, E. T., Kumela, T., Analysis of stress-strain and deflection of flexible pavements using finite element method case study on Bako-Nekemte Road. Journal of Civil. Construction and Environmental Engineering, 2(4), 100-111, 2017.

[35] Khazanovich, L., Gotlif, A., Evaluation of joint and crack load transfer final report. Technical Report No. FHWA-RD-02-088, Federal Highway Administration, 2003.

*Teknik Dergi, 2021 11361-11380, Paper 637*

# Data Collection for Implementation of the Mechanistic-Empirical Pavement Design Guide (MEPDG) in Izmir, Turkey

**Mohammad Razeq SHAKHAN**[1]
**Ali TOPAL**[2]
**Burak ŞENGÖZ**[3]

## ABSTRACT

Developing countries like Turkey are trying to implement the Mechanistic-Empirical Pavement Design Guide (MEPDG). The implementation of this method requires comprehensive local data collection, evaluation, and, if necessary, a local calibration. The objective of this study is to prepare local data such as climate, traffic, and materials for evaluation and local calibration of MEPDG for Izmir City. For this purpose, the climate and traffic data were obtained, analysed, and converted to the MEPDG format. Besides, the bound and unbound pavement material properties were determined. Since some of the obtained local data like climate, vehicle classification, traffic growth factor, and axle load distribution cannot be directly used as design inputs, they were developed and converted to a suitable format to be used in the MEPDG. The output of this study can be used as design inputs for the evaluation and local calibration of the MEPDG in Izmir and serves as a guide for data preparation for other parts of the country.

**Keywords:** Climate, data collection, materials, mechanistic-empirical pavement design guide (MEPDG), traffic.

## 1. INTRODUCTION

The MEPDG is an advanced and the most sophisticated pavement analysis and design method that calculates pavement structure responses and predicts different pavement performances under the combination of traffic loading and environmental conditions taking

Note:
- This paper was received on November 26, 2019 and accepted for publication by the Editorial Board on May 23, 2020.
- Discussions on this paper will be accepted by January 31, 2022.
- https://dx.doi.org/10.18400/tekderg.651399

1 Dokuz Eylul University, The Graduate School of Natural and Applied Sciences, Izmir, Turkey - raziqshakhan@yahoo.com - https://orcid.org/0000-0002-9756-7331

2 Dokuz Eylul University, Department of Civil Engineering, Izmir, Turkey - ali.topal@deu.edu.tr https://orcid.org/0000-0002-2601-1926

3 Dokuz Eylul University, Department of Civil Engineering, Izmir, Turkey - burak.sengoz@deu.edu.tr https://orcid.org/0000-0003-0684-4880

into various material properties consideration. The MEPDG consists of two models: 1) Mechanistic Model calculating the pavement responses (stresses and strains) based on engineering mechanics law. 2) Empirical Model predicts pavement distresses (rutting, top-down, bottom-up, and thermal cracking as well as the International Roughness Index (IRI)) using transfer regression equations [1], [2]. The implementation of the MEPDG in other parts of the world would require verification, local calibration, and validation for local materials, conditions, and construction policies since the MEPDG was calibrated based on the Long-term Pavement Program (LTPP) database in the USA. To carry out such efforts, comprehensive local data (e.g., materials, traffic, climate, and pavement distresses) are required to be collected [3], [4], [5].

Several countries have tried to collect local design data, to conduct sensitivity analysis, and to carry out the local calibration so as to facilitate the implementation of the MEPDG. In Italy, the local data such as traffic (e.g., vehicle classification, truck distribution, and truck axle load distribution), materials properties, and climate data were collected and analysed to conduct the local calibration of the MEPDG [6]. Traffic and climate data were collected to facilitate the implementation of MEPDG in India [7]. The local data (e.g., traffic, climate, pavement structure, materials, and pavement distresses) were collected and the local calibration of the MEPDG was conducted in New Mexico. The MEPDG prediction model error was successfully reduced [8]. Climate data were extracted from the World Weather Online website, analysed, and converted to the MEPDG format to conduct the sensitivity analysis in Egypt [9]. To implement and use the MEPDG in Egypt, pavement distresses prediction models were developed for the non-freezing zone and design data was extracted from the LTPP database [10]. The material properties and specifications were determined from the Qatar Highway Design Manual (QHDM), climate data of Needles Airport in California were adapted, and the default traffic design inputs (Level 3) were used to conduct the sensitivity analysis in the State of Qatar [11]. In China, the local material properties was collected and default (Level 3) axle load distribution and climate data were used in local calibration of the thermal cracking model [12]. In Saudi Arabia, local design data such as traffic, climate, and material are prepared to be used for local calibration of the MEPDG [13]. The traffic data (e.g., vehicle classification, growth rate, and truck distribution factors) was collected and the sensitivity analysis for various climate condition was carried out in Lebanon [14]. The experience of other countries has shown that local data collection is a laborious effort and some of the local data should be analysed and converted to the AASHTOWare Pavement ME Software format. Turkey is one of the countries that is trying to leave the existing empirical pavement design guide (AASHTO 1993) to the adaptation of MEPDG. In this regard, some initial works have been performed by Turkish General Directorate of Highways [15]. In this study, local design data (e.g., climate, traffic, and materials) were collected for different state highways in Izmir region from various government agencies.

## 2. OBJECTIVE

The main objective of this study is to prepare local design data (obtaining, analysing, and converting) to be used as design inputs for local calibration of the MEPDG in Izmir. With the aiming of achieving the objective, the following activities are performed.

a) Climate data were obtained, analysed and converted to the text file with ".hcd" extension.

b) Traffic data were obtained, analysed, and converted to a suitable format required by the MEPDG.

c) Bound and unbound material properties were determined.

## 3. LOCAL DATA COLLECTION METHODOLOGY

Different road sections were selected in Izmir to collect the local design data such as material properties, traffic characteristics, and climate data. The selected road segments are located in the North, North-South, West, West-East, and South that can cover the whole zone (Table 1).

*Table 1 - Selected roadway segments*

| Roadway section number | Number of lanes | Direction/Location |
|---|---|---|
| D240 | 4 | North |
| D550 | 4 | North-South |
| D505 | 2 | West |
| D300 | 4 | West-East |
| D310 | 4 | South |

### *3.1.1. Climate Data*

It is well known that flexible pavement is significantly affected by environmental conditions. The asphalt concrete (AC) is affected by air temperature gradient while the unbound layers and subgrade are sensitive to moisture variation and freezing-thawing cycles [16], [17]. The MEPDG uses different climate data such as hourly temperature, hourly precipitation, hourly wind speed, hourly sun shine, and hourly humidity as design inputs to calculate the environmental effects on pavement performance using the Enhanced Integrated Climatic Model (EICM) software. The EICM is a powerful software that calculates the temperature and moisture effects on pavement structure. The USA and Canada's climate data are embedded in the Pavement ME Design Software, however the climate data is required to be collected for local conditions. In Turkey, the climate model has not yet been calibrated and the climate data files have not been created in EICM format [4], [5]. A five year period (2013-2018) climate data was taken from the Turkish State Meteorological Services, the data was analysed and various missing weather data were identified. The missing data (hours) were calculated using the average before and after the missing data points. The missing data (days, months, or years) were also adapted from the nearest weather stations. Seventeen weather stations were selected, which cover the entire Izmir state (Table 2). The climate data were converted to the text file with extension ".hcd" based on Pavement ME Design Software format. Each climatic file consists of: date (YYYY/mm/dd/hr), air temperature (°C), precipitation (mm), wind speed (m/hr), sunshine (%), and humidity (%) (Figure 1).

*Table 2 - Selected weather stations*

| Station number | Station name | Latitude | Longitude |
|---|---|---|---|
| 17180 | Dikili | 39.0737 | 26.888 |
| 17787 | Aliaga | 38.7922 | 26.9682 |
| 17742 | Konak | 27.171 | 53.000 |
| 17789 | Menemen | 38.6237 | 27.0433 |
| 17219 | Izmir Adnan Menderes Airport | 38.295 | 27.1481 |
| 17822 | Ödemis | 38.2157 | 27.9642 |
| 17854 | Selcuk | 37.9423 | 27.3669 |
| 18447 | Kiraz | 38.2192 | 28.2028 |
| 18029 | Tire | 38.133 | 27.8165 |
| 18443 | Buca | 38.375 | 27.1953 |
| 18031 | Bornova | 38.4666 | 27.2166 |
| 17218 | Cigli Airport | 38.5127 | 27.0144 |
| 17749 | Kemalpaşa | 38.4639 | 27.3705 |
| 17221 | Cesme | 38.3036 | 26.3724 |
| 18028 | Urla | 38.3628 | 26.8322 |
| 18444 | Güzelbahce | 38.3717 | 26.8908 |
| 18032 | Karaburun | 38.6401 | 26.5081 |

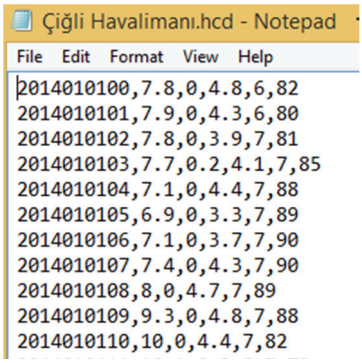


*Figure 1 - An example of climate data in MEPDG required format*

### *3.1.2. Traffic Data*

The MEPDG requires extensive detailed traffic inputs which are categorized in four main parts [1], [18].

a) Base Year Traffic Information (Initial Two Way Annual Average Daily Truck Traffic (AADTT), Number of Lanes in Design Direction, Percent Trucks in Design Direction, Percent Trucks in Design Lane, Operational Speed).

b) Traffic Volume Adjustment Factors (Monthly Adjustment Factors, Vehicle Class Distribution, Hourly Distribution, Traffic Growth Factors).
c) Axle Load Distribution Factors,
d) General Traffic Inputs (number of axles per truck, axle configuration, wheelbase, and lateral traffic wander).

In this study, traffic data were collected from the Turkish General Directorate of Highways published reports such as Traffic and Transportation Information [19] and Characteristics and Trends of Heavy Truck Traffic and Good Transportation [20].

### *3.1.3. Vehicle Classification*

The MEPDG uses ten vehicle classes (4-13) in which Class 4 indicates buses and Class 5 through 13 indicate trucks and trailers. In the MEPDG, vehicles are classified based on truck types, axle numbers, and axle types (single, tandem, triple, and quad) [1], [18], while in Turkey, vehicles are classified based on vehicle types in five groups: 1) cars, 2) medium goods vehicles (MGV), 3) buses, 4) Trucks, and 5) Trailers [15]. This classification cannot be used in the MEPDG as design inputs. Therefore, comprehensive efforts have been made to develop a new truck classification to be used in the MEPDG. The observed trucks in Turkey were categorized in seven classes based on truck types, axle numbers and axle types (single, tandem, and tridem). Thus, first of all, Class 1 (cars) were removed from the proposed vehicle classification. Secondly, Class 2 (medium goods vehicles) with 3.5-10 tons weigh was merged into other classes since it consists of buses and trucks (30% bus and 70% truck). The Class 3 (buses) was remained unchanged and it is equivalent to Class 4 in the MEPDG. The Class 4 (trucks) has been divided into three subclasses (5-7) based on axles numbers and axle types. The Class 5 representing the trailers, has been grouped into three subclasses (8-10). In the proposed truck classification: Class 1 is buses, Classes 2, 3, and 4 are single-unit trucks, and Class 5-7 indicate the single unit trailers. The vehicle classes 11, 12, and 13 have not been observed in Turkey (Table 3) [19], [20].

*Table 3. Trucks classification*

| MEPDG | Existing | Proposed classification | Axles types/numbers | Description |
|---|---|---|---|---|
| 4 | Buses | 1 | 1.2, 1.21, 1.22 | Buses |
| 5 | Trucks | 2 | 1.1, 1.2 | Two-axle, six-tire, single unit trucks |
| 6 | | 3 | 1.21, 1.22 | Three-axle, single-unit trucks |
| 7 | | 4 | 11.21, 11.22, 1.122, 1.122, 1.211, 11.121, 11.122 | Four or more axle, single unit trucks |

*Table 3. Trucks classification (continue)*

| MEPDG | Existing | Proposed classification | Axles types/numbers | Description |
|---|---|---|---|---|
| 8 | Trailers | 5 | 1.2+11, 1.2+22 | Four axle, single trailer trucks |
| 9 | | 6 | 1.21+22, 1.22+11, 1.22+22, 1.2+111, 1.2+122, 1.2+222 | Five axle, single trailer trucks |
| 10 | | 7 | 1.22+111, 1.22+222 | Six or more axles, single trailer trucks |
| 11 | - | - | - | Five axle, multi trailer trucks |
| 12 | - | - | - | Six axle, multi trailer trucks |
| 13 | - | - | - | Seven or more, multi trailer trucks |

### *3.1.4. Average Annual Daily Truck Traffic (AADTT)*

The Turkish General Directorate of Highways uses hundreds of automatic vehicle counting devices to measure traffic volume and classify the vehicles. The average annual daily traffic (AADT) is available only for current vehicle classification (cars, MGV, buses, trucks, and trailers) which cannot be directly used for the proposed truck classification. Therefore, the truck distribution factors of proposed truck classification were extracted from [19], [20] (Table 4).

*Table 4 - Truck distribution percentage for proposed truck classification*

| Current vehicle classification | Proposed truck classification | Truck distribution (TD) % |
|---|---|---|
| Buses | 4 | 100 |
| Trucks | 5 | 18.56 |
| | 6 | 50.39 |
| | 7 | 30.96 |
| Trailers | 8 | 1.35 |
| | 9 | 98.36 |
| | 10 | 0.28 |

The AADTT for the proposed vehicle classification was calculated using the following equation (Equation 1).

$$AADTT_{pi} = AADTT_{ci} \times \mathrm{TD}_i \quad (1)$$

Where, $AADTT_{pi}$ is the average annual daily truck traffic for class$_i$ of proposed truck classification. $AADDT_{ci}$ is the average annual daily truck traffic for class$_i$ of current vehicle classification, and $TD_i$ is the truck distribution percentage. As the Medium Goods Vehicles class includes 30% buses and 70% trucks, its AADT was added to Class 4 and 5.

### *3.1.5. Vehicle Class Distribution Factors (VCDF)*

The share percentage of trucks are indicated by vehicle class distribution factors (VCDF) which was calculated by (Equation 2).

$$VCDF_i = \frac{AADTT_i}{AADTT} \times 100 \quad (2)$$

Where, $VCDF_i$ is the vehicle class distribution factor for class*i,* $AADDT_i$ is the average annual daily truck traffic for class*i,* and AADDT is the average annual daily truck traffic for classification.

At the end of calculation, the sum of VCDF must be equal to 100. As seen in (Figure 2), the vehicle distribution percentage of vehicle classes 5, 6, and 9 are high in state roads in Izmir.

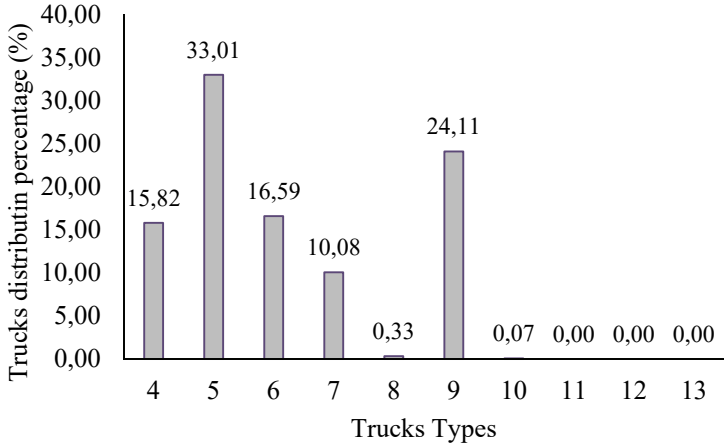


*Figure 2 - Vehicle class distribution factors*

### *3.1.6. Vehicle Growth Rate*

Because the AADT is available for the current vehicle classification (cars, medium goods vehicles, trucks and trailers), a single growth rate was calculated for 5, 6, 7 and 8, 9, 10 classes. As seen in (Table 5), the truck growth rate of classes 8, 9, and 10 are significantly high (13.37) that should be considered in pavement structural analysis and design in the future.

*Table 5 - Vehicle class distribution factors and truck growth rates for state roads*

| Vehicle class | Distribution (%) | Growth rate (%) | Growth function |
|---|---|---|---|
| 4 | 15.82 | 1.76 | Linear |
| 5 | 33.01 | 2.80 | Linear |
| 6 | 16.59 | 2.80 | Linear |
| 7 | 10.08 | 2.80 | Linear |
| 8 | 0.33 | 13.37 | Linear |
| 9 | 24.10 | 13.37 | Linear |
| 10 | 0.07 | 13.37 | Linear |
| 11 | 0.00 | 0 | - |
| 12 | 0.00 | 0 | - |
| 13 | 0.00 | 0 | - |
| Total | 100 | | - |

### *3.1.7. Monthly Adjustment Factors*

The whole year traffic variation is indicated by traffic monthly adjustment factors (MAF). The monthly adjustment factors were calculated by (Equation 3). The sum of monthly adjustment factors should be equal to 12. The monthly adjustment factors were presented in (Table 6) and (Figure 3) [21].

$$MAF_i = \frac{AMDTT_i}{\sum_{i=1}^{12} AMDTT_i} \times 12 \tag{3}$$

Where, $MAF_i$ is the vehicle monthly adjustment factor for class*i,* $AMDTT_i$ is the average monthly daily truck traffic for class*i.*

*Table 6 - Trucks monthly adjustment factors*

| Month | Trucks Classes | | | | | | | | | |
|---|---|---|---|---|---|---|---|---|---|---|
| | 4 | 5 | 6 | 7 | 8 | 9 | 10 | 11 | 12 | 13 |
| Jan | 0.83 | 0.84 | 0.84 | 0.84 | 0.8 | 0.8 | 0.8 | 0 | 0 | 0 |
| Feb | 0.79 | 0.8 | 0.8 | 0.8 | 0.77 | 0.77 | 0.77 | 0 | 0 | 0 |
| Mar | 0.88 | 0.96 | 0.96 | 0.96 | 0.94 | 0.94 | 0.94 | 0 | 0 | 0 |
| Apr | 0.9 | 0.99 | 0.99 | 0.99 | 0.96 | 0.96 | 0.96 | 0 | 0 | 0 |
| May | 1.03 | 1.07 | 1.07 | 1.07 | 1.05 | 1.05 | 1.05 | 0 | 0 | 0 |

*Table 6 - Trucks monthly adjustment factors (continue)*

| Month | Trucks Classes | | | | | | | | | |
|---|---|---|---|---|---|---|---|---|---|---|
| | 4 | 5 | 6 | 7 | 8 | 9 | 10 | 11 | 12 | 13 |
| Jun | 1.07 | 1.07 | 1.07 | 1.07 | 1.05 | 1.05 | 1.05 | 0 | 0 | 0 |
| Jul | 1.25 | 1.1 | 1.1 | 1.1 | 1.13 | 1.13 | 1.13 | 0 | 0 | 0 |
| Aug | 1.28 | 1.08 | 1.08 | 1.08 | 1.12 | 1.12 | 1.12 | 0 | 0 | 0 |
| Sep | 1.05 | 1.03 | 1.03 | 1.03 | 1.07 | 1.07 | 1.07 | 0 | 0 | 0 |
| Oct | 1.04 | 1.08 | 1.08 | 1.08 | 1.12 | 1.12 | 1.12 | 0 | 0 | 0 |
| Nov | 0.92 | 0.99 | 0.99 | 0.99 | 1.04 | 1.04 | 1.04 | 0 | 0 | 0 |
| Dec | 0.95 | 0.99 | 0.99 | 0.99 | 0.95 | 0.95 | 0.95 | 0 | 0 | 0 |
| Total | 12 | 12 | 12 | 12 | 12 | 12 | 12 | 0 | 0 | 0 |

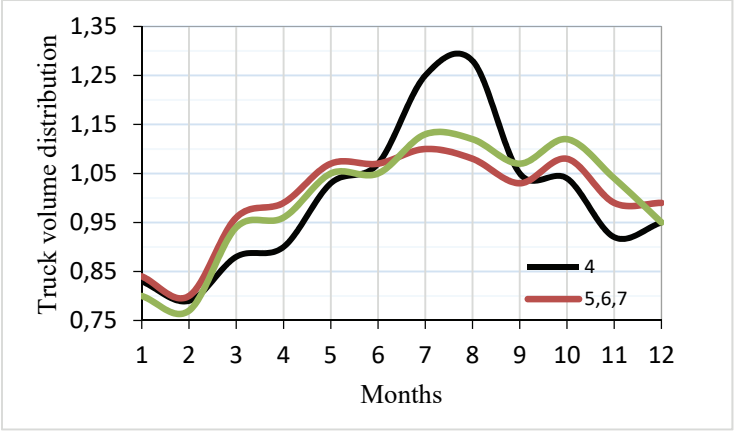


*Figure 3 - Truck monthly adjustment factors*

As seen (Figure 3), truck traffic volumes are decreased in the winter season and are then increased in the summer season.

### *3.1.8. Truck Hourly Distribution Factors*

The truck hourly distribution factors represent the percentage of the total truck traffic within each hour of the day. The sum of 24-hourly distribution factors must be equal to 100 (Table 7) and (Figure 4). For state roads in Turkey, the truck hourly distribution percentage was extracted from Highway Traffic Flow Properties and Traffic Parameters [21].

*Table 7 - Truck hourly distribution factors*

| Time period | Distribution (%) | Time period | Distribution (%) |
|---|---|---|---|
| 00:00 - 01:00 | 3.6 | 12:00 - 13:00 | 5.0 |
| 01:00 - 02:00 | 3.0 | 13:00 - 14:00 | 4.9 |
| 02:00 - 03:00 | 2.4 | 14:00 - 15:00 | 5.0 |
| 03:00 - 04:00 | 2.2 | 15:00 - 16:00 | 5.3 |
| 04:00 - 05:00 | 2.1 | 16:00 - 17:00 | 5.4 |
| 05:00 - 06:00 | 2.4 | 17:00 - 18:00 | 5.5 |
| 06:00 - 07:00 | 3.1 | 18:00 - 19:00 | 5.3 |
| 07:00 - 08:00 | 3.9 | 19:00 - 20:00 | 5.5 |
| 08:00 - 09:00 | 4.1 | 20:00 - 21:00 | 4.8 |
| 09:00 - 10:00 | 4.4 | 21:00 - 22:00 | 4.4 |
| 10:00 - 11:00 | 4.7 | 22:00 - 23:00 | 4.1 |
| 11:00 - 12:00 | 5.0 | 23:00 - 24:00 | 3.9 |
| Total | 40.9 | Total | 59.1 |

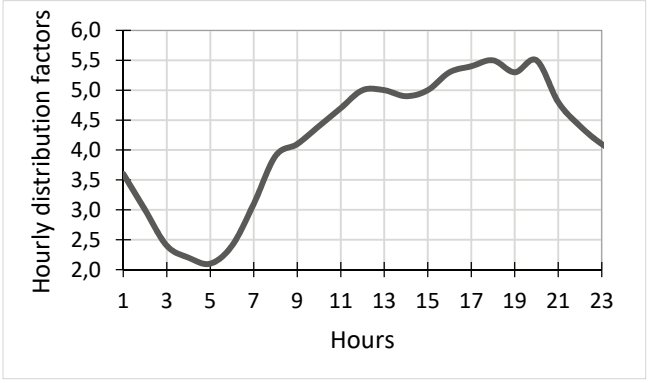


*Figure 4 - Truck hourly distribution factors*

As seen in (Figure 5) and (Table 7), the traffic volume is high during the day and reaches to the highest value at 18:00, the traffic volume decreases at 21:00 and reaches at the lowest level at 5:00.

### *3.1.9. Axle Load Distribution Factors*

The Turkish General Directorate of Highways uses a weighbridge system placed at 350 stations to measure the axle loads associated with trucks. Consequently, they collect the

distribution of axle loads at 1000 kg intervals unlike the MEPDG requesting axle load distribution at different intervals [20].

- Single axles from 1361 kg to 18597 kg in intervals of 454 kg.
- Tandem axles from 2722 kg to 37197 kg in intervals of 907 kg.
- Tridem axles from 5443 kg to 46266 kg in intervals of 1360 kg.

The measured and collected axle loads in Turkey should be converted to the MEPDG required standard. The axle load distribution factors were obtained by the following three steps.

1. The measured axle load distribution (single, tandem, and tridem) was converted into the 454 kg, 907 kg, and 1360 kg intervals. The difference between measured axle load distribution and converted axle load distribution are not significant (Figure 5), (Figure 6), and (Figure 7).
2. The collected axle load distributions are shared between all types of trucks (i.e., class 5, 6, 7, 8, 9, and 10), therefore, at first, the share percentage of each truck was determined, and then the axle load distributions (single axle, tandem axle, and tridem axle) were calculated (Figure 8).
3. The axle load distribution factors were calculated by (Equation 4) [13].

$$ALDF_{ijk} = \frac{No.\ of\ axles_{ijk}}{Total\ No.\ of\ axles_{ij}} \times 100 \tag{4}$$

Where *ALDF* is the axle load distribution factor, *i* is vehicle class from 4-10, *j* represents the month from 1-12, and *k* is the load interval.

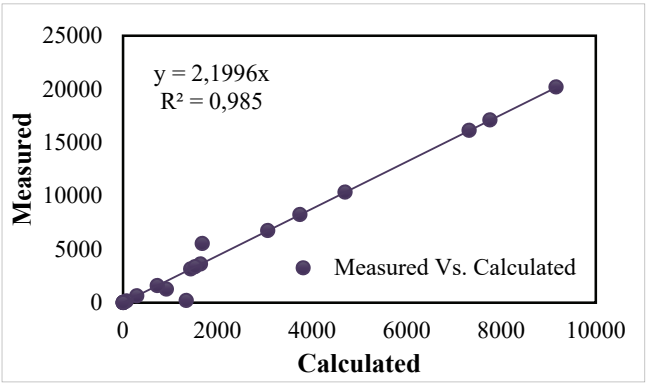


*Figure 5 - Single axle load distribution (measured vs. calculated)*

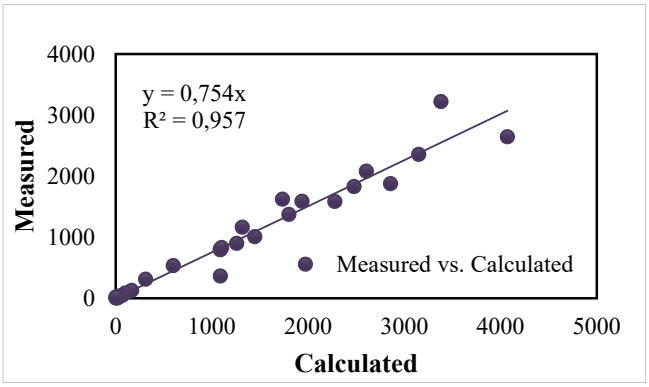


*Figure 6 - Tridem axle load distribution (measured vs. calculated)*

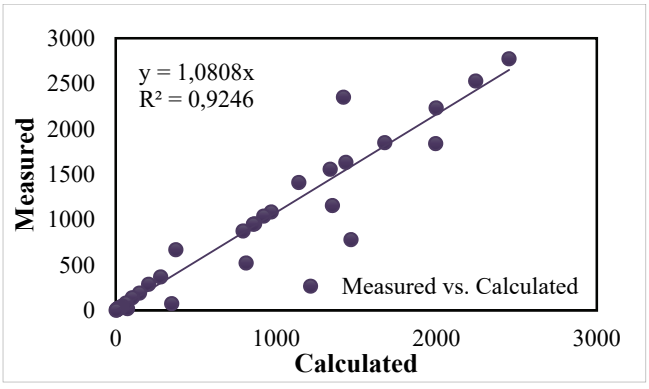


*Figure 7 - Tandem axle load distribution (measured vs. converted)*

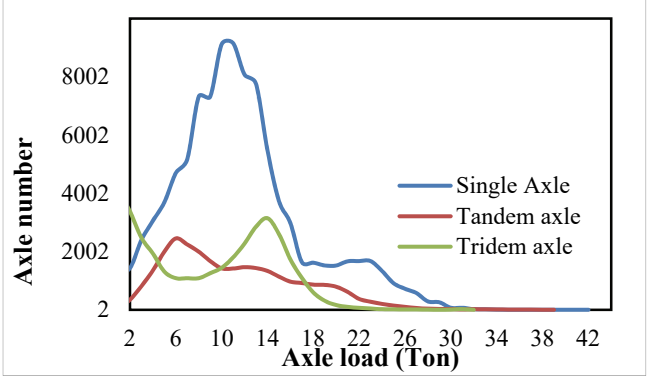


*Figure 8 - Axle load distribution*

In Turkey, monthly axle load distribution is not available, so only one axle load distribution factors is obtained for all months (Figure 9). Besides, axle load regarding buses (Class 4) is not measured in Turkey, so the default axle load distribution factors were chosen [20].

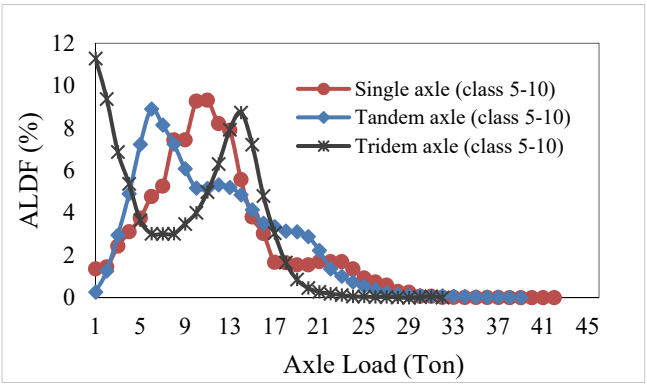


*Figure 9 - Axle load distribution factors*

### *3.1.10. General Traffic Inputs*

The following local design inputs were collected for Izmir, Turkey.

*3.1.10. 1. Lateral traffic wander*

- *Mean wheel location,* the distance between outer edge of the wheel and the edge marking for the pavement. The default value of 460 mm is used for Izmir region.
- *Traffic wander standard deviation*, the default value of 256 mm is used for Izmir region.
- *Design lane width,* the value of 3.5 m is used for Izmir region.

*3.1.10. 2. Number of axles per truck*

The average number of axles for each truck class (Class 4 to 10) for each axle type (single, tandem, and tridem) is called the number of axles per truck. The number of axles per truck was calculated for state roads in Izmir (Table 8).

*Table 8 - The average number of axles per truck*

| Vehicle class | Single | Tandem | Tridem | Quad |
|---|---|---|---|---|
| 4 | 1.96 | 0.04 | 0.00 | 0 |
| 5 | 2.00 | 0.00 | 0.00 | 0 |
| 6 | 1.00 | 1.00 | 0.00 | 0 |
| 7 | 1.33 | 0.33 | 0.68 | 0 |
| 8 | 2.00 | 1.00 | 0.00 | 0 |

*Table 8 - The average number of axles per truck (continue)*

| Vehicle class | Single | Tandem | Tridem | Quad |
|---|---|---|---|---|
| 9 | 1.99 | 0.03 | 0.99 | 0 |
| 10 | 1.00 | 1.00 | 1.00 | 0 |
| 11 | 0 | 0 | 0 | 0 |
| 12 | 0 | 0 | 0 | 0 |
| 13 | 0 | 0 | 0 | 0 |

*3.1.10. 3. Axle configuration*

The axle configuration and axle spacing were presented in Table 9 and Table 10, respectively [22].

*Table 9 - Truck Axle Configuration for Izmir*

| Axle configuration | Values (MEPDG) | Values (Turkey) |
|---|---|---|
| Average axle width (m) | 2.59 | 2.45 |
| Dual tire spacing (mm) | 305 | 305 |
| Tire pressure (psi) | 120 | 101 |

*Table 10 - Axle Spacing for Izmir*

| Axle types | Average axle spacing (MEPDG), m | Average axle spacing (Turkey), m |
|---|---|---|
| Tandem | 1.45 | 1.36 |
| Tridem | 1.68 | 1.25 |
| Quad | 1.32 | NA* |

* Not applicable in Turkey

*3.1.10. 4. Wheelbase*

The spacing between steering axle and first axle in a truck is named as wheel base and divided in three ranges of short, medium, and long. Typically Class 5 indicates short trucks; Class 6 and 7 indicate medium trucks and Class 8-13 indicate long trucks. Table 11 presents default values used in this study.

*Table 11 - Truck wheelbase*

| Axle types | Average axle spacing between axle group, m | Percent of truck % |
|---|---|---|
| Short | 3.66 | 33 |
| Medium | 4.57 | 33 |
| Long | 5.49 | 34 |

## 4. MATERIAL PROPERTIES

The MEPDG requires various and detailed material properties in three hierarchical input levels. In Level 1, design inputs are obtained through the laboratory or site tests. In Level 2, design inputs were collected using the correlation with other material properties. In Level 3, embedded design inputs in the Pavement ME Design Software were used or obtained using empirical predictive equations [1]. In this study, comprehensive efforts have been carried out to collect Level 2 and Level 3 design inputs. Therefore, several documents such as Turkish Highway Technical Specification [23], Asphalt Mixture Laboratory Studies [24], and Turkish Flexible Pavement Design Guide [15] were carefully reviewed and local design data were obtained as explained in the following subtitles.

### *4. 1. Hot Mixed Asphalt Material Properties*

The asphalt binder properties, asphalt volumetric properties and aggregate gradation that is commonly used in wearing course and binder course in Izmir are presented in Table 12, 13 and 14, respectively.

*Table 12 - Binder inputs (Input Level 3)*

| Inputs | Values |
|---|---|
| Penetration grade, (0.1 mm) | 50/70 |
| Performance graded, (PG) | 64-16 and 64-22 |

*Table 13 - Volumetric inputs (Input Level 3)*

| Inputs | Wearing course | Binder course (Type 1) | Binder course (Type 2) |
|---|---|---|---|
| Maximum specific gravity, (kN/m$^3$) | 25 | 25 | 25 |
| Bulk specific gravity, (kN/m$^3$) | 24 | 24 | 24 |
| Effective binder content by volume $V_{be}$ (%) | 8 | 8 | 8 |
| Air voids $V_a$ (%) | 4-5 | 4-6 | 4-6 |
| Voids in mineral aggregates *VMA* (%) | 14-16 | 13-15 | 12-14.5 |
| Voids filled with asphalt *VFA* (%) | 65-75 | 60-75 | 55-75 |

*Table 14 - Aggregate gradation (Input Level 3)*

| Inputs | Wearing course | Binder course (Type 1) | Binder course (Type 2) |
|---|---|---|---|
| % Passing the No.200 sieve | 3-8 | 2-7 | 0-8 |
| Cumulative % retained on in No.4 sieve | 58-28 | 70-48 | 70-38 |
| Cumulative % retained on in 3/8" sieve | 28-0 | 52-30 | 57-25 |
| Cumulative % retained on in 3/4" sieve | 0 | 20-0 | 40-10 |

Inputs Level 3 were selected based on other design inputs such as poison's ratio, surface shortwave absorptivity, coefficient of thermal contraction of the mix, reference temperature, thermal conductivity, heat capacity of asphalt, asphalt indirect tensile strength, and asphalt creep compliance.

### *4. 2. Unbound and Subgrade Material Properties*

The MEPDG requires the Resilient Modulus ($M_R$) of subgrade and base materials. The $M_R$ can be obtained through laboratory tests or predicted via empirical predictive equations. In Turkey, the resilient modulus of subgrade and unbound materials were determined through an empirical equation (Equation 5) [25].

$$M_R = 1750(D_{BSK} + K)^{0.438} \times CBR^{0.4} \left( \frac{1}{1+\log(No.200)} \right)^{0.35(LL \times PI+1)^{0.06}} \times \left( \frac{\gamma_{\max}^{\ 2}}{No.4} \right)^{0.09\log(\omega_{opt})} \quad (5)$$

Where;

$M_R$ = resilient modulus

$D_{BSK}$ = HMA layer total thickness

CBR = California bearing ratio (%)

ω = moisture content

γ = maximum dry density

LL = liquid limit

PI = plasticity index

No.200 = % passing the No. 200 sieve

No.4 = % passing the No.4 sieve

K = depth correction factor (k=0 for base and subbase, k=17 for subgrade)

It seems that (Equation 6) significantly underestimates the resilient modulus of unbound materials comparing to the equation suggested by MEPDG in (Table 15) and (Figure 10).

$$M_r(psi) = 2555CBR^{0.64} \quad (6)$$

In this study, the equation suggested by MEPDG was used to predict the resilient modulus for base and subbase instead of Equation 5. The CBR values for base layer and subbase layer was taken as 100% and 50%, respectively, based on the information found in the Turkish Technical Specification for Highways and Turkish Flexible Pavement Design Guide.

*Table 15 - Comparison between MEPDG and local predictive equations*

| CBR (%) | 10 | 20 | 30 | 40 | 50 | 60 | 70 | 80 | 90 | 100 |
|---|---|---|---|---|---|---|---|---|---|---|
| $M_R$ (ksi) by Equation 5 | 11.2 | 17.4 | 22.5 | 27.1 | 31.2 | 35.1 | 38.8 | 42.2 | 45.5 | 48.7 |
| $M_R$ (ksi) by Equation 6 | 9.2 | 12.1 | 14.2 | 15.9 | 17.4 | 18.7 | 19.9 | 21.0 | 22.0 | 23.0 |

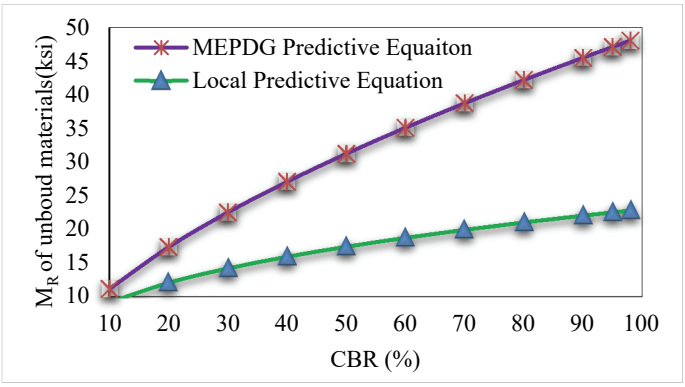


*Figure 11 - Comparison between MEPDG and local predictive equations*

## 5. CONCLUSIONS

In this study, climate data, traffic characteristics and material properties have been obtained from various local sources to be used for local implementation of the MEPDG in Izmir. The collected local data were analysed and some of the data were found to be deficient for direct use as a design input. Therefore, the data was converted to the MEPDG required format which is summarized in the following paragraphs:

- The obtained climate data were analysed, and various missing weather data were observed. The missing data were completed by using the average of data before and after the missing points. The values were adapted from other closest weather stations. Finally, climate data were converted to the text file with extension ".hcd".
- In Turkey, vehicles are classified based on their types into five groups which significantly differ from the MEPDG truck classification standard. Therefore, vehicles were classified in 10 classes according to the vehicle type, axle number, and axle spacing.

- The truck distribution indicates that vehicles in class 5 and 9 have the highest share percentage while trucks in classes 9 and 10 have little distribution.
- The growth rate of trucks in classes 8, 9 and 10 are very high.
- In Turkey, only the axle loads of the heavy trucks (5, 6, 7, 8, 9, and 10) are measured using weighbridge method at the interval of 1000 kg regarding all axle types (single, tandem, and tridem). The quad axle load has not been measured. In this study, the axle load distributions were calculated at the intervals of default axle load distribution factors, which were used for class 4, and quad axle load distribution factors were set to zero.
- The local resilient modulus predictive equation significantly underestimates the resilient modulus in comparison with the equation suggested by MEPDG. In this study the equation suggested by MEPDG is used.

**Acknowledgment**

The authors would like to express their profound gratitude to the Department of Scientific and Research Project, Dokuz Eylul University, Izmir, Turkey for their financial support (Project Number: 2019.KB.FEN.038). They also thank and appreciate the Graduate School of Natural and Applied Sciences, Dokuz Eylul University for their valuable supports.

## References

[1] AASHTO, Mechanistic empirical pavement design guide. American Association of State Highway and Transportation Officials, Washington, D.C., USA, 2008.

[2] Timm, D. H., Roobin, M. M., Tran N., Rodezno C., Flexible pavement design – State of the practice, NCAT Report 14-04, National Asphalt Pavement Association, USA, 2014.

[3] AASHTO, Guide for the local calibration of the mechanistic-empirical pavement design guide. Washington, D.C: American Association of State Highway and Transportation Officials (AASHTO), Washington, D.C., USA, 2010.

[4] Öztürk, H. I., Tan, E. B., Şengün, E., Yaman, İ. Ö., Farklı trafik, zemin, malzeme ve iklim koşulları için mekanistik-ampirik (M-E) yöntemle tasarlanan derzli donatısız rijit üstyapı sistemlerinin karşılaştırılması, J. Fac. Eng. Archit. Gazi Univ., 34(2), 771–783, 2019.

[5] E. Şengün, E. H. I. Öztürk, H. I. and İ. Ö. Yaman, İ. Ö., Mekanistik-Ampirik ve Geleneksel Beton Yol Tasarım Yöntemlerinin Karşılaştırılması: Afyon-Emirdağ Deneme Kesimi, Tek. Dergi, 31 (5), 2020.

[6] Caliendo, C., Local calibration and implementation of the mechanistic-empirical pavement design guide for flexible pavement design, J. Transp. Eng., 138(3), 348–360, 2012.

[7] Ghosh, A., Padmarekha, A., Krishnan, J. M., Implementation and proof-checking of mechanistic-empirical pavement design for Indian highways using AASHTOWARE Pavement ME Design Software, Procedia - Soc. Behav. Sci., 104, 119–128, 2013.

[8] Tarefder, R., Rodriguez-Ruiz, J. I., Local calibration of MEPDG for flexible pavements in New Mexico, J. Transp. Eng., 139(10), 981–991, 2013.

[9] Elshaeb, M. A., El-Badawy, S. M., Shawaly, E. S. A., Development and impact of the Egyptian climatic conditions on flexible pavement performance, Am. J. Civ. Eng. Archit., 2(3), 115–121, 2014.

[10] M. Dadwan, M. Abo-Hashema, H. Faheem, and M. Hashem, "Modeling Pavement Performance Using LTPP Database for Flexible Pavements," Tek. Dergi, 31(4), 2020.

[11] Sadek, H. A., Masad, E. A., Sirin, O., Al-Khalid, H., Sadeq, M. A., Little, D., Implementation of mechanistic-empirical pavement analysis in the state of Qatar, Int. J. Pavement Eng., 15(6), 495–511, 2014.

[12] Ma, H., Wang, D., Zhou, C., Feng, D., Calibration on MEPDG low temperature cracking model and recommendation on asphalt pavement structures in seasonal frozen region of China, Adv. Mater. Sci. Eng., Vol. 2015, 1–11, 2015.

[13] Alqaili, A. H., Alsoliman H. A., Preparing data for calibration of mechanistic-empirical pavement design guide in central Saudi Arabia, World Acad. Sci. Eng. Technol. Int. J. Urban Civ. Eng., 11(2), 248–255, 2017.

[14] Chhade, R. H., Mrad, R., Houssami, L., Chehab, G., Asce, A. M. Formulation of traffic inputs required for the implementation of the M-E PDG formulation of traffic inputs required for the implementation of the M-E PDG in data-scarce regions : Lebanon case study, J. Mater. Civ. Eng. ASCE, 30(9), 04018198-14, 2018.

[15] Turkish General Directorate of Highways, Karayolları esnek üstyapılar projelendirme rehberi. Ankara, Turkey, 2008.

[16] Huang, Y. H., Pavement Analysis and Design, Second Edi. Pearson/Prentice Hall, USA, 2004.

[17] Schwartz, C. W., Carvalho, R. L., Evaluation of Mechanistic-Empirical Design Procedure, SP0077B41, University of Maryland, Maryland State, USA, 2007.

[18] AASHTO, Mechanistic-empirical pavement design. American Association of State Highway and Transportation Officials,Washington, D.C., USA, 2015.

[19] Turkish General Directorate of Highways, Trafik ve ulaşım bilgileri, Trafik Güvenliği Dairesi Başkanlığı Ulaşım Etütleri Şubesi Müdürlüğü, Ankara, Turkey, 2018.

[20] Turkish General Directorate of Highways, Karayollarında ağır taşıt trafiğinin ve yük taşımacılığının özellikleri ve eğilimleri, Trafik Güvenliği Dairesi Başkanlığı Ulaşım Etütleri Şubesi Müdürlüğü, Ankara, 2016.

[21] Turkish General Directorate of Highways, Devlet yolları trafik akımı özellikleri ve trafik parametreleri, Strateji Geliştirme Daire Başkanlığı Ulaşım ve Maliyet Etütleri Şubesi Müdürlüğü, Ankara, Turkey, 2009.

[22] Özcana, S., Akpinar, M. V., Esnek Üstyapılarda Kritik Tekerlek ve Aks Konfigürasyonların Mekanistik Analizlere Göre Tespit Edilmesi, Teknik Dergi, 25(121), 6625-6654, 2014.

[23] Turkish General Directorate of Highways, Karayolu teknik şartname, Vol. 1. Turkish General Directorate of Highways, Ankara, Turkey, 2013.

[24] Orhan, F., Bitümlü karışımlar lab. çalışmaları, Karayolları Genel Müdürlüğü, Ar-Ge Dairesi Başkanlığı Üstyapı Geliştirme Şubesi Müdürlüğü, Ankara, 2012.

[25] Güngör, A. G., Sağlık, A., Mekanistik ampirik üstyapı tasarımında esneklik modülünün şartnamelere uyarlanması, 5th Eurasphalt & Eurobitume, 455–463, 2012.

*Teknik Dergi, 2021 11381-11405, Paper 638*

# Experimental Study on the Behavior of Header End - Plate Connections under Cyclic Loading

**Adem KARASU**[1]
**Cüneyt VATANSEVER**[2]

## ABSTRACT

This paper presents the results from an experimental study on the actual behavior of header end-plate connections. To better understand the hysteretic behavior of these connections in terms of the stiffness and the strength, sixteen specimens were considered and subjected to cyclic loads. The effect of some parameters such as thickness of the header end-plate, depth of the connection and the number of bolt rows on the behavior of header end-plate connections has been investigated by the help of experimental tests and finite element (FE) analyses. The moment-rotation relations of the connections governed by three parameters such as initial stiffness, moment capacity and rotation capacity were obtained. Results revealed that the moment capacity increases with the increase in end-plate thickness and depth of connection. However, for the equal connection depth, increasing the number of bolt rows has not influenced the connection behavior in any noticeable way.

**Keywords:** Steel structures, semi-rigid connections, header end-plate, experimental study, finite element method.

## 1. INTRODUCTION

The use of bolted end-plate connections has become popular due to ease of fabrication, erection and proper seismic behavior. After the 1994 Northridge earthquake, bolted end-plate connections have seen a rise in popularity as engineers seek alternatives to the welded connections. Moreover, these connections exhibited more suitable results than rigid welded connections (Chen et al. [1]). These connections have the advantage of less supervision and shorter assembly time than welded connections.

Research in bolted end-plate connections provided liability of bolted extended and flush end-plate connections to serve as moment resisting connections. One of them presented by Sherif

Note:
- This paper was received on January 14, 2020 and accepted for publication by the Editorial Board on May 23, 2020.
- Discussions on this paper will be accepted by January 31, 2022.

• https://dx.doi.org/10.18400/tekderg.674889

1 Istanbul Technical University, Department of Civil Engineering, Istanbul, Turkey - karasuad@itu.edu.tr https://orcid.org/0000-0002-1063-8484

2 Istanbul Technical University, Department of Civil Engineering, Istanbul, Turkey - cuneyt.vatansever@itu.edu.tr - https://orcid.org/0000-0002-9954-925X

et al. [2] and Bing et al. [3] have studied cyclic behavior of flush end-plate and extended end-plate connections, respectively. Cyclic behavior of bolted extended end-plate connections was evaluated and responses of the specimens were examined in ABAQUS software presented by Ismail et al. [4] and Haghollahi and Jannesar [5]. Fang et al. [6] has investigated the cyclic performance of extended end-plate connections equipped with shape memory alloy (SMA) bolts numerically and experimentally. It was clearly observed from the test results that longer SMA bolts resulted in higher ductility. Dessouki et al. [7], Adey [8] and Johnstone and Walpole [9] have used the yield line theory to propose equations for the four bolts and multiple row extended end-plate connections. However, limited number of experimental investigations in the area of cyclic behavior of header end-plate connections has been carried out.

Header end-plate connection is a kind of bolted end-plate connection whose length is less than the depth of the beam. Since they have limited stiffness and strength, these types of connections are also called a shear end-plate connection in the AISC-LRFD specifications [10] and fall in the category of flexible connections (Kishi et al. [11]). Moment-rotation characteristics of these type of steel connections are indicative of the connection's stiffness, strength and ductility. Stiffness, strength and ductility of the connections are believed to be critical factors for structures located in seismic areas. Furthermore, in seismic design, the flexible semi-rigid connections might be alternatively employed to offer sufficient plastic rotations. Jaspart and Demonceau [12] presented design sheets that contain practical ways to satisfy the ductility and rotation requirements of header end-plate connections.

A joint may be classified as full-strength, nominally pinned or partial strength by comparing moment resistance, and can be categorized as fully-rigid, nominally pinned or semi-rigid according to its initial rotational stiffness according to Eurocode (EN 1993-1-8, [13]). The design of joints within this partial strength/semi rigid approach is becoming more and more popular, because actual behavior of the connections significantly influence the distribution of the internal forces and overall deformations of the structure. Therefore, the studies on header end-plate connections have concentrated on experimental tests and analytical studies for achieving the moment-rotation relations (Sommer [14], Aggarwal [15], Pilgr [16]) under monotonic loading.

Most of the experimental studies were conducted on monotonic loading on header end-plate connections. The lack of cyclic test results of header end-plate connections motivated the study presented in the paper. That is the reason why the hysteretic response of this type of connection must be investigated to better understand the behavior of structural system under seismic loads when these connections are used as a beam-to-column connections. In this study, therefore, we experimentally investigated the nonlinear behavior of bolted header end-plate connections under cyclic loading. The behavior of the bolted header end-plate steel connections is entirely dependent upon and highly sensitive to the connection's geometric variables. It is essential that the influence of these parameters on the performance of header end-plate connections must be investigated to make proper assessment. The studied parameters were as follows: end-plate thickness, depth of the connection and number of bolt rows. Also, we examined the applicability of these connections according to AISC provisions (AISC341-16, [17]) by presenting moment-rotation hysteretic response of the connections. Thus, it may be possible to provide a contribution to the energy dissipated during the

earthquake, if gravity frames with these connections are used combining with the special moment frames.

## 2. EXPERIMENTAL PROGRAM

### 2.1. Test Specimens

The study included a total of sixteen full scale tests that were performed in the Structural and Earthquake Engineering Laboratory of Istanbul Technical University. Two specimens with the characteristics of T5-20, whose details will be described later, were prepared and one of these was used in the pilot test to ensure that the test setup worked properly. Pilot test results are identical to the test results mentioned in the paper for the other specimen of T5-20. An extensive parametric study was conducted with the different configurations of end-plate as shown in Figure 1. The main test parameters for header end-plate connections were end-plate thickness, depth of the connection and number of bolt rows. Each specimen consisted of a column and a cantilever beam connected to the column flange at column's mid-height. The length of the column was 3020 mm and the length of the beams were 1760 mm, 1755 mm and 1750 mm, respectively. As for the end-plate thicknesses; 10 mm, 15 mm and 20 mm were considered. M20 high strength bolts of grade 10.9 (yield strength, $F_{yb}$ is 900 N/mm$^2$, tensile strength, $F_{ub}$ is 1000 N/mm$^2$) were employed for the connections. All bolts were fully tightened to the specified pretension force of 172 kN (TCDCSS, [18]) which is defined as the minimum pretension force for M20-10.9 bolts, using a torque wrench previously calibrated for each specimen. The bolts had the same dimensions and different arrangements for each type of the connection, as illustrated in Figure 1. The beam web was attached to the end-plate with double-sided fillet welds. For the current study the column and its flange were designed to have negligible deformation. Stiffener plates with a thickness of 10 mm were also placed between the column flanges on both sides of the column web at the level of beam flanges to limit the bending deformation of the column flange. The throat size of the fillet weld used for connecting beam web to end-plate was 10 mm and 6 mm fillet weld throat size was used for the stiffener connection to beam and column for all specimens. Because the moment resistance of the connection varies significantly to the depth of the end-plate, it was varied from 180 mm to 240 mm. The moment resistance of the connection is also affected by the number of bolts. Therefore, bolt rows changing from two to four were considered.

The tests were set-up using hot rolled European steel sections. To obtain the material characteristics of steel for each individual member involved in the connections, tensile tests were conducted considering three coupons for each member. For beams' (IPE 300) materials, all coupons were extracted from the web of IPE 300 profiles and as for columns (HEB 300) one coupon was cut from the flange, other two were extracted from the web. In total, 21 coupons were considered and average values for yield stress and elastic modulus are listed in Table 1. The results show that the experimental values were higher than the specified values of yield strength $F_y$ as expected.

The naming convention used for the sample identification (TX-Y) is a combination of the type of the end-plate configurations (TX) and the thickness of the end-plate (Y) in mm. For example, a test designation of T3-20 indicates that the type of connection configuration is T3 and the thickness of the end-plate is 20 mm. Joint details for type 3 (T3-10,15,20) are given in Figure 2.

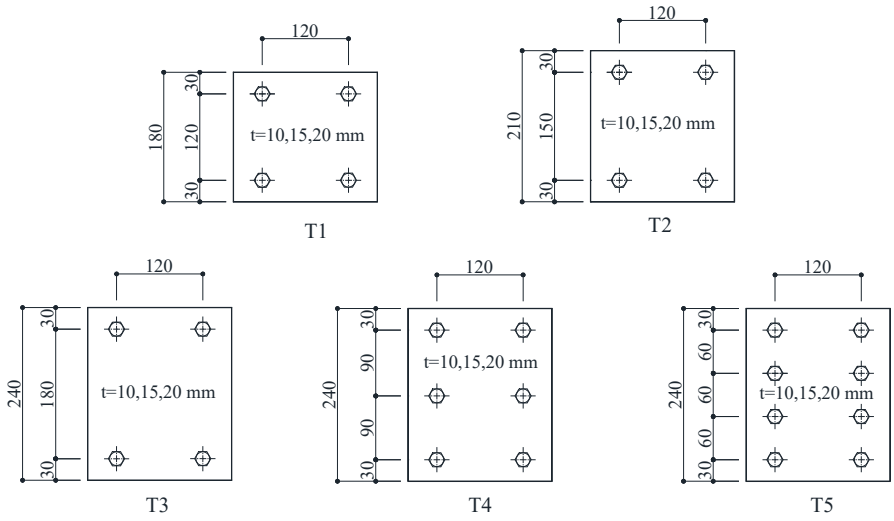


*Figure 1 - Different header end-plate configurations*

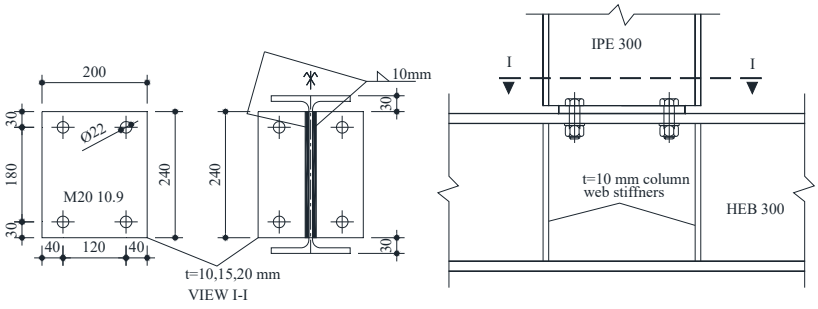


*Figure 2 - Details of header end-plate connections for T3*

*Table 1 - Coupon test results*

| Specimen | | $F_y$ (N/mm$^2$) | $F_u$ (N/mm$^2$) | E (N/mm$^2$) |
|---|---|---|---|---|
| End plate thickness t=10mm T(1,2,3,4,5)-10 | Endplate t=10 mm (S235) | 287.08 | 419.88 | 203316.66 |
| | Beam / IPE 300 (S275) | 325.03 | 442.91 | 205392.00 |
| | Column / HEB 300 (S275) | 346.88 | 478.80 | 205568.00 |
| End plate thickness t=15mm T(1,2,3,4,5)-15 | Endplate t=15 mm (S235) | 280.35 | 392.09 | 194955.00 |
| | Beam / IPE 300 (S275) | 300.54 | 425.37 | 214514.00 |
| | Column / HEB 300 (S275) | 346.89 | 478.80 | 205568.00 |

*Table 1 - Coupon test results (continue)*

| Specimen | | $F_y$ (N/mm$^2$) | $F_u$ (N/mm$^2$) | E (N/mm$^2$) |
|---|---|---|---|---|
| End plate thickness t=20mm T(1,2,3,4,5)-20 | Endplate t=20 mm (S235) | 278.29 | 415.03 | 198171.66 |
| | Beam / IPE 300 (S275) | 332.95 | 470.80 | 208492.00 |
| | Column / HEB 300 (S275) | 346.89 | 478.80 | 205568.00 |

### 2.2. Test Setup and Instrumentations

Test setup and instrumentation used in the present study are shown in Figure 3. The test setup consists of a servo-controlled MTS hydraulic actuator with the loading capacity of ± 250 kN, stroke capacity of ± 300 mm and steel posts mounted on the strong floor. A load cell installed in the hydraulic actuator to measure the cyclic load. The column was connected to the supports via a pin connection using two rollers at both sides. It was assumed that the column is pin supported at mid-story. Also the length of the cantilever beam was considered more than five times the depth of the beam section that is exactly sufficient to idealize the flexural behavior. Besides, out of plane movement of the beam was prevented by using support frame, as seen in Figure 4.

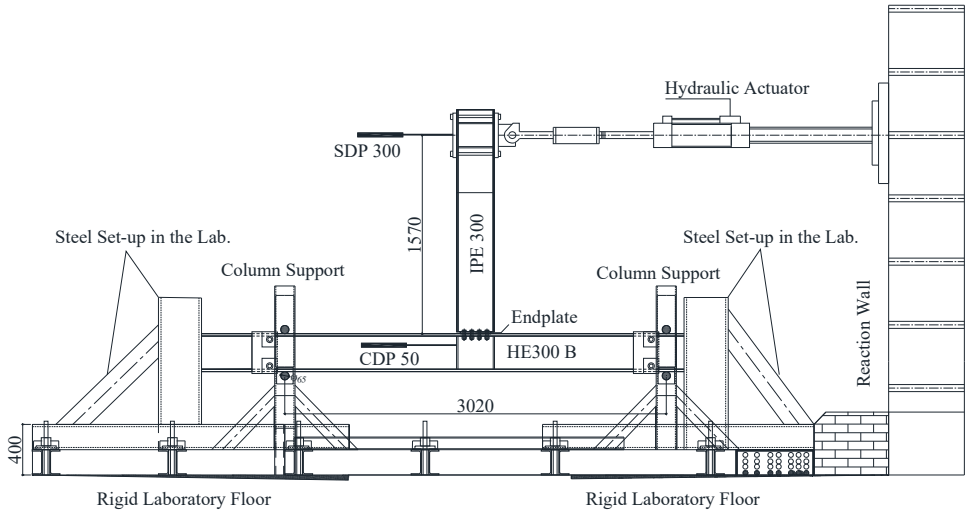


*Figure 3 - The experimental setup*

Linear variable differential transformers (LVDTs) were employed to measure lateral displacements of the beam and deformations of the connection during the tests. Strain gauges were placed on the end-plate and beam web at the connection, as shown in Figure 5, to determine the stress distribution and to monitor the progress of plasticity of the connection. The positions of the strain gauges were chosen at the positions of the expected maximum tensile strains as predetermined by the FE analyses results. One LVDT (SDP 300) was placed

to measure the top displacement at 1570 mm above the column flange surface. The other LVDT (CDP 50) was used to measure possible slippage of the specimen. The relative displacement of the beam top was calculated by deducting the horizontal displacement of the column from the total displacement of the beam top.

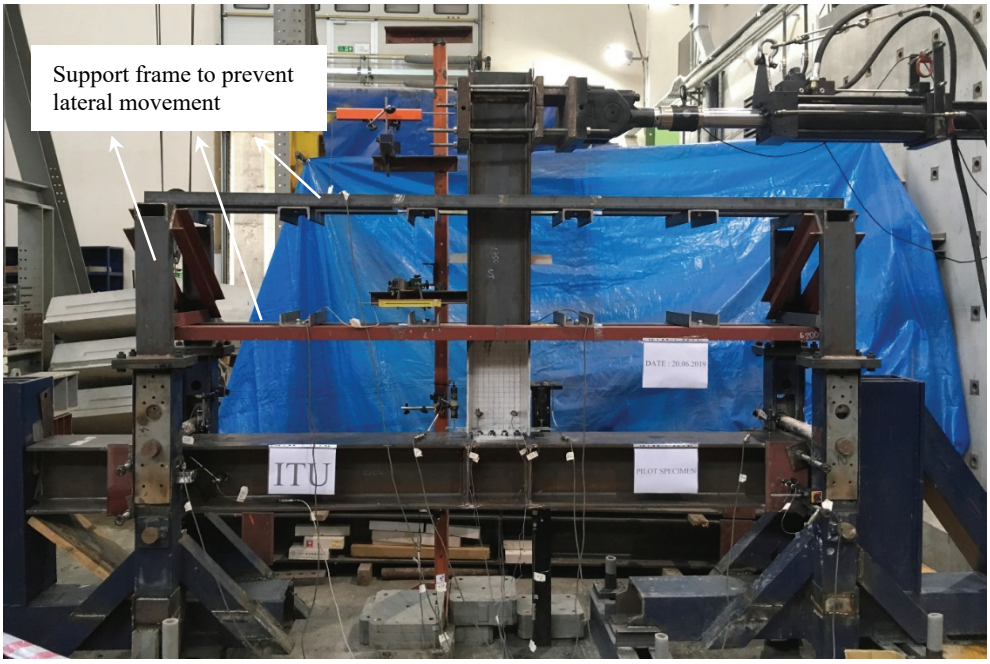


*Figure 4 - Photographic view of the test setup*

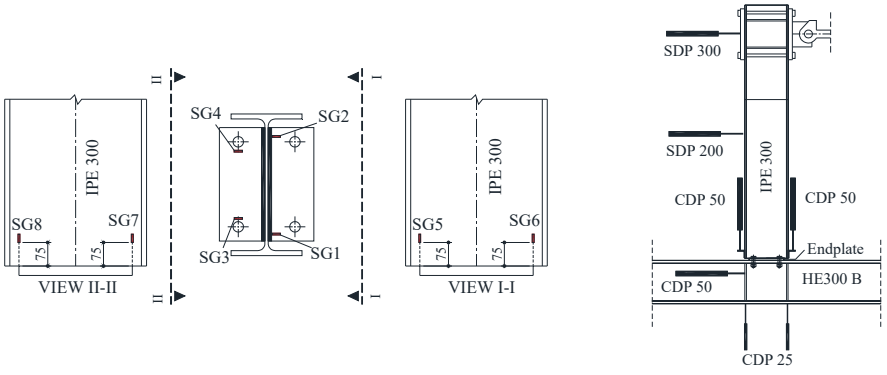


*Figure 5 - Strain gauges and LVDT layout*

### 2.3. Test Procedure

As previously described, to ensure a sufficient initial stiffness, full pretension was applied to each bolt. After bolt pretension process, the cyclic load was applied by the hydraulic jack at the beam top using a displacement control procedure. The loading protocol recommended by AISC (AISC341-16, [17]) was followed (Figure 6). This protocol uses drift angle, $\theta_b$ (relative displacement of beam divided by arm length (1570 mm)) as the main parameter, and the sequence of loading drifts are: 0.00375 (six cycles), 0.005 (six cycles), 0.0075 (six cycles), 0.01 (four cycles), 0.015 (two cycles), 0.02 (two cycles), 0.03 (two cycles), 0.04 (two cycles) and subsequent loadings at increments of $\theta_b$=0.01 rad, with two cycles of loading at each step. For each loading, a set of readings were taken for displacement and applied load.

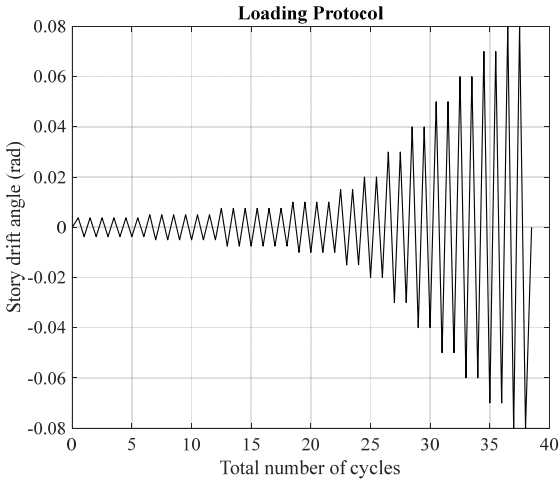


*Figure 6 - Loading protocol*

## 3. TEST RESULTS AND DISCUSSION

During the loading process, the shear action was well resisted via the friction between the end-plate and column flange face with no slippage observed. The bending moments at the connection are calculated by multiplying the load at the actuator with the distance to the column flange face. The failure conditions were considered to have reached when an abrupt or significantly large reduction occurred in the moment capacity.

The study mainly identified three types of behavior for the header end-plate connections. First, thin plate behavior where the end-plate is weaker and yields before the yielding and rupture of the beam web, secondly, intermediate plate behavior in which the end-plate and beam web plastify simultaneously and so both of them yield together, and finally thick plate behavior where the end-plate is stronger than the beam web and therefore, the beam web governs the flexural strength. According to the test results, increasing the number of bolt rows has negligible effect on the flexural capacity of the connections with thick plate, where the failure is governed by the beam web rupture. For these types of connections the test of each specimen was terminated after the rupture of the beam web. Experimental results are

summarized in Table 2, in which $R_i$, $M_{max}$, $\theta_{max}$ are the initial stiffnesses of the connections, the maximum moments achieved in the tests and the maximum rotations of the connections attained at the moment of the failure in the tests, respectively. Initial stiffnesses of the connections were determined by regression analysis considering a few data points in elastic region. The effect of each parameter on the connection behavior is assessed in the following sections.

*Table 2 - Summary of the test results*

| | $R_i$ (kNm/rad) | $M_{max}$ (kNm) | $\theta_{max}$ (rad) | Failure Mode |
|---|---|---|---|---|
| **T1-10** | 5494.0 | 18.44 | 0.09 | End-plate tearing |
| **T1-15** | 5471.1 | 35.51 | 0.08 | End-plate tearing |
| **T1-20** | 6179.3 | 41.69 | 0.04 | Rupture of beam web |
| **T2-10** | 7078.0 | 24.75 | 0.08 | End-plate tearing |
| **T2-15** | 7386.0 | 45.51 | 0.09 | End-plate tearing |
| **T2-20** | 8355.0 | 53.49 | 0.03 | Rupture of beam web |
| **T3-10** | 9667.1 | 29.62 | 0.07 | End-plate tearing |
| **T3-15** | 9792.9 | 57.89 | 0.09 | End-plate tearing |
| **T3-20** | 9755.6 | 67.98 | 0.02 | Rupture of beam web |
| **T4-10** | 9481.3 | 34.77 | 0.08 | End-plate tearing |
| **T4-15** | 10122 | 63.11 | 0.09 | End-plate tearing |
| **T4-20** | 9402.2 | 69.33 | 0.03 | Rupture of beam web |
| **T5-10** | 8962.9 | 38.90 | 0.08 | End-plate tearing |
| **T5-15** | 9825.2 | 64.44 | 0.08 | Both End-plate tearing and Rupture of beam web |
| **T5-20** | 9708.5 | 64.98 | 0.02 | Rupture of beam |

### 3.1. End-Plate Thickness

For the purpose of the discussion of the test results, the connection moment versus rotation hysteretic loops of all types of the connections are plotted in the same graph, as shown in Figure 7, to distinguish the behavior of the connections according to the end-plate thicknesses. As understood from the figures, the connections with the end-plates of 10 mm and 15 mm thicknesses exhibit more ductile behavior than those with the end-plates of 20 mm thickness because the flexural yielding of the end plate governs the behavior, which is defined as thin plate behavior. Moreover, the flexural capacities of the connections with 15 mm thick end-plate increase by about 70-100% when compared to those of the connections with 10 mm thick end-plate. Due to damage with the ductile tearing of the end-plate adjacent to the fillet welds, strength deterioration was observed at large rotations for 10 mm and 15 mm thick end-plates. Then, further increase in the end-plate thickness from 15 mm to 20 mm

has a little effect on the connection capacity as the behavior turns into the thick plate behavior. Furthermore, the ductility of the thicker end-plate connections is smaller than that of the other connections since the beam web in tension controls the behavior, which is described as the thick plate behavior.

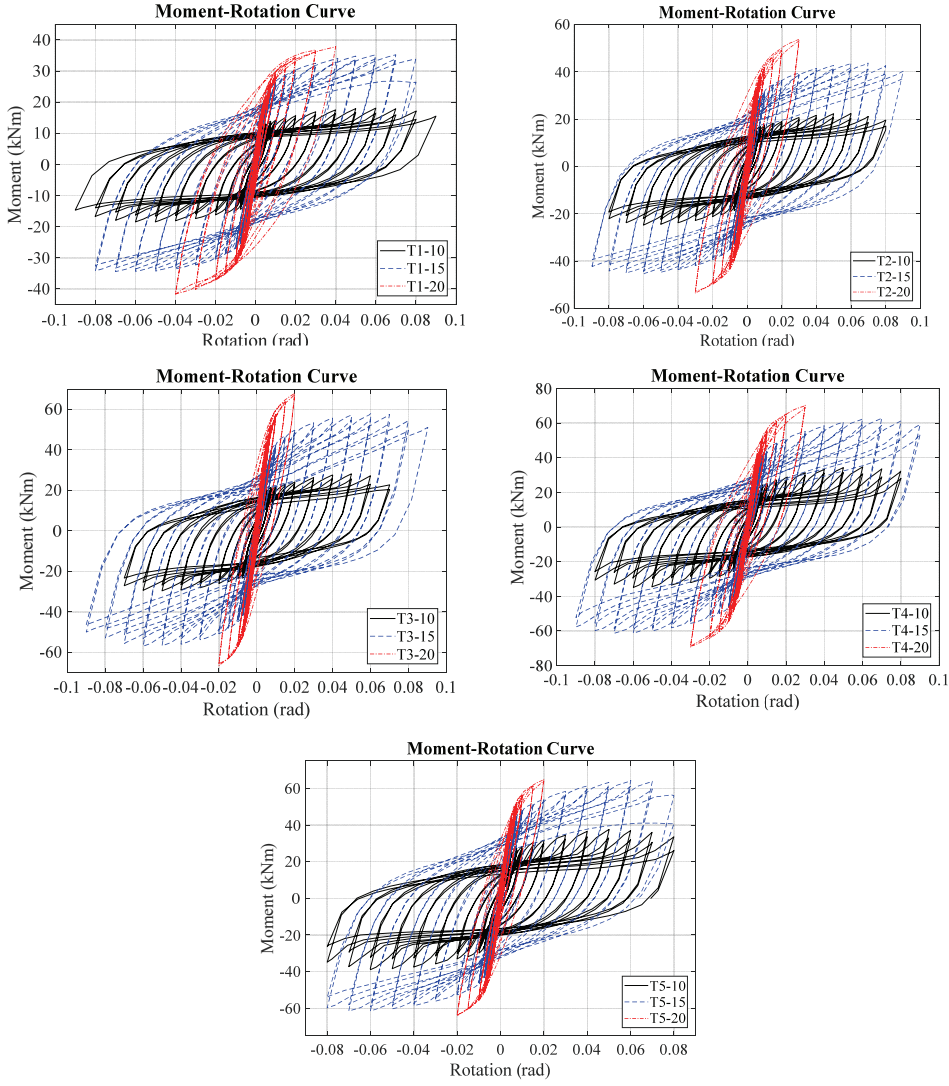


*Figure 7 - Moment-rotation hysteretic loops*

As seen from the Figure 7, the hysteretic loops are stable and the connections behave in a stiff linear manner at the beginning of the loading till reaching yield strength of either end-plate or beam web. Increasing the end-plate thickness has not significantly affected the initial

stiffness of the connections due to beam web playing a governing role in the elastic region. After yielding, the behavior becomes non-linear because of the plastic deformations occurred in both beam web and end-plate. It is apparent that end-plate thickness affects the behavior of the header end-plate connections significantly. According to the test results, specimens with end-plates of t=10 mm and t=15 mm show a higher ductility level while the specimen with the end-plate of t=20 mm develops the largest moment capacity with limited ductility. In these connections (t=20mm), further deformations cause the beam web to enter the inelastic range that leads to stiffness deterioration. For the connections with t=15 mm, the occurrence instant of the tearing of the end-plate together with the fracture of the beam web was so close as it would not recognize which one was earlier than the other for the specimens.

According to the observations during the tests shown in Figure 8, the connection with 10mm thick end-plate (relatively thin end-plate) reached the flexural capacity with the plastification of the end-plate. The flexural strength of the connection with 15mm thick end-plate (intermediate end-plate) was reached by yielding of both end-plate and the beam web while the yielding of the beam web governed the flexural capacity of the connection having 20mm thick plate (relatively thick end-plate). One indication that shows the flexural deformation of the end-plate is the amount of the separation observed between the surfaces of the end-plate and the column flange at the contact surface. As shown in the Figure 8, the sizes of the separations that took place at the connections with relatively thinner end-plates were larger than others with thicker ones. Spalling of whitewash, as seen in Figure 8 within the connection with 15 mm and 20 mm thick end-plate, indicates that the beam web yields. Strain gauge readings (S7) shown in Figure 9 also showed yielding occurred within the beam web. However, neither strain gauge readings (S5, S6, S7 and S8) nor observations during the test showed that the beam web of the specimen having 10mm thick header end-plate yields. Failure of the connection with the end-plate of 20mm thick occurred by rupture of the beam web adjacent to the fillet welds before the end-plate experienced sufficient flexural deformation to ensure ductility and rotational capacity. Therefore, the connection had relatively limited ductility and exhibited limited rotation capacity. Also, the parallel yield lines were observed at both bolt line and beam web-end-plate junction in addition to diagonal yield lines due to complete yielding of the end-plate of the specimen T5-10 and T5-15, while no complete yielding occurred in the end-plate of the specimen T5-20, as shown in Figure 10.

T5-10 T5-15 T5-20

*Figure 8 - Failure modes of the samples*

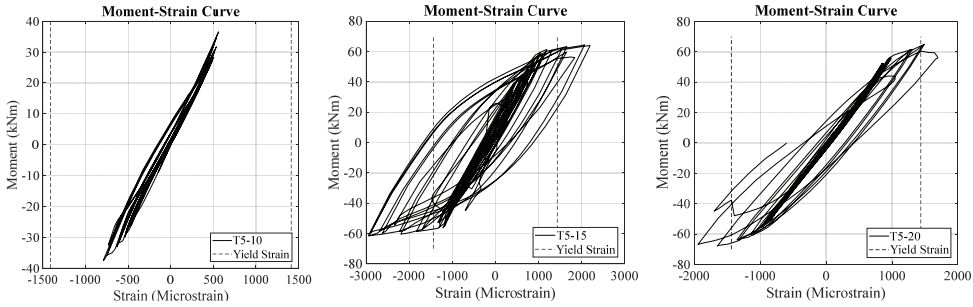


T5-10 T5-15 T5-20

*Figure 9 - Moment-Beam web strain curves for T5 samples (S7)*

*Figure 10 - End-plate deformations (left to right; T5-10, T5-15, T5-20)*

At the completion of tests, it was observed that effect of the prying forces that induced moment on bolt in addition to tensile forces, were more remarkable on the bolts in the connection with the end-plate of t=15mm than that with the end-plate of t=20mm due to larger flexural deformation of the end-plate occurred transversely. As seen in Figure 11, it is clear that the thicker the end-plate becomes, the smaller is the effect of the prying action .

T3-15 T3-20

*Figure 11 - Deformed shape of the bolts*

### 3.2. Depth of the Connection

As the depth of the end-plate increases from 180 mm to 240 mm, moment capacity of the connections is increased by about 60-65% for thin, intermediate and thick plates as shown in Figure 12. This is because the use of deep end-plate has developed longer lever-arm. Besides, a long lever-arm tends to reduce the connection rotation capacity as more applied load is needed to develop high moment resistance. Therefore the rotation capacity of the connection was less for deep end-plates than shallow end-plate.

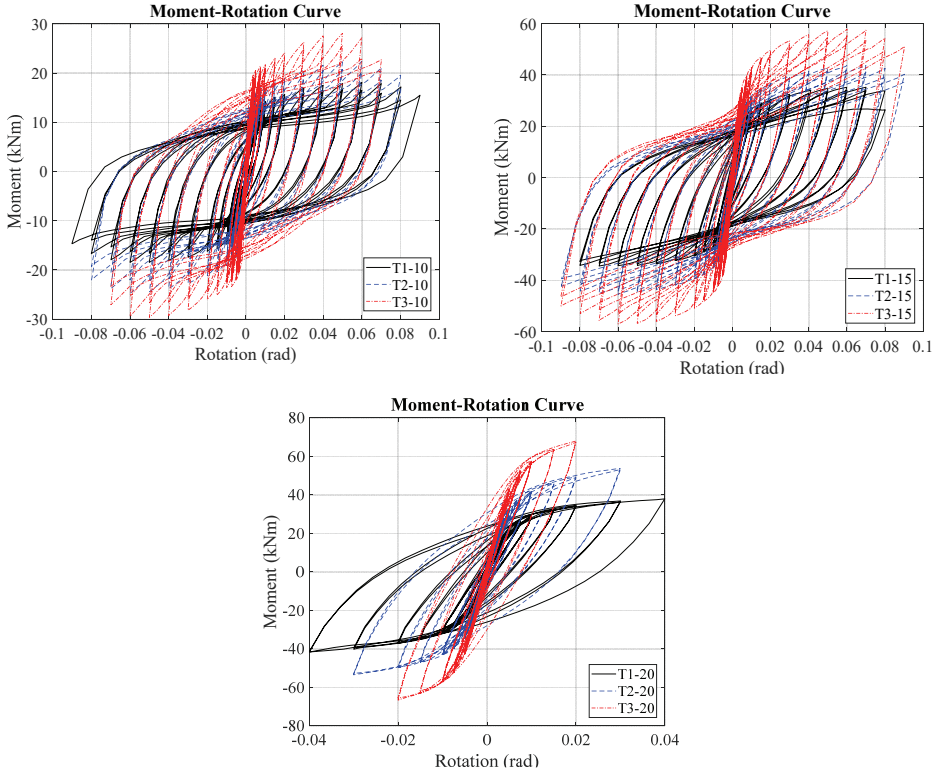


*Figure 12 - Moment-rotation hysteretic loops at different end-plate height*

### 3.3. Number of Bolt Rows

Figure 13 shows the moment-rotation curve of the connections having different end-plate configurations; with altogether 3, 4 and 5 with the thickness of 10 mm, 15 mm and 20 mm, respectively. The moment capacity of the joint increased when the number of bolt row increased for the end-plate with t=10 and 15 mm, because more bolt row provides more fixed points on the end-plate that leads to larger yielding capacity. However, effect of the number of bolt rows for the end-plate with t=20 mm was found to be negligible because beam web yielding governed the behavior of the joint.

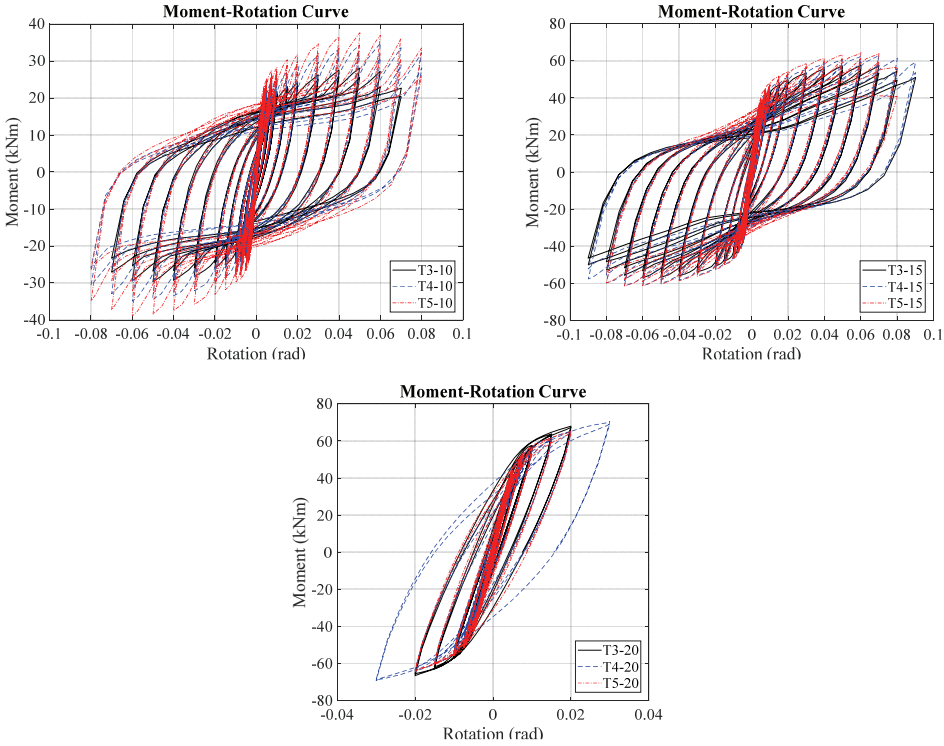


*Figure 13 - Moment-rotation hysteretic loops for equal end-plate height with different numbers of bolt rows*

### 3.4. Classification of the Connections according to Eurocode 3

Considering the stiffness, a connection can be classified as nominally pinned (NP), semi-rigid (SR) or rigid through the comparisons with $EI_b/L_b$, where $E$, $I_b$, and $L_b$ are the modulus of elasticity, second moment of area and the span of the connected member. The span of the connected member will be taken as 3.14 m (twice of the span of the cantilever beam and if the tested specimen beam section size is applied in 6 m span frames, the ratio in Table 3 ($R_i/(E_bI_b/L_b)$) will be almost doubled). According to the Eurocode 3 (EN 1993-1-8, [13]), connections having end-plates of t=15 mm and t=20 mm (T3, T4, T5) transfer more than 25% of the beam plastic moment capacity. Therefore they are called partial-strength (PS) connection while the connection with end-plate of t=10 mm is classified as nominally pinned. Furthermore, the results indicate that all of the specimens are categorized as semi-rigid connections because the ratio of $R_i/(E_bI_b/L_b)$ is between 0.5 and 25. Finally, for sufficient rotation capacity, end-plate thickness should be limited. In this study, based on the experimental results, end-plate thickness of 15 mm was found to be critical thickness. Therefore, the connection with 20mm thick end-plate exhibited insufficient behavior in terms of ductility and rotation capacity.

Connection assessment in terms of maximum moment of the connection $M_{max}$, to the ratio of the plastic moment capacity of the beam and initial stiffness of the connection to the ratio of the flexural stiffness of the beam according to Eurocode 3 (EN 1993-1-8, [13]) is given in the Table 3.

*Table 3 - Connection assessment based on Eurocode classification*

| | $R_i$ (kNm/ rad) | $\frac{E_b I_b}{L_b}$ | $\frac{R_i}{E_b I_b / L_b}$ | $M_{max}$ (kNm) | $M_{pl,IPE}$ | $\frac{M_{max}}{M_{pl,IPE}}$ | EC3 classfic. |
|---|---|---|---|---|---|---|---|
| **T1-10** | 5494.0 | 5465.9 | 1.00 | 18.44 | 204.1 | %9 | SR/NP |
| **T1-15** | 5471.1 | 5708.0 | 0.96 | 35.51 | 188.4 | %19 | SR/NP |
| **T1-20** | 6179.3 | 5441.8 | 1.13 | 41.69 | 209.1 | %20 | SR/NP |
| **T2-10** | 7078.0 | 5465.9 | 1.29 | 24.75 | 204.1 | %12 | SR/NP |
| **T2-15** | 7386.0 | 5708.0 | 1.29 | 45.51 | 188.4 | %24 | SR/NP |
| **T2-20** | 8355.0 | 5441.8 | 1.54 | 53.49 | 209.1 | %26 | SR/PS |
| **T3-10** | 9667.1 | 5465.9 | 1.76 | 29.62 | 204.1 | %15 | SR/NP |
| **T3-15** | 9792.9 | 5708.0 | 1.72 | 57.89 | 188.4 | %31 | SR/PS |
| **T3-20** | 9755.6 | 5441.8 | 1.79 | 67.98 | 209.1 | %33 | SR/PS |
| **T4-10** | 9481.3 | 5465.9 | 1.73 | 34.77 | 204.1 | %17 | SR/NP |
| **T4-15** | 10122 | 5708.0 | 1.77 | 63.11 | 188.4 | %34 | SR/PS |
| **T4-20** | 9402.2 | 5441.8 | 1.73 | 69.33 | 209.1 | %33 | SR/PS |
| **T5-10** | 8962.9 | 5465.9 | 1.64 | 38.90 | 204.1 | %19 | SR/NP |
| **T5-15** | 9825.2 | 5708.0 | 1.72 | 64.44 | 188.4 | %34 | SR/PS |
| **T5-20** | 9708.5 | 5441.8 | 1.78 | 64.98 | 209.1 | %31 | SR/PS |

Tests on the header end-plate connections revealed that the behavior of the specimens with the end-plate of t=15 mm and t=20 mm (T3, T4, T5) has satisfied requirements stipulated by the Eurocode 3 for partial strength and semi-rigid connections. The connections with 15 mm thick end-plate experienced rotation levels beyond 0.04 rad. However, the rotation capacity of the connection with end-plate thickness of t=20 mm was not more than 0.04 rad and they seem not to be suitable for use together with the special moment frames because this requires that the rotation capacity of the connection be at least 0.04 rad according to AISC provisions (AISC341-16, [17]). Additionally, the behavior of the connection was significantly improved with 15 mm thickness when compared to that with 10 mm thick header end-plate.

## 4. NUMERICAL INVESTIGATIONS ON HEADER-END PLATE CONNECTIONS

### 4.1. Flexural Resistance Based on the Obtained Yield Line Configurations

The flexural strength of the end-plate is determined by using yield line (YL) analysis which estimates the yield moment of the end-plate (Bruneau et al. [19]). For this purpose, based on the experimental and the FE analyses results, yield line pattern as shown in Figure 14, is determined and in order to obtain the flexural strength, the equality of the work done by the internal forces to that done by the external forces is generated.

General expression for internal work stored by the yield line pattern is as follows.

$$W_i = \sum_{n=1}^{N} (m_p \theta_{nx} l_{nx} + m_p \theta_{ny} l_{ny}) \tag{1}$$

Where $\theta_{nx}$ and $\theta_{ny}$ are the x and y components of the relative rotation of the rigid plate segments along the yield line. $l_{nx}$ and $l_{ny}$ are the x and y components of the yield line length and $m_p$ is the plastic moment strength of the plate per unit length which is defined as below.

$$m_p = F_y \frac{t^2}{4} \tag{2}$$

Where $t$ is the thickness and $F_y$ is the actual yield strength of the end-plate (Table 1). For the samples of T4-10 and T5-10, the total internal work $W_i$ stored in the yield lines can be calculated with Eq. 3, and external work $W_e$, due to external moment $M$, can be calculated with Eq. 4.

$$\begin{aligned} W_I &= m_p \times g \times [\frac{h_1}{m_f} + \frac{h_2}{p_f} + \frac{h_2}{s}] \times \theta^\circ + ... \\ &... + 8 \times m_p \times [(g_p + m_f) \times \frac{h_0}{g} + (p_f + s) \times \frac{h_2}{g} + 0.5(p_f + m_f) \frac{h_0 + h_2}{2g}] \times \theta^\circ \end{aligned} \tag{3}$$

$$W_e = \frac{M}{h} \theta h \tag{4}$$

Where $M_{pl}$ is the end plate flexural strength and $\theta$ is the applied virtual displacement that is equal to $1/h$, where $h$ is the height of the end-plate. Besides, $g$, $h_0$, $h_1$, $h_2$, $p_f$, $g_p$, $m_f$ and $s$ are the distances that define the geometric properties of the end-plate as shown in Figure 14.

In the FE models and the tests, the actual material properties have been used while the effect of the strain hardening has not been considered in the yield line analysis. Therefore, flexural capacities $M_{pl}$, from yield line method indicates the level of the moment at the beginning of

the plastification of the connection obtained by the FE method and experimental tests as shown in Figure 19. The flexural capacity value and end-plate yield line mechanism parameter $Y_p$ are given in Table 4, obtained by the following equations;

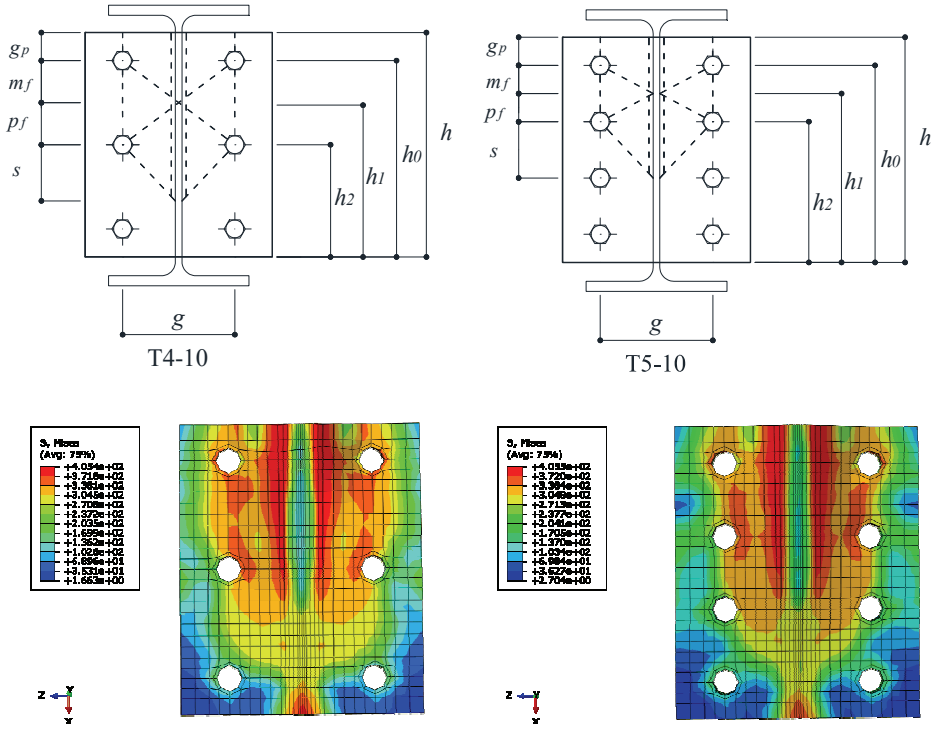


*Figure 14 - Yield line patterns and Stress contour diagram (FE results) of end-plates of T4-10 and T5-10*

$$M_{pl} = F_y \times t^2 \times Y_P \tag{5}$$

$$Y_P = \frac{g}{4}\left[\frac{h_1}{m_f} + \frac{h_2}{p_f} + \frac{h_2}{s}\right] + 2\left[(g_p + m_f) \times \frac{h_0}{g} + (p_f + s) \times \frac{h_2}{g} + 0.5(p_f + m_f)\frac{h_0 + h_2}{2g}\right] \tag{6}$$

$$\frac{\partial W}{\partial s} = 0 \rightarrow s = \frac{g}{2\sqrt{2}} \tag{7}$$

*Table 4 - Moment capacity (YL) of the connections with 10mm thick plate*

| Specimen | $t$ (mm) | $Y_p$ | $F_y$ (N/mm$^2$) | $M_{pl}$ (kNm) |
|---|---|---|---|---|
| T4-10 | 10 | 835.96 | 287 | 23.98 |
| T5-10 | 10 | 917.13 | 287 | 26.31 |

To limit the complexity of the equations, the plate material removed by drilling bolt holes is not considered and beam web thickness is taken to be zero as presented in Murray and Sumner [20].

### 4.2. Mechanical Model

In order to understand and to represent the elastic behavior of the connection before yielding, the initial stiffness of the connection must be known. Herein, initial stiffness of the end-plate connections can be estimated according to Faella et al. [21] based on the simulation of the connection by using a set of rigid or flexible components. It is easy to recognize that the prediction of the joint behavior involves the following components:

- Column web in shear (cws)
- Column web in compression (cwc)
- Column flange in bending (cfb)
- End-plate in bending (epb)
- Bolts in tension (bt)
- Column web in tension (cwt)
- Beam flange and web in compression (bfc)
- Beam web in tension (bwt)

For the extended and flush end-plate connections, the first six components govern the flexural resistance and initial rotational stiffness. Conversely, the last two components must be considered in the evaluation of the joint flexural resistance only. However, beam web strains control the initial stiffness of the header end-plate connections. Therefore, for the initial stiffness of the header end-plate connection, beam web in tension must be taken into consideration as an elasto-plastic spring component as shown in Figure 15. The effect of the beam flange and web in compression can be neglected for rotational stiffness of the connection.

The evaluation of the initial stiffness requires a knowledge of the effective stiffness coefficient of the first tension bolt row that is obtained by a set of springs in series. Then, the initial stiffness $S_{j,ini}$ can be determined through the Eq. 8 where $K_i$ is the stiffness coefficient representing $i$ component and $h_z$ is the lever arm. Translational stiffness of the other bolts were ignored.

$$S_{j,ini} = \frac{h_z^2}{\frac{1}{K_{cwt}} + \frac{1}{K_{cfb}} + \frac{1}{K_{epb}} + \frac{1}{K_{bwt}} + \frac{1}{K_{bt}} + \frac{1}{K_{cws}} + \frac{1}{K_{cwc}}} \quad (8)$$

As a result, initial stiffnesses of the specimens T5-10, T5-15 and T5-20 are 9122 kNm/rad, 9780 kNm/rad and 10047 kNm/rad, respectively. These values proved to be a close approximation of the experimental results of 8962.9 kNm/rad, 9825.2 kNm/rad and 9708.5 kNm/rad, respectively.

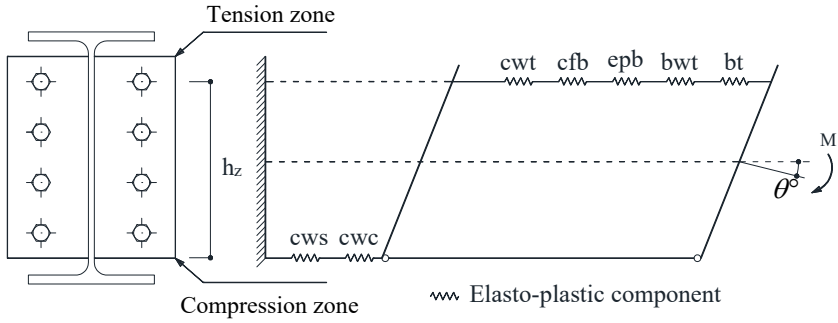


*Figure 15 - Characterization of the beam-to-column joints components*

### 4.3. Finite Element Model

In order to identify the effect of different parameters on the behavior of connection and to understand important local effects which are difficult to measure with sufficient accuracy, 3-D FE models which account for both geometrical and material nonlinearities were developed using the multi-purpose software package ABAQUS [22] (Figure 16). To simulate the projected test setup, the column was assumed to be pin connected at the ends and the lateral displacement of the column was prevented. A point load was applied to tip of the beam (To reference point, $X^{RP-1}$ in Figure 16) which is allowed to deflect horizontally in x-direction in the same manner as in the test. The beam was laterally supported to prevent any possibility of premature failure caused by lateral torsional buckling, as done in the tests.

For more reliable performance, the eight-node brick elements C3D8I with incompatible modes are used. Since having additional degree of freedoms, C3D8I has the capability to capture bending behavior better. Modelling the contact interaction; between the outer surfaces of the column flange and header end-plate and between the bolt head/nut and column flange/end-plate requires two different interaction properties. First one is 'hard contact' property and the second one is tangential behavior of the contact. The friction coefficient between the contact surfaces was taken as 0.30. Also, to get acceptable results under flexural moment, at least four layers were formed through the member thickness in element meshing. The optimal solution is to use a fine mesh in areas of high stress and a coarser mesh in the remaining areas. Hexagonal bolt heads and nuts are idealized as circular bolt heads and nuts

to simplify the model and washers are not modeled. Bolt holes are assumed to be 2 mm larger than the nominal bolt diameter ($d_b$=20 mm). The FE analyses of the model were done using two load steps. The first load step was to apply pretension forces to the bolts by applying displacements to the ends of the bolts. The prescribed bolt displacements corresponding to the axial force of 172 kN were calculated considering axial rigidity of the bolts. The second load step was employed to define cyclic loading path applied by imposing horizontal displacement to the free end of the beam. The available material test data was in the form of engineering stress and strain. Therefore, in the FE models the material data converted from engineering stress $\sigma_{eng}$ and strain $\varepsilon_{eng}$ to true stress $\sigma_{true}$ and strain $\varepsilon_{true}$ based on the following equation. The plasticity behavior in the joint was represented by the combined hardening assumption and Von Mises yield criterion. Figure 17 and Figure 18 display the deformed shape of the connections at the maximum target displacement (0.07, 0.08 and 0.02 rad rotation for specimens; T5-10, T5-15 and T5-20, respectively) and equivalent plastic strain distributions at the end of the FE analysis, respectively. Quantitative comparison in terms of bending strength and initial stiffness between the experimental and the simulated capacity is given in Figure 19. When the force applied at the end of the beam is a push force, the rotation is negative, and in case of pull force, the rotation is positive in the given moment-rotation curves.

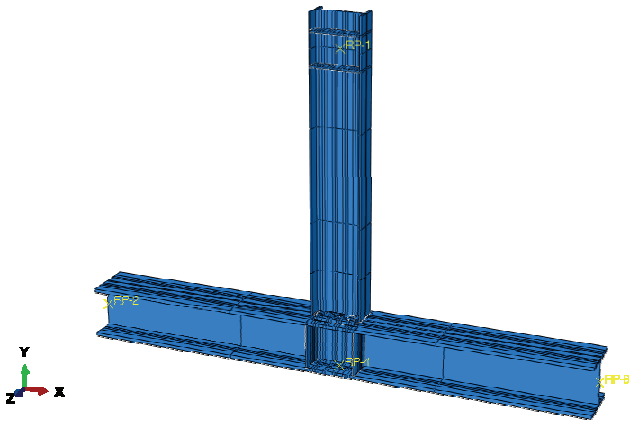


*Figure 16 - 3D FE model in ABAQUS (T5-15)*

$$\sigma_{true} = \sigma_{eng}(1+\varepsilon_{eng}); \qquad \varepsilon_{true} = \ln(1+\varepsilon_{eng}); \tag{9}$$

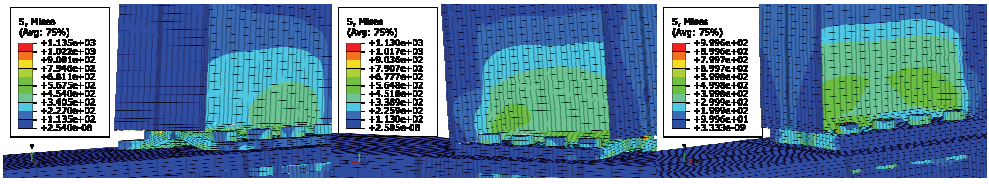

T5-10 T5-15 T5-20

*Figure 17 - Stress contour diagram and deformed shape of the specimens T5*

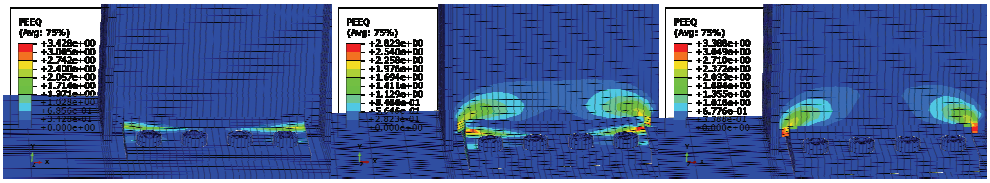

T5-10 T5-15 T5-20

*Figure 18 - Equivalent plastic strain distributions for the specimens T5*

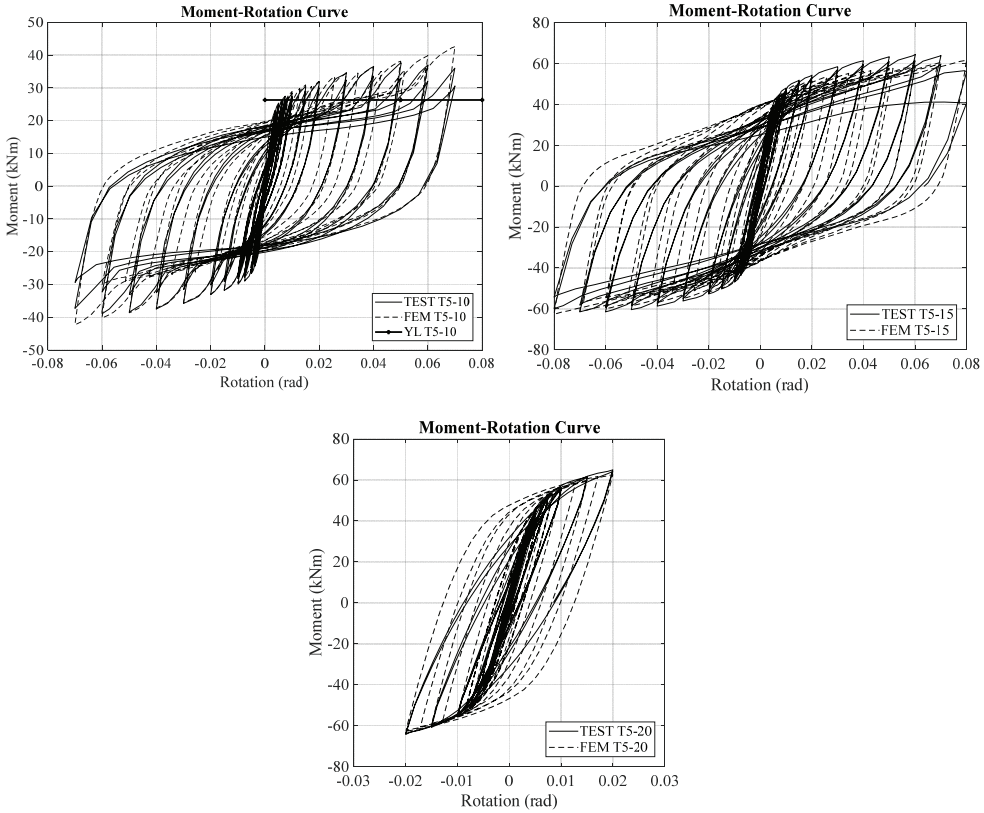


*Figure 19 - Comparison of the FE model and experimental test results*

It can easily be seen that, the achieved numerical results provided satisfactory agreement with the experimental test results. Although of the high accuracy of the results obtained, the main defect that the inability of FE model to reflect the stiffness deterioration in hysteretic loops as in the actual test behavior of the specimen T5-20, because the decrease in the stiffness due to yielding of the beam web at the connection could not exactly be represented in the FE model.

Equivalent plastic strain (PEEQ) index was employed to measure inelastic strain demands which are defined as the ratio of the equivalent plastic strain to the yield strain. PEEQ index for the end-plate of the specimen T5-20 is very less compared to the end-plates of the T5-10 and T5-15. In this basis, it can be stated that by use of thin or intermediate end-plates, the potential of ductile behavior provided by plastic hinge formation within the end-plate increases when compared to the connections with thick plates.

### 4.4. Recommendation to Determine the Critical Thickness

Based on the test results, the behavior of header-end plate connections is controlled by two limit states such as end-plate tearing and rupture of the beam web. According to this study, thin plate behavior should be adopted to ensure that the connections have enough rotation capacity under cyclic loading when more energy dissipation, as expected from a structural system, is intended during the earthquakes. A limit for header-end plate thickness, called critical thickness, should be defined to distinguish between thick and thin end plate behaviour. Critical thickness, t can be determined by ensuring that the flexural capacity of end-plate is smaller than that of the portion of the beam web which is effective in bending (Eq.10).

$$F_y \times t^2 \times Y_P \le F_{ybw} \times \frac{t_w \times h_{eff}^{\ 2}}{4} \qquad h_{eff} \cong 1.23 \times h \le d_b \tag{10}$$

$$t \le \sqrt{\frac{0.38 \times h^2 \times F_{ybw} \times t_w}{F_y \times Y_P}} \tag{11}$$

In which, $h_{eff}$ is the height of beam web which is assumed to be effective in bending based on the experimental and FE analyses results. $F_y$ and $F_{ybw}$ are actual yield stresses of end plate and beam web material, respectively. Thickness of end plate and of beam web are designated by t and $t_w$, respectively.

## 5. CONCLUSIONS

Sixteen specimens with different header end-plate configurations have been tested under cyclic loading in order to investigate the actual behavior of the header end-plate connections. Detailed FE analyses were also carried out to support the investigation. The parameters considered were the thickness of the end-plate, height of the end-plate and the number of bolt rows. According to the test results, the following conclusions can be drawn:

End-plate thickness has remarkable influence on the hysteretic behavior of the connections. The relatively thick end-plate connections (in this study, t=20mm) have higher flexural capacity. However, the energy dissipation capacities are limited due to premature rupture of the beam web that occurred when the Von Mises stresses reached to ultimate stress of the

beam web. Therefore, the increase in the end-plate thickness did not result in an increase in the connection ductility. The specimen having t=15 mm thick end-plate has stable hysteretic loops and energy was dissipated by flexural behavior of the end-plate and beam web. If the end-plate thickness is relatively thin the connection can be called nominally pinned. As long as the thinner and intermediate end-plates were employed, prying forces which increase the tensile stresses in the bolts became more pronounced.

Since the amount of end plate cross-sectional area in yielding along the folding lines is not significantly increased with increasing bolt rows, the effect of using more bolt rows on the behaviors of the connections with thin and intermediate end-plates has been found small. However, it is found that increasing the bolt row has no effect on the connections with thick plates because the failure mode of the connections has been controlled by the rupture of the beam web. Moreover, for the same thickness, increasing the depth of the connection has shown enhanced capacity for all types of the end-plate configurations. It is also noticed that the stiffness of the connection increases with the increase in the depth of the end-plate.

Tests on the header end-plate connections showed that the actions of the specimens with the end-plate thickness t=15 mm and t=20 mm (T3, T4, T5) met the Eurocode 3 criteria for partial strength and semi-rigid connections. However, the specimens with a thickness of the end-plate t=20 mm do not have sufficient rotational capacity.

Additionally, finite element model results have shown good correlation with the experimental results and were proven to simulate the behavior of the connection effectively. Yield moment capacity of the header end-plate connection attained by the tests and FE analysis under cyclic loading was compared by the results obtained based on the yield line theory.

A mechanical model was proposed for obtaining rotational stiffness of the connection. In the measurement of the rotational stiffness, the response of the beam web controlling the initial stiffness of the header end-plate connections must be considered in the mechanical model.

From the above discussion, it is suggested that for the header end-plate connections in bending, it is necessary to limit the thickness of the end-plate in order to avoid brittle failure of beam web and to obtain ductile joints by yielding of the end-plate in bending. This can be accomplished by designing the end plate whose flexural capacity is smaller than that of the effective cross-section in bending within the beam web. If it is so, such connections also would help to dissipate energy imposed by earthquakes.

**Symbols**

| | | |
|---|---|---|
| *bfc* | : | Beam flange and web in compression |
| *bt* | : | Bolts in tension |
| *bwt* | : | Beam web in tension |
| *cfb* | : | Column flange in bending |
| *cwc* | : | Column web in compression |
| *cws* | : | Column web in shear |

| | | |
|---|---|---|
| *cwt* | : | Column web in tension |
| $d_b$ | : | Beam web depth |
| $E$ | : | Modulus of Elasticity (N/mm$^2$) |
| *epb* | : | End-plate in bending |
| $F_u$ | : | Actual tensile strength of the material (N/mm$^2$) |
| $F_{ub}$ | : | Tensile strength of the bolt material (N/mm$^2$) |
| $F_y$ | : | Actual yield stress of the end-plate (N/mm$^2$) |
| $F_{yb}$ | : | Yield strength of the bolt material (N/mm$^2$) |
| $F_{ybw}$ | : | Actual yield stress of the beam web (N/mm$^2$) |
| $g, h_0, h_1, h_2, p_f, g_p, m_f, s$ | : | The distances that define the geometric properties of the end-plate |
| $h$ | : | Height of the end-plate |
| $h_{eff}$ | : | Height of the effective region within beam web in bending |
| $h_z$ | : | Lever arm of the end-plate |
| $I_b$ | : | Second moment of area of the connected member |
| $K_i$ | : | Stiffness coefficient representing *i* component |
| $l_{nx}$ , $l_{ny}$ | : | x and y components of the yield line length |
| $L_b$ | : | Span of the connected member |
| $m_p$ | : | Plastic moment strength of the plate per unit length |
| $M$ | : | External moment |
| $M_{max}$ | : | Maximum moment attained just before failure in the tests |
| $M_{pl}$ | : | Flexural strength capacity of end plate |
| *NP* | : | Nominally-Pinned |
| *PS* | | Partial-Strength |
| $R_i$ | : | Initial stiffness of the connection (Test results) |
| *SR* | : | Semi-Rigid |
| $S_{j,ini}$ | : | Initial stiffness of the connection according to Eurocode 3 |
| $t$ | : | End-plate thickness |
| $t_w$ | : | Beam web thickness. |
| $W_e$ | : | External work due to external moment |

| | | |
|---|---|---|
| $W_i$ | : | Total internal work stored in the yield lines |
| $Y_p$ | : | End-plate yield line mechanism parameter |
| $\varepsilon_{eng}$ | : | Engineering strain |
| $\varepsilon_{true}$ | : | True strain |
| $\theta$ | : | Applied virtual displacement |
| $\theta_b$ | : | Drift angle (relative displacement of beam divided by arm length) |
| $\theta_{max}$ | : | maximum connection rotation attained before failure |
| $\theta_{nx}$, $\theta_{ny}$ | : | x and y components of the relative rotation of the rigid plate segments |
| $\sigma_{eng}$ | : | Engineering stress |
| $\sigma_{true}$ | : | True stress |
| $\phi$ $(d_b)$ | : | Nominal bolt diameter (mm) |

**Acknowledgments**

This research was financially supported by Research Fund of the Istanbul Technical University. Project Number: 41573

**References**

[1] Chen, W., Kishi, N. and Komuro, M., Semi-Rigid Connections Handbook, J. Ross Publishing, U.S.A, 2011.

[2] Sherif, H.M.H., Hazem, M. R., M. Nabil, A. and Sherif, A. M., Experimental study of prequalified status of flush end plate connections, Journal of Housing and Building National Research Center, HBRC journal, 12, 25-32, 2014.

[3] Bing, G., Qiang, G. and Feng, L., Experimental Behavior of Stiffened and Unstiffened End-Plate Connections under Cyclic Loading, Journal of Structural Engineering ASCE, 132(9), 1352-1357, 2006.

[4] Ismail, R.E.S., Fahmy, A.S., Khalifa, A.M. and Mohamed, Y.M., Numerical study on ultimate behavior of bolted end-plate steel connections, Latin American Journal of Solids and Structures, 13(1), 1–22, 2016.

[5] Haghollahi, A. and Jannesar, R., Cyclic behavior of bolted extended end-plate moment connectionswith different sizes of end plate and bolt stiffened by a rib plate, Civil Engineering Journal, 4(1), 200-211, 2018.

[6] Fang, C., Yam, M.C.H., Lam, A.C.C. and Xie, L., Cyclic performance of extended end-plate connections equipped with shape memory alloy bolts, Journal of Constructional Steel Research, 94, 122–136, 2014.

[7] Dessouki, A.K., Youssef, A.H. and Ibrahim, M.M., Behavior of I-beam bolted extended end-plate moment connections, Ain Shams Engineering Journal, 4, 685-699, 2013.

[8] Adey, B.T., Extended End Plate Moment Connections under Cyclic Loading, Master's thesis, University of Alberta, Alberta, Canada, 1997.

[9] Johnstone, N.D., Walpole, W.R., Behavior of steel beam-column connections, made using bolted end plates, Bulletin of the New Zealand National Society for Earthquake Engineering, 15(2), 82-92, 1982.

[10] AISC, Load and Resistance Factor Design Specifications for Structural Steel Buildings, 2nd Edition, American Institute of Steel Construction; Chicago, USA, 1994.

[11] Kishi, N., Komuro, M. and Chen, W., Four-parameter power model for Moment-rotation curves of end-plate connections, ECCS/AISC Workshop Connections in Steel Structures V, (c), 99–110, Amsterdam, The Netherlands, 2004.

[12] Jaspart, J.P., Demonceau, J.F., European design recommendations for simple joints in steel structures, Journal of Constructional Steel Research, 64, 822-832, 2008.

[13] EN 1993-1-8:2005, Eurocode 3: Design of Steel Structures-part 1-8: Design of Joints, European Committee for Standardization; Brussels, Belgium, 2005.

[14] Sommer, W.H., Behaviour of Welded Header Plate Connections, Master's thesis, University of Toronto, Toronto, Canada, 1969.

[15] Aggarwal, A.K., Behaviour of flexible end plate beam-to-column joints, Journal of Constructional Steel Research, 16, 111–134, 1990.

[16] Pilgr, M., Experimental verification of actual behaviour of header plate connections, The Nordic Steel Construction Conference, 2009.

[17] AISC 341-16, Seismic provisions for structural steel buildings, American Institute of Steel Construction; Chicago, IL, USA, 2016.

[18] TCDCSS, Turkish code for design and construction of steel structures 2016, Ministry of Environment and Urbanization; Ankara, Turkey, 2016.

[19] Bruneau, M., Uang, C.M. and Sabelli, R., Ductile Design of Steel Structures, (2nd Edition), McGraw Hill, New York, USA, 2011.

[20] Murray, M. and Sumner, E.A., Design Guide 4 Extended End-Plate Moment Connections Seismic and Wind Applications, (2nd Edition), American Institute of Steel Construction, Chicago, 2003.

[21] Faella, C., Piluso, V. and Rizzano, G., Structural Semi-Rigid Connections, Design and Software. Boca Raton FL: CRC Press LLC, USA, 2000.

[22] ABAQUS 2017, Dassault Systemes Simulia Corp., Abaqus/CAE User's Guide, Providence, RI, USA.

*Teknik Dergi, 2021 11407-11422, Paper 639*

# Effect of the Gravel Zone Thickness Created in the Deep Well Test Simulation on the Operating Characteristics of the Pump and Head Loss

**Nuri ORHAN**[1]
**Osman ÖZBEK**[2]
**Ali Yavuz ŞEFLEK**[3]

## ABSTRACT

This study was conducted in a deep well simulator used for typical irrigation studies. In this work, the changes in the pump flow rate, drawdown, noise level, and pump pressures were analyzed for three different gravel zone thicknesses used in the well.

From the study, it was found that a high gravel zone thickness increased the well's drawdown levels during pumping. For drawdown values of 40, 45, 50 and 55 $m^3\ h^{-1}$, an increase in the gravel thickness by 10 cm increased these values by 2.92, 2.41, 2.38 and 2.37 times, respectively. When the gravel thickness was doubled (from 5 cm to 10 cm), the hydraulic conductivity decreased by about half and head loss doubled. As a result, gravel thickness directly affected the drawdown rate of the pump. It was shown that different drawdown values resulting due to different gravel thicknesses should be taken into consideration when placing the pump in a deep well.

**Keywords:** Irrigation deep well, gravel zone thickness, pumping, drawdown, head losses, hydraulic conductivity.

## 1. INTRODUCTION

Deep wells, which have an important place in agricultural irrigation, are dug by drilling and are of different diameters. In addition, these wells are equipped with closed or screen pipes.

Note:
- This paper was received on February 20, 2020 and accepted for publication by the Editorial Board on May 23, 2020.
- Discussions on this paper will be accepted by January 31, 2022.
- https://dx.doi.org/10.18400/tekderg.691948

1 University of Selcuk, Dep. of Agricultural Machinery and Technologies Engineering, Konya, Turkey - nuriorhan@selcuk.edu.tr - https://orcid.org/0000-0002-9987-1695

2 University of Selcuk, Dep. of Agricultural Machinery and Technologies Engineering, Konya, Turkey - ozbek@selcuk.edu.tr - https://orcid.org/0000-0003-0034-9387

3 University of Selcuk, Dep. of Agricultural Machinery and Technologies Engineering, Konya, Turkey - seflek@selcuk.edu.tr - https://orcid.org/0000-0003-1009-6635

The area around the screen pipe is filled with gravel material and increases the filtering efficiency.

In addition, to prevent the pumping of foreign materials such as sand or silt, the gravel is also placed to support the aquifer.

Size is important when choosing gravel material [1]. The suitable particle size of the gravel material as compared to the aquifer material substantially prevents sand from entering the well [2, 3].

It is necessary to have at least 35% of the porosity ratio of the gravel material used [4].

The thickness of the gravel placed in the well should generally be between 7.5 cm and 20 cm [1, 2, 5]. Sterrett [6] in their work stated that the gravel thickness should not exceed 12.5 cm and the optimum thickness should be 7.6 cm.

Driscoll [7] reported that the maximum gravel thickness should be about 20 cm. Using large quantities of gravel does not increase the efficiency of the well significantly and does not prevent more foreign materials (such as the sand from the sand formation) from entering the well [2].

The drawdown during pumping from irrigation wells is the sum of head losses caused by parameters such as aquifer loss, aquifer thickness, gravel pack, and screen [8]. In other words, the head losses due to the turbulent water flow around the filtered well are the predominant factor in the drawdown [9].

In this study, the effects of different gravel zone thicknesses on the well's water level during pumping decrease or drawdown (Δ), the pump noise level (G), the pump inlet (Pe), and the outlet pressure (Pb) were investigated. In addition, different drawdown levels observed for wells having different gravel thicknesses have been associated with head losses. The head losses caused by the pump and measurement pipes have been neglected.

## 2. MATERIALS AND METHODS

The study was carried out using the Deep Well Testing Simulator at the Selcuk University Faculty of Agriculture, Agricultural Machinery and Technology Engineering. The technical specifications of the equipment used in the test tower are given in Table 1.

*Table 1 - Some technical specifications of the measuring instruments*

| | |
|---|---|
| Pump | Nominal diameter 6"–7"–8", radial wheel, 4.5 mm terminal opening |
| Electric Machine | Suver, 380 V, 8.2 A, 50 Hz, 2869 1/min, 4.5 kW, shaft diameter :25 mm, water-cooler, 3×2.5mm$^2$ cable cross-section |
| Flow meter | S MAG 100 TİP, DN 80/H/316 electromagnetic flow meter, 220 V power supply, digital indicator Adjustable between 4–20 m/A plus. Operational flow-rates 1–280 m$^3$/h, operational pressure 16 bars. |
| Manometer | WİKA, 0–10 bar, 4–20 m/A output. |

| | |
|---|---|
| Level Sensor | Hydrotechnik model, 010 type/1.5 V |

*Table 1 - Some technical specifications of the measuring instruments (continue)*

| | |
|---|---|
| Temperature Sensor | Truck model, 10–24 VDC, –50...100 °C, 4–20mA output. |
| Noise Sensor | CT–2012 model, input 4 mA, DC 24V power supply output indicator. Sound level Transmitter model: TR-SLT1A4, Measurement range:30–80 dB, 50–100 dB, 80–130 dB, output 4–20 mA, 90–260 ACV 50Hz/60Hz, Operation temperature 0–50 °C. |
| Computer | Asus Intel core i7. |

In the experiments, approximately 2 $m^3$ clean and washed gravel was used to fill different gravel casing pipes. The gravel used is shown in Figure 1.

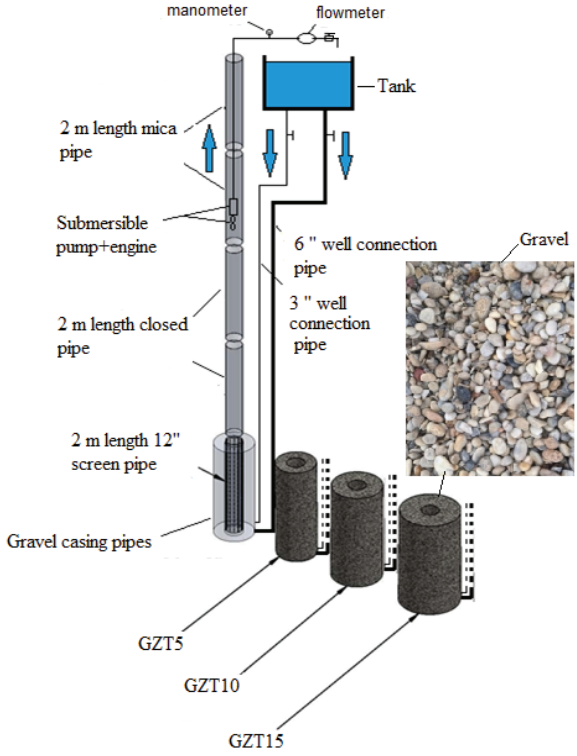


*Figure 1 - Well equipment and working principle for gravel zone thickness*

The average of some of the physical properties of the gravel, determined from the measurements made on 100 gravel samples taken from the gravel pile, are shown in Table 2 [10, 11].

From Table 2, it can be seen that 76% of the gravel used in the experiments is between 7–15 mm. Furthermore, the porosity of the gravel using in the well is over 35%.

The inlet pressure (Pe) of the pump was measured with a U-type differential pressure gauge placed at the suction nozzle. For the U-type differential pressure gauge, a 2 m long and 6 mm diameter transparent hose and 200 g mercury were used.

In the experiments, a 4 m long-closed pipe, 4 m long mica pipe and a 2 m long and 12" diameter vertical oblong filter were used. This combination was kept constant in all gravel experiments. The gravel was filled around the screen pipe with the help of specially prepared gravel casing pipes.

Different thicknesses of gravel were piled in each well and the wells were labeled GZT5, GZT10, and GZT15, corresponding to gravel zone thicknesses of 5 cm, 10 cm, and 15 cm, respectively. In this way, three different well types (GZT5, GZT10, GZT15) were formed.

Water inlet to the deep well constructed for the experiments was provided from the tank consisting of 6" and 3" diameter pipes. On establishing these connections, the deep well test tower works according to the compound containers method (Figure 1). The measurement and calculation of the pump's operating characteristics were made according to EN ISO 9906 and the noise levels were measured according to EN ISO 3740 [12, 13].

*Table 2 - Some physical properties of gravel used in experiments*

| **Physical property** | **Average value** |
|---|---|
| Bulk density (kg $dm^{-3}$) | 1.54 |
| Density (kg $dm^{-3}$) | 2.75 |
| Porosity (%) | 44 |
| Thickness (mm) | 14.3 |
| Length (mm) | 19.6 |
| Thickness (mm) | 9.1 |
| Geometric diameter (mm) | 13.5 |
| Globularness (%) | 70 |
| Natural agglomeration angle (°) | 22.76 |
| Metal-gravel static friction coefficient (-) | 41.9 |
| Frequency distribution of particles in terms of geometric diameter | |
| 7.68 mm (min.) –10.00 mm (%) | 8 |
| 10.01 mm –13.50 mm (%) | 46 |
| 13.51 mm –15.00 mm (%) | 22 |
| 15.01 mm –18.00 mm (%) | 12 |
| 18.01 mm–21.94 mm (max.) (%) | 12 |

The noise level was measured by placing the noise measurement device from the tower control center platform approximately 1 m below the space between the pump column and the plexiglass pipe [14-16].

The hydraulic conductivity (K) of the different well types was calculated according to the Darcy law (Darcy, 1856).

In each of the well types having different gravel zone thicknesses, with the submersible pump (D) operating at the optimum operating speed, for five different flow ranges (40, 45, 50, 55, 60 $m^3\ h^{-1}$) the drawdown (Δ)/submergence (S), pump noise level (G), pump outlet pressure (Pb), pump inlet pressure (Pe), ambient temperature ($T_1$) and water temperature ($T_2$) values were measured (Figure 2). After the pump was run at a particular flow rate, the initial values were recorded and then the other flow values were attempted.

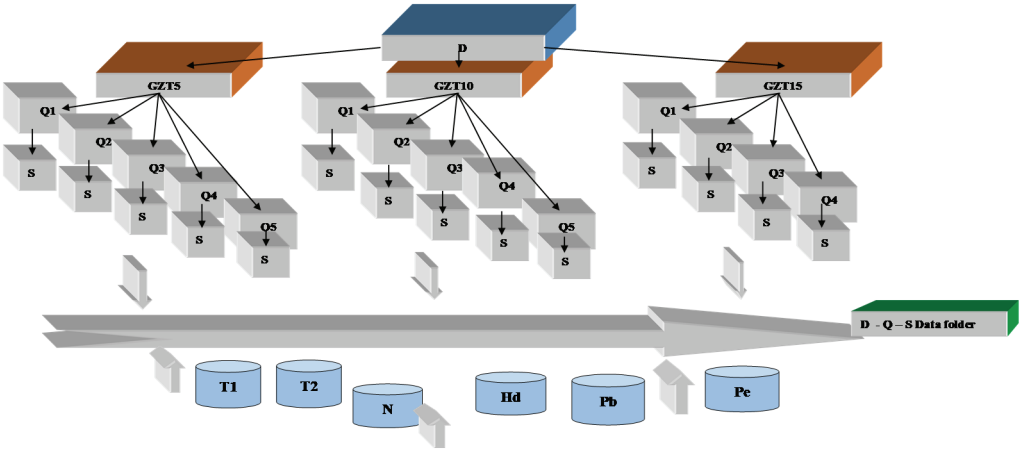


*Figure 2 - Trial plan*

Software and automation systems were made to record the measured data. The information received from the sensors located in the system was wirelessly transferred to the central computer via a data acquisition card and a Bluetooth module. The information stored in the central computer for the required range was recorded with a suitable name that was given by the operator via the software interface. Record action was set to record one measurement per second. After the pump entered the working regime, the record-process was started and 50 data recordings were taken from one sensor.

The experiments were carried out at a plunge depth (constant hydraulic head) of 188 cm. The measurement of the drawdown (Δ) was made by the level meter.

## 3. RESULTS AND DISCUSSION

During the experiments, the average air and water temperatures were 15 °C and 12 °C, respectively.

The experiments were started under a constant hydraulic head of 188 cm and at a level of 89 cm of static water.

### 3.1. Effect of the Gravel Zone Thickness on the Drawdown

The results of the least square difference (LSD) test and the averages of the drawdown levels corresponding to the different thickness of the gravel zone in each well type are given in Table 3.

*Table 3 - The different gravel zone thickness and values drawdowns (cm)*

| Q | GZT5 | GZT10 | GZT15 | Q |
|---|---|---|---|---|
| **40** | $41.00^{k}$ | $65.67^{h}$ | $94.02^{e}$ | $66.91^{d}$ |
| **45** | $49.67^{j}$ | $82.57^{f}$ | $119.97^{c}$ | $84.07^{c}$ |
| **50** | $62.17^{i}$ | $100.03^{d}$ | $148.02^{b}$ | $103.41^{b}$ |
| **55** | $74.00^{g}$ | $119.13^{c}$ | $176.03^{a}$ | $123.05^{a}$ |
| | | **LSD=2.284** | | **LSD=1.318** |
| **GZT** | $56.71^{c}$ | $91.85^{b}$ | $134.52^{a}$ | |
| | | **LSD=1.142** | | |

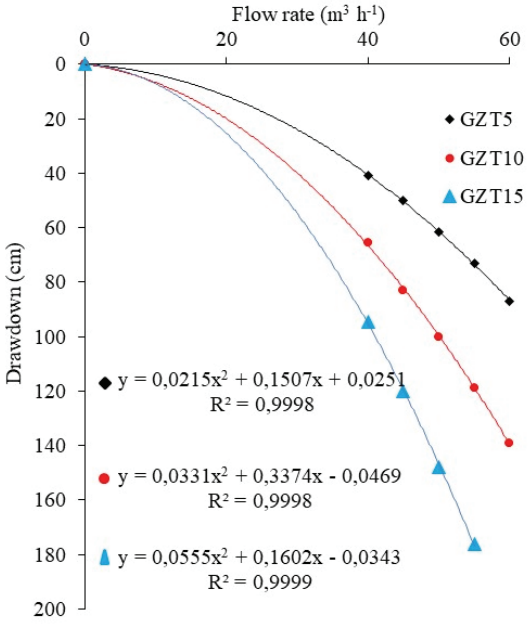


*Figure 3 - The relationship between gravel zone thickness and drawdown*

The data could not be retrieved due to too much drawdown in the 60 $m^3 h^{-1}$ flow rate in the well type GZT15. Thus, it has not been included in Table 3.

The values of the drawdown in wells having different gravel zone thicknesses are plotted in Figure 3.

The highest drawdown measured was 134.52 cm in the GZT15 well type with the least drawdown of 56.71 cm in GZT5 well type. The measured drawdown values for constant flow rates were found to be 66.91 cm at a flow rate of 40 $m^3 h^{-1}$, 84.07 cm at a flow rate of 45 $m^3 h^{-1}$, 103.41 cm at a flow rate of 50 $m^3 h^{-1}$ and 123.05 cm at a flow rate of 55 $m^3 h^{-1}$. It can be seen from Table 3 that there is a statistically significant difference between the values. On determining the variance of the drawdown values, the flow, gravel zone thickness, and the interaction of these two parameters were found to be statistically different ($P<0.01$). As the flow rate in all the well types increased, the drawdown level in them increased as well. The $R^2$ values corresponding to this increase is very high. From Fig. 3, it can be clearly seen that increasing the gravel thickness at the same flow rate increases the drawdown levels.

### 3.2. Hydraulic Conductivity of the Different Well Types, Hydraulic Conductivity of the Gravel, and Reynolds Number

The hydraulic conductivity of the gravel material used and the different well types constructed were calculated separately. The hydraulic conductivity of gravel was calculated using the Hazen–Williams (1892–1911) equation. This equation is based on the relationship between the grain size and permeability and is given by Equation (1).

$$k = C.d_{10}^{2}\,(0.7 + 0.03T)$$
$$C = 400 + 40\,(n - 26) \quad (1)$$

where k is permeability (m $s^{-1}$), $d_{10}$ is the effective grain size, which is thinner by ten percent by weight (mm), T is the temperature of water (°C), C is the Hazen-Williams coefficient calculated according to porosity, and n is the porosity. The $d_{10}$ value of the gravel used in the experiments was found to be 12 mm. The average water temperature was 14 °C during the experiments. The permeability of the gravel was calculated to be $1.8 \times 10^{-1}$ m $s^{-1}$. The hydraulic permeability coefficient of the different well types was calculated according to the Darcy law Eqn. (2) given below. According to the Darcy law, the flow rate (Q) of the liquid passing through a medium is directly proportional to the cross-sectional area (A) perpendicular to the flow, the head loss (Δh) and the coefficient of hydraulic permeability coefficient (K) and is inversely proportional to the distance traveled by the liquid (ΔL).

$$Q = A.K.i$$
$$i = \frac{\Delta h}{\Delta L} \quad (2)$$

The values of the flow rate obtained for the different well types by applying Darcy's law are plotted in Fig. 4. The hydraulic permeability coefficient of the different well types calculated from Darcy's law has also been indicated here.

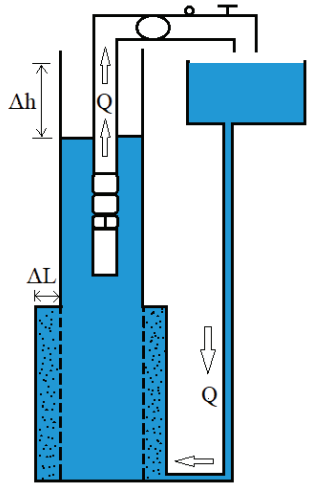


*Figure 4 - Method of application of Darcy's law in well types*

The relation between hydraulic permeability coefficient (K) and the drawdown levels is shown in Fig. 5.

An increase in the gravel zone thickness was found to reduce the hydraulic permeability coefficient at a constant flow rate. Houben *et al.,* (Houben and Hauschild [17]) reported that the lower the hydraulic conductivity, the higher is the drawdown. The average hydraulic permeability coefficient values corresponding to the GZT5, GZT10, and GZT15 well types were calculated to be 0.012, 0.0036 and 0.0016, respectively. This difference in the hydraulic permeability coefficient values was found to be due to the different gravel zone thicknesses in the wells. The flow regime can be determined by calculating the Reynolds number, which is determined using the following expression [4, 18, 19]:

$$\mathrm{Re} = \frac{\rho . v . d}{\mu} \tag{3}$$

where;

ρ = Density of water (at 14 °C, it is 999.85 kg $m^{-3}$),

v = water inlet speed (m $s^{-1}$),

μ = dynamic viscosity of water (at 14 °C, it is 0.0013097 kg $m^{-1}$ $s^{-1}$),

d = Characteristic length (m); the average gravel grain size was taken as the characteristic length here.

If Re ≤ 10 in porous environments, the flow is considered to be laminar [18]. If Re > 100, the flow is assumed to be turbulent [18, 20]. In this study, the Reynolds number in all the flow values ranged between 1100 and 1800. A turbulent flow was detected in the gravel region.

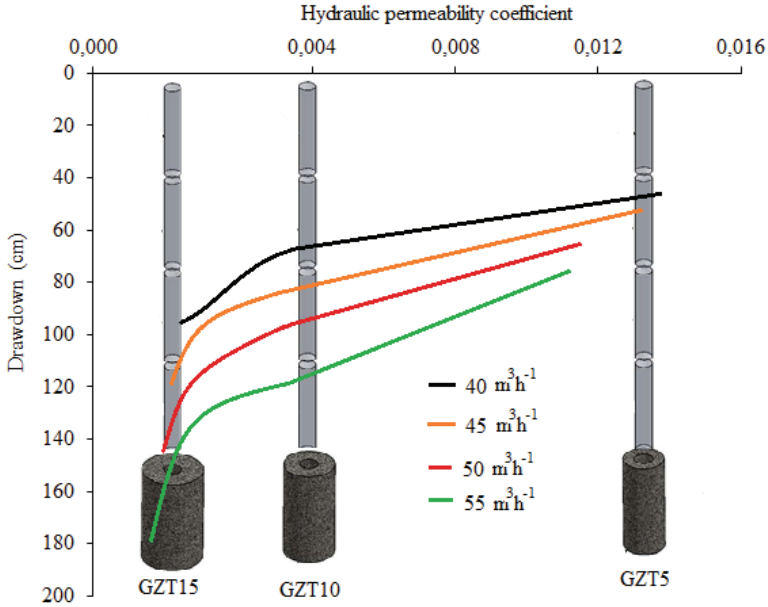


*Figure 5 - The hydraulic permeability coefficient and drawdown relation of different well types*

### 3.3. Head Loss for Different Gravel Thicknesses

Many researchers have stated that the drawdown in the wells corresponds to head losses [8, 20-22]. The reason for the different drawdown at the same flow rate and different gravel zone thickness in the well is caused by the head loss. These head losses are expressed as the sum of laminar and turbulent head losses. The turbulent loss is limited to the well filter area [20, 23].

For the three different well types, the head loss due to a change in the gravel thickness by 5 cm and 10 cm was considered. The head loss due to an increase in the gravel thickness by 5 cm was obtained from the drawdown differences in the GZT5 and GZT10 well types, while the head loss due to an increase in the gravel thickness by 10 cm was obtained from the drawdown differences in the GZT5 and GZT15 well types.

As a result, since all components of each well type are fixed except for the gravel thickness, the only reason the different drawdown is obtained is due to the different gravel thickness.

As a function of the flow rate, the head losses for an increase in the gravel thickness by 5 cm and 10 cm are plotted in Fig. 6.

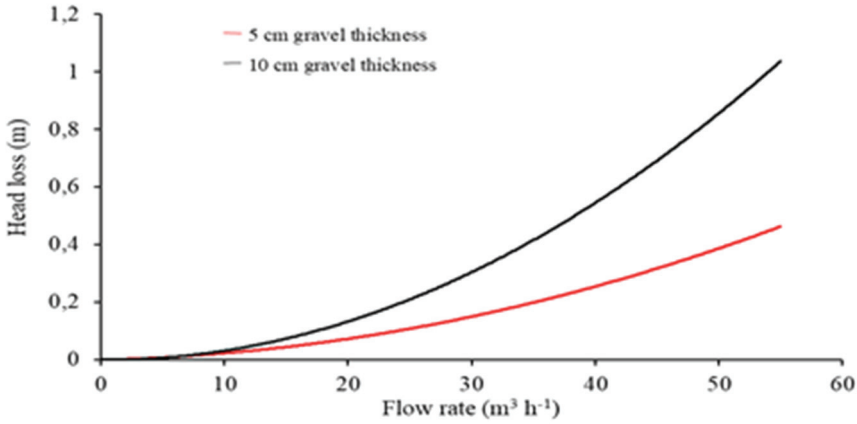


*Figure 6 - Relationship between gravel thickness increase and head loss*

For each flow rate, an increase in the gravel thickness by 10 cm caused a larger head loss as compared to the case where the gravel thickness was increased by 5 cm (Fig. 6). At a flow rate of 55 $m^3 h^{-1}$, a 0.46 m head loss corresponding to an increase in the gravel thickness by 5 cm, was found to increase to 1.03 m for an increase in the gravel thickness by 10 cm.

We explain the increased head loss with increasing gravel thickness by the distance traveled by water from the gravel to the filter under water. The head loss increases by increasing this distance, which can also be understood from the Darcy-Weisbach [24] turbulent flow equation.

Houben [20] has estimated that different gravel thicknesses cause different head losses in the case of low hydraulic conductivity wells. In his study, Byung-Woo [21] found different drawdown values for the same flow rate for the case of gravel and gravel + granular screen zones combinations. The addition of gravel to the well is shown to increase the drawdown value.

*Table 4 - The drawdown values per unit cm of the gravel zone well types*

| Q ($m^3 h^{-1}$) | GZT5-GZT10 Δ (m $cm^{-1}$) | GZT5-GZT15 Δ (m $cm^{-1}$) | Average Δ (m $cm^{-1}$) |
|---|---|---|---|
| 40 | 0.049 | 0.054 | 0.051 |
| 45 | 0.066 | 0.07 | 0.068 |
| 50 | 0.077 | 0.087 | 0.082 |
| 55 | 0.092 | 0.103 | 0.098 |
| 60 | 0.104 | - | 0.104 |

The head loss per unit gravel thickness is given in Table 4. The unit gravel width was calculated by dividing the head losses due to the increasing gravel thickness in the GZT5, GZT10, and GZT15 well types by the difference of the gravel thickness values used in these wells.

For the GZT5-GZT10 and GZT5-GZT15 well types, the head loss values per unit cm are close to each other.

The average rates show an increase of 0.098 m $cm^{-1}$ for a flow rate of 55 $m^3$ $h^{-1}$ while for a flow rate of 40 $m^3$ $h^{-1}$, it is 0.051 m $cm^{-1}$. The values of the average head loss per unit cm in the different well types are plotted in Fig. 7. It can be seen from the figure that the head loss per unit of gravel thickness increases as the flow rate increases. This is consistent with the work of Houben [8], where a similar observation was found.

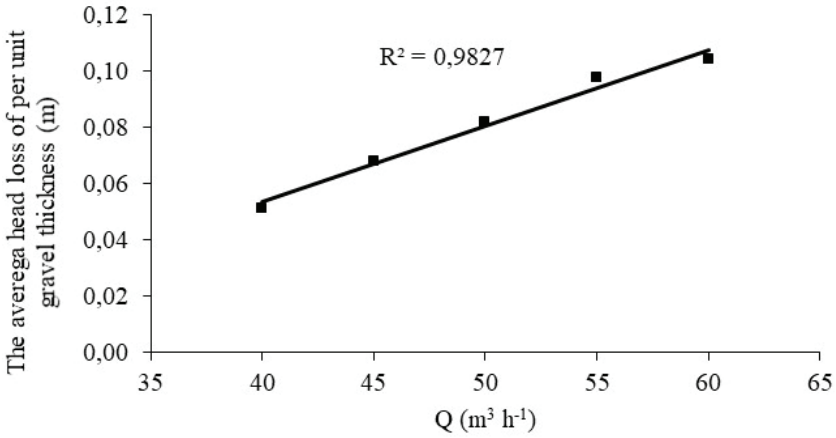


*Figure 7 - Average unit gravel thickness per head loss and flow change*

### 3.4. The Effect of the Gravel Zone Thickness on the Noise Level

The effect of different gravel zone thicknesses on the noise level of the pump for different flow values is illustrated in Fig. 8a.

The figure shows that an increase in the gravel zone thickness does not have a significant effect on the noise level. In a previous report, Çalışır, et al. [25] stated that the noise level of the pump decreased for the flow rate corresponding to the optimum efficiency point of the pump, which in their study was found to be 48–52 $m^3$ $h^{-1}$. The optimum efficiency point of the pump we used in the study was measured as 50 $m^3$ $h^{-1}$. At the optimum efficiency point flow rate (50 $m^3$ $h^{-1}$), increasing the gravel zone thickness led to an increase in the noise level (Fig. 8a).

The average noise levels in the pump fixed in the GZT5, GZT10 and GZT15 well types for flow rates of 40,45, 50 and 55 $m^3$ $h^{-1}$ were measured to be 74.5, 75.1, 72.7 and 76.3 dB, respectively. The minimum noise level was obtained at the optimum efficiency point of the pump.

The average of the noise levels obtained in the GZT5, GZT10, and GZT15 well types for all flow rates were found to be 73.05, 75.30, and 76.68 dB, respectively. The average of the noise levels obtained at different flow rates of the pump increased as the gravel thickness increased.

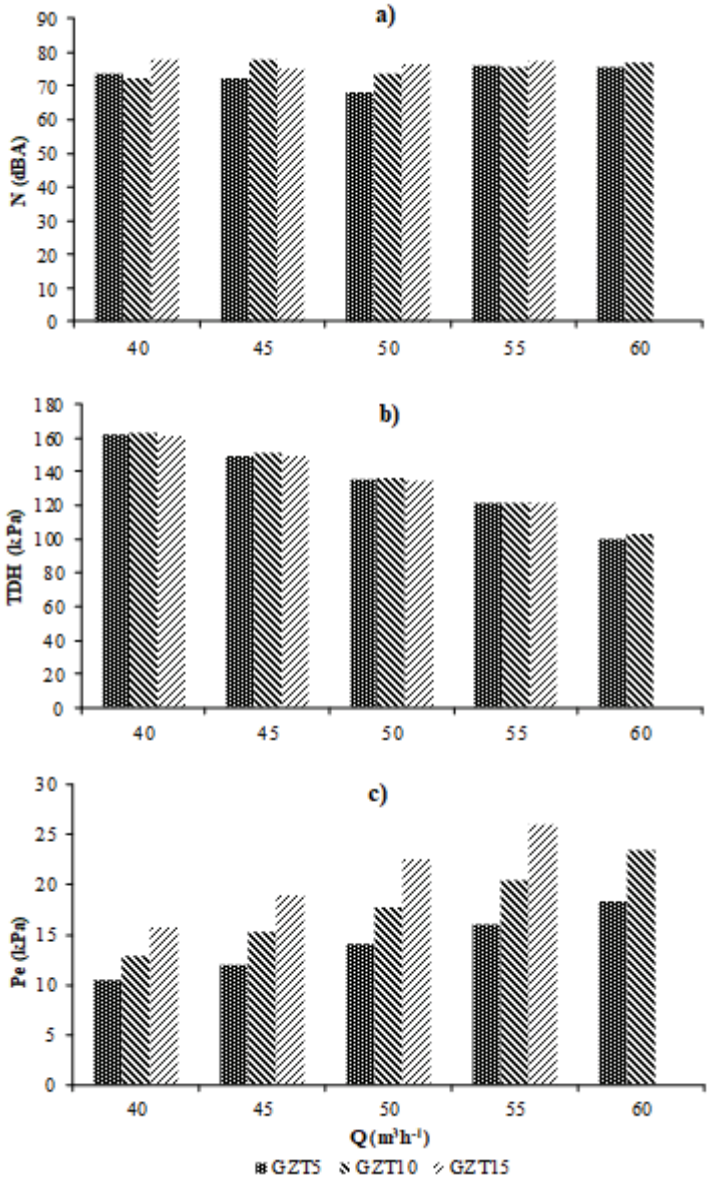


*Figure 8 - Difference between gravel zone thickness, flow rate, and noise*

### 3.5. Effect of the Gravel Zone Thickness on the Total Dynamic Head (TDH) and TDH Components of the Pump

The effect of the gravel zone thickness on the TDH developed by the pump is shown in Fig. 8b.

From the figure, it is seen that as the flow rate in the three well types increases, the TDH rates are seen to decrease. In the case of constant flow rates, the effect of gravel zone thickness was not observed.

The numerical values of TDH and TDH components as a function of the different gravel zone thicknesses are given in Table 5.

*Table 5 - TDH (total dynamic head) and TDH components in different gravel zone thicknesses and flow rates*

| | Q ($m^3 h^{-1}$) | $P_b$ (kPa) | $H_d$ (m) | $V^2/2g$ (m) | TDH (kPa) |
|---|---|---|---|---|---|
| **GZT5** | 40.1 | 146.5 | 1.30 | 0.27 | 161.9 |
| | 45.0 | 132.4 | 1.39 | 0.34 | 149.4 |
| | 50.1 | 118.7 | 1.51 | 0.43 | 138.1 |
| | 55.1 | 100.4 | 1.63 | 0.52 | 121.4 |
| | 60.1 | 76.6 | 1.76 | 0.61 | 99.9 |
| **GZT10** | 40.2 | 144.8 | 1.55 | 0.27 | 162.7 |
| | 45.1 | 130.3 | 1.72 | 0.35 | 150.6 |
| | 50.2 | 113.2 | 1.89 | 0.43 | 136.4 |
| | 54.9 | 94.5 | 2.08 | 0.52 | 120.2 |
| | 60.0 | 74.3 | 2.28 | 0.62 | 102.7 |
| **GZT15** | 40.0 | 140.8 | 1.84 | 0.27 | 161.5 |
| | 44.9 | 125.2 | 2.09 | 0.35 | 149.1 |
| | 50.1 | 106.8 | 2.37 | 0.43 | 134.2 |
| | 55.0 | 90.5 | 2.65 | 0.52 | 121.5 |

From the table, it is observed that as the gravel zone thickness is increased while the flow rate is constant, the TDH and velocity (or the kinetic energy) do not change, the pump outlet pressure (Pb) decreases and the dynamic height (Hd) rate increases. The reason for these changes is the drawdown.

Also, on examining the effect of the gravel zone thickness and flow rate on the inlet pressure, the pump inlet pressure rates show an increase both as the gravel zone thickness increases for a constant flow rate as well as when the flow rate increases for a constant gravel zone thickness (Fig. 8c).

## 4. CONCLUSION

The arrangement of the gravel zone in the well design is one of the effective parameters pertaining to head losses while pumping from a well. During the pumping process, different gravel zone thicknesses were observed giving rise to different head losses occurring at the well inlet. These head losses caused different drawdown for the same flow rate of the pump.

A 10 cm increase in the gravel thickness for flow rates of 40, 45, 50 and 55 $m^3h^{-1}$ caused an increase by 2.92, 2.41, 2.38 and 2.37 times, respectively in the drawdown values. The difference between the average values of the drawdown rates has been found to be statistically significant. Furthermore, the drawdown rates per unit gravel thickness were found to increase with increasing flow rate.

Hydraulic permeability coefficient was found to decrease in well types having higher gravel thickness. The average head loss per unit of gravel thickness for all flow rates was found to be 0.0805 m $cm^{-1}$. When the gravel thickness doubled (from 5 cm to 10 cm), the hydraulic conductivity decreased by about half and the head loss doubled.

An increase in the gravel thickness resulted in an increase in the average noise levels at different flow rates of the pump. As the increase in gravel thickness affects the drawdown, the pump has a reduced outlet pressure rate and requires an increased inlet pressure rate. However, the total dynamic head of the pump does not change depending on the gravel thickness.

As a result, different gravel thicknesses directly affect the drawdown rate of the pump. The dependence of the head losses on the gravel zone thickness, which is one of the important factors in a well design, has emerged from the experiments in this work with the deep well testing unit. In addition, well design analyses were performed for the gravel type used in the experiments.

Firms designing wells and Engineers working in the company can benefit from the results of this study. Experts who want to make use of this context can choose the pump by examining the effects of gravel zone thickness on the well design and the reduction in the well.

**Symbols**

$\rho$ = Water density (kg $m^{-3}$)

$\mu$ = dynamic viscosity (kg $m^{-1}$ $s^{-1}$)

$\Delta$ = Drawdown (cm);

Hd = Dynamic head (mm);

G = Pump noise level (dBA);

GZT5 = 5 cm gravel zone thicknesses

GZT10= 10 cm gravel zone thicknesses

GZT15= 15 cm gravel zone thicknesses

K = Hydraulic conductivity (m $s^{-1}$);

i = hydraulic gradient (-)

Re = Reynolds number (-)

Pb = Output pressure (kPa);

Pe = Inlet pressure (kPa);

Q = Flow rate ($m^3$ $h^{-1}$);

S = Submergence (mm);

v = water inlet speed (m $s^{-1}$)

TDH = Total dynamic head (kPa);

T1 = Ambient temperature (°C);

T2 = Water temperature (°C);

## References

[1] K. Rafferty, "Specification of water wells," American Society of Heating, Refrigerating and Air-Conditioning Engineers Transactions, vol. 107(2), 2001.

[2] B. Boman, S. Shukla, and J. Hardin, "Design and construction of screened wells for agricultural irrigation systems," EDIS University of Florida, 2003.

[3] Çebi T, "Design Techniques in Drinking and Potable Water Supply Wells in Groundwater.," Journal of Geological Engineering, vol. 44-45, 7, 1994 p. 70-81.

[4] G. J. Houben, J. Wachenhausen, and C. R. G. Morel, "Effects of ageing on the hydraulics of water wells and the influence of non-Darcy flow," Hydrogeology Journal, vol. 26, no. 4, 2018, p. 1285-1294.

[5] K. Akpınar, "Su Kuyularının Açılması ve İşletilmesi, Sorunları ve Çözümleri" ISBN 975-94033-0-7. Ankara, 1999, p.1-695

[6] R. J. Sterrett, "Groundwater and wells, 3rd edn. Johnson Screens, New Brighton, MN.," 2007.

[7] F. G. Driscoll, "Groundwater and wells, 2nd edn. Johnson Division, St. Paul, MN," 1986.

[8] G. J. Houben, "Hydraulics of water wells—head losses of individual components," Hydrogeology journal, vol. 23, no. 8, 2015, p. 1659-1675.

[9] V. Batu, Aquifer hydraulics: a comprehensive guide to hydrogeologic data analysis. John Wiley & Sons, 1998.

[10] TS EN 1097-3, Tests for mechanical and physical properties of aggregates- Part 3: Determination of loose bulk density and voids, Turkish Standardization Institute, Ankara, 1999.

[11] TS EN 933-3, Experiments for Geometric Properties of Aggregates.,Turkish Standardization Institute. Ankara., 2004.

[12] TS EN ISO 9906, Rotodynamic Pumps-Hydraulic Performance Acceptance Tests, Class 1 and Class 2, Turkish Standardization Institute, Ankara, 2012.

[13] TS 11146/T1, Submersible Pumps for Clean Water, Turkish Standardization Institute, Ankara, 2016.

[14] M. Binama, A. Muhirwa, and E. Bisengimana, "Cavitation effects in centrifugal pumps-A review," Binama Maxime. Int. Journal of Engineering Research and Applications, vol. 6, no. 5, 2016, p. 52-63.

[15] M. Čdina, "Detection of cavitation phenomenon in a centrifugal pump using audible sound," Mechanical systems and signal processing, vol. 17, no. 6, 2003, p. 1335-1347.

[16] M. Čudina and J. Prezelj, "Detection of cavitation in operation of kinetic pumps. Use of discrete frequency tone in audible spectra," Applied Acoustics, vol. 70, no. 4, 2009, p. 540-546.

[17] G. J. Houben and S. Hauschild, "Numerical Modeling of the Near-Field Hydraulics of Water Wells," Groundwater, vol. 49, no. 4, 2011, p. 570-575.

[18] J. Bear, Hydraulics of Groundwater. New York: Dover Publication 2007.

[19] F. Tügel, G. J. Houben, and T. Graf, "How appropriate is the Thiem equation for describing groundwater flow to actual wells?," Hydrogeology Journal, vol. 24, no. 8, 2016, p. 2093-2101.

[20] G. J. Houben, "Hydraulics of water wells—flow laws and influence of geometry," Hydrogeology Journal, vol. 23, no. 8, 2015, p. 1633-1657.

[21] K. Byung-Woo, "Effect of Filter Designs on Hydraulic Properties and Well Efficiency," Groundwater S1 (52), 2014, p. 175-185.

[22] M. Janssen Lok, "Analysis and improvement of well capacities in fine grained sand aquifers," 2013.

[23] D. E. Williams, "Modern techniques in well design," Journal-American Water Works Association, vol. 77, no. 9,1985, p. 68-74.

[24] J. L. Weisbach, Lehrbuch der ingenieur-und maschinen-mechanik (Textbook of engineering and machine mechanics). Vieweg, 1863.

[25] S. Çalışır, T. Eryılmaz, H. Hacıseferoğulları, and H. O. Mengeş, "Noise in Centrifugal Pumps," Journal of Agricultural Machinery Science, vol. 3, no. 2, 2007, p. 105-110.

# *DISCUSSION*

*Teknik Dergi, 2021 11423-11427, Paper 640,* ***Discussion***

# Evaluation of Two Vegetation Indices (NDVI and VCI) Over Asi Basin in Turkey[†]

**Discussion by A. Ünal ŞORMAN**[*]

The paper published by the authors in Teknik Dergi presents an agricultural drought analysis using vegetation indices by considering the historical drought archives and applying them to the Asi Basin. The authors apply the NDVI and VCI indices, which have gained importance in recent literature, by using the remote sensing method. The work concludes that the NDVI index was more appropriate for the Asi Basin than the VCI index to monitor drought.

**Aims of discussion:**

This discussion serves as a commentary for future research with similar objectives. As an illustrative purpose, results from a preliminary study are presented to highlight alternative approaches to strengthen the vegetation index calculation under drought conditions.

Broadly, suggestions emphasize that future studies should:

- Indicate the importance of selecting the derived VCI parameter compared to the NDVI resulting from MODIS/ NOAA.
- Highlight the link between the vegetation condition parameters to the meteorological drought indices (SPEI; SPI) for the specific threshold values (extreme, severe and moderate).
- Support the use of VCI or NDVI with satellite data on soil moisture content using ERA5-Interim values to detect and confirm moisture content in the soil, dry/wet.

Additionally, VCI and ERA5 are also discussed in detail in the last section – in overall discussions.

Literature also suggests that the NDVI satellite data may need some simple noise correction (see references [1-3]). Further research also recommends coupling the findings of VCI and ERA5 to represent and include agricultural products (yields) to manage crops and water.

**Illustrative Example for Central Anatolian provinces in Turkey:**

To illustrate this point, the commenting author would like to reference some early research results as a case study (unpublished). The presented Figures 1 and 2 indicate the comparison of the meteorological drought indices for Central Anatolian provinces in Turkey.

---

[†] Mehmet DIKICI, Murat AKSEL, Teknik Dergi Volume 32, Issue 4, July 2021. 10995-11011

* Middle East Technical University, Department of Civil Engineering, Ankara, Turkey
sorman@metu.edu.tr

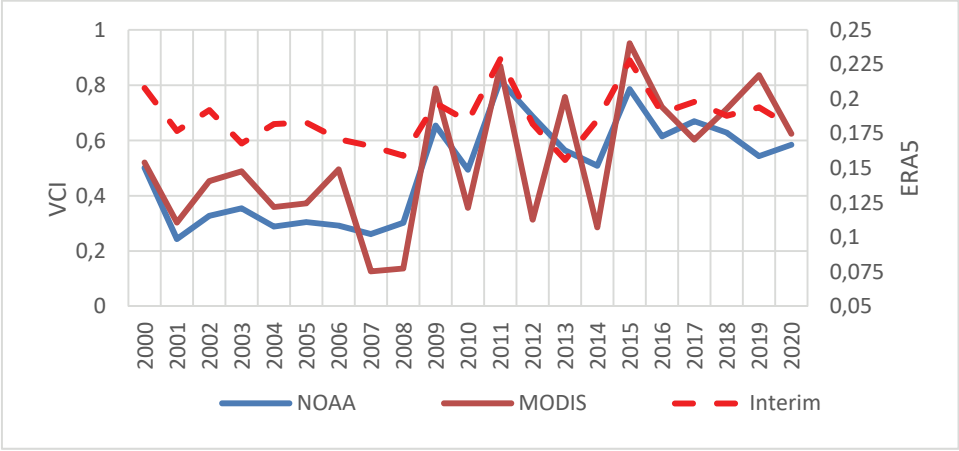


*Figure 1 - Comparison of VCI (MODIS), VCI (NOAA) & SM (ERA5)*

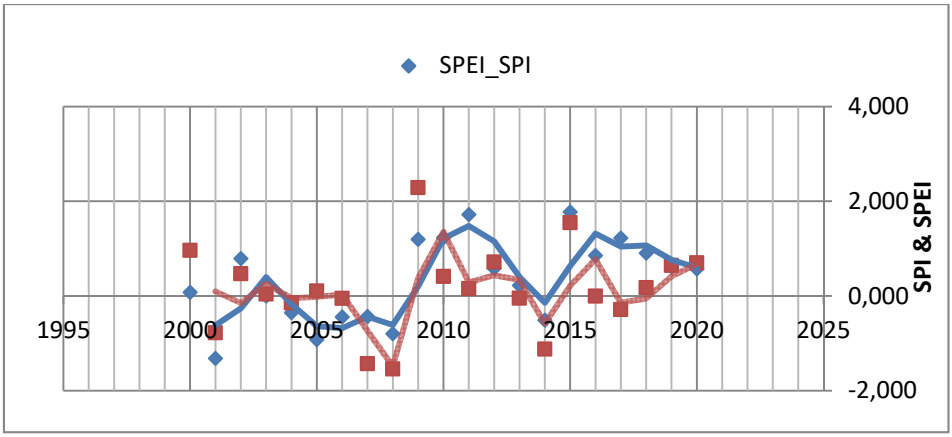


*Figure 2. Comparison of Drought Indices (SPI & SPEI)*

The graphical comparison in Figure 1 illustrates data of VCI's using either (MODIS indicated as VCI average) and (NOAA as VCI_3M) satellite images for three months (June, July and August covering the period 2000-2021) and are compared with the soil moisture content values of ERA5-Interim (ERA 3M) for the same period.

Figure 2 presents the meteoroidal drought index variations, namely Standardized Precipitation Index (SPI) and Standardized Precipitation Index (SPEI), to enhance findings on VCI and agricultural drought yield.

Table 1 indicates the correlation coefficients between meteorological drought parameters (SPEI-SPI) and among NOAA (VCI-3M) with MODIS (VCI basin averages) are 0.638, 0.744 respectively.

*Table 1 - Data on the meteorological drought indices of SPEI, SPI, and the vegetation condition indices VCI derived from NOAA and MODIS for Central Anatolia in Turkey between the period 2000-2020.*

| | **Meteorological Drought Indices** | | **Satellite Images NDVI calculations** | | **Soil Moisture** |
|---|---|---|---|---|---|
| DATE | MDI | MDI | NOAA | MODIS | Interim |
| [Jun-Aug] | SPEI_JJA | SPI_Ave | VCI_3M | VCI_Ave | ERA5_3M |
| 2000 | 0.079 | 0.966 | 0.501 | 0.521 | 0.208 |
| **2001** | **-1.316** | **-0.773** | **0.243** | **0.303** | **0.177** |
| 2002 | 0.793 | 0.473 | 0.328 | 0.453 | 0.192 |
| 2003 | 0.002 | 0.043 | 0.355 | 0.488 | 0.168 |
| 2004 | -0.350 | -0.141 | 0.289 | 0.360 | 0.182 |
| 2005 | -0.920 | 0.109 | 0.305 | 0.373 | 0.183 |
| 2006 | -0.439 | -0.049 | 0.292 | 0.495 | 0.171 |
| **2007** | **-0.431** | **-1.427** | **0.261** | **0.127** | **0.166** |
| **2008** | **-0.796** | **-1.538** | **0.302** | **0.137** | **0.159** |
| 2009 | 1.197 | 2.291 | 0.654 | 0.789 | 0.197 |
| 2010 | 1.237 | 0.415 | 0.495 | 0.356 | 0.184 |
| 2011 | 1.723 | 0.157 | 0.817 | 0.869 | 0.229 |
| 2012 | 0.587 | 0.719 | 0.687 | 0.313 | 0.182 |
| 2013 | 0.225 | -0.045 | 0.564 | 0.757 | 0.156 |
| **2014** | **-0.509** | **-1.118** | **0.509** | **0.286** | **0.185** |
| 2015 | 1.776 | 1.549 | 0.786 | 0.952 | 0.228 |
| 2016 | 0.859 | 0.000 | 0.615 | 0.721 | 0.19 |
| 2017 | 1.226 | -0.284 | 0.669 | 0.603 | 0.198 |
| 2018 | 0.909 | 0.179 | 0.628 | 0.714 | 0.188 |
| 2019 | 0.620 | 0.648 | 0.544 | 0.836 | 0.194 |
| 2020 | 0.575 | 0.704 | 0.585 | 0.24 | 0.18 |

**Overall Discussion:**

Here, further explanations are emphasized for meteorological drought, vegetative crop index and soil moisture parameters and their interrelations.

The Vegetation Condition Index (VCI):

VCI values are derived using NDVI's, either by NOAA obtained for each province for the three-month- averages for June, July and August in Central Anatolia, Turkey, OR by using

MODIS images for the province averages for more extended term periods. To detect the effect of weather, NDVI needs to be enhanced by separating long-term ecosystem changes from the short term weather-related NDVI fluctuations from the ecosystem. Also, noise reduction techniques for the time series data need to be applied to derive more accurate results.

For this purpose, VCI was introduced and published initially by Kogan (1990,1995) [4,5]. The derived parameter VCI as presented by the Equation (2) in the published paper, considers the additional terms (max and min) of NDVI for each grid cell for the entire time records for the basin.

As proposed by Kogan [4,5] VCI is expected to represent the weather component better than NDVI due to mild/warm climate and shows the drought stress impact on crop condition much better than NDVI [6].

The VCI values between 15-35% indicate extreme to moderate vegetation drought conditions. The commenting author also notes that the meteorological drought indices (as shown in detail in Figure 2 derived from Table 1-SPI and SPEI of the illustrative example) are mostly negative during the drought years 2001, 2007-08 and 2014 (indicated in bold).

When the values of VCI go above 35% with a slight increase of soil moisture (EPA5$\geq$ 0.18), the agricultural crop yield results above the average crop yield value for the following years to follow. This result may be due to the mild (fair to good) vegetation condition resulting from dry/warm micro-climatic factors.

Soil moisture estimation using ERA5 Interim /Land:

Additionally, the ERA5 term provides a global, integrated soil moisture assessment (SM) [7, 8]. The land surface analysis (LSA) is also relevant to foster research for climate change studies providing initial land conditions to forecast models. The methodology includes ECMWF's Interim analysis (ERA5) and NASA's analysis recommended for research and applications (MERRA). This product is a new land surface data set in cooperated LSM with bias precipitation correction, which can be freely downloaded at (https://www.ecmwf.int/en/forecasts/datasets/reanalysis-datasets/era-interim).

## References

[1] Rahman, M. S., Di, L., Shrestha, R., Eugene, G. Y., Lin, L., Kang, L., & Deng, M. (2016, July). Comparison of selected noise reduction techniques for MODIS daily NDVI: An empirical analysis on corn and soybean. In 2016 Fifth International Conference on Agro-Geoinformatics (Agro-Geoinformatics) (pp. 1-5). IEEE.

[2] Michishita, R., Jin, Z., Chen, J., & Xu, B. (2014). An empirical comparison of noise reduction techniques for NDVI time-series based on a new measure. ISPRS Journal of Photogrammetry and Remote Sensing, 91, 17-28.

[3] Hird, J. N., & McDermid, G. J. (2009). Noise reduction of NDVI time series: An empirical comparison of selected techniques. Remote Sensing of Environment, 113(1), 248-258.

[4] Kogan, F. N. (1995). Droughts of the late 1980s in the United States as derived from NOAA polar-orbiting satellite data. Bulletin of the American Meteorological Society, 76(5), 655-668.

[5] Kogan, F. N. (1990). Remote sensing of weather impacts on vegetation in non-homogeneous areas. International Journal of Remote Sensing, 11(8), 1405-1419.

[6] Rousta, I., Olafsson, H., Moniruzzaman, M., Zhang, H., Liou, Y. A., Mushore, T. D., & Gupta, A. (2020). Impacts of drought on vegetation assessed by vegetation indices and meteorological factors in Afghanistan. Remote Sensing, 12(15), 2433.

[7] Balsamo, G., Albergel, C., Beljaars, A., Boussetta, S., Brun, E., Cloke, H., ... & Vitart, F. (2015). ERA-Interim/Land: a global land surface reanalysis data set. Hydrology and Earth System Sciences, 19(1), 389-407.

[8] Albergel, C., Dutra, E., Munier, S., Calvet, J. C., Munoz-Sabater, J., Rosnay, P. D., & Balsamo, G. (2018). ERA-5 and ERA-Interim driven ISBA land surface model simulations: which one performs better?. Hydrology and Earth System Sciences, 22(6), 3515-3532.

# Authors' Closure

The authors thank the commenting author for this discussion part, which emphasizes the importance of the subject by making detailed explanations and the results and discussions presented in the article.

A large part of Turkey is classified in "Hot-summer Mediterranean Climate" class under "Group C: Temperate Climates" according to the Köppen–Geiger climate classification system (Beck et al., 2018). Also Turkey is defined as "highly vulnerable to climate change" in projections (Kammila, 2021). In the light of this situation (i.e., ecoregion of Turkey), the issues of drought monitoring and water management are immensely important for Turkey and increase their importance year by year. As commenting author pointed out, various drought indices in the detection of drought in Turkey enable the monitoring of drought processes and making projections for the future with the improvement of remote sensing technologies. It is noteworthy that the graphics provided by commenting author are also compatible with the drought periods and periods in the study.

Authors are agreeing with the future studies which were suggested by commenting author, and in addition, changes in land use data, climate change effect on microclimate zones and changes in soil quality especially after forest fires should be examined for better predictions.

Beck, H. E., Zimmermann, N. E., McVicar, T. R., Vergopolan, N., Berg, A., & Wood, E. F. (2018). Present and future Köppen-Geiger climate classification maps at 1-km resolution. Scientific Data, 5(1), 180214. https://doi.org/10.1038/sdata.2018.214

Kammila, S. (2021). Turkey. UNDP Climate Change Adaptation. https://www.adaptation-undp.org/explore/europe-and-central-asia/turkey

# TEKNİK DERGİ MANUSCRIPT DRAFTING RULES

1. The whole manuscript (text, charts, equations, drawings etc.) should be arranged in Word and submitted in ready to print format. The article should be typed on A4 (210 x 297 mm) size paper using 10 pt (main title 15 pt) Times New Roman font, single spacing. Margins should be 40 mm on the left and right sides and 52.5 mm at the top and bottom of the page.
2. Including drawings and tables, articles should not exceed 25 pages, technical notes 10 pages.
3. Your contributed manuscript must be sent over the DergiPark system. (http://dergipark.gov.tr/tekderg)
4. The text must be written in a clear and understandable language, conform to the grammar rules. Third singular person and passive tense must be used, and no inverted sentences should be contained.
5. Title must be short (10 words maximum) and clear, and reflect the content of the paper.
6. Sections should be arranged as: (i) abstract and keywords, (ii) title, abstract and keywords in the other language, (iii) main text, (iv) symbols, (v) acknowledgements (if required) and (vi) references.
7. Both abstracts should briefly describe the object, scope, method and conclusions of the work and should not exceed 100 words. If necessary, abstracts may be re-written without consulting the author. At least three keywords must be given. Titles, abstracts and keywords must be fitted in the first page leaving ten line space at the bottom of the first page and the main text must start in the second page.
8. Section and sub-section titles must be numbered complying with the standard TS1212.
9. Symbols must conform to the international rules; each symbol must be defined where it appears first, additionally, a list of symbols must be given in alphabetic order (first Latin, then Greek alphabets) at the end of the text (before References).
10. Equations must be numbered and these numbers must be shown in brackets at the end of the line.
11. Tables, drawings and photographs must be placed inside the text, each one should have a number and title and titles should be written above the tables and below the drawings and photographs.
12. Only SI units must be used in the manuscripts.
13. Quotes must be given in inverted commas and the source must be indicated with a reference number.
14. Acknowledgement must be short and mention the people/ institutions contributed or assisted the study.
15. References must be numbered (in brackets) in the text referring to the reference list arranged in the order of appearance in the text. References must include the following information:

    If the reference is an article: Author's surname, his/her initials, other authors, full title of the article, name of the journal, volume, issue, starting and ending pages, year of publication.

    Example : Naghdi, P. M., Kalnins, A., On Vibrations of Elastic Spherical Shells. J. Appl. Mech., 29, 65-72, 1962.

    If the reference is a book: Author's surname, his/her initials, other authors, title of the book, volume number, editor if available, place of publication, year of publication.

    Example : Kraus. H., Thin Elastic Shells, New York. Wiley, 1967.

    If the reference is a conference paper: Author's surname, his/her initials, other authors, title of the paper, title of the conference, location and year.

    If the source is a thesis: Author's surname, his/her initials, thesis title, level, university, year.

    If the source is a report: Author's surname, his/her initials, other authors, title of the report, type, number, institution it is submitted to, publication place, year.
16. Discussions to an article published in Teknik Dergi should not exceed two pages, must briefly express the addressed points, must criticize the content, not the author and must be written in a polite language. Authors' closing remarks must also follow the above rules.
17. A separate note should accompany the manuscript. The note should include, (i) authors' names, business and home addresses and phone numbers, (ii) brief resumes of the authors and (iii) a statement "I declare in honesty that this article is the product of a genuinely original study and that a similar version of the article has not been previously published anywhere else" signed by all authors.
18. Copyright has to be transferred to UCTEA Turkish Chamber of Civil Engineers. The standard copyright form signed by the authorised author should therefore be submitted together with the manuscript.

# CONTENTS



**ISSN: 1300-3453**